Pointing Model evolution for GMRT antennas over the last decade

by Subhashis Roy

NCRA-TIFR
Pune-7

Pointing model evolution for GMRT antennas over the last decade

Nov 27, 2021

1 Introduction

Any mechanical structure built following a plan would suffer from imperfections. For example, the azimuth axis of radio astronomical telescopes or antennas may not be truly vertical or the elevation axis may not truly be lying along the horizontal plane. Depending on elevation angle, reflecting surface of an antenna could deviates from a true parabola due to changes in its support structure caused by gravitational bending. Such errors would cause systematic difference between the apparent and true azimuth (AZ) measured from North through rotation of its vertical axis. The same would manifest in difference between apparent and true elevation (EL) angles of the antennas as shown by the rotation of horizontal axis from horizon. Given that misalignment of axis is geometrical in nature, the resulting pointing errors could be corrected if the amount of misalignment of the two axis for each antennas can be measured. If gravitational bending of support structures cause the effective axis of the antennas to shift by small amount, it also could be modelled. Hence, measuring pointing errors of the antennas as a function of elevation and azimuth are needed, and if found to be significant, there is need to model and apply corrections.

Initial measurements of pointing errors for modelling the antenna characteristics were done as described in Kantharia et al. (2007) by observing a single calibrator from rise to set. This was repeated on a few calibrators to cover a reasonable portion of the AZ plane. It showed significant systematic variation of pointing error as a function of azimuth and elevation for GMRT antennas. They used the model of Greve et al. (1996, A&AS, 115, 379) to estimate the axis misalignment and gravitational bending parameters of the GMRT antennas. They found that by using Greve et al. (1996) model, the residual rms pointing error of the antennas could be brought down to $\sim 1'$. They claimed the resultant model to satisfactorily correct the elevation pointing errors up to about 6 months, whereas the azimuth pointing errors could not be properly corrected beyond a couple of months.
Subsequently, as described in Roy & Kulkarni, (2009), they found that the inclination of azimuth axis along the N-S direction (called P4 in Greve et al. 1996) as determined from the EL data were systematically higher than values derived from the AZ data for almost all the antennas. This indicated that Greve et al. (1996) model may not describe the pointing errors of the GMRT antennas adequately.

Roy & Kulkarni (2009) found it possible to empirically model the AZ and EL dependent pointing errors separately using seven parameters (3 parameters for AZ and 4 parameters for EL). They also included refraction correction of radio waves through the neutral atmosphere. The parameters of the model appeared to remain stable (except the constant offsets terms) over a timescale of an year, and using it could reduce typical pointing errors by ~ 2. The model was then applied through Online for regular observations. They concluded that the model parameters could change on timescales of $\gtrsim 1$ year.

Subsequently, these test observations were followed up regularly. Set of calibrators were observed all across the sky in L-band to determine pointing errors typically once or twice an year to check if applying the then existing pointing model could still reduce the pointing errors of the antennas. Also, model parameters were redetermined from these observations to see how these numbers change with time. When errors from certain antennas did not show any improvement using the existing pointing model, we did identify possible mechanical issues with the antennas, which were subsequently fixed. In a few cases, when model parameters were systematically off from the best fit values over a few epochs of testing, the parameters were updated for the antennas. The present work summarises on how the pointing model parameters of the antennas behaved over the last decade and how effective it is in reducing the pointing errors.

2 Observing technique and data reductions:

Need for accurate measurement of antenna pointing errors was felt from the beginning of GMRT construction, and strategies to measure pointing offsets accurately initiated. To measure pointing errors, antennas were used to scan a strong source ($\sim$a few hundred Jy) with known angular speed and total power data for antennas recorded. However, this was possible only if a strong radio sources in the sky was visible (only a few of which are known), and one also needed to switch the automatic level controls (ALCs) off. Measurements of pointing errors were performed by fitting a Gaussian beam pattern to the observed total power as a function of time, which needed the speed of the scan and the start time of the scans to be accurately known. However, occasionally at least one of the above (perhaps the start time) was not correct and the pointing errors appeared unrepeatable for a few antennas when repeated. Also, the shape of the beam showed indications of saturation in some cases. Therefore, a new routine was written for the legacy Online system of GMRT, where a calibrator is observed using interferometric techniques at different known offsets from the pointing centre for all the available antennas in both AZ and EL (developed by Jitendra Kodilkar and A. Pramesh Rao). It is called 'Grid-pointing', during which a calibrator is observed with 5 to 9 known offsets for $\sim$1 minute at each grid points either in AZ or EL and the source offsets change from one grid point to the next and the maximum offset is $\sim$2 of the FWHM of the antenna primary beam. This method is used to carry out all the pointing error measurements described here.

To measure the pointing errors for the GMRT antennas, several observations during test times were carried out for $\gtrsim$10 hours of duration. Typically seven grid points were used for each set of AZ and EL Grid-pointing and the grid size was $6'$. Observing frequency was chosen to be 1280 MHz, so that the primary beam sizes remain small thereby improving the accuracy of the pointing error measurements. We used the programme 'gngrpntg' (developed by Vasant Kulkarni) to measure AZ and EL pointing errors from the Grid-pointing observations. All the pointing errors with weights (reliability) less than 3 were rejected. These pointing errors were fitted by the pointing model as developed in Roy & Kulkarni (2009) using 'gnuplot' (uses non-linear least square fit),

$$\Delta\mathrm{AZ} = A \times \cos(\mathrm{AZ}) + B + C \times \cos(\mathrm{EL}) \tag{1}$$

$$\Delta\mathrm{EL} = 0.933.\cot(\mathrm{EL}) + a \times \cos(\mathrm{EL}) + b + c \times \cos(\mathrm{AZ} - d) \tag{2}$$

where A, B, C and a, b, c, d are model parameters to be determined from fit. All the angles are measured in degrees. The first term in Eqn. (2) is due to refraction correction from neutral atmosphere (COESA 1976).
We note that there could exist significant correlation between the different parameters. While fitting the data from typical pointing observations of ∼10 hours (∼30 pointing scans), 'gnuplot', showed highly significant anti-correlation between B & C (at ∼95% level), and between 'a' and 'b' (at ∼95% level). Therefore, the individual values of the above coefficients may not be uniquely determined from the fits.

After the model parameters were finalised in May 2008, the subsequent AZ pointing error observations were done on 29 Jan 2009, 18 Nov 2009, 10 May 2010, 31 May 2011, 26 Jan 2014, 05 Apr 2015, 28 Aug 2017, 17 Feb 2019, 25 Nov 2019 and 16 Dec 2020.
The EL pointing error observations were done on 21 Nov 2008, 04 Nov 2009, 10 May 2010, 22 Aug 2010, 06 Sept 2010, 31 May 2011, 15 Sept 2012, 11 Oct 2012, 18 May 2013, 26 Jan 2014, 04 Apr 2015, 28 May 2016, 23 Aug 2017, 03 Mar 2019, 14 Nov 2019 and 02 Dec 2020.

3 Results & Discussions:

3.1 Azimuth

Measured pointing model parameters as a function time in months are shown in Fig. 1. Where month no. are measured from May 2008 when the model coefficients were implemented for the first time. The model coefficients for the model of May 2008 are shown by a '+' sign in the plots corresponding to month-0. Also, the existing model coefficients which were last renewed in Jun 2019 are shown by the same symbol for the month 133 in the plots. As can be seen from Fig. 1, despite fitting Eqn. 1 for each epoch, the reduced χ^2 for C00, C02, C05 and W01 were >4 (assuming error in measurements is $1'$) for up to 40 months from May 2008. These antennas had certain mechanical issues, and were pointed out during 2008. The problems were corrected by 2011. However, the χ^2 for C01 is typically >4 from the year 2017 which cannot be addressed by the model.

From the plots we find that the value of parameter 'A' is either quite stable or changes slowly over time for most of the antennas. However, the value of parameter 'C' appears pretty unstable. This could happen as the DC offset (B) is significantly anti-correlated with C. If that is the case, then the value of B+C would remain stable over time. However, as shown in the same plot, the value of B+C also to be unstable and varies in the same way as C. This suggests that epoch to epoch variation of B is not responsible for the variation of C. We also note that the actual model parameter values used for GMRT are often quite different than what is determined by independent fitting for all the parameters at each epochs. Therefore, we also checked for the reduced χ^2 of the pointing errors from Aug 2017 after applying the latest pointing model (after May 2008, pointing model was updated for certain antennas in Jul 2017 and then again in Jun 2019), which are shown in Table-1. From Table-1, most of the antennas show typical reduced $\chi^2 < 1$, though a few of antennas have $\chi^2 > 2$. This indicates the model of Jun 2019 adequately describes the AZ pointing errors for almost all the antennas. It also indicates lack of consistency of C (Fig. 1) among the epochs and variation of some of the individual model parameters have little impact on the overall pointing error.

Fig. 1: C00 Azimuth pointing coefficients

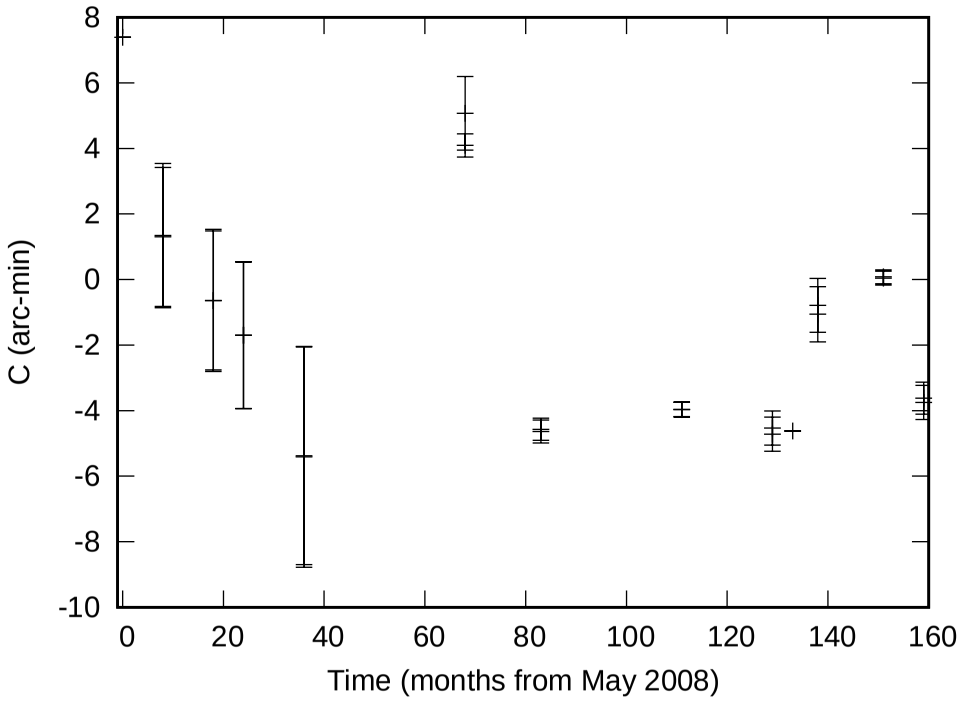

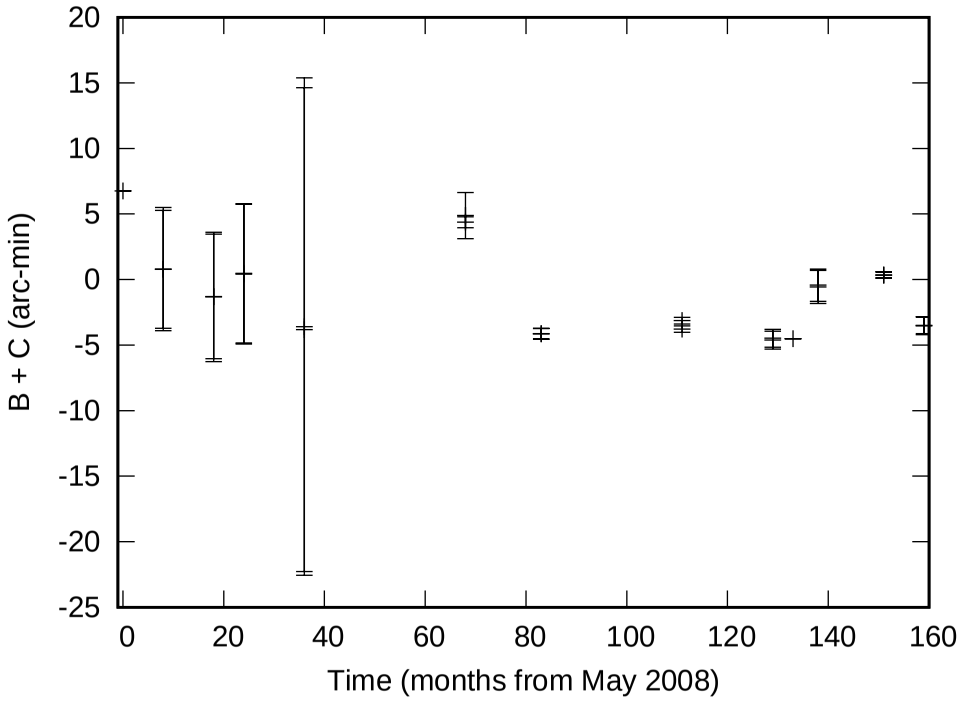

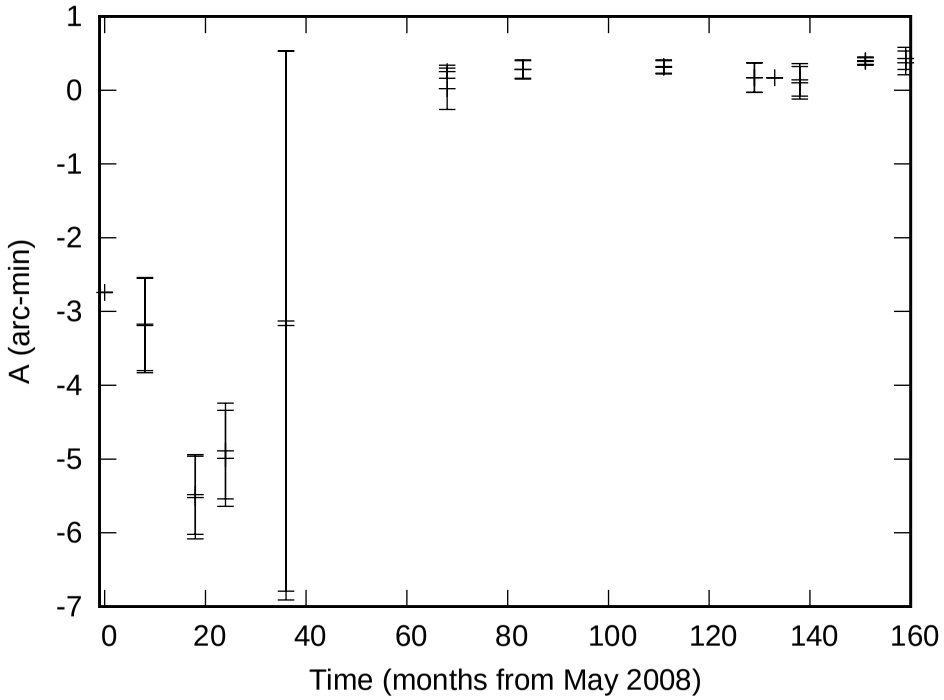

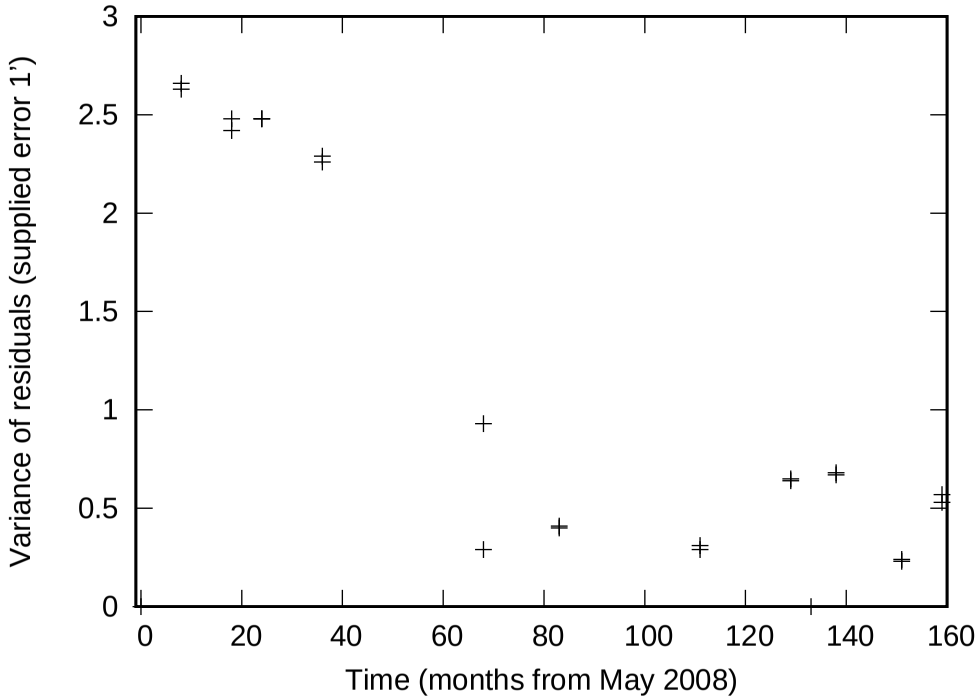

Fig. 1: C01 Azimuth pointing coefficients

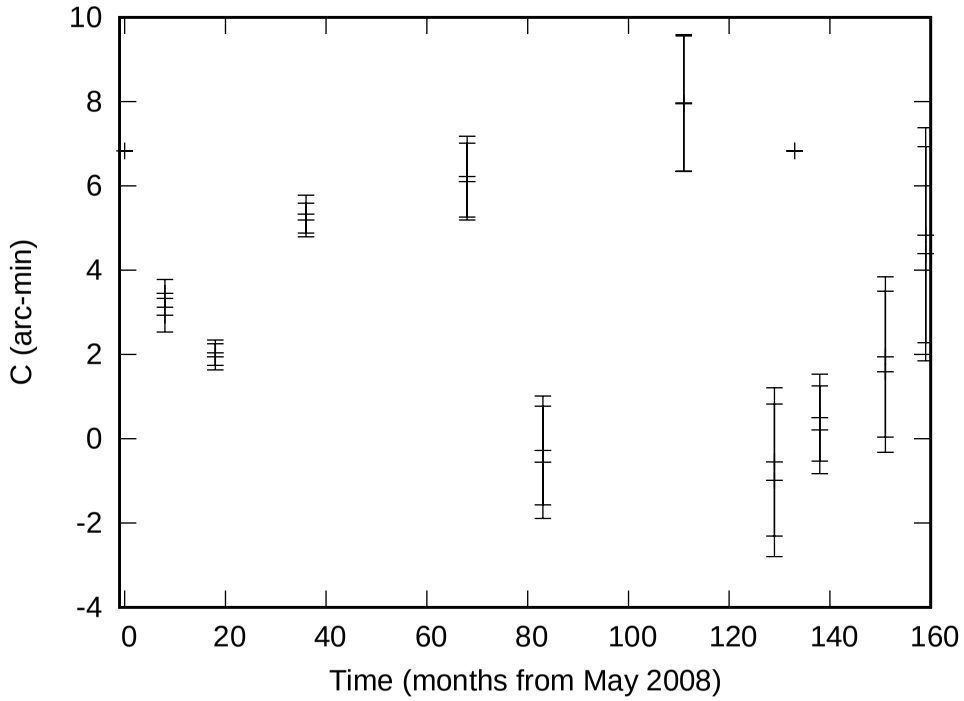

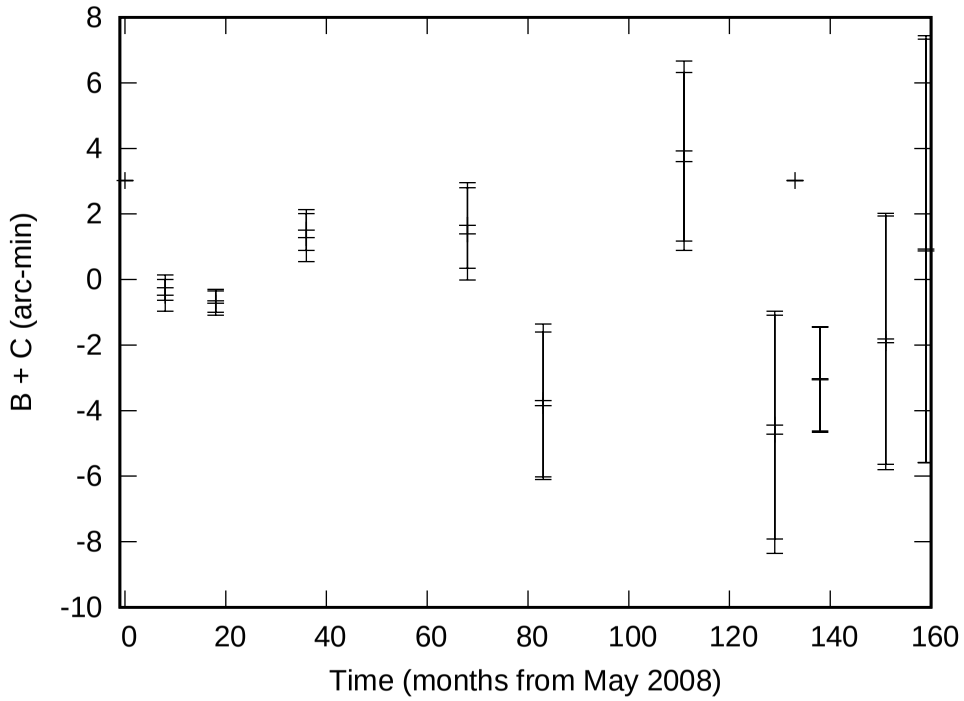

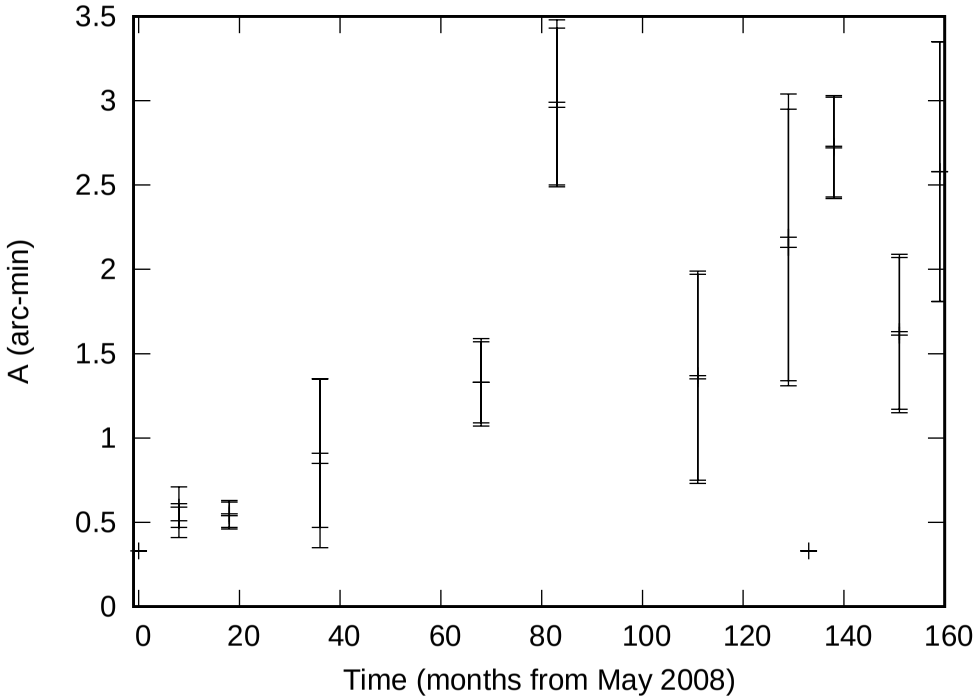

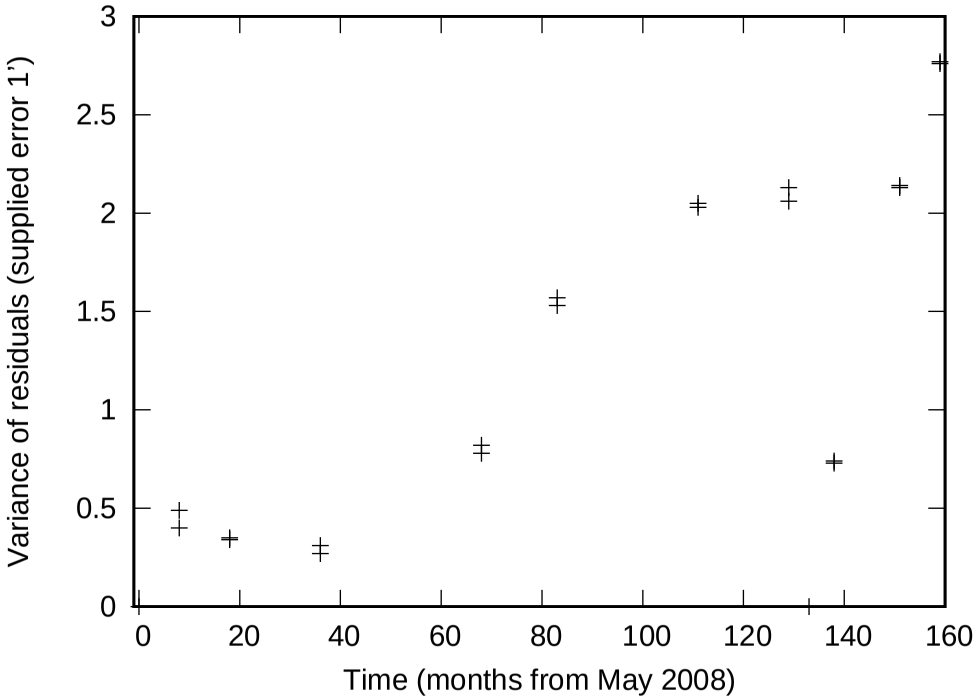

Fig. 1: C02 Azimuth pointing coefficients

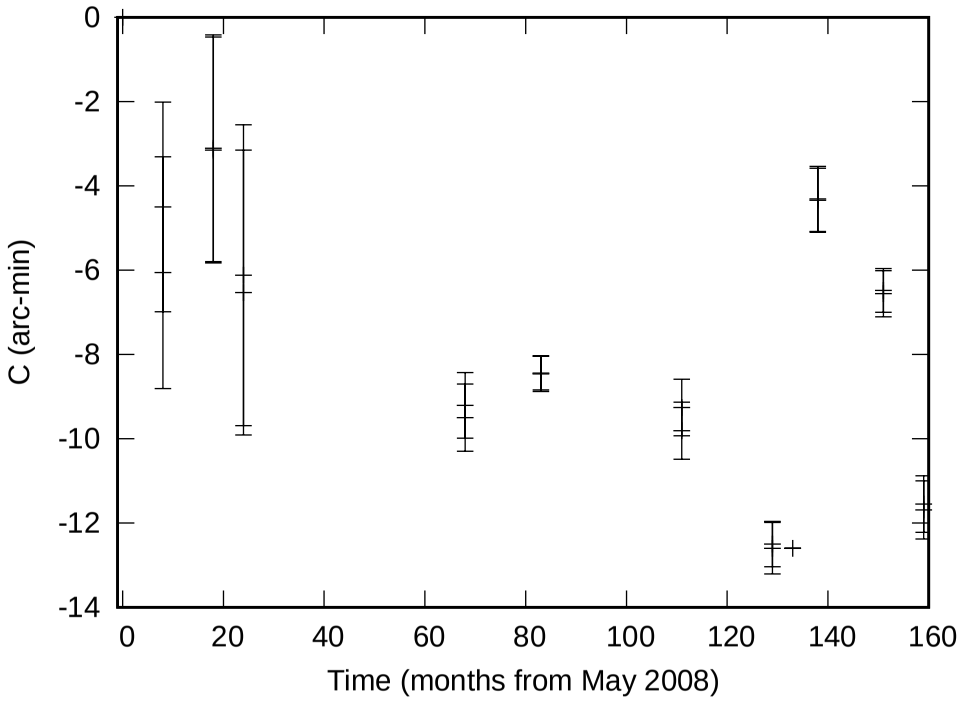

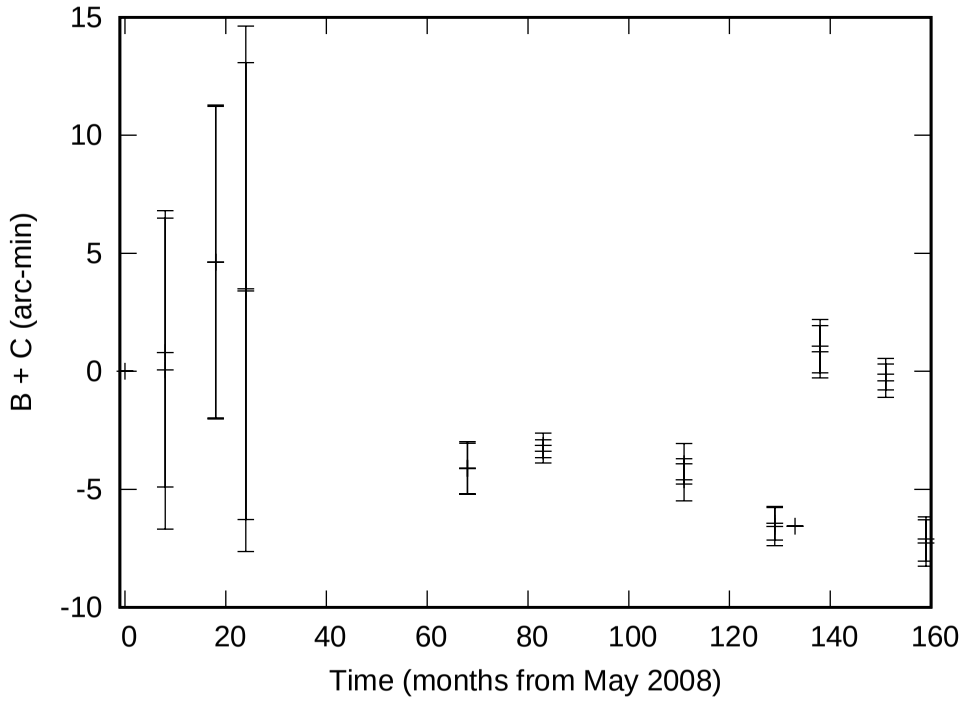

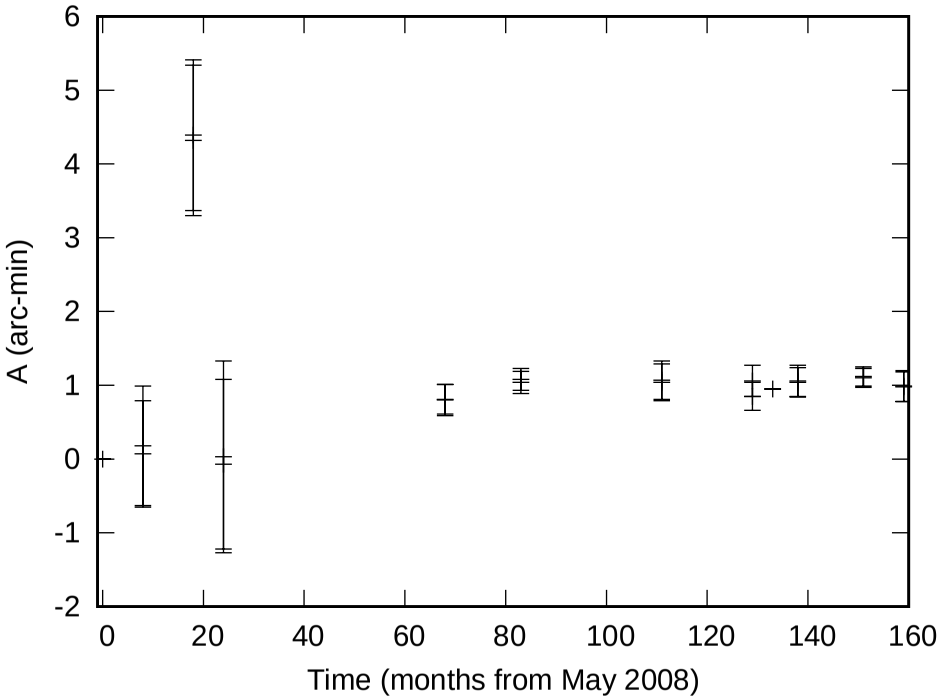

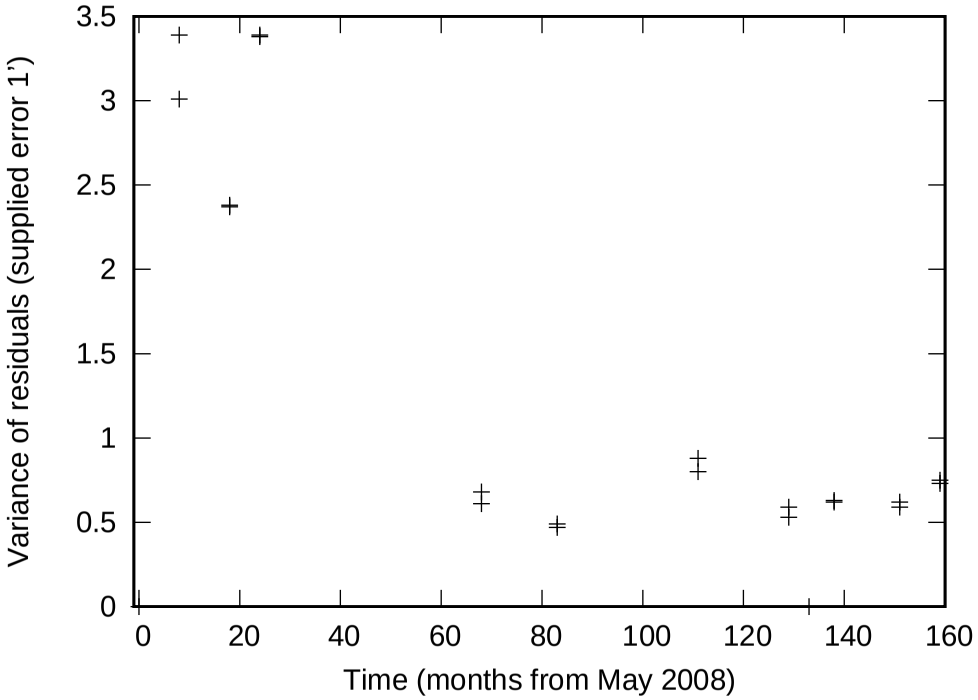

Fig. 1: C03 Azimuth pointing coefficients

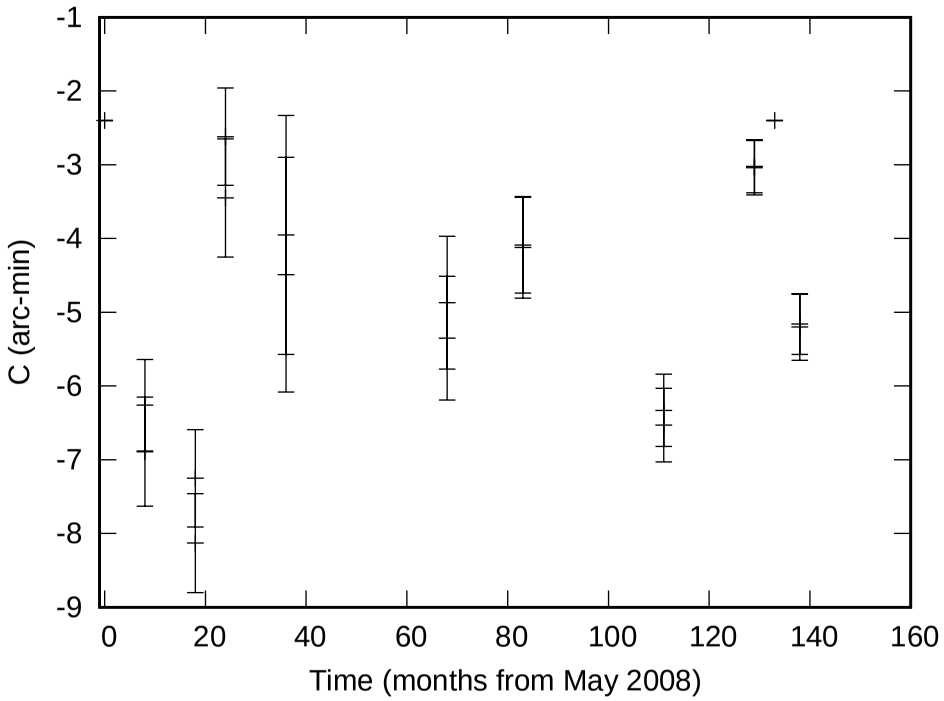

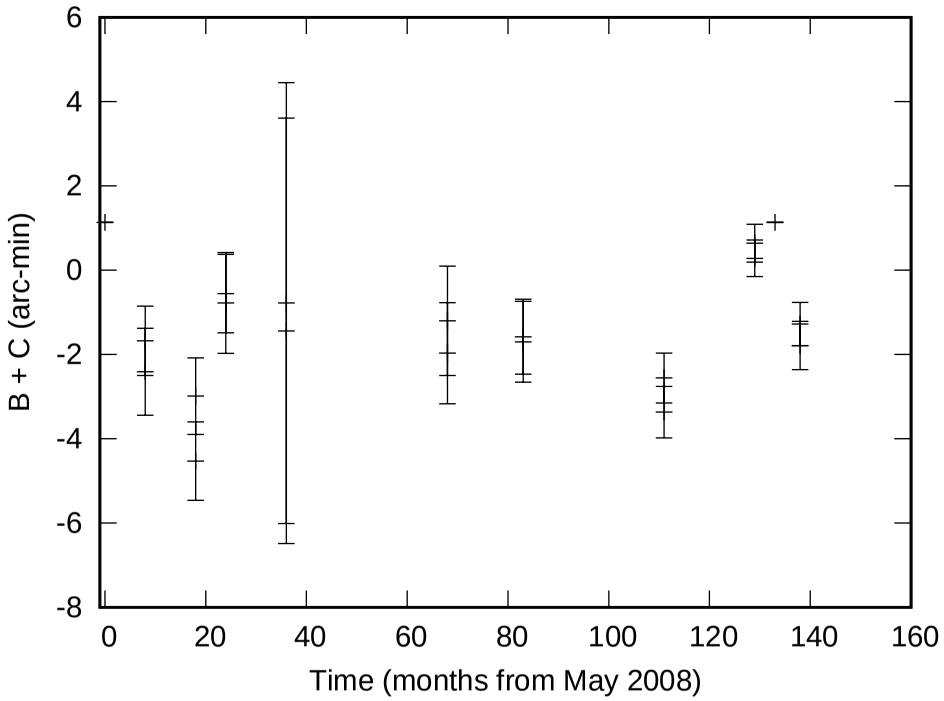

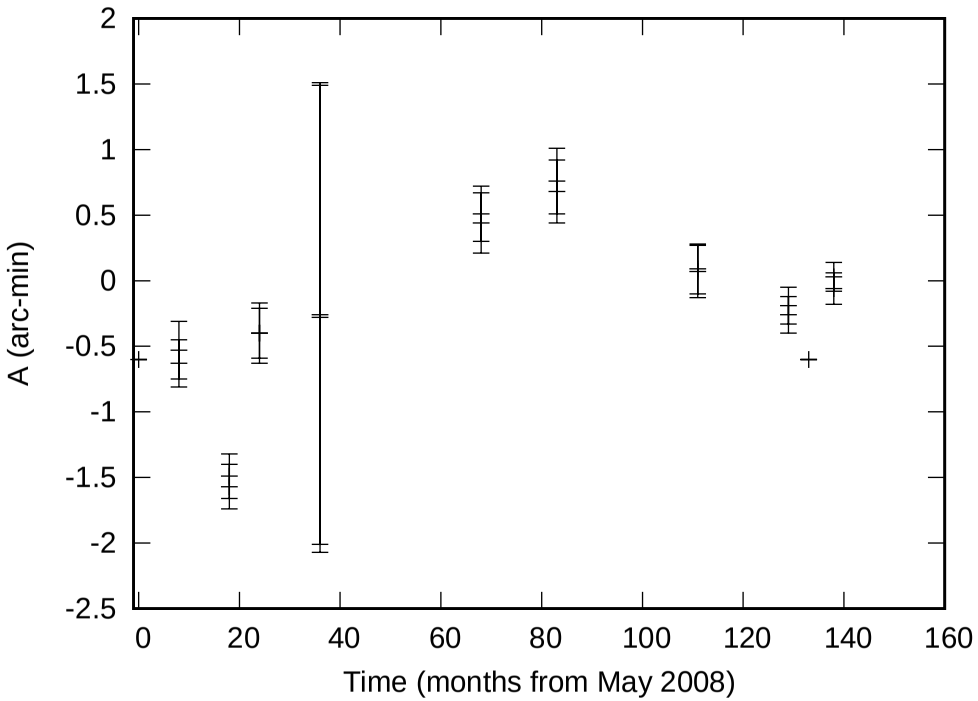

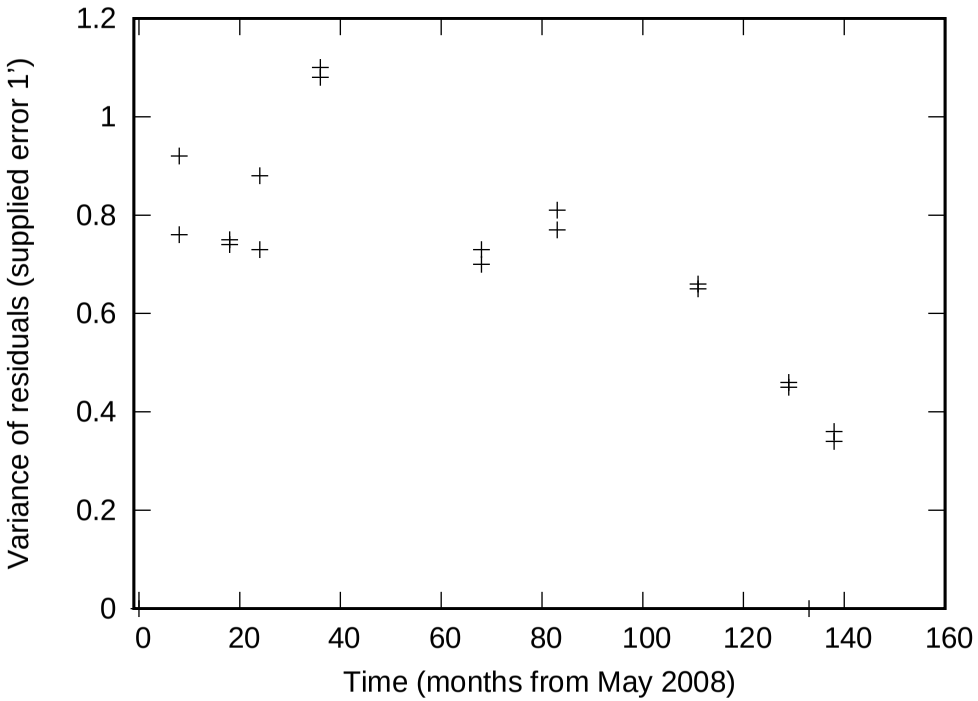

Fig. 1: C04 Azimuth pointing coefficients

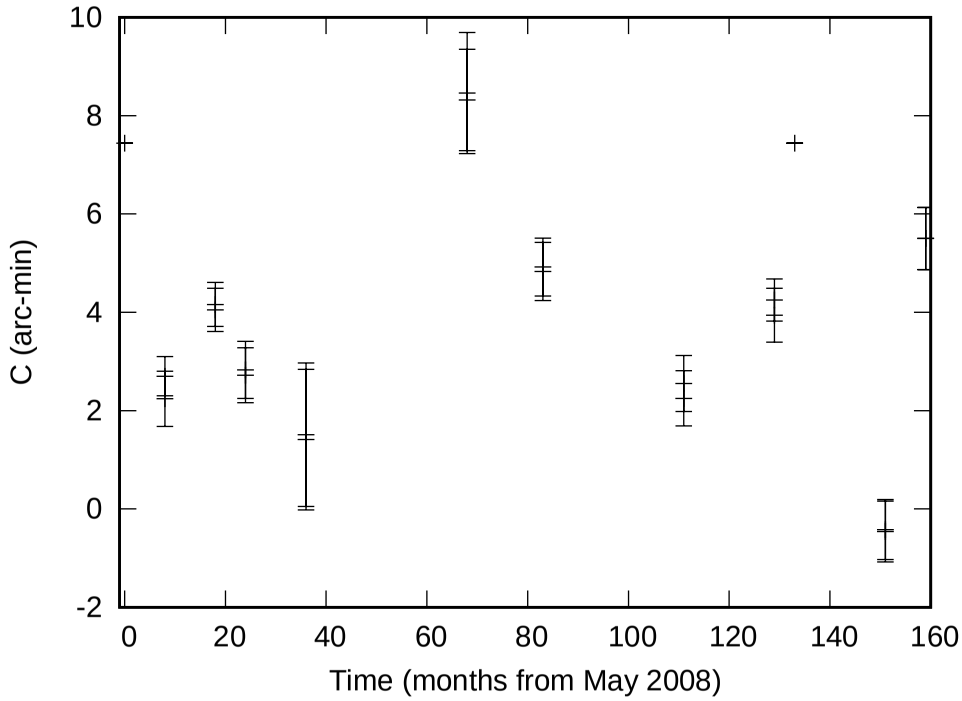

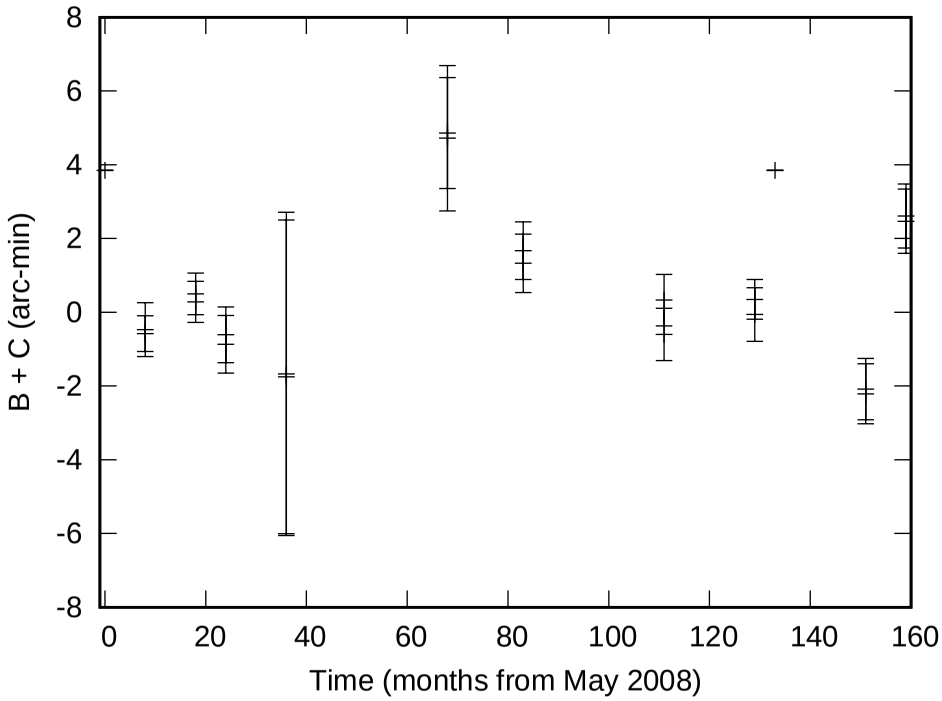

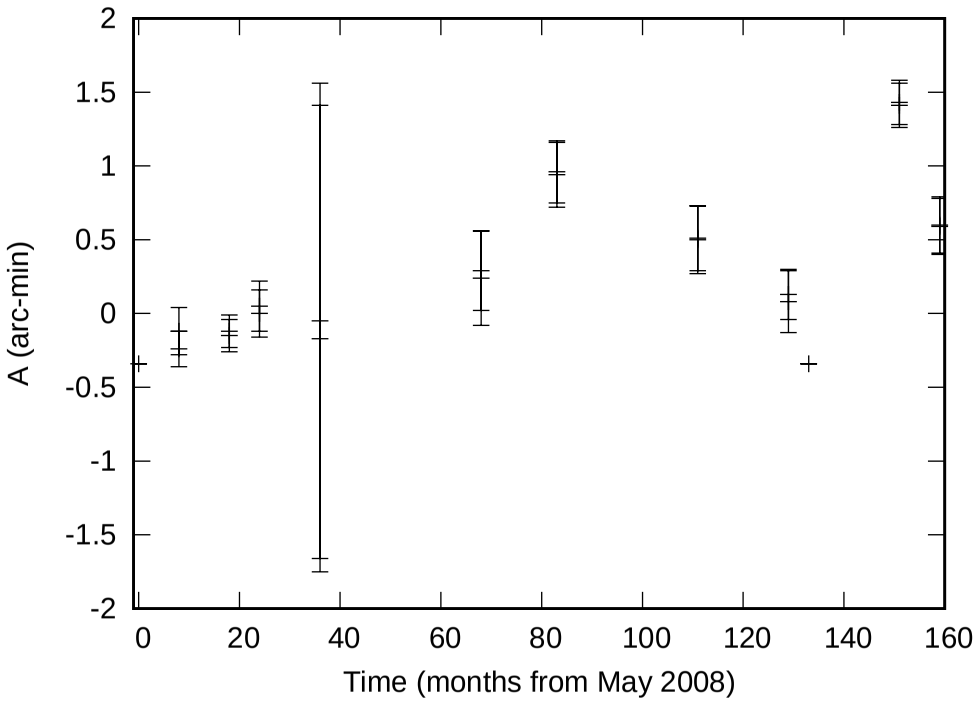

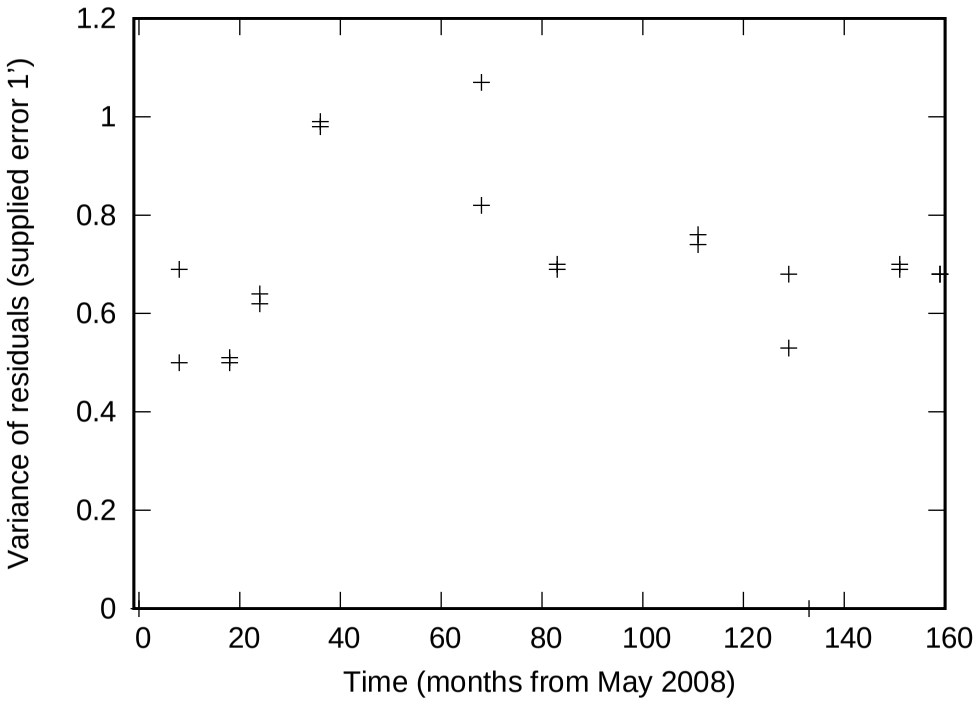

Fig. 1: C05 Azimuth pointing coefficients

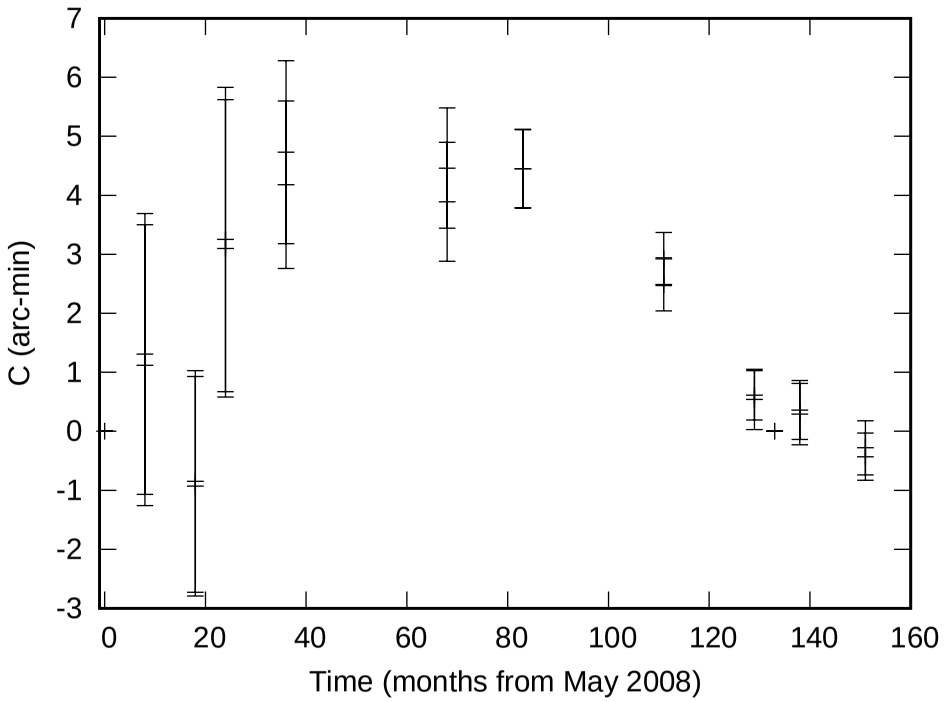

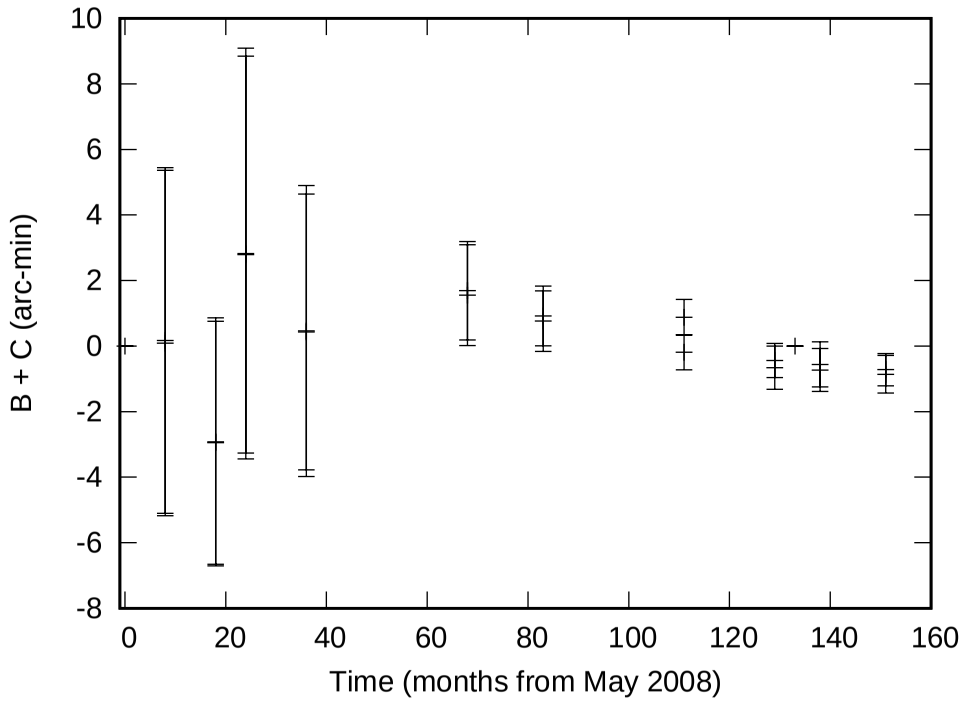

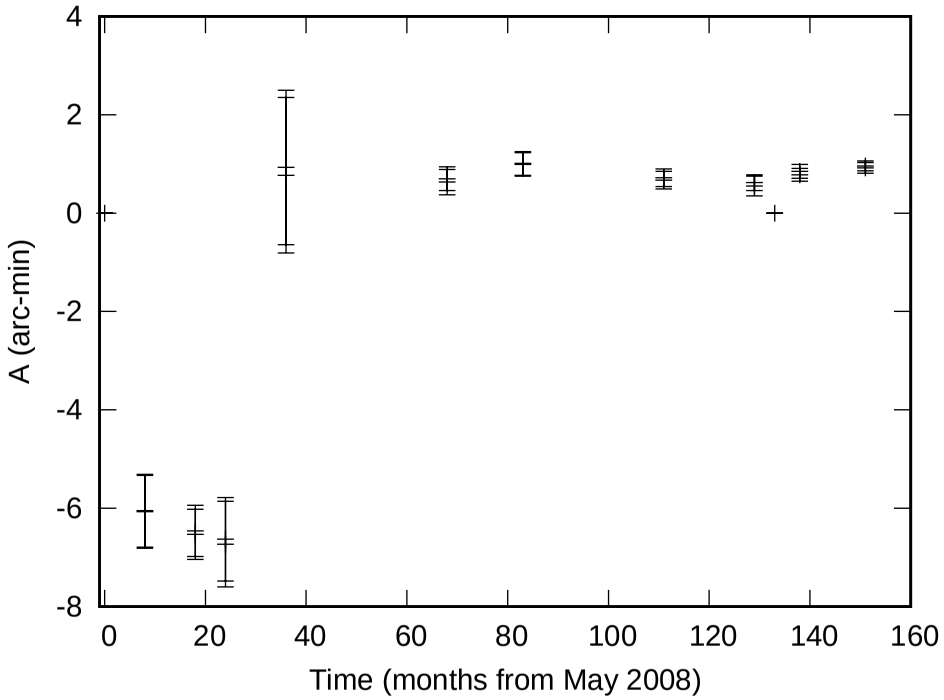

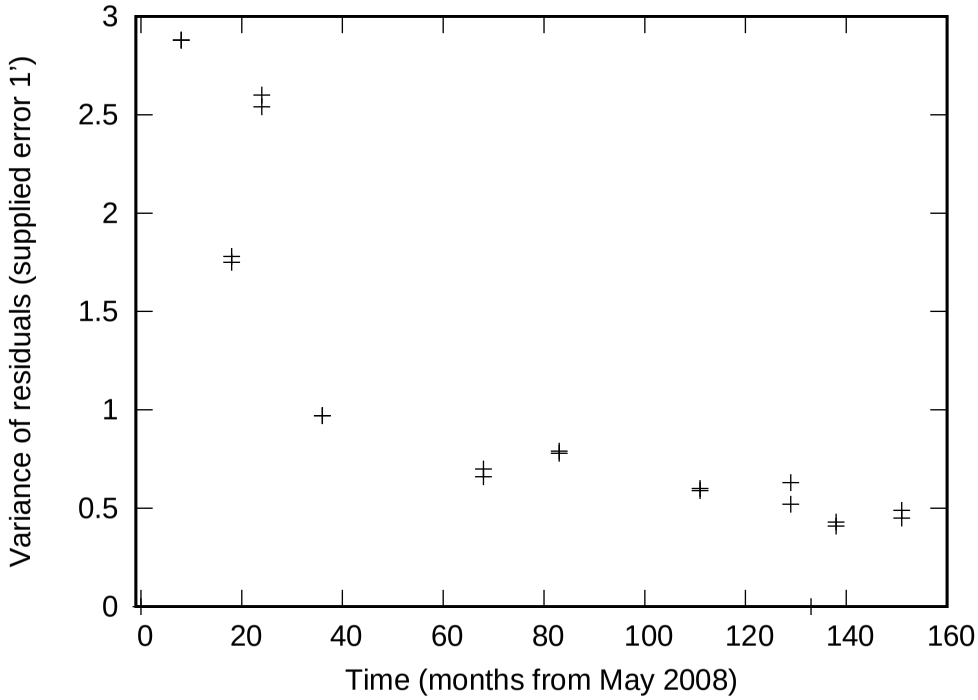

Fig. 1: C06 Azimuth pointing coefficients

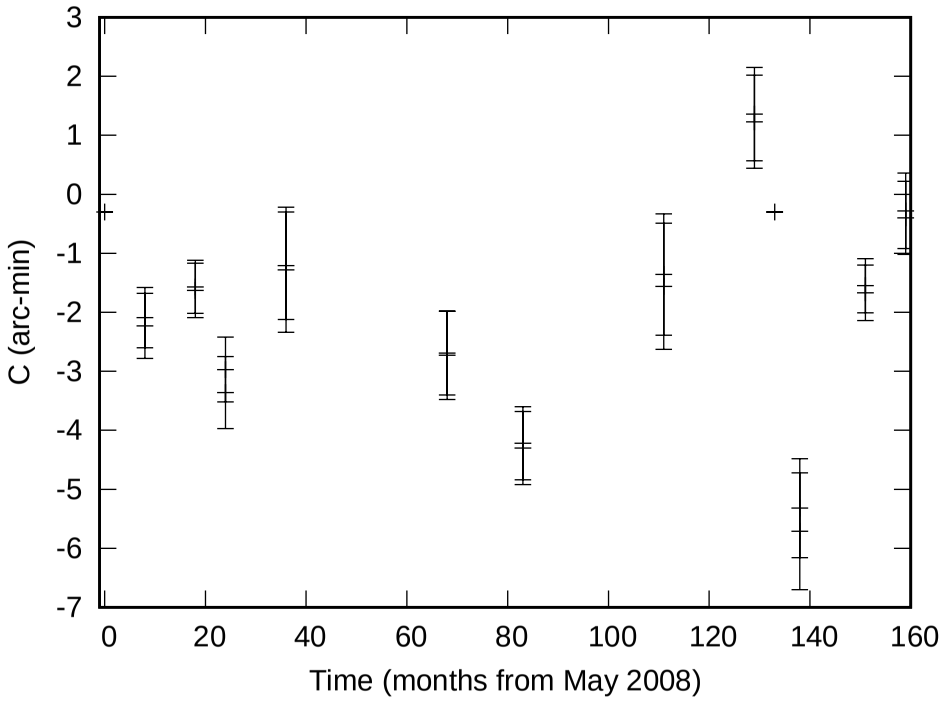

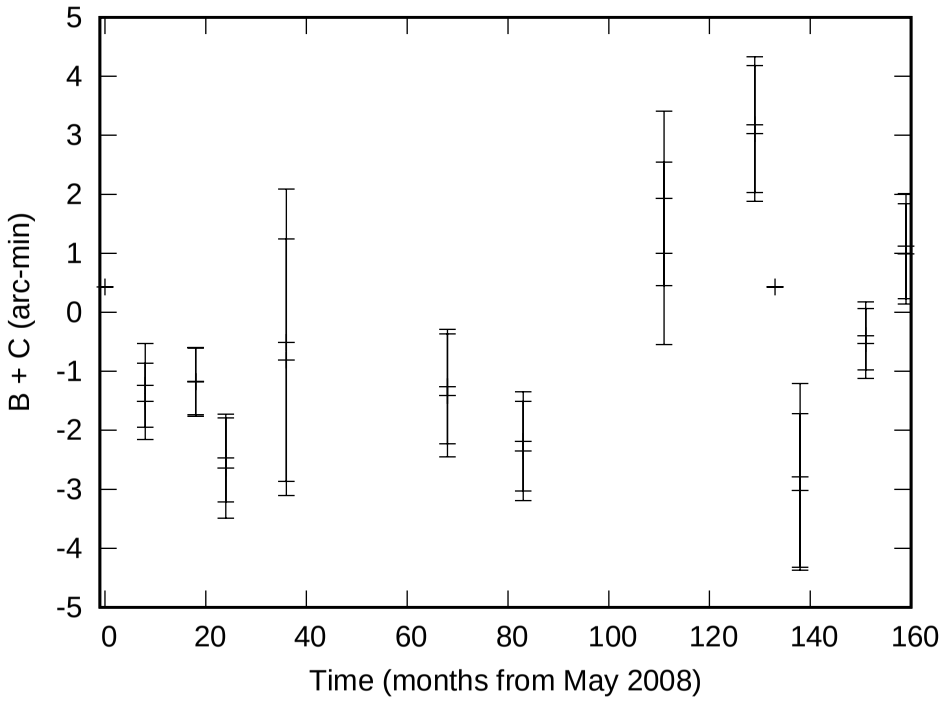

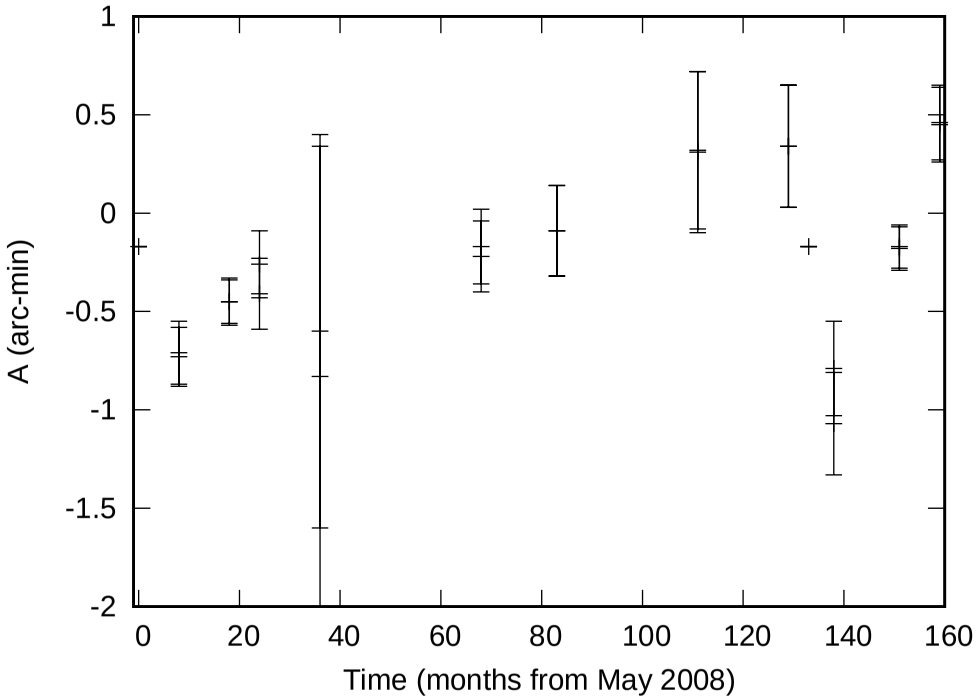

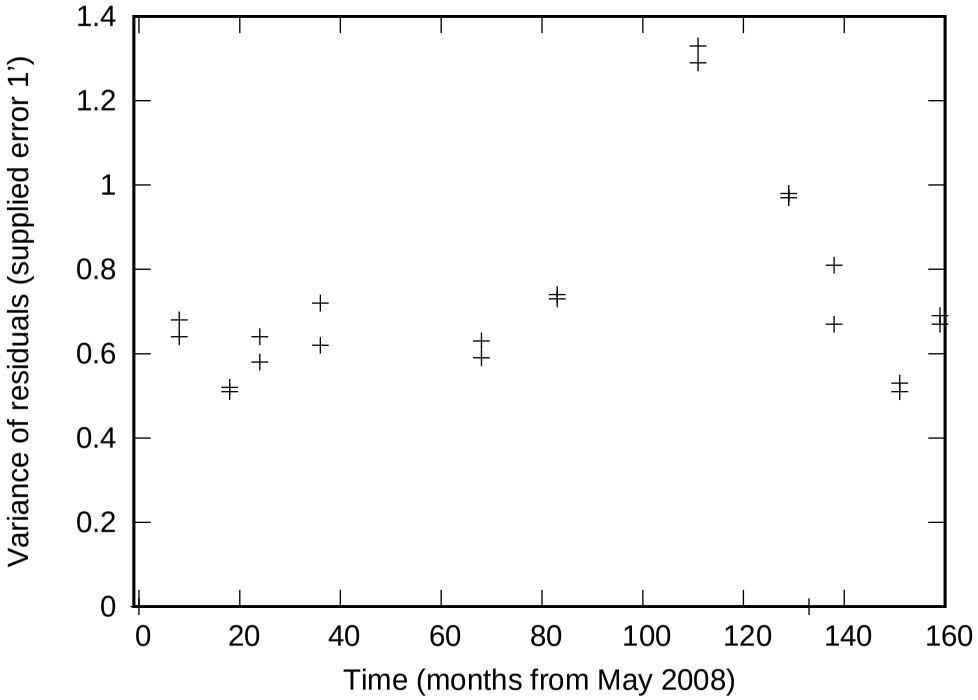

Fig. 1: C08 Azimuth pointing coefficients

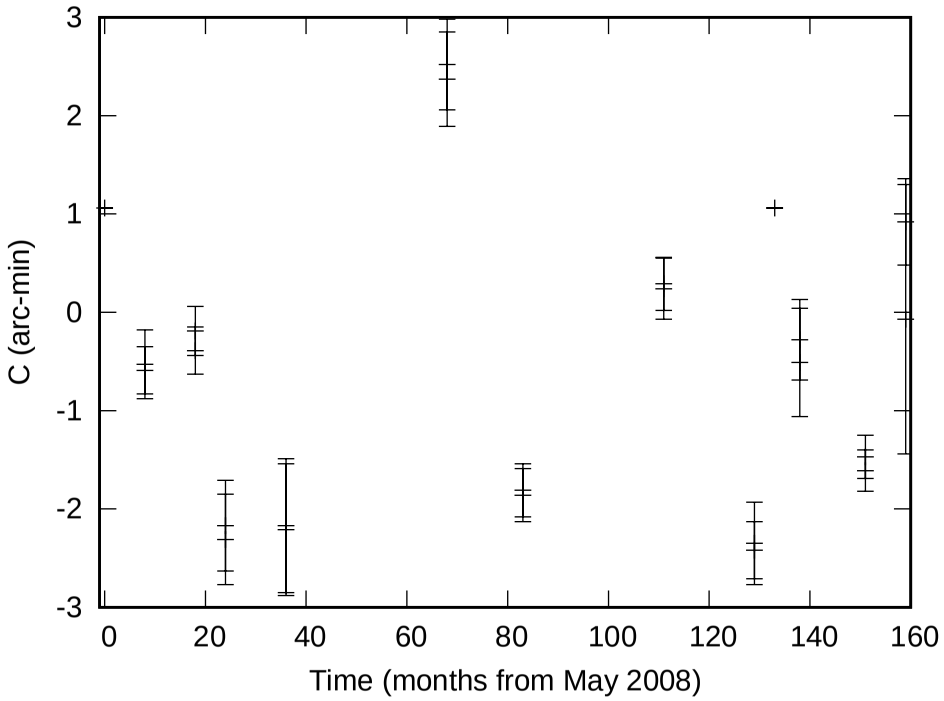

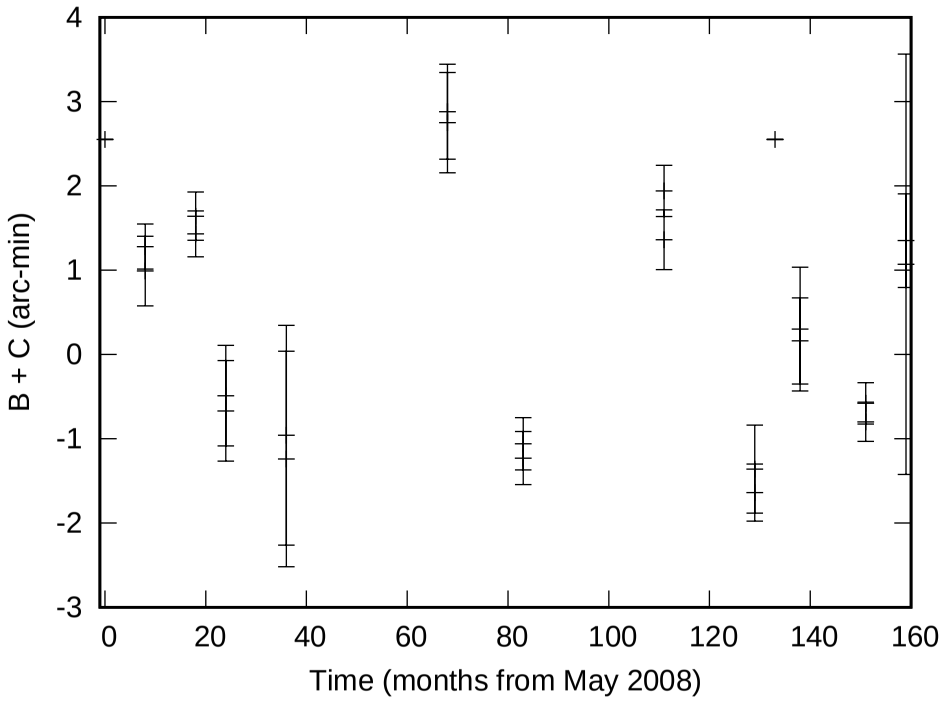

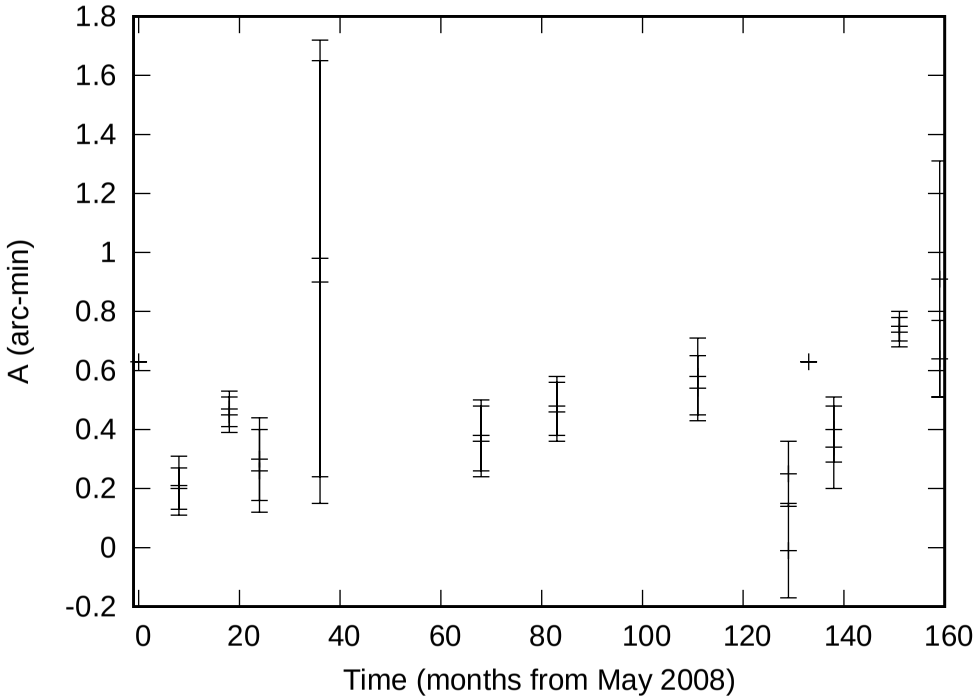

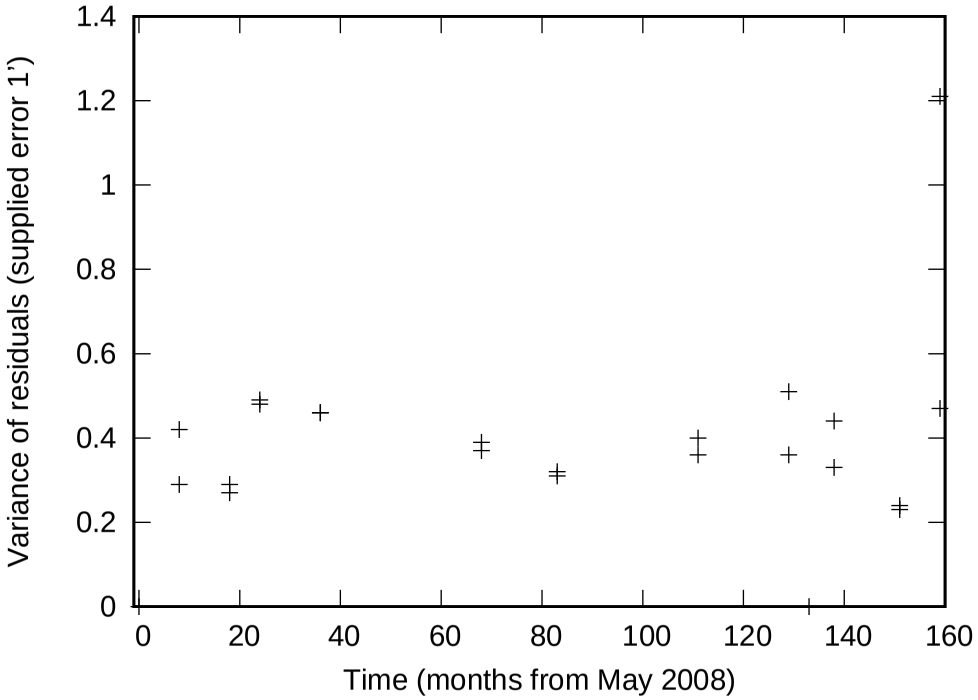

Fig. 1: C09 Azimuth pointing coefficients

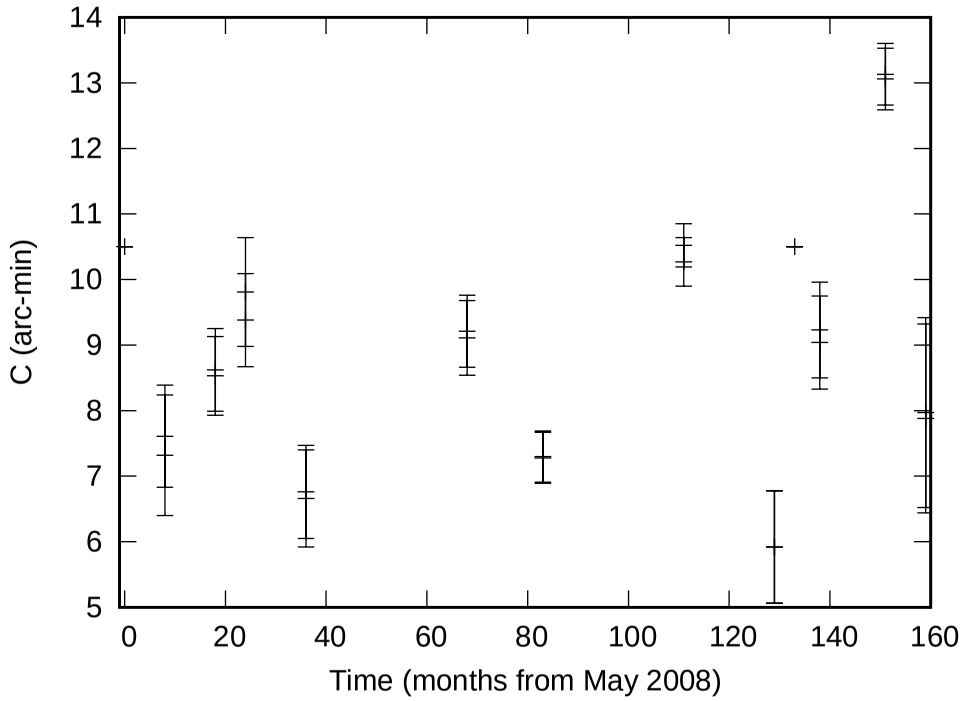

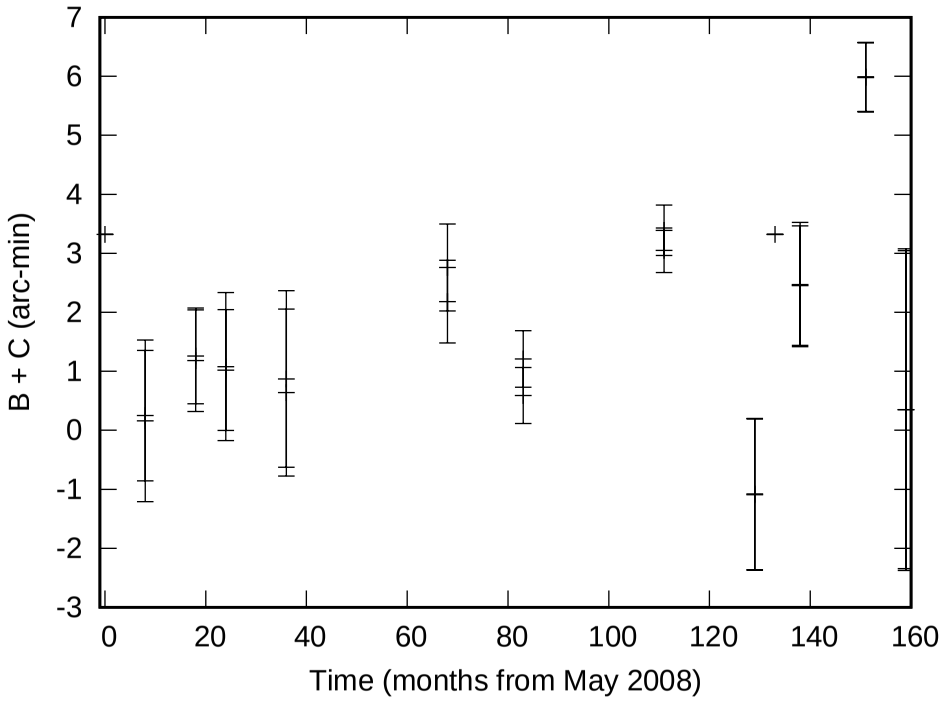

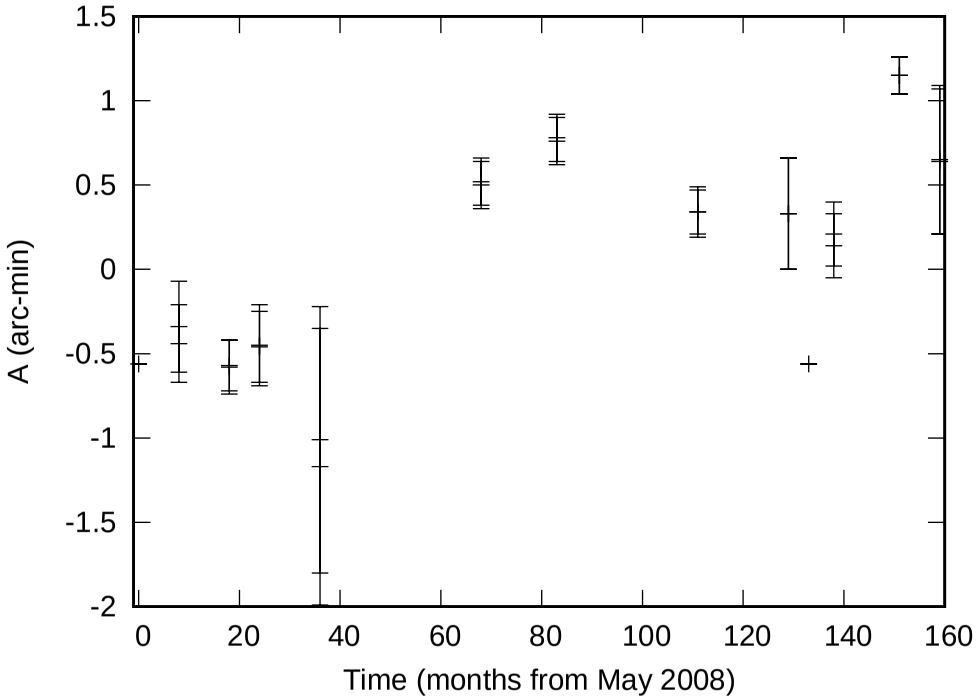

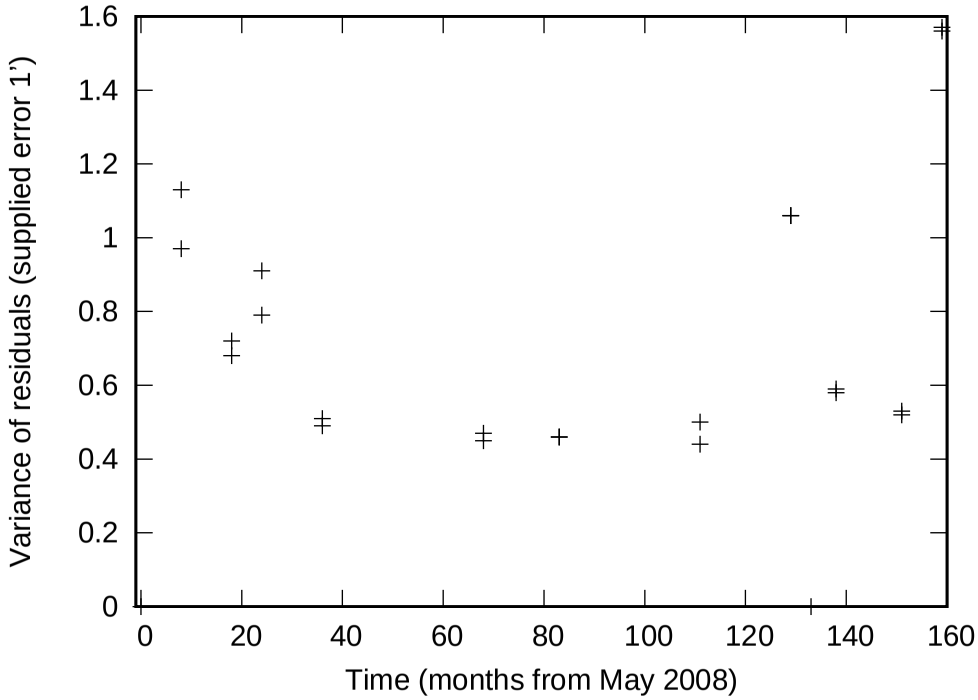

Fig. 1: C10 Azimuth pointing coefficients

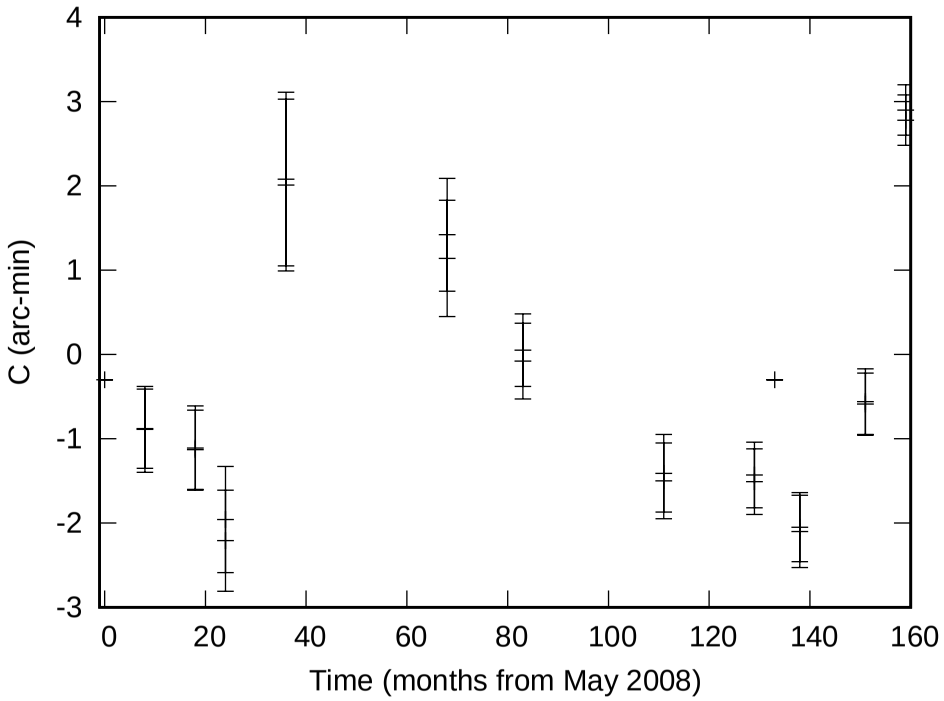

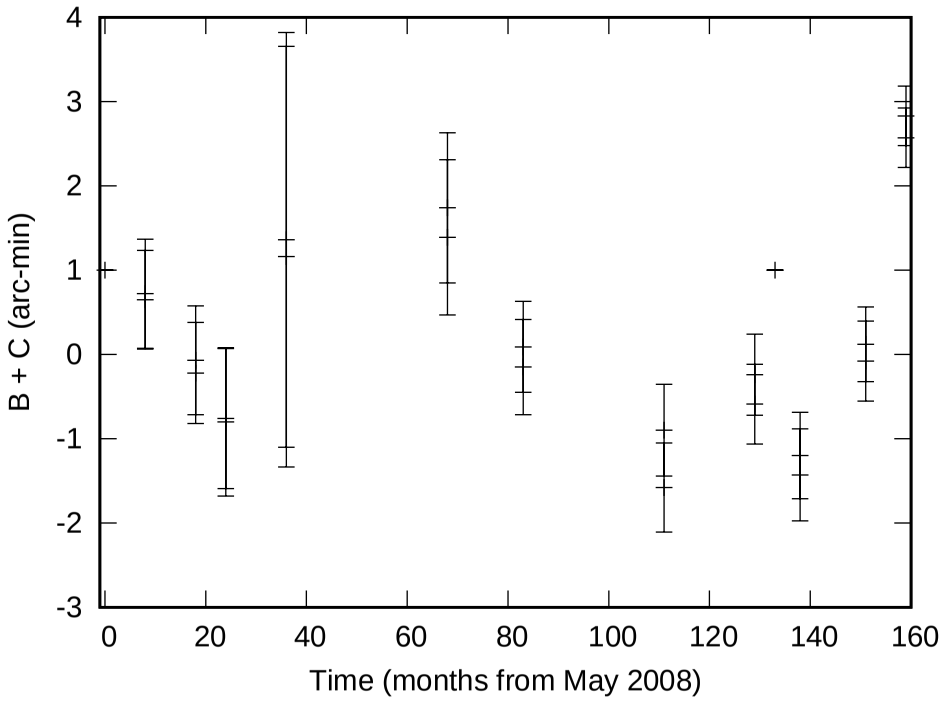

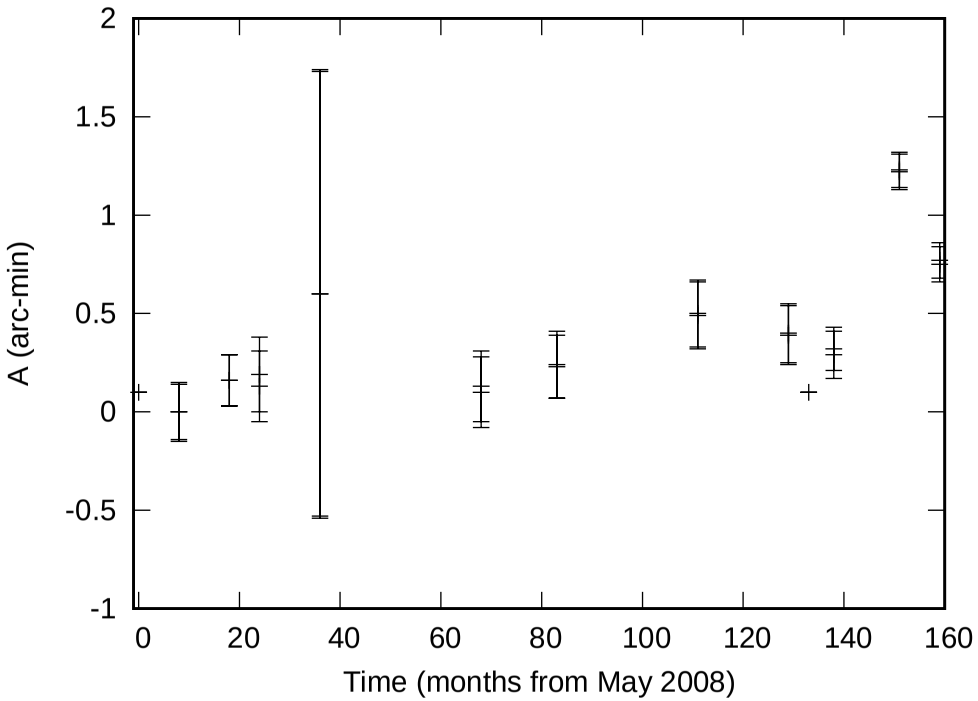

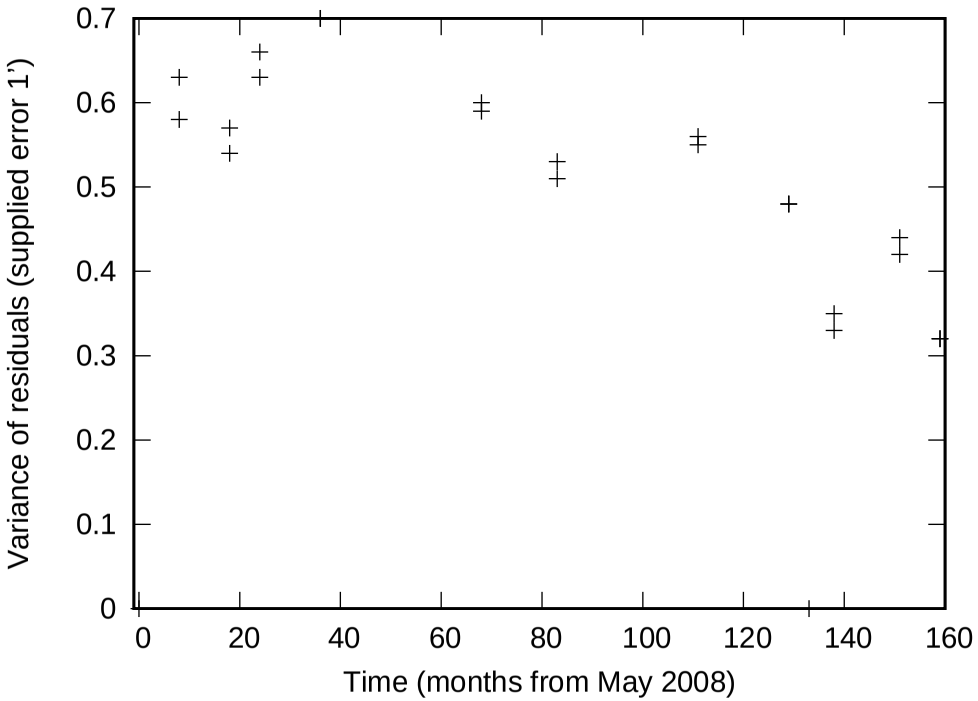

Fig. 1: C11 Azimuth pointing coefficients

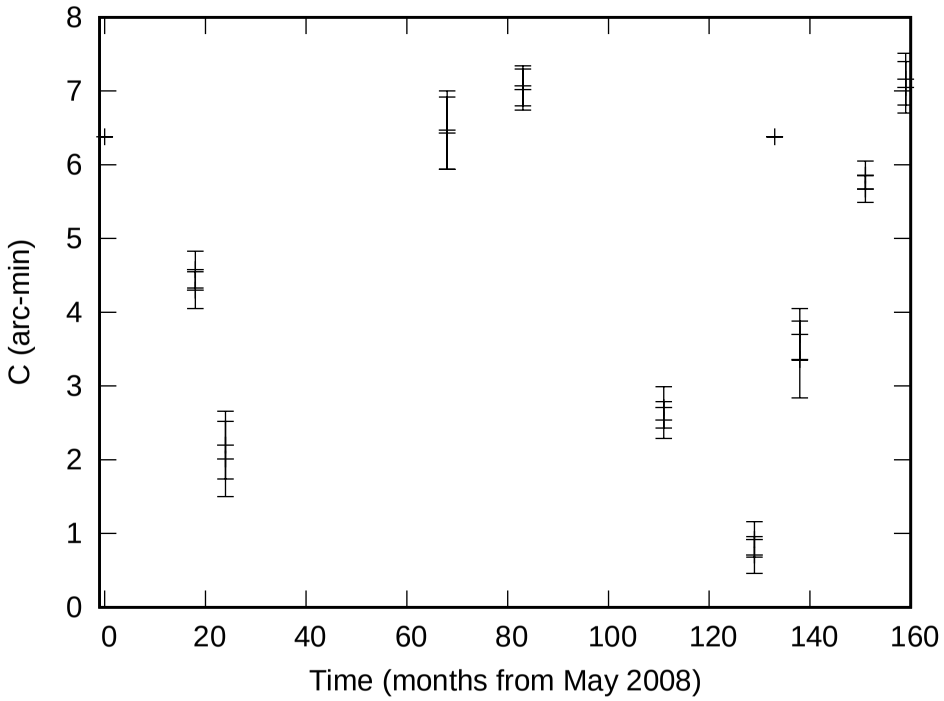

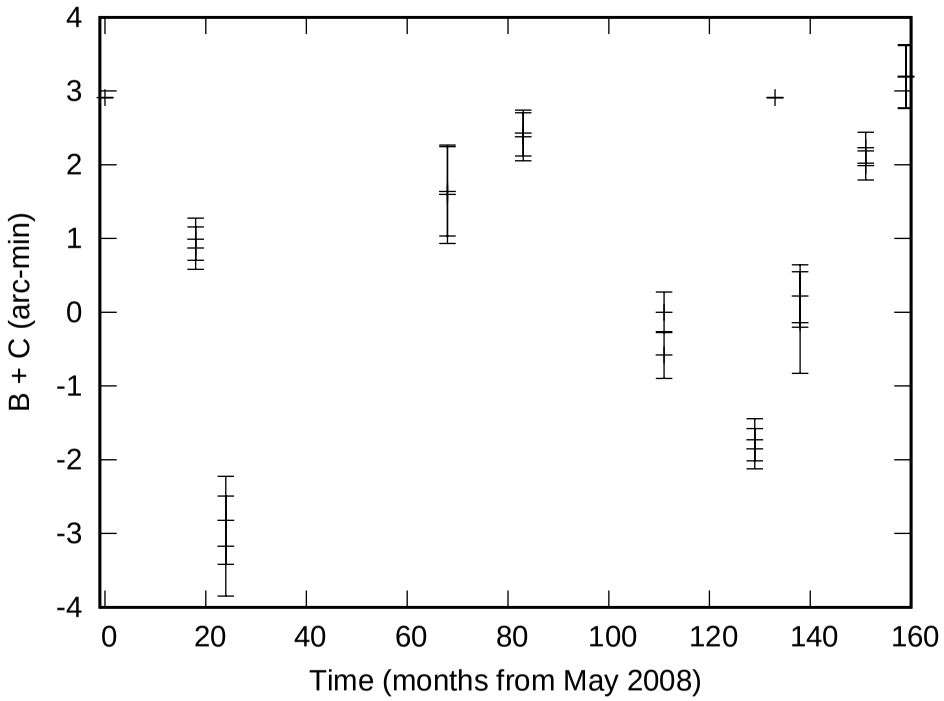

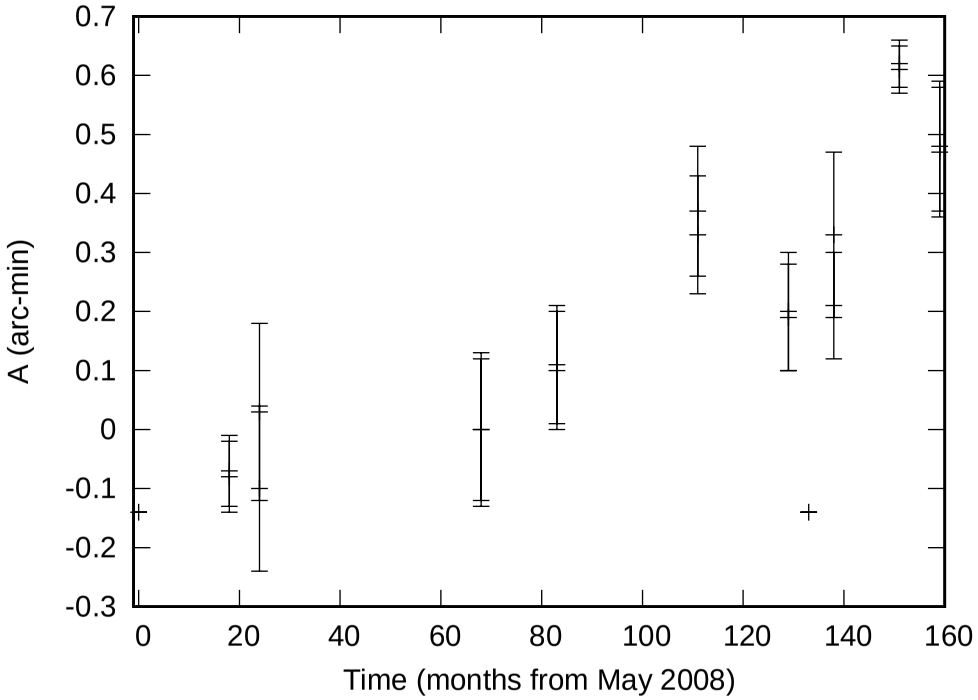

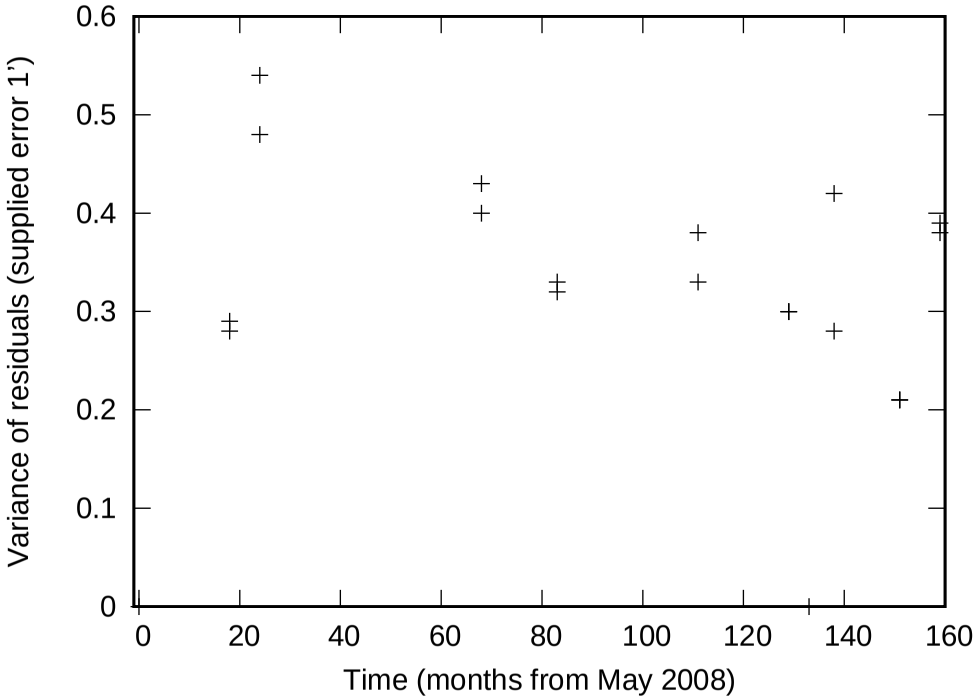

Fig. 1: C12 Azimuth pointing coefficients

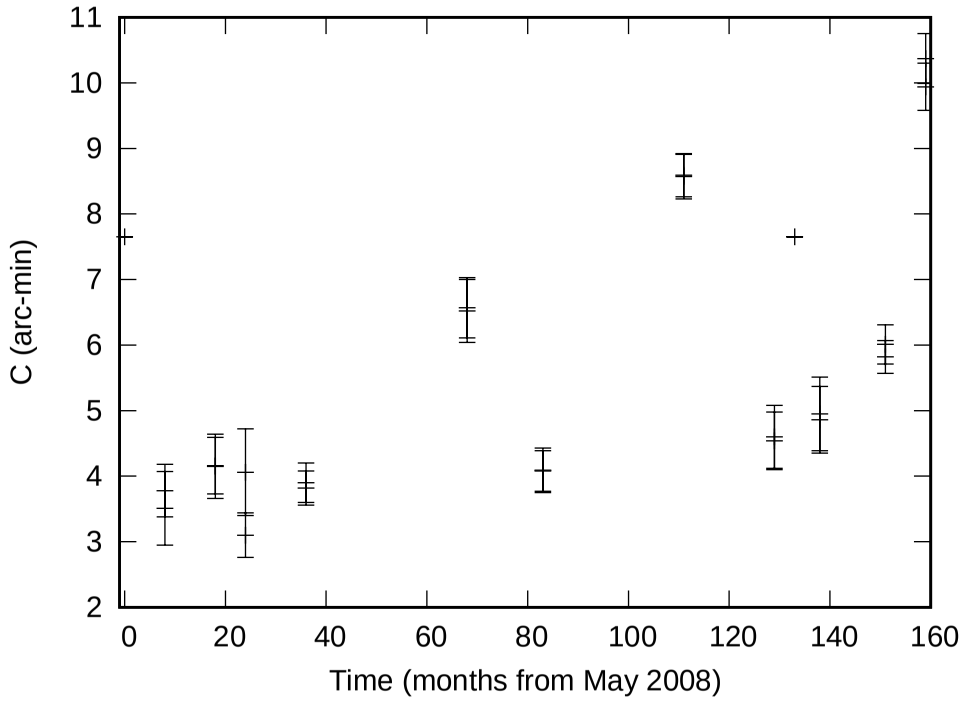

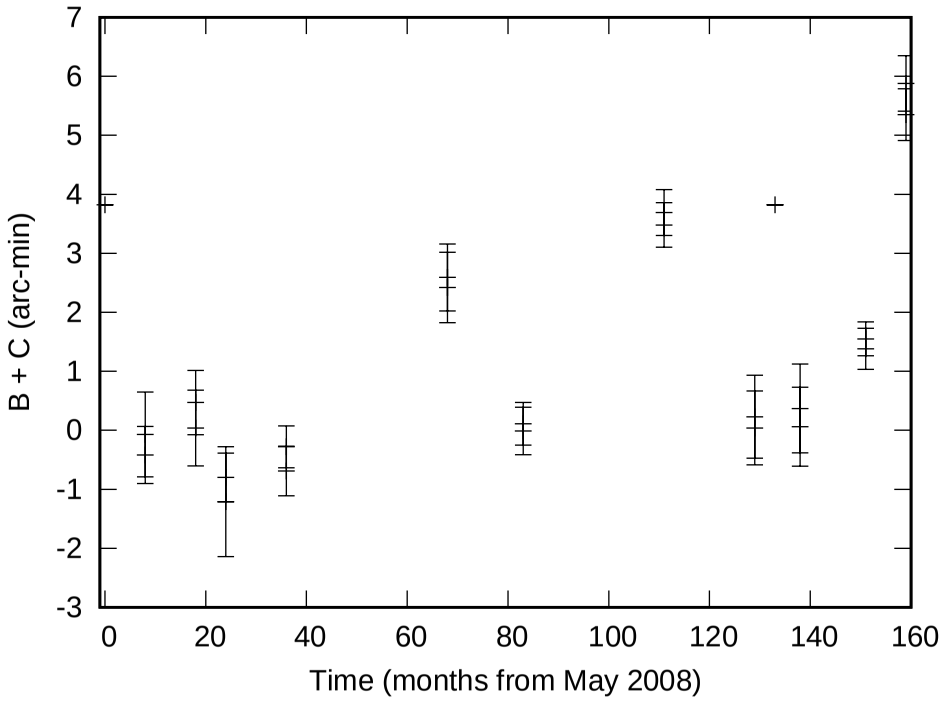

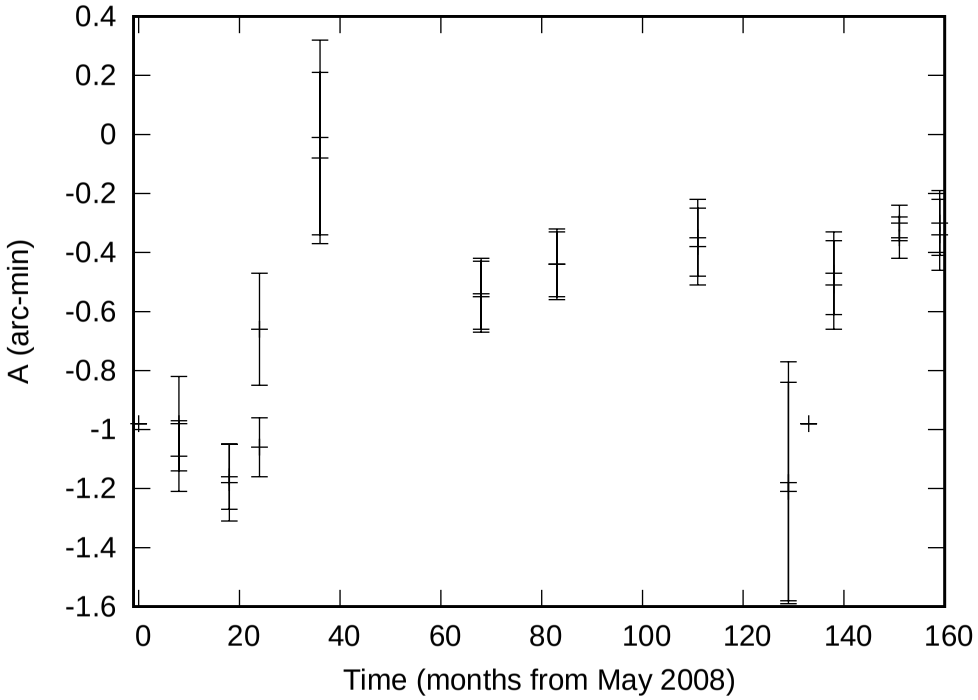

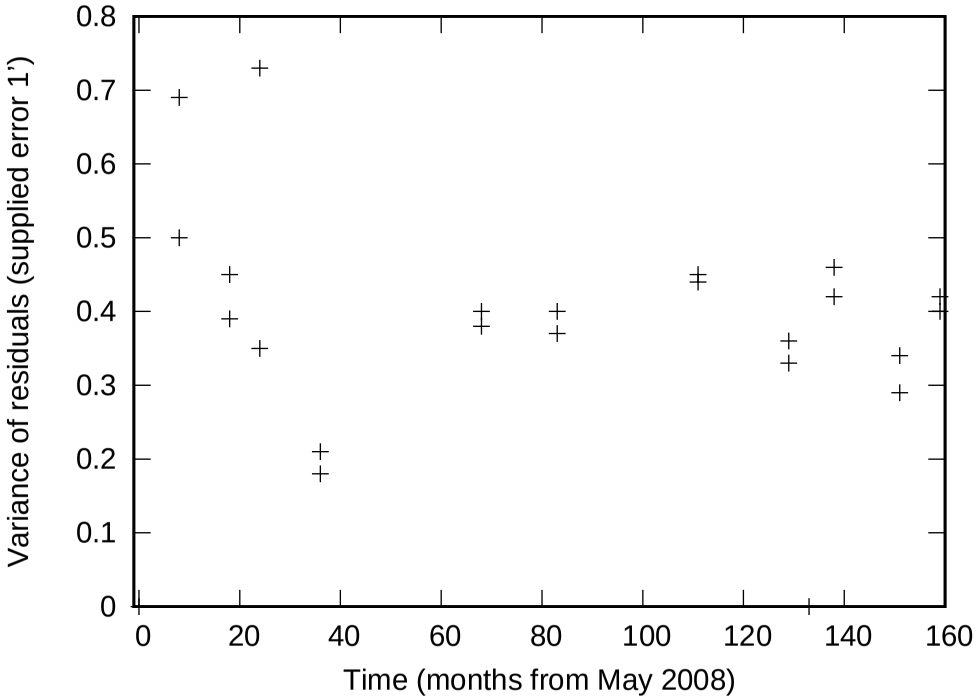

Fig. 1: C13 Azimuth pointing coefficients

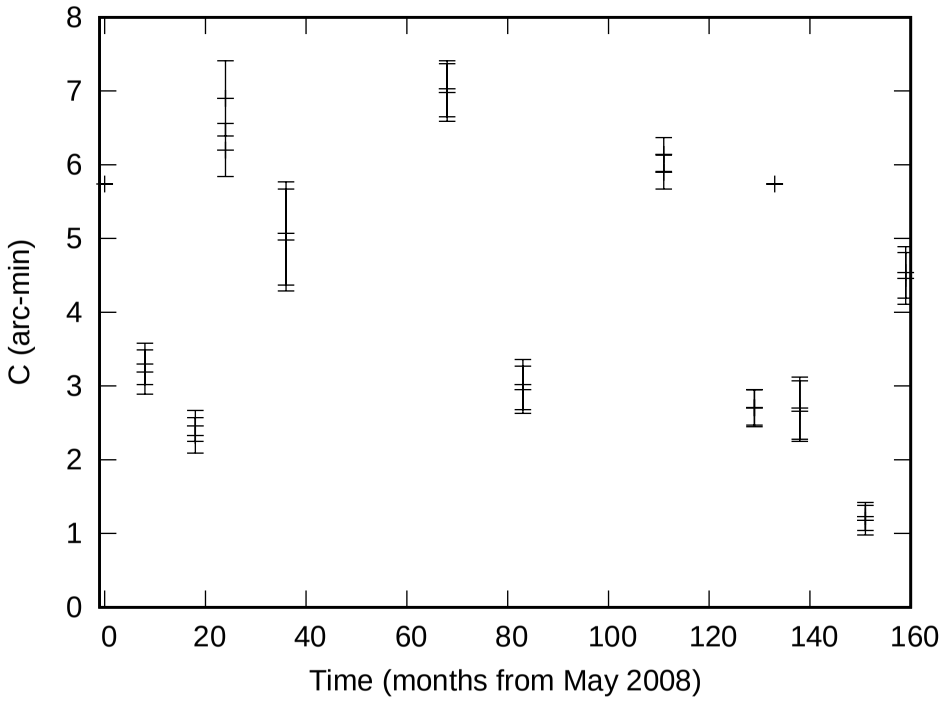

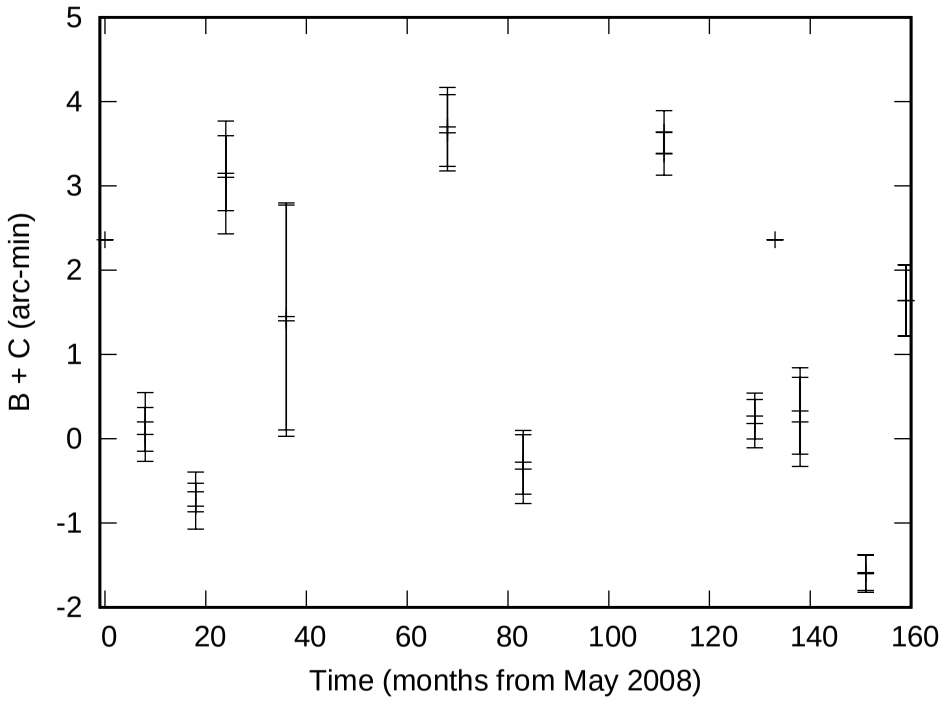

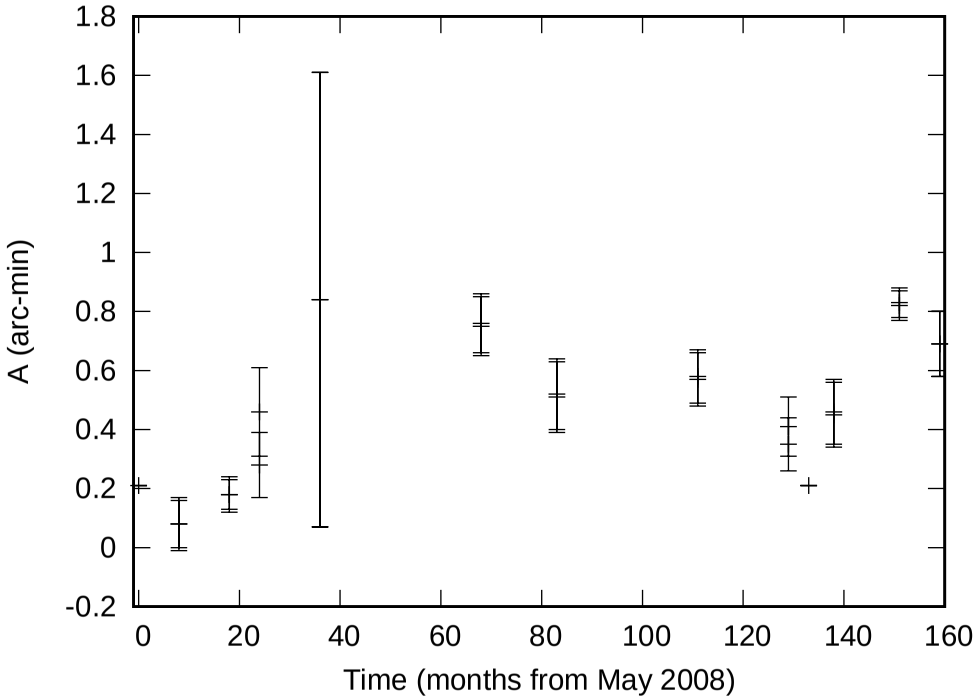

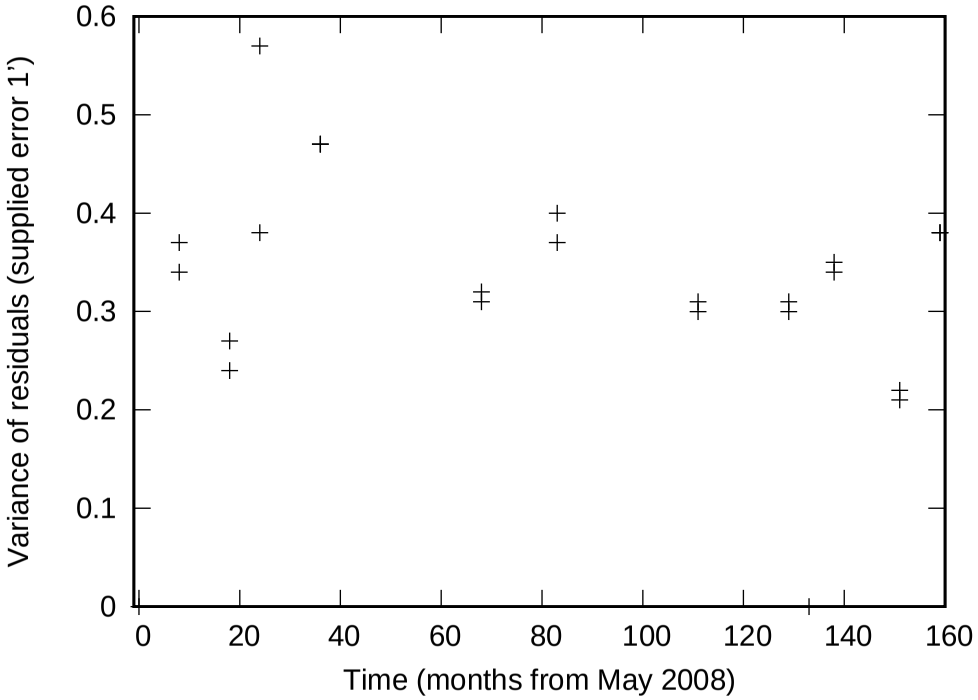

Fig. 1: C14 Azimuth pointing coefficients

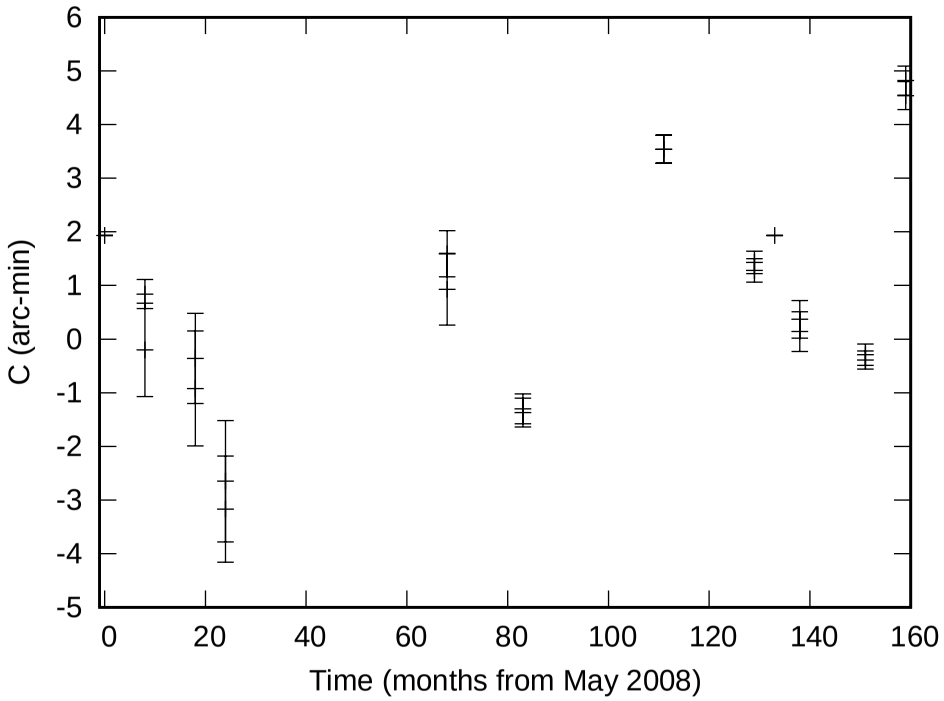

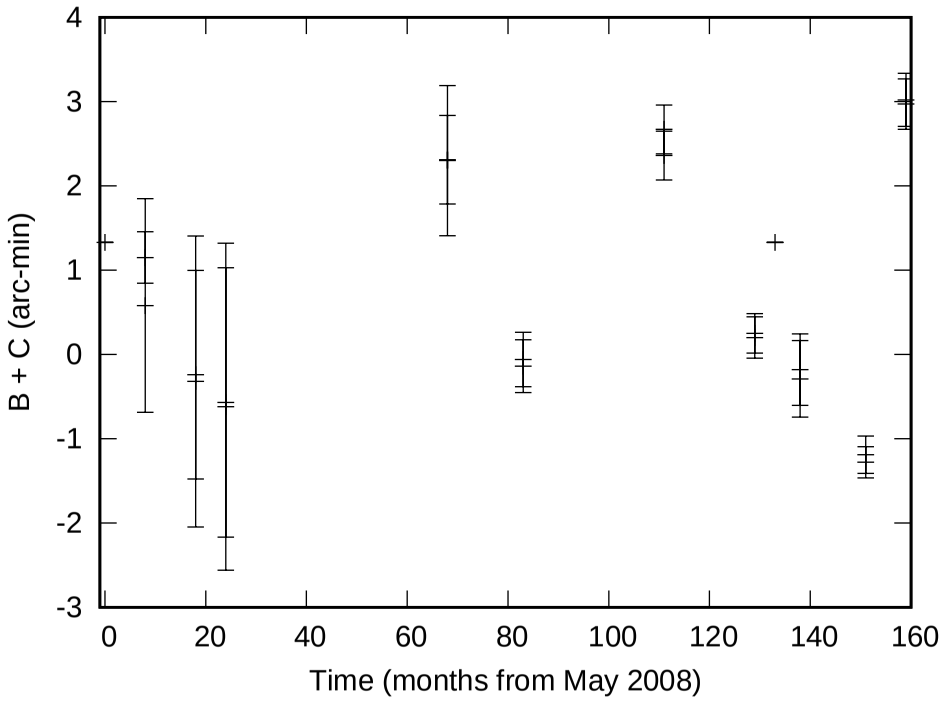

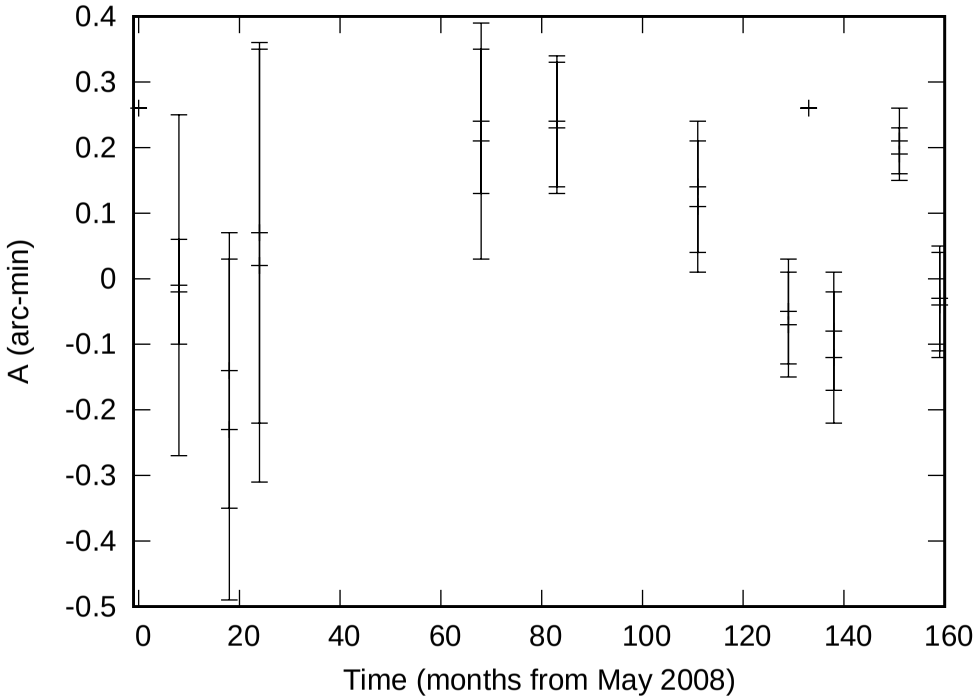

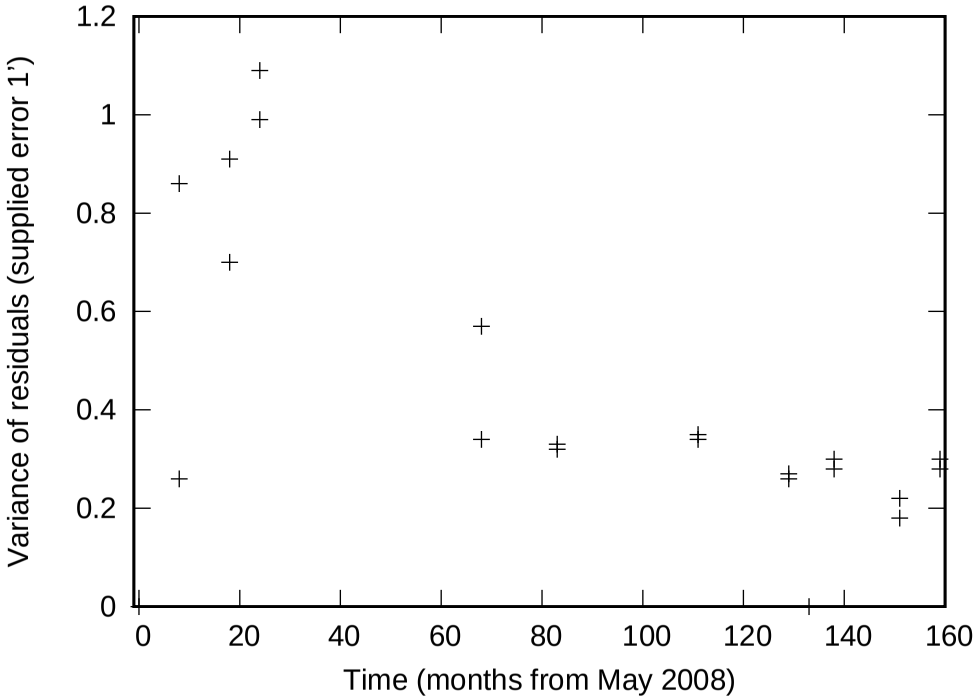

Fig. 1: E02 Azimuth pointing coefficients

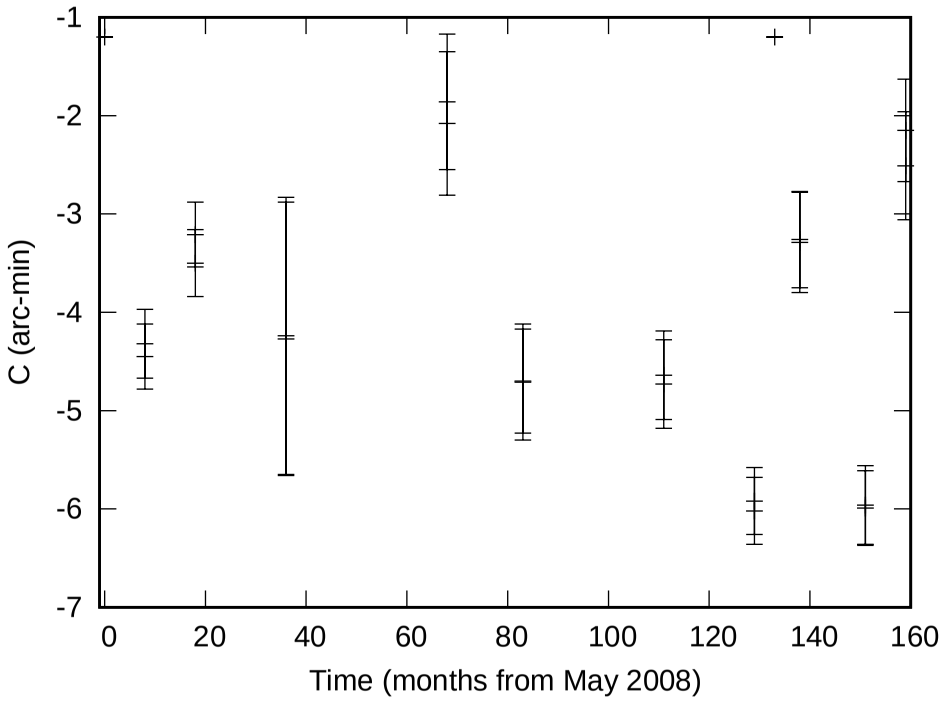

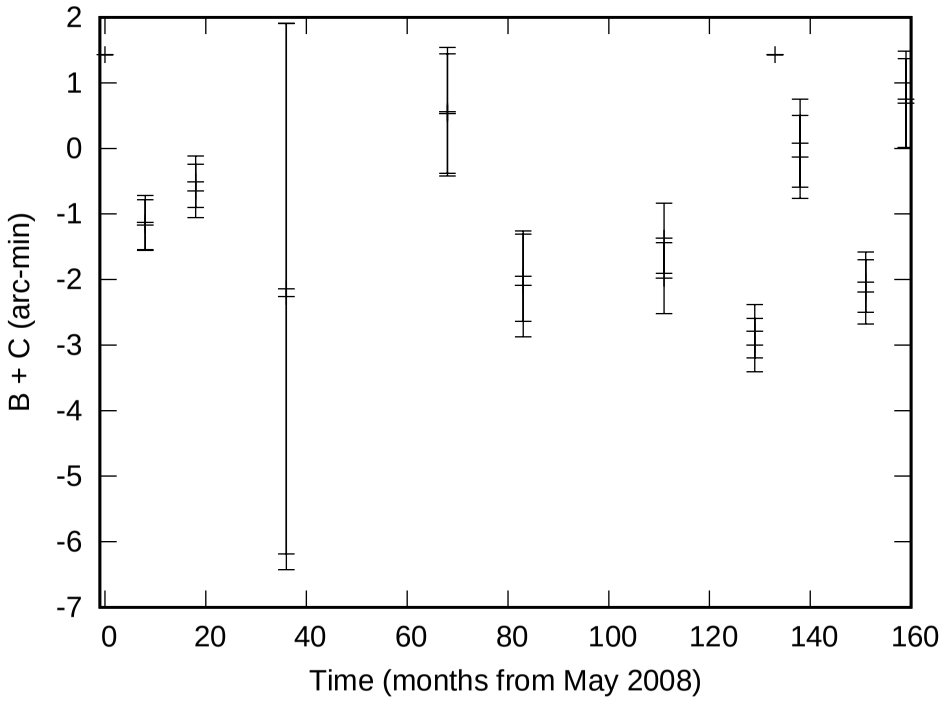

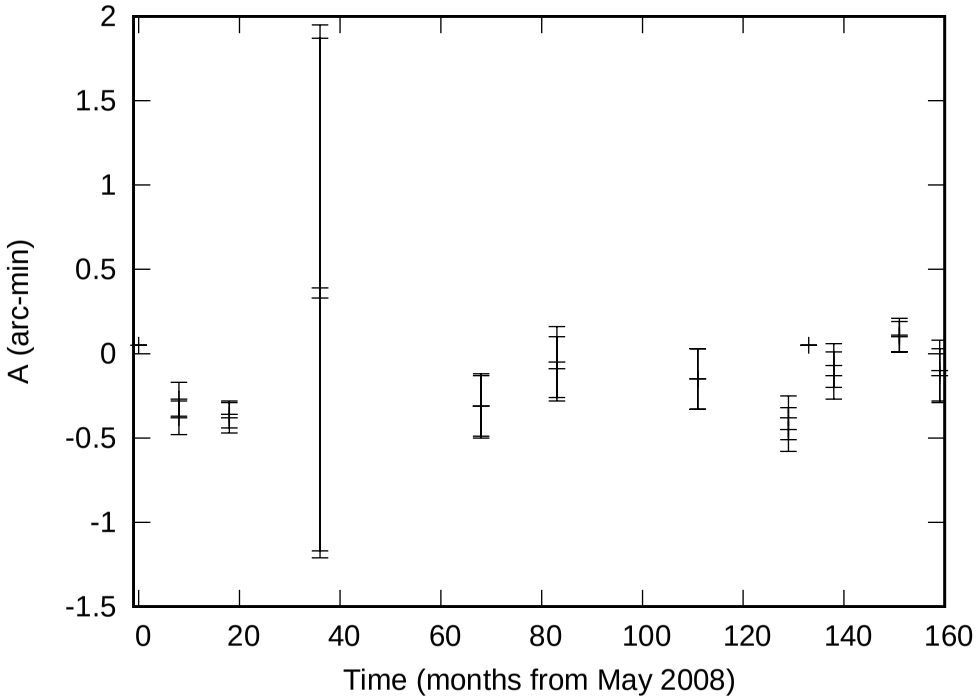

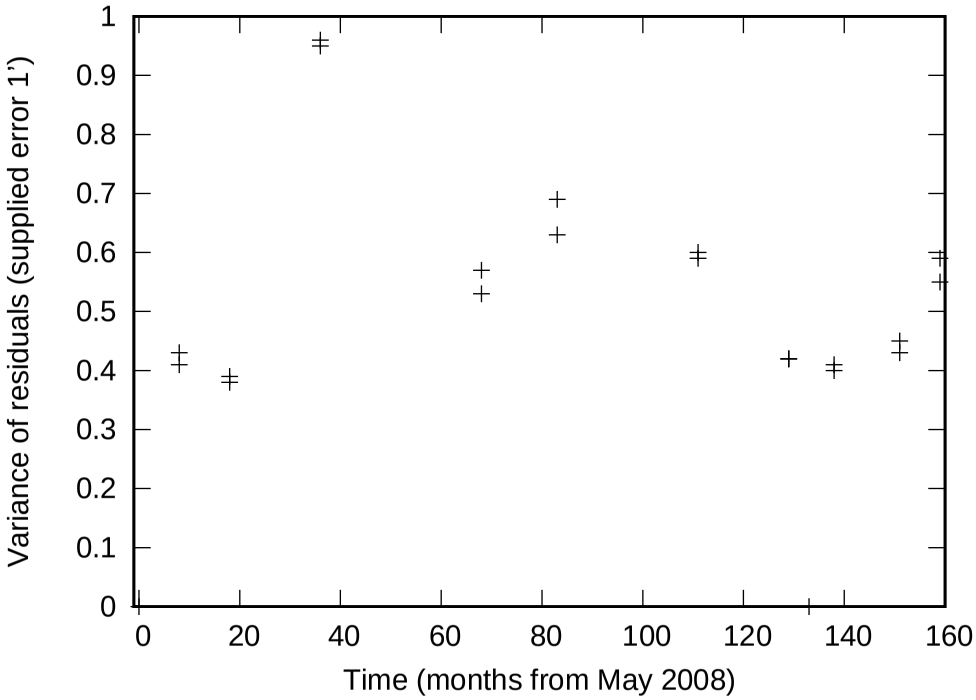

Fig. 1: E03 Azimuth pointing coefficients

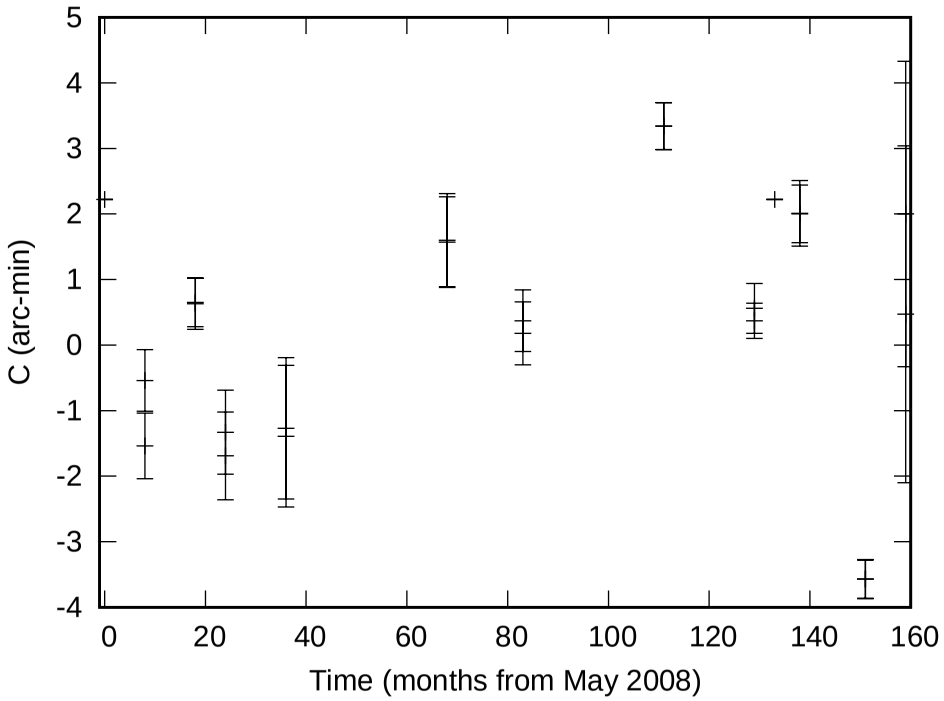

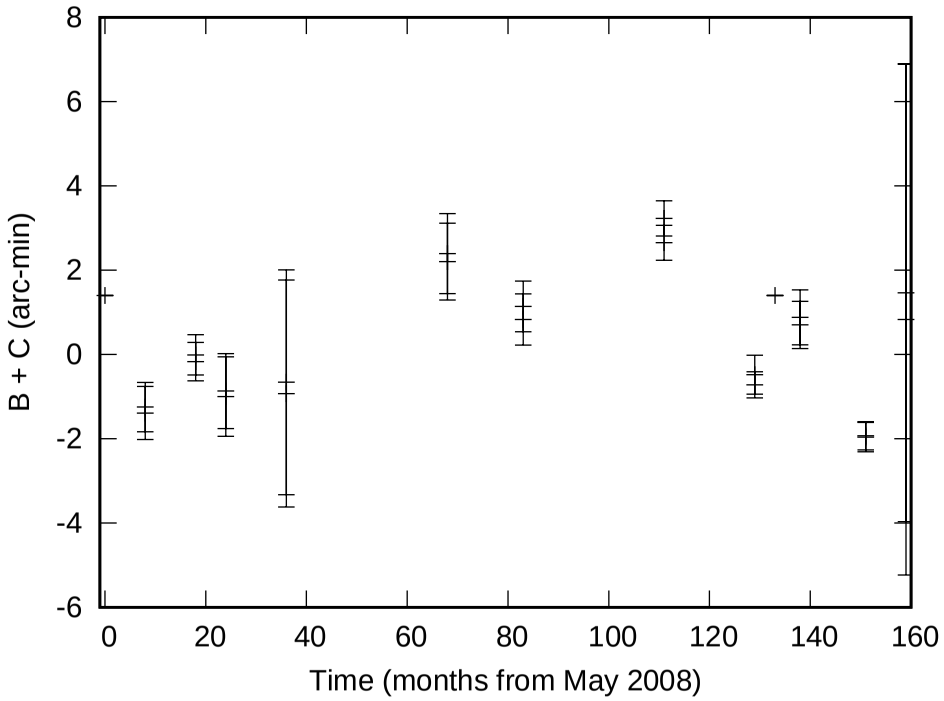

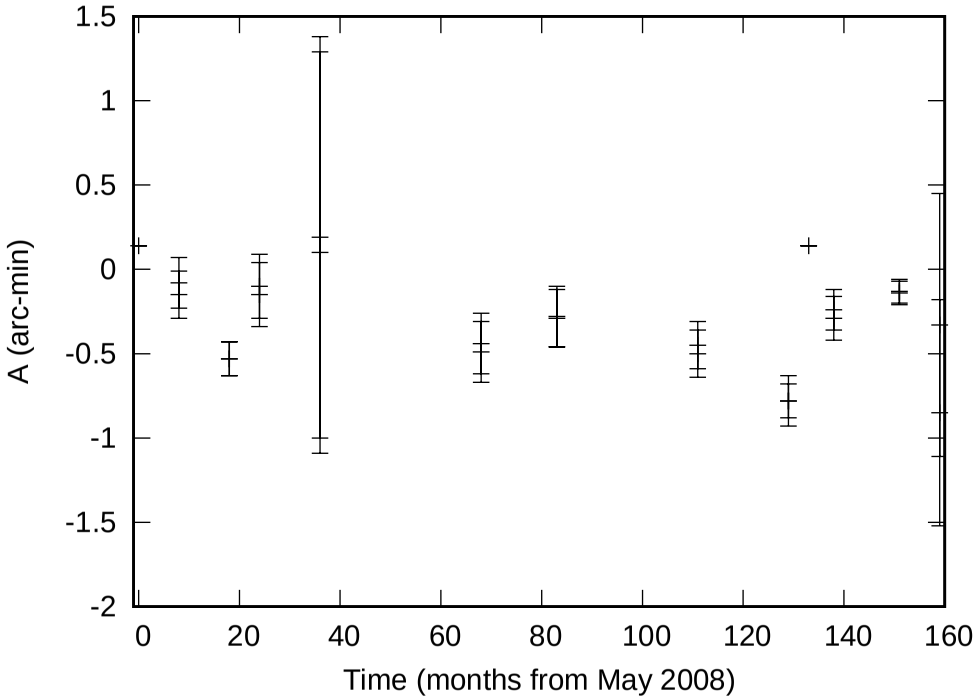

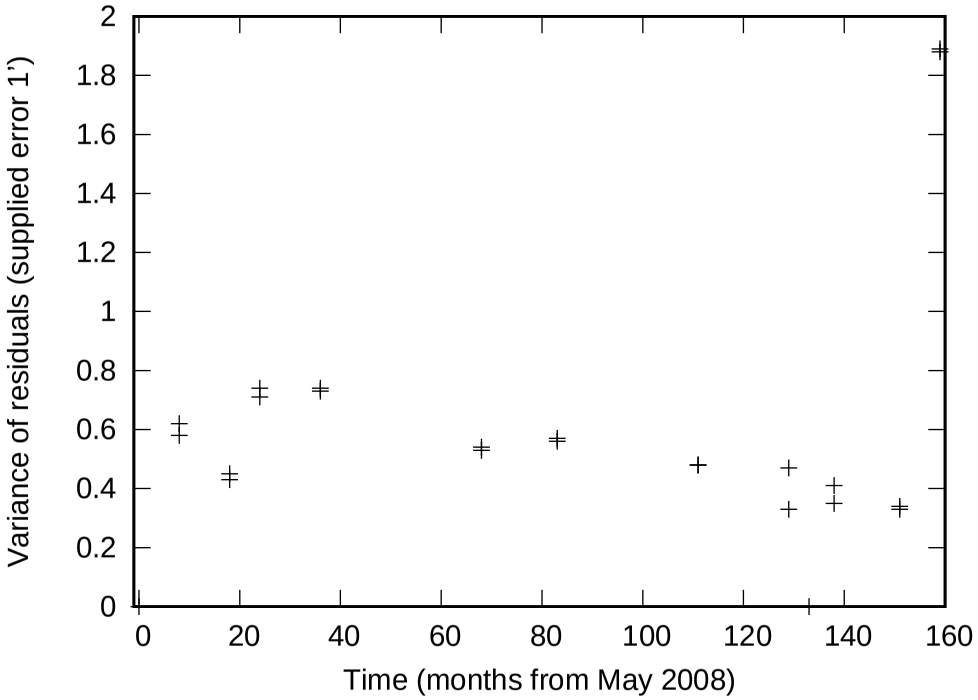

Fig. 1: E04 Azimuth pointing coefficients

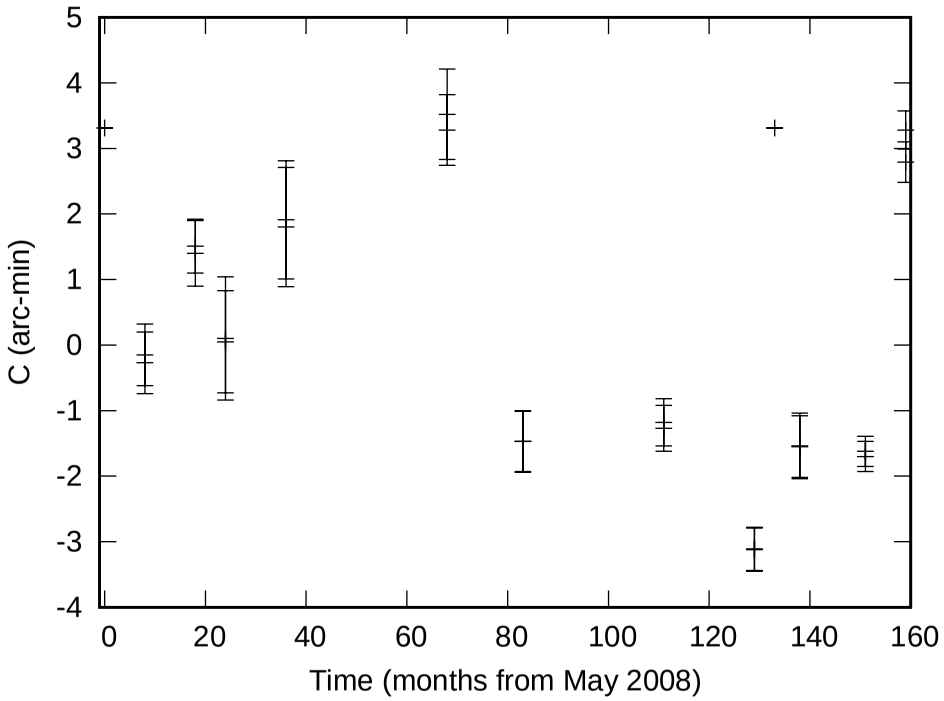

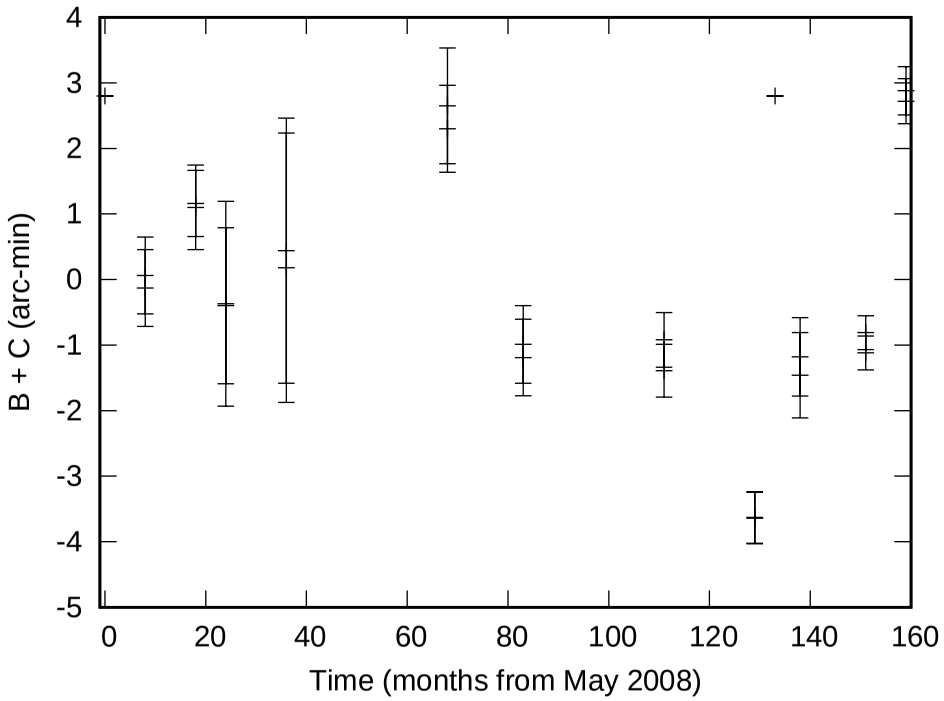

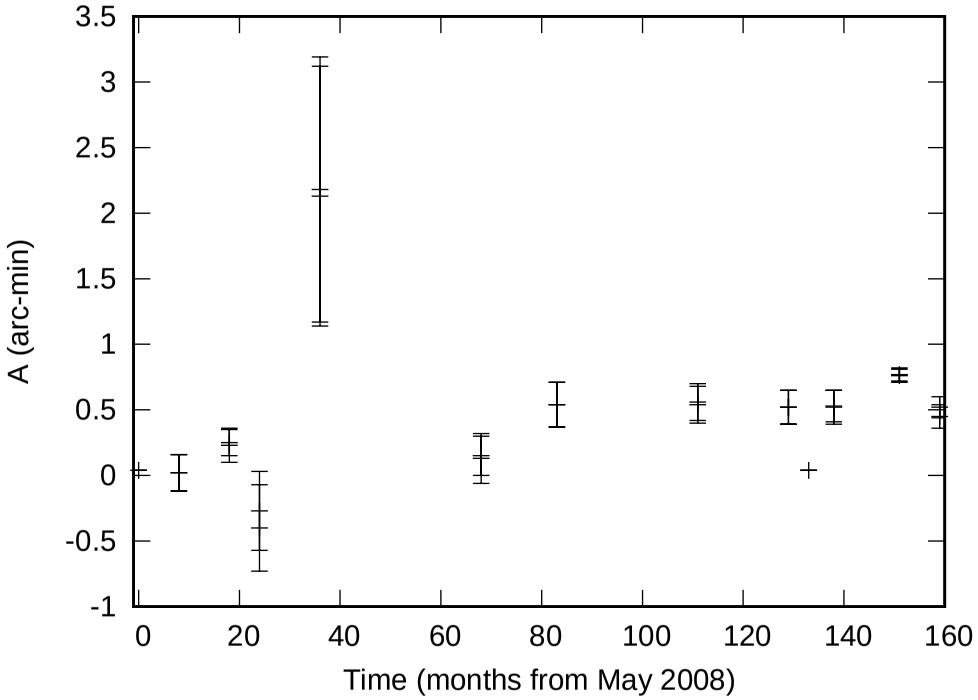

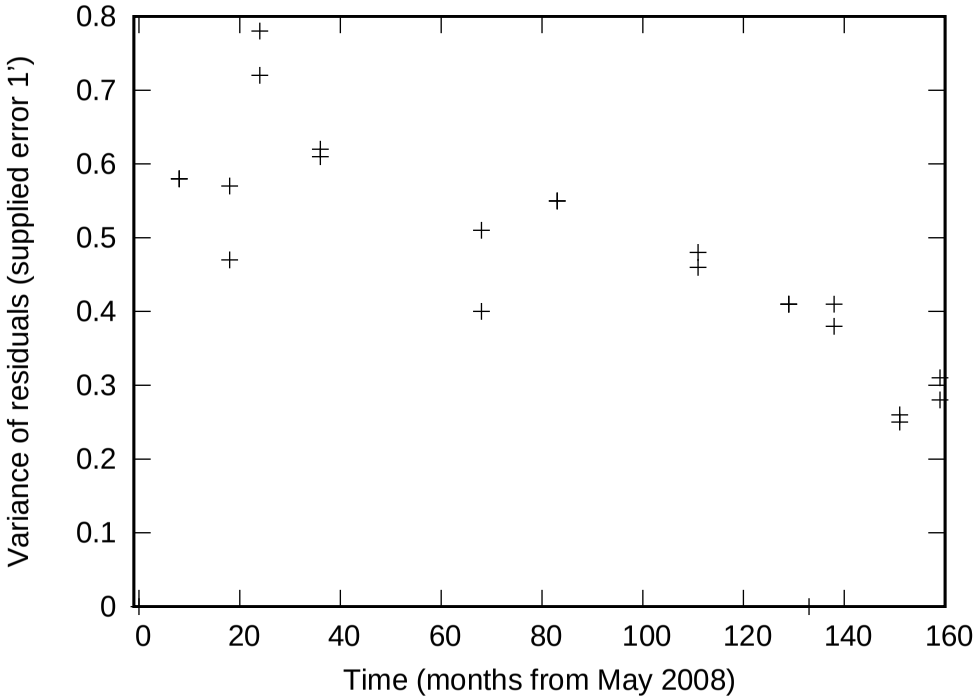

Fig. 1: E05 Azimuth pointing coefficients

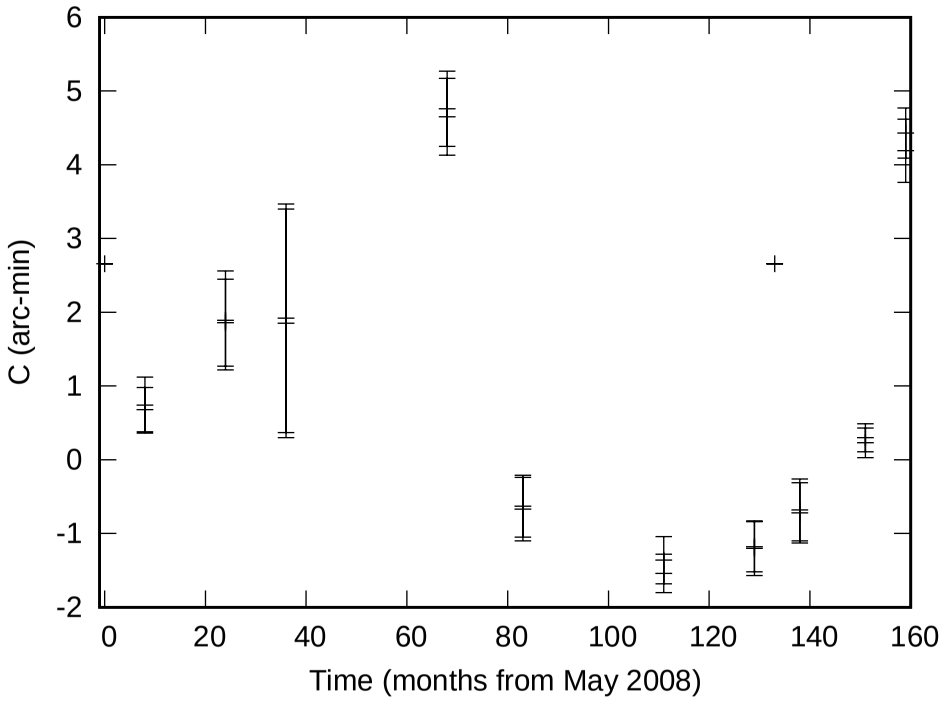

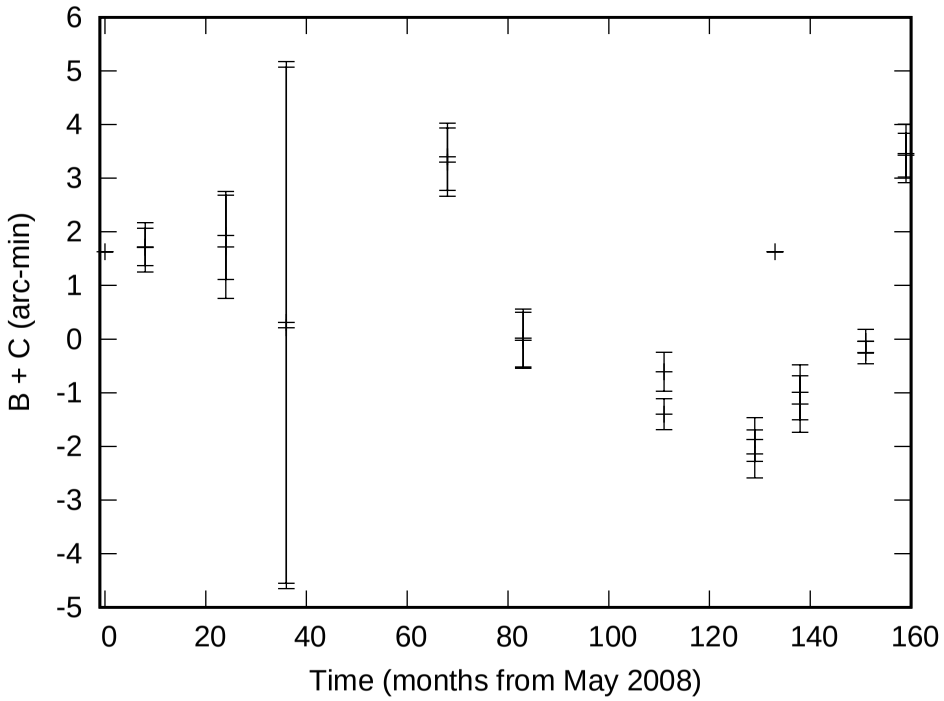

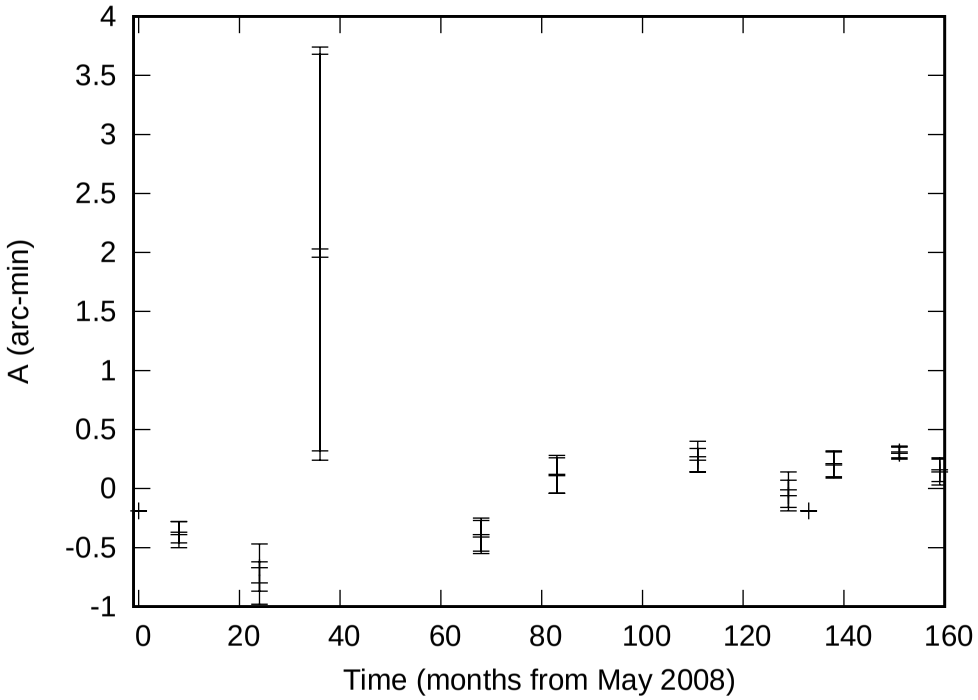

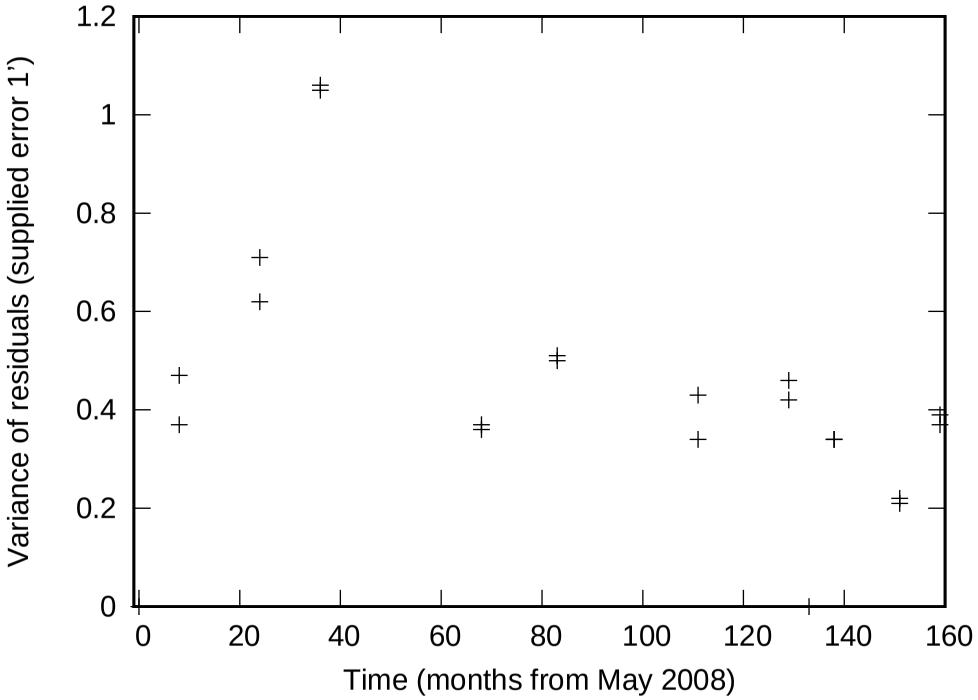

Fig. 1: E06 Azimuth pointing coefficients

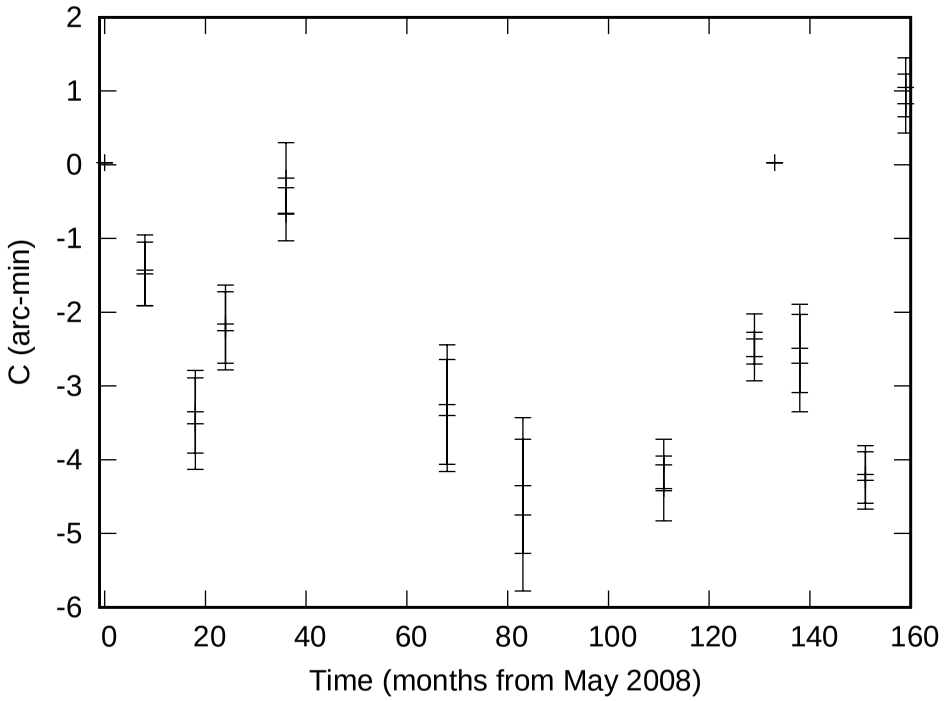

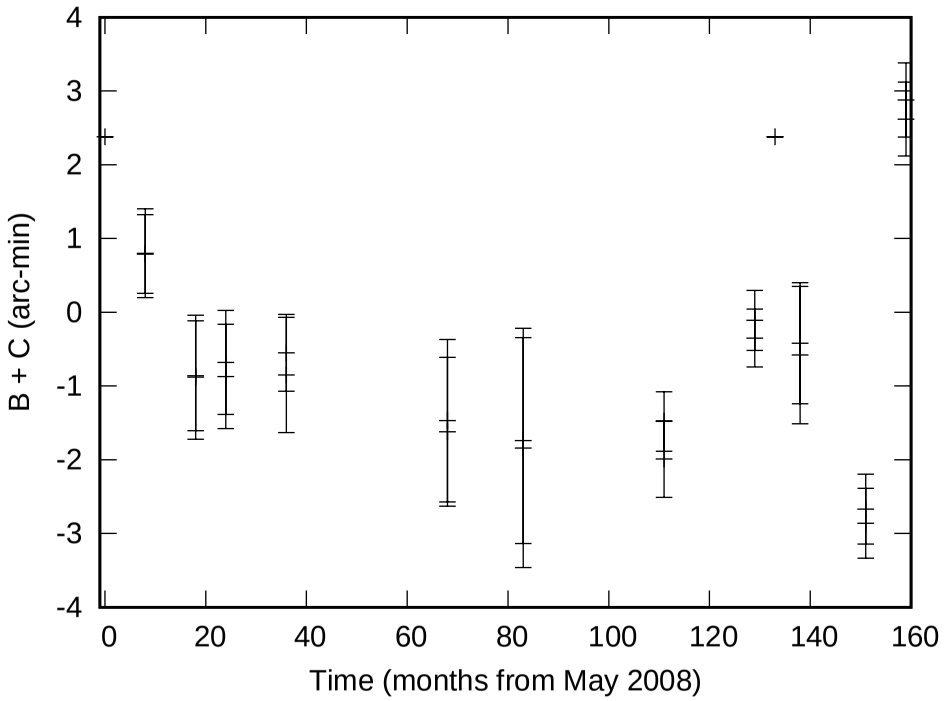

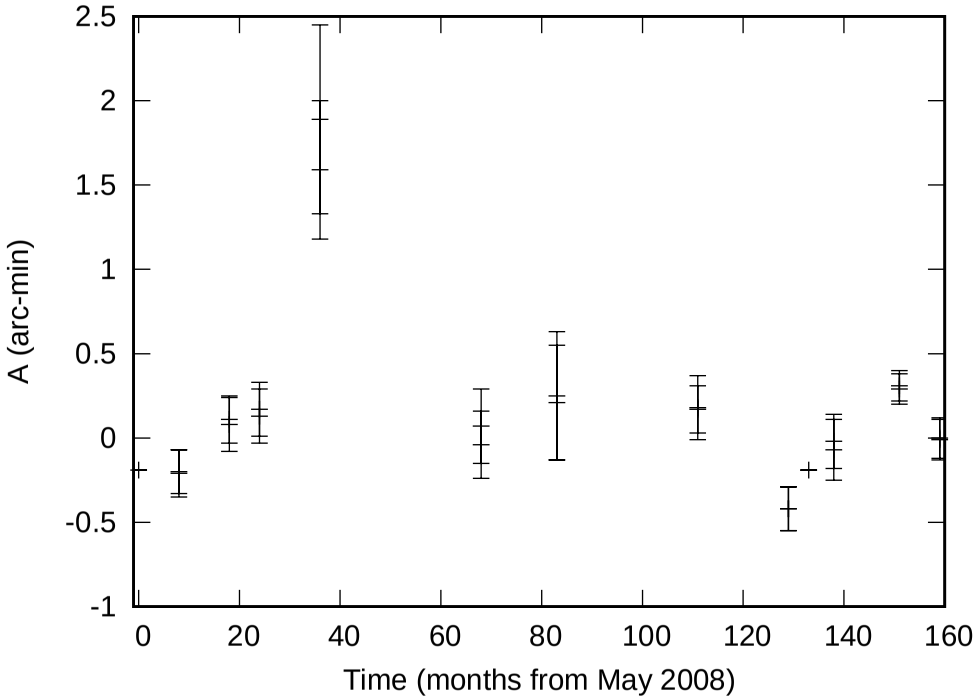

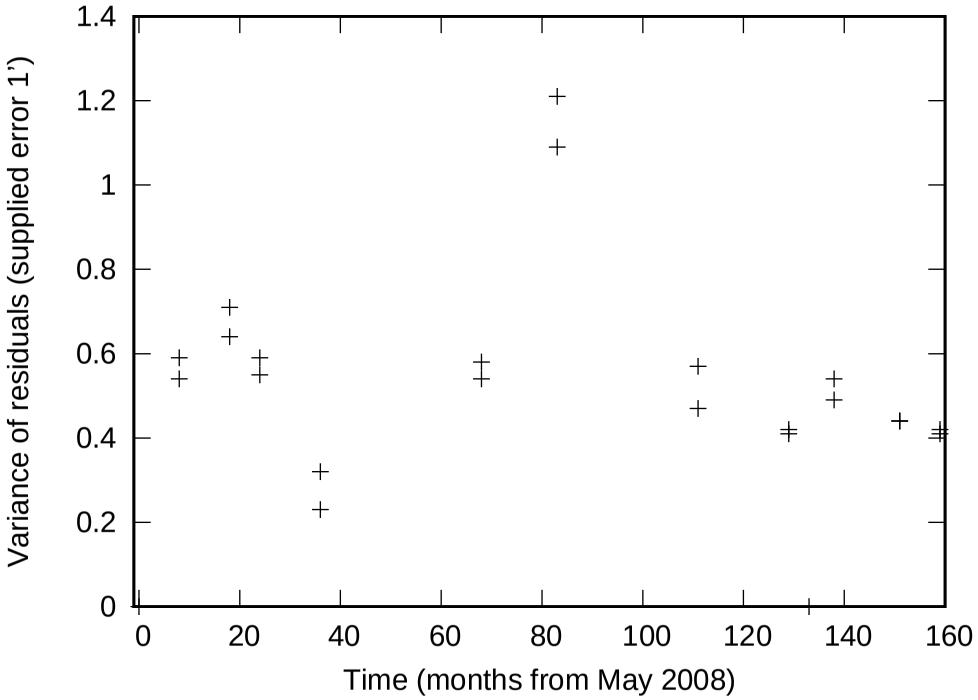

Fig. 1: S01 Azimuth pointing coefficients

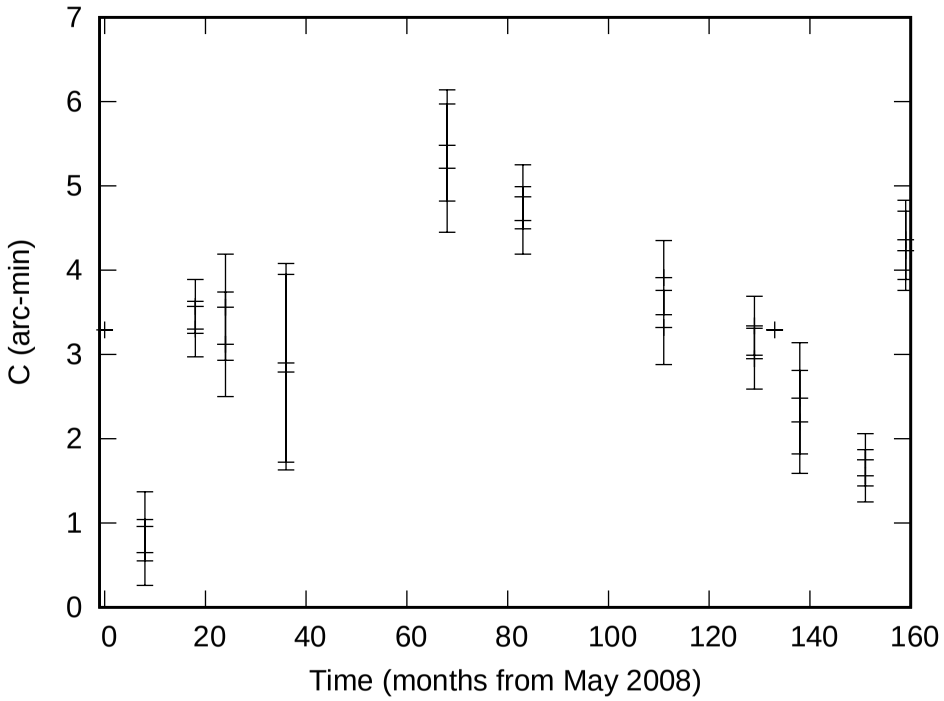

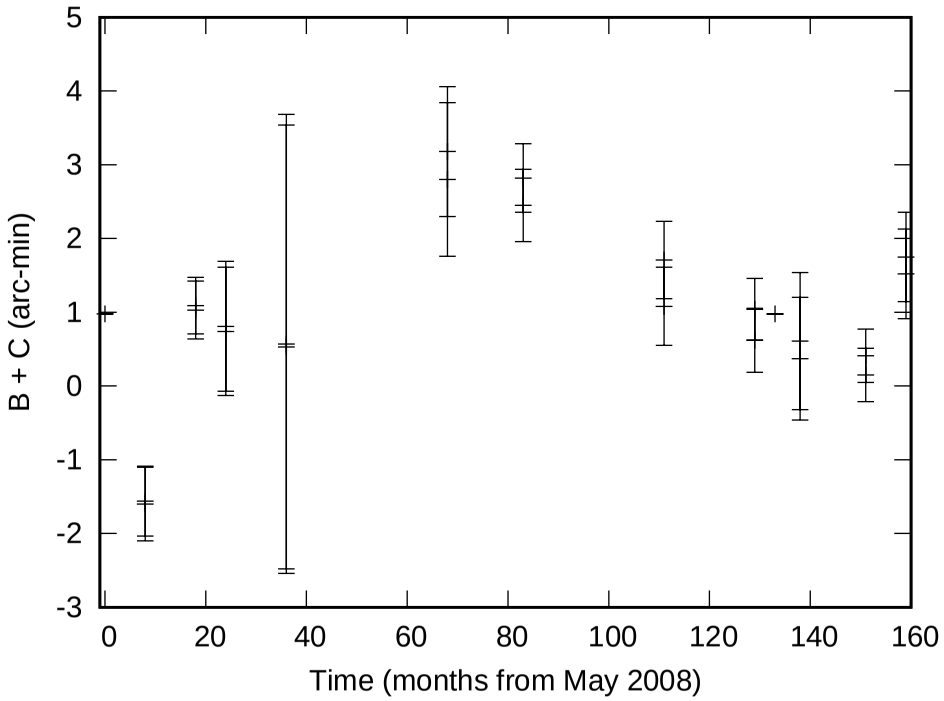

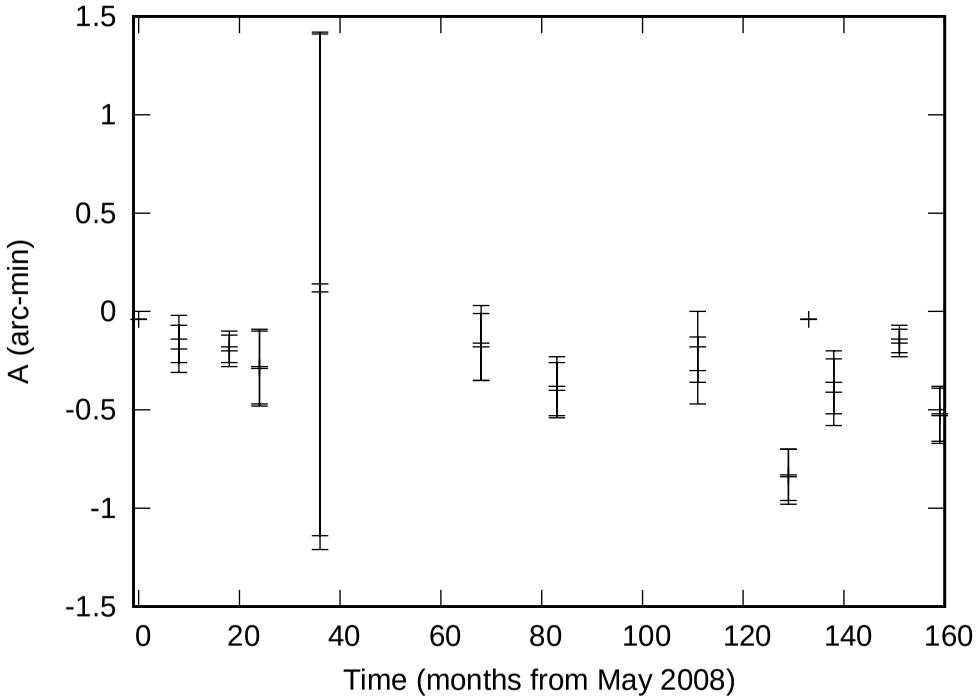

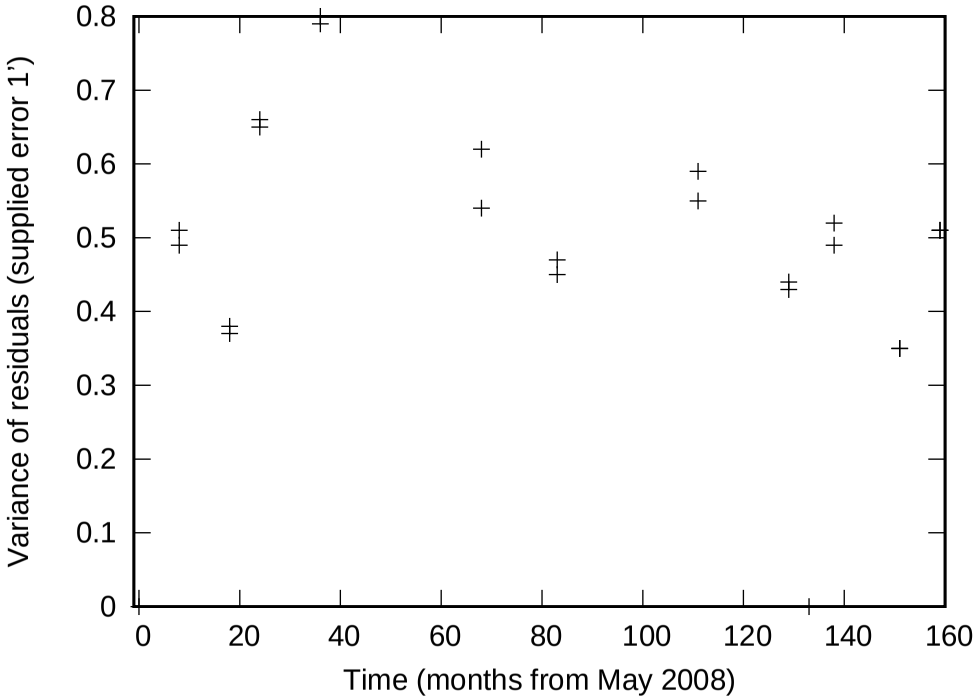

Fig. 1: S02 Azimuth pointing coefficients

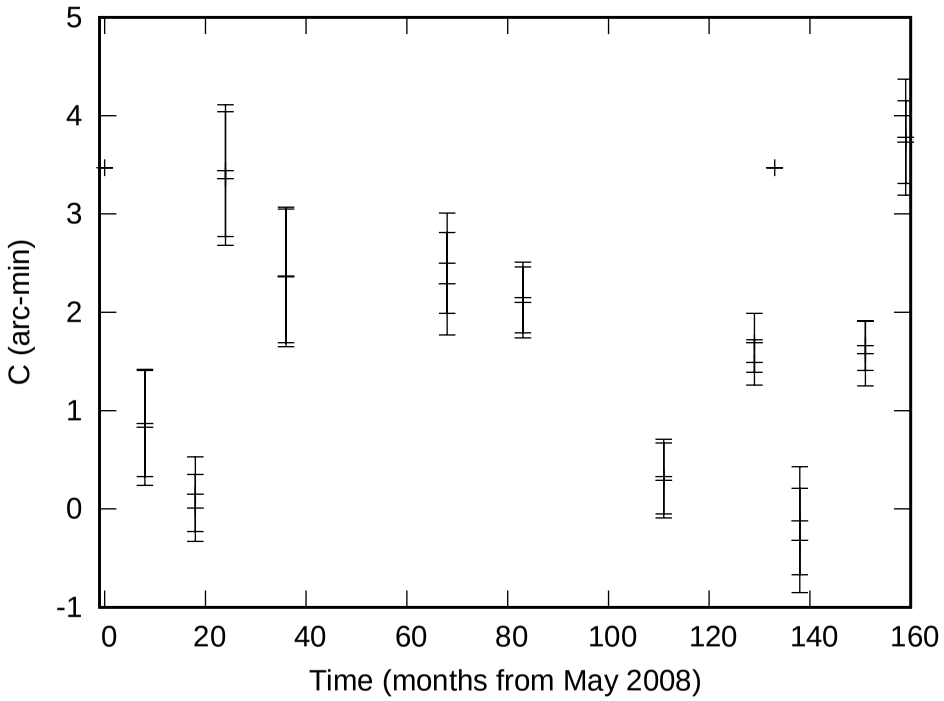

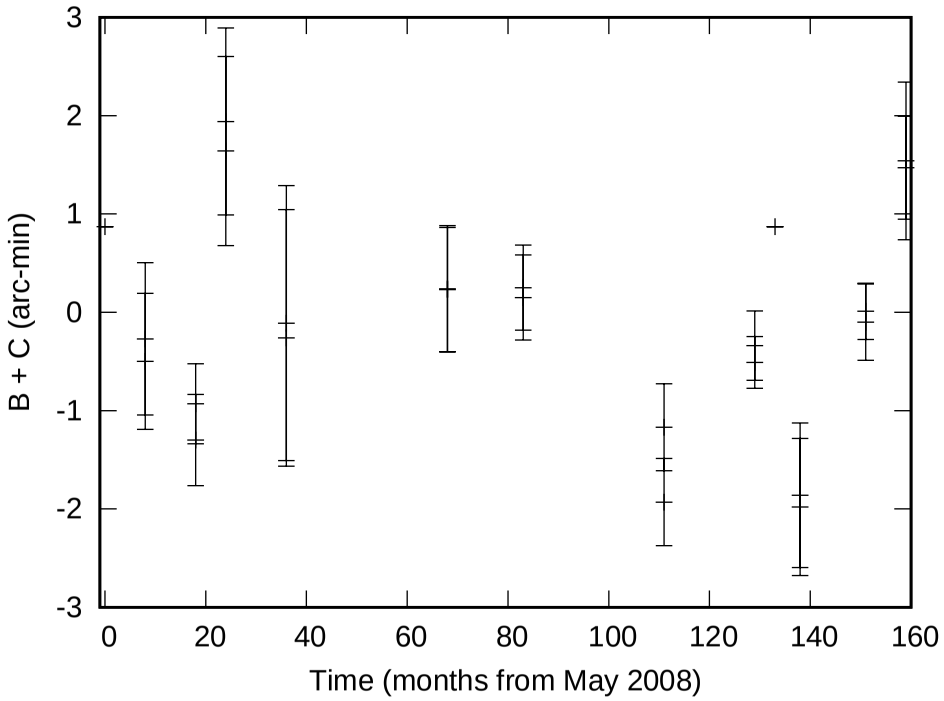

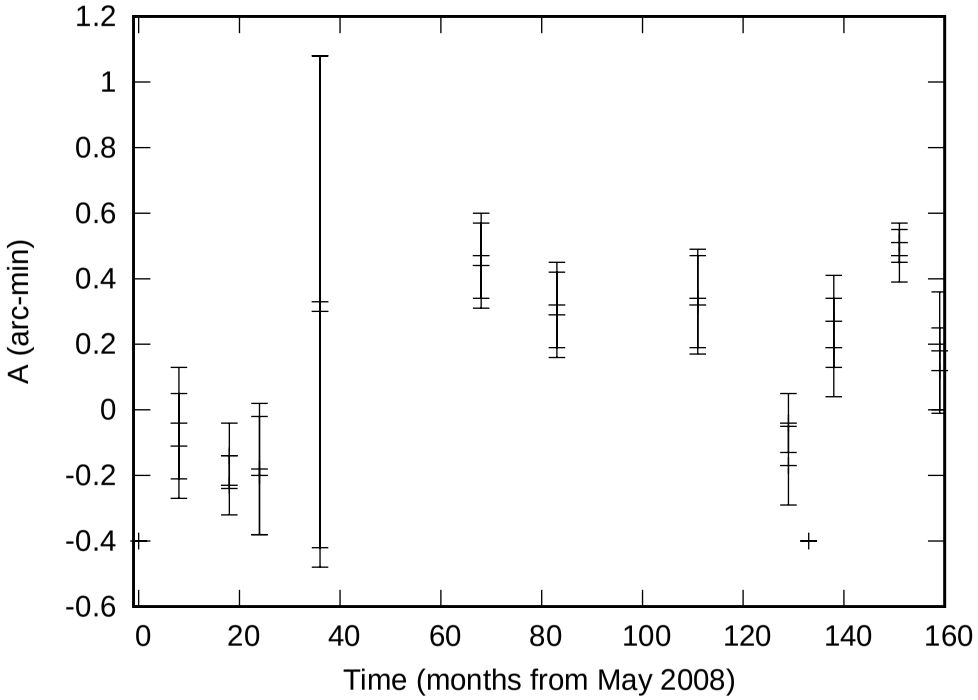

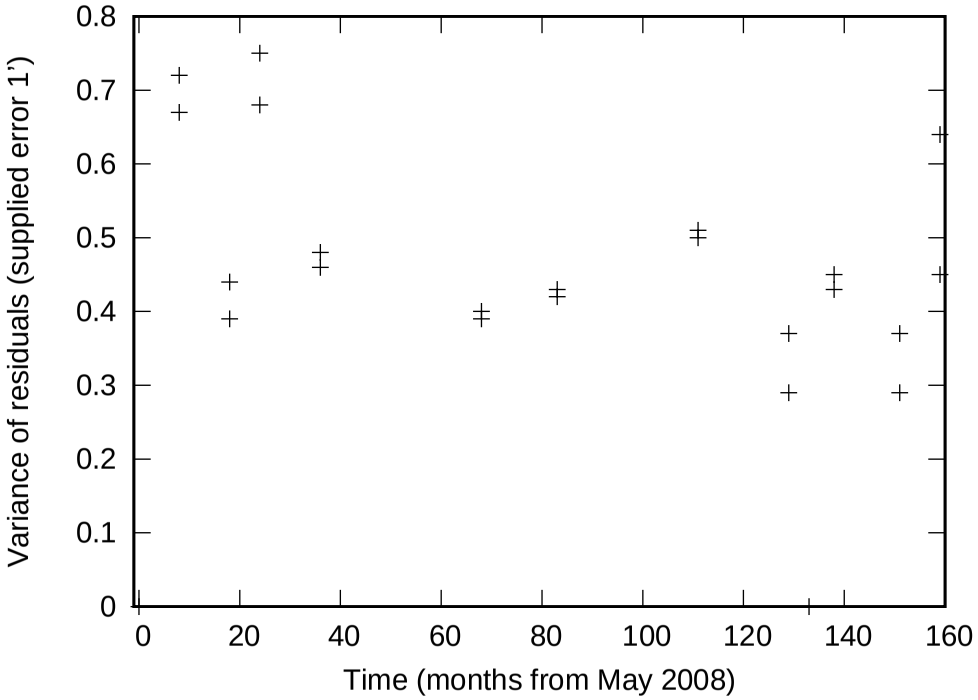

Fig. 1: S03 Azimuth pointing coefficients

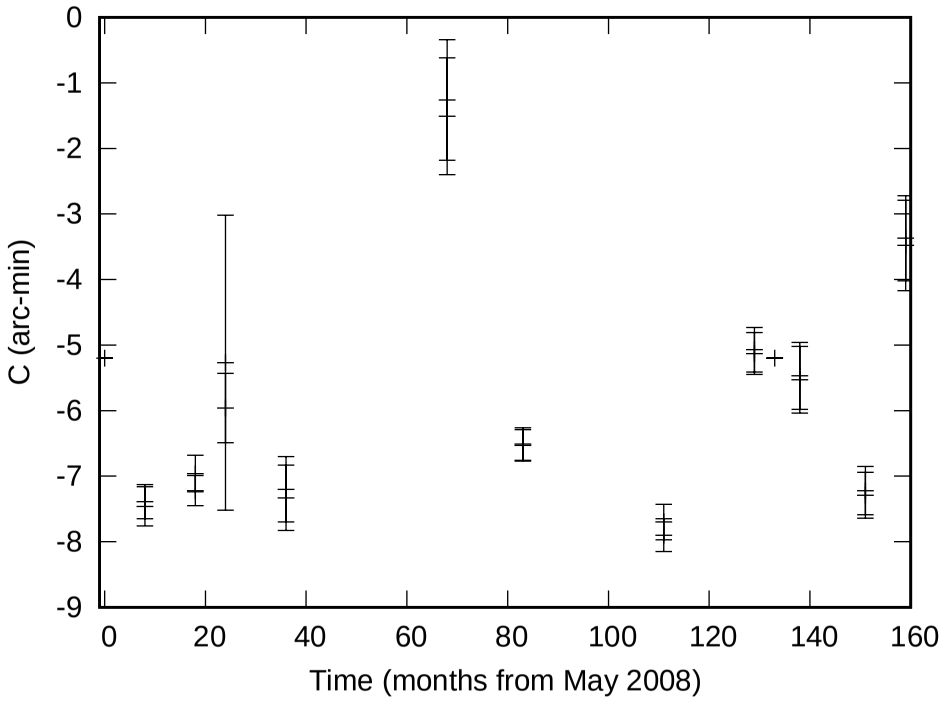

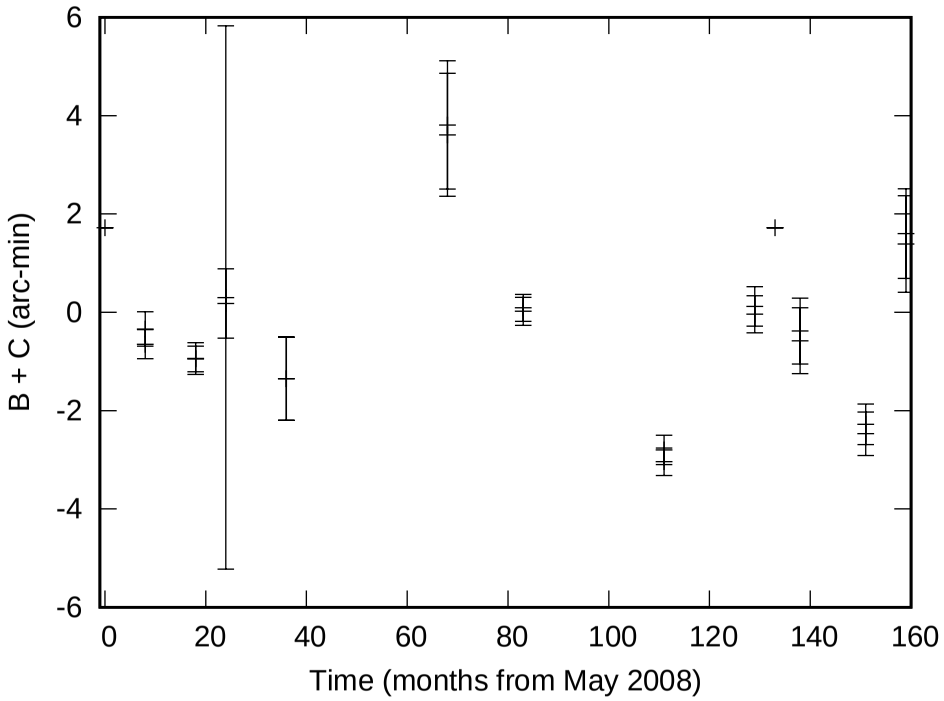

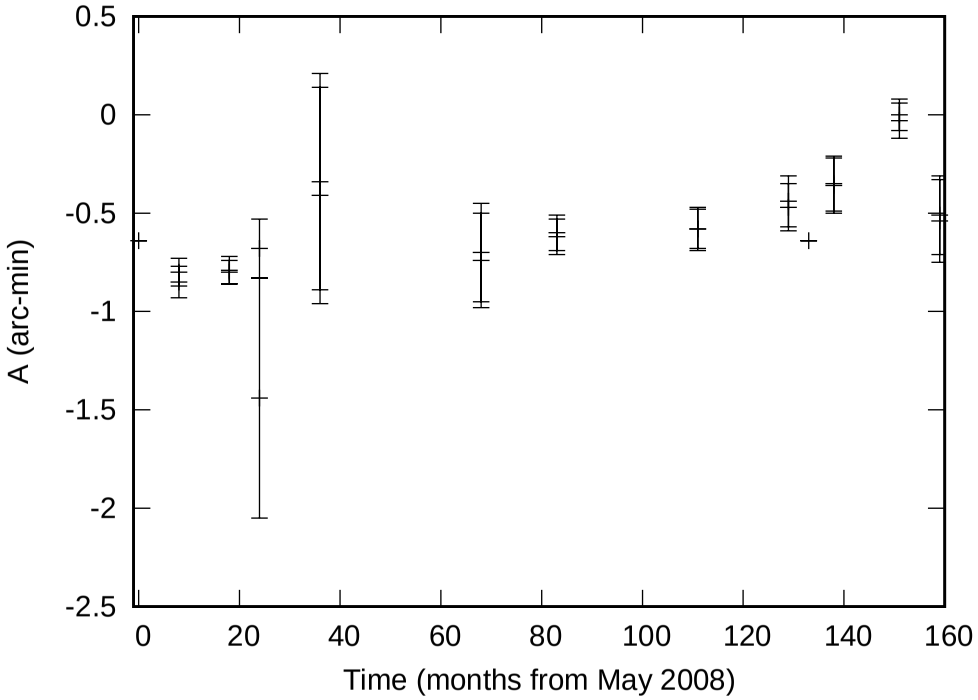

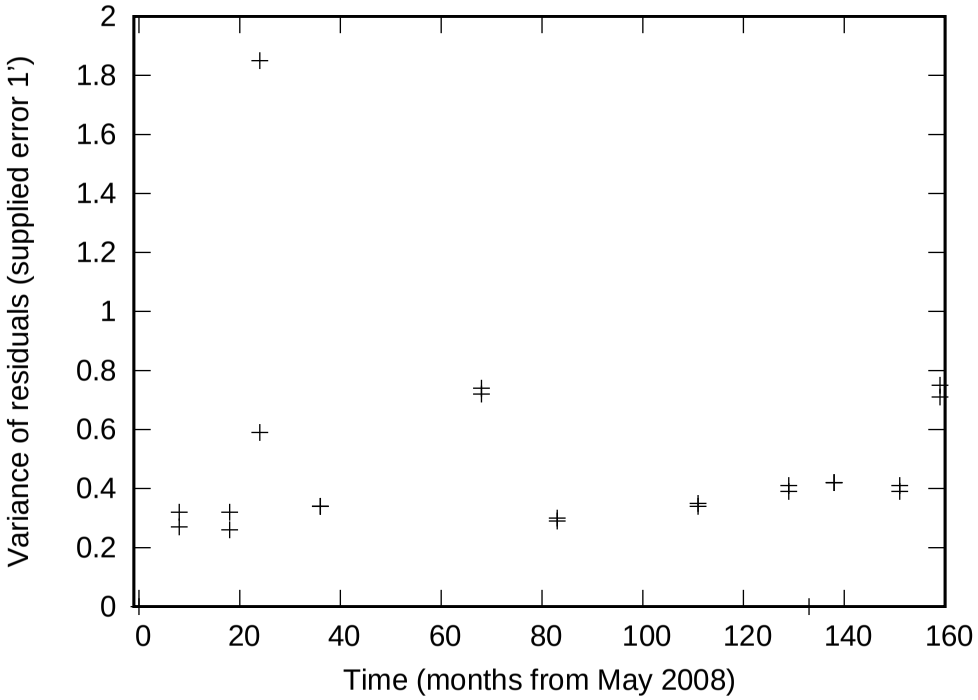

Fig. 1: S04 Azimuth pointing coefficients

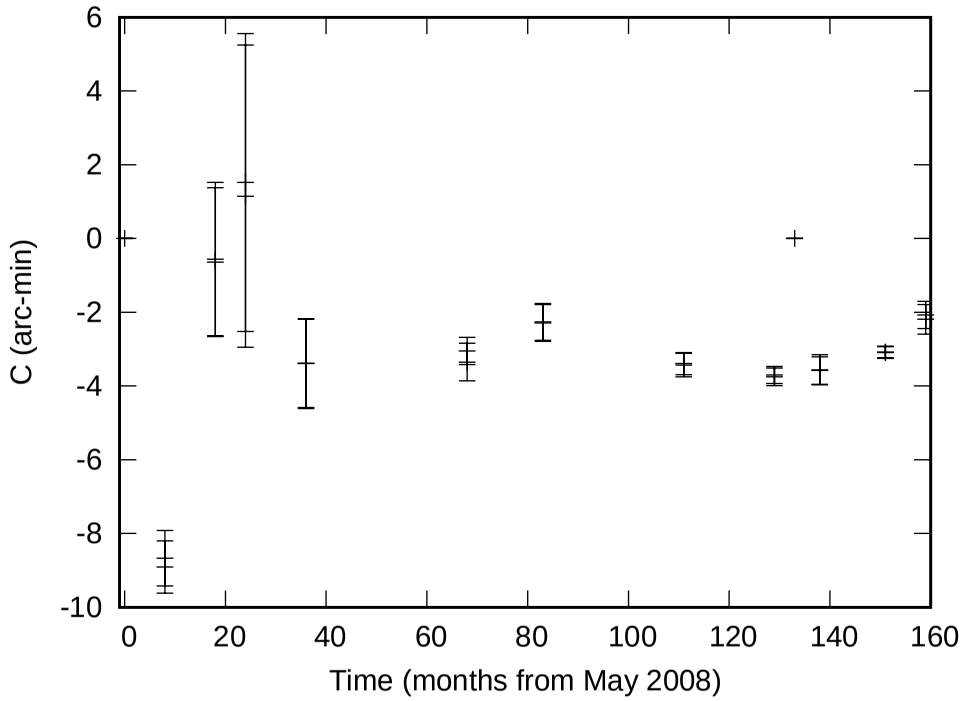

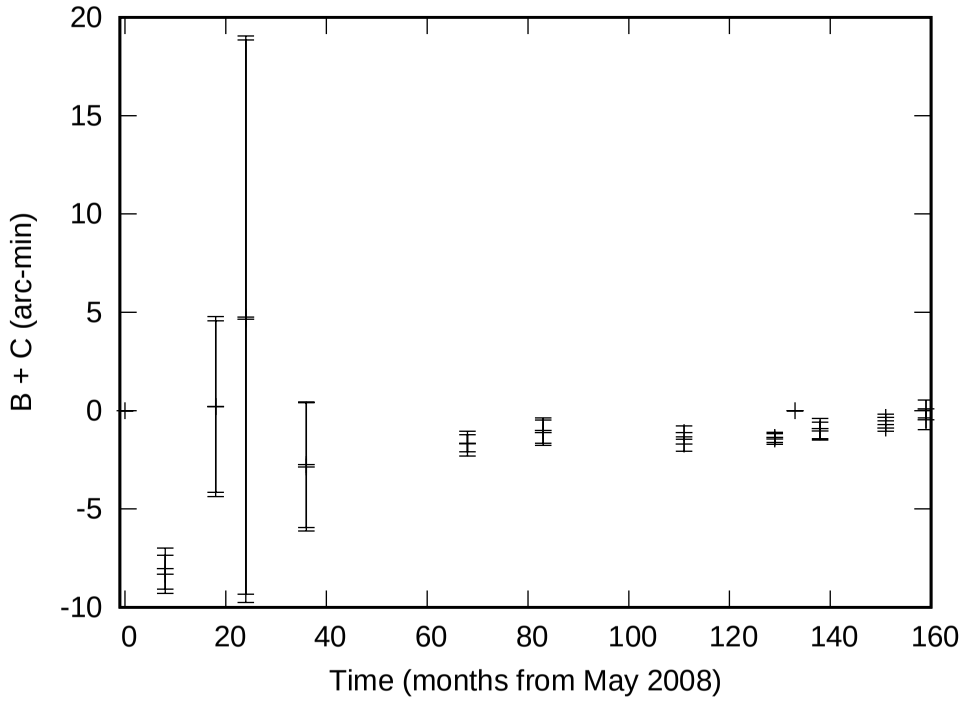

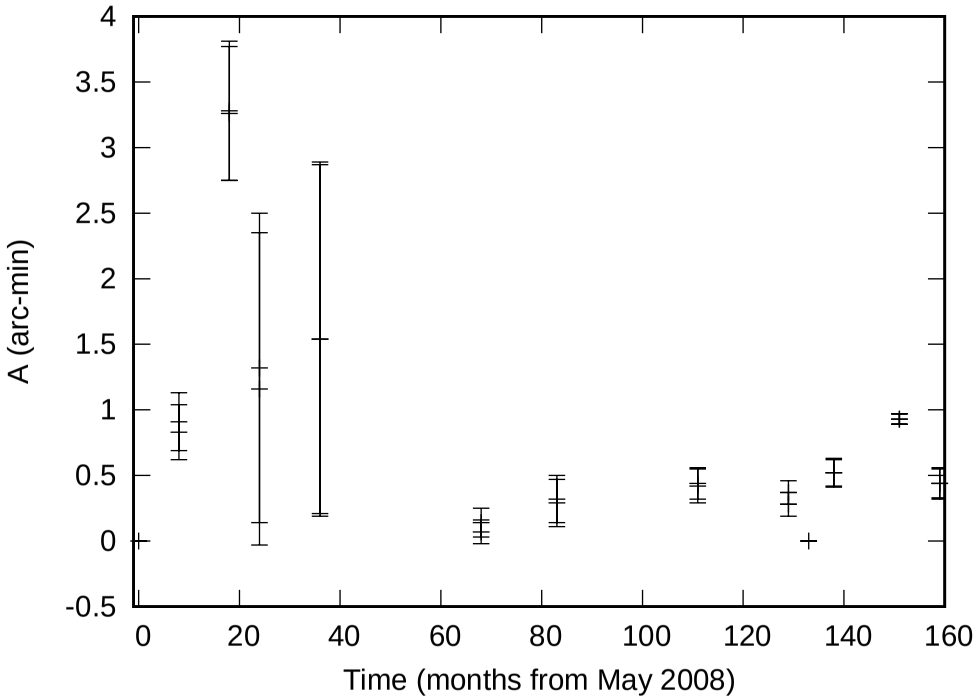

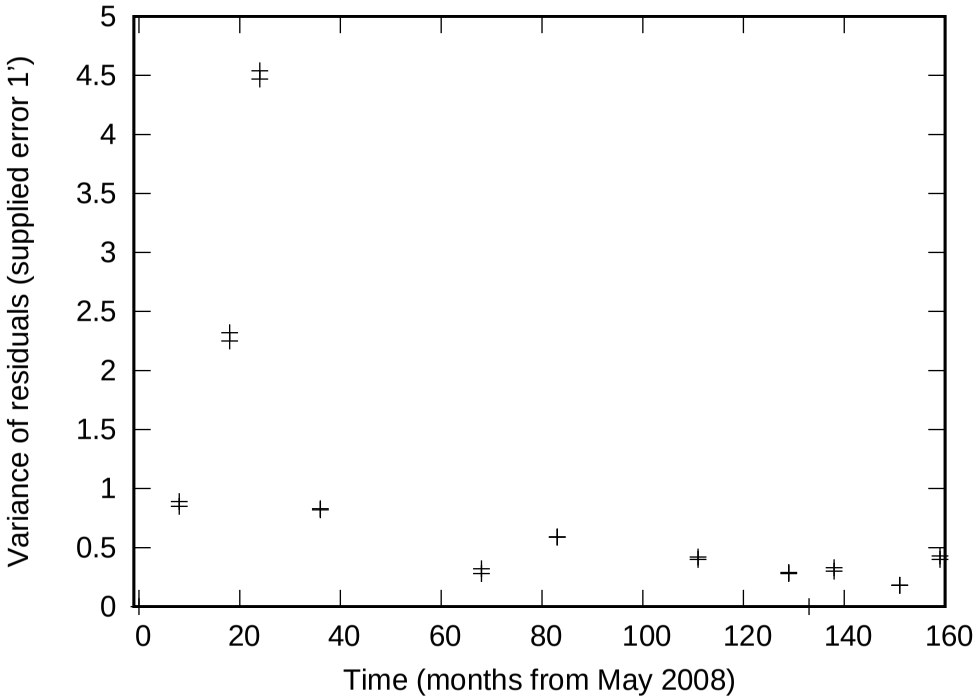

Fig. 1: S06 Azimuth pointing coefficients

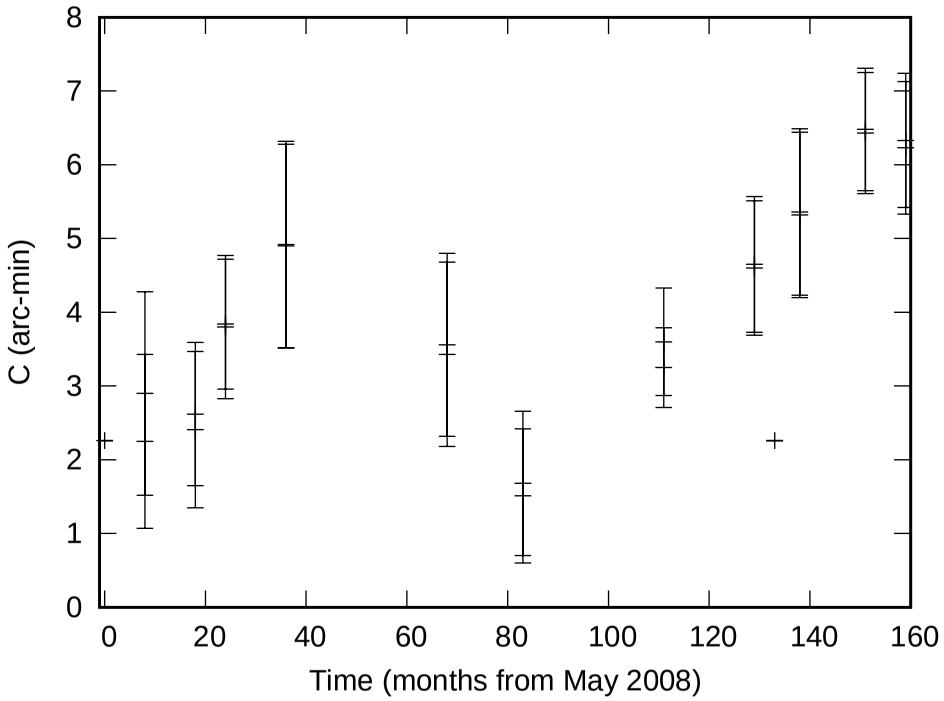

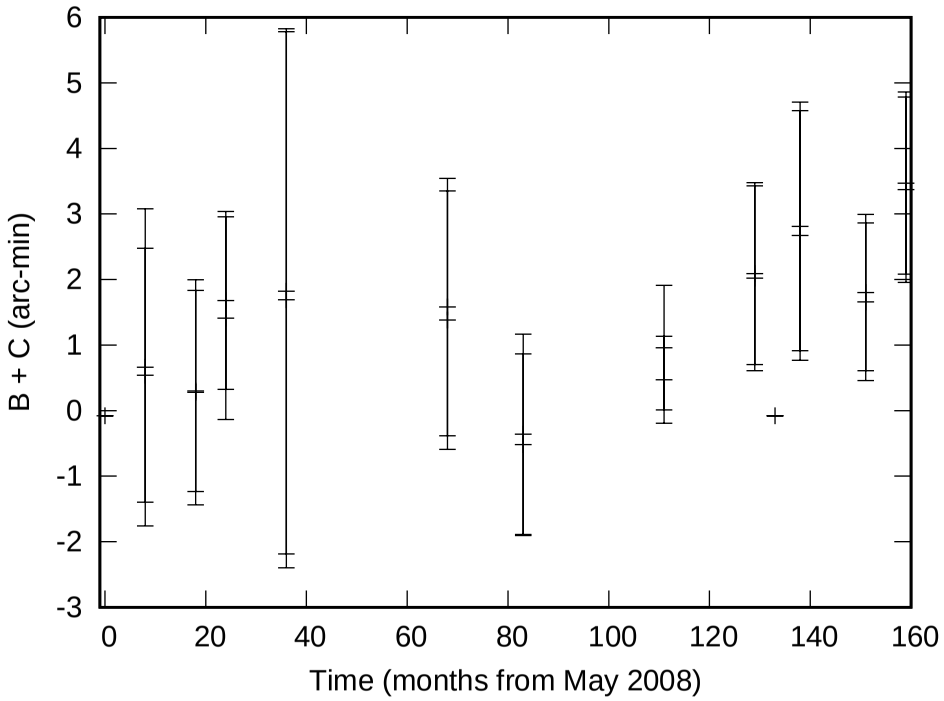

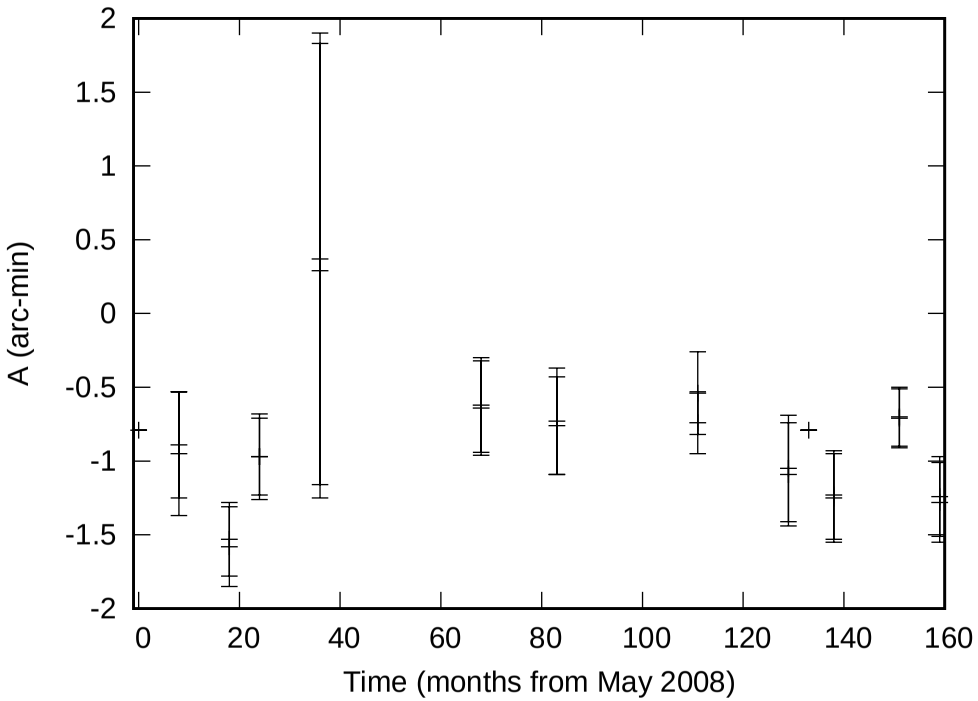

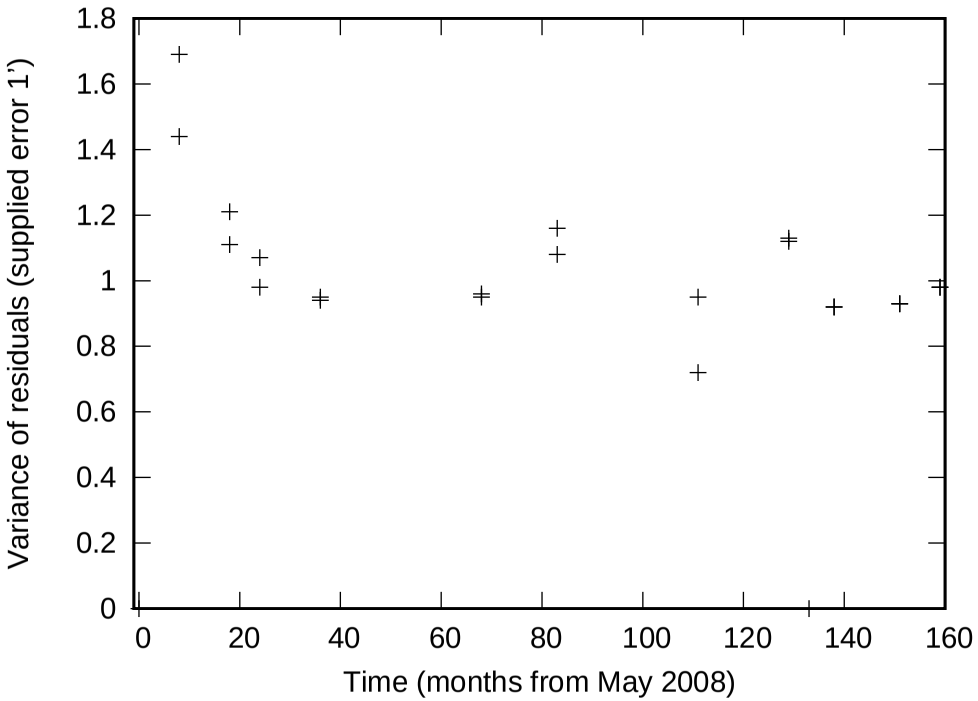

Fig. 1: W01 Azimuth pointing coefficients

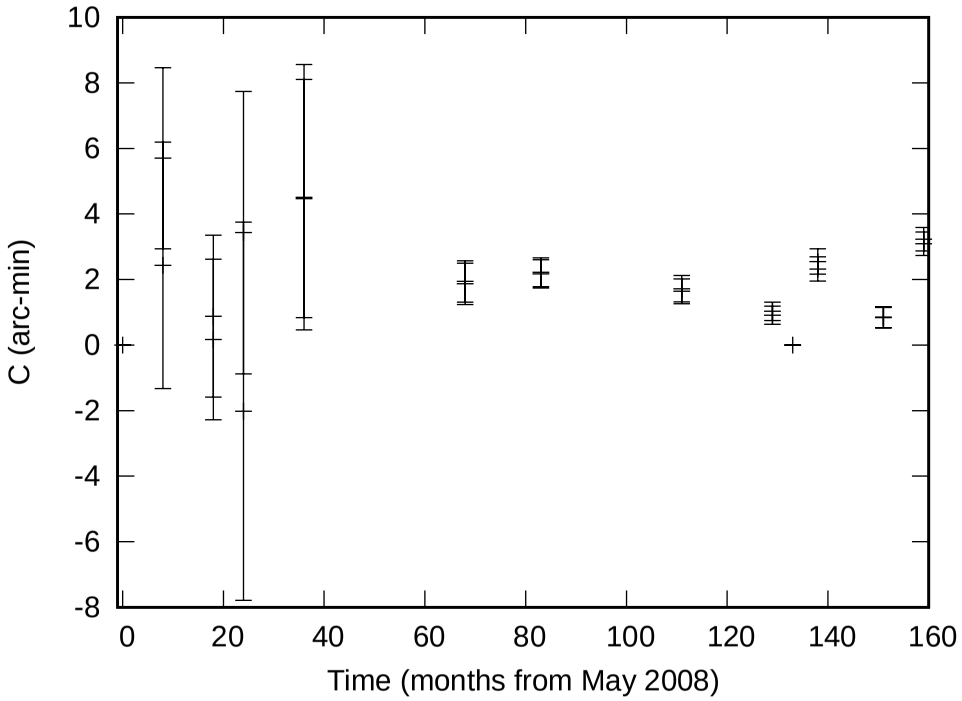

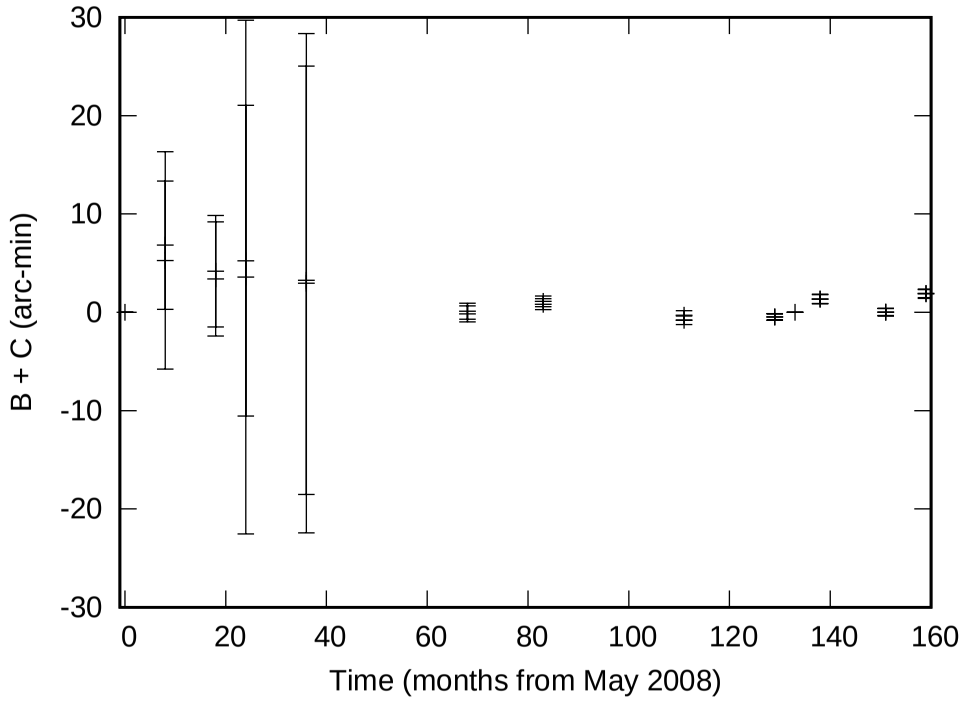

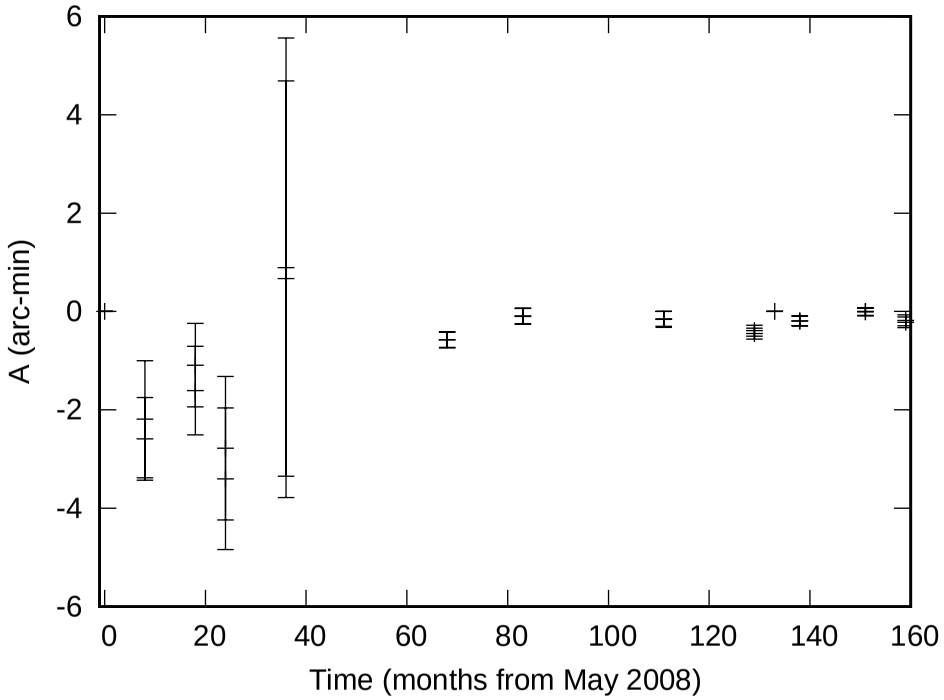

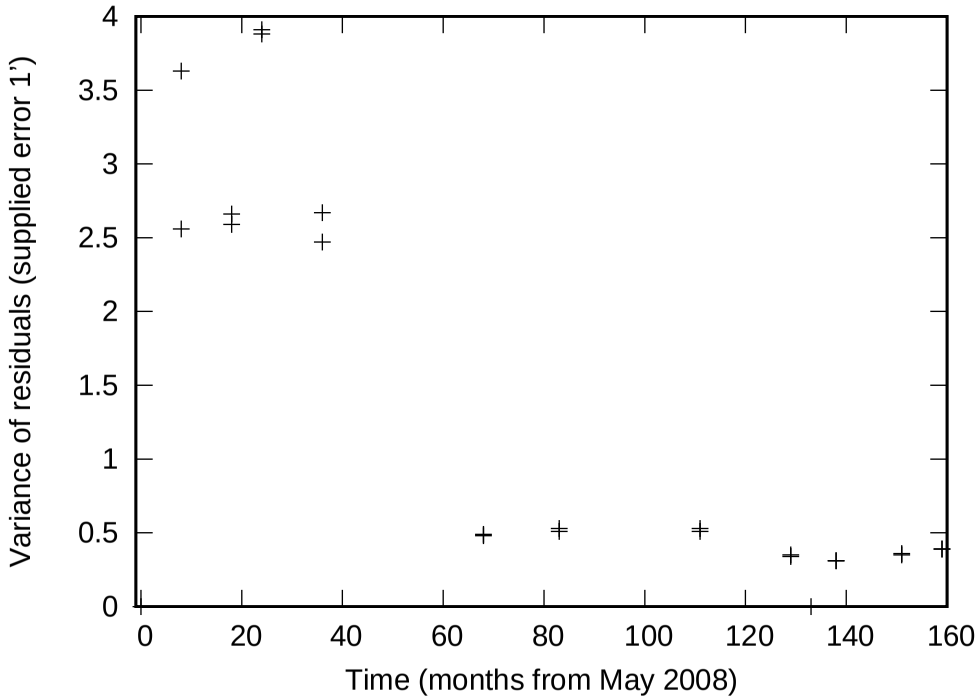

Fig. 1: W02 Azimuth pointing coefficients

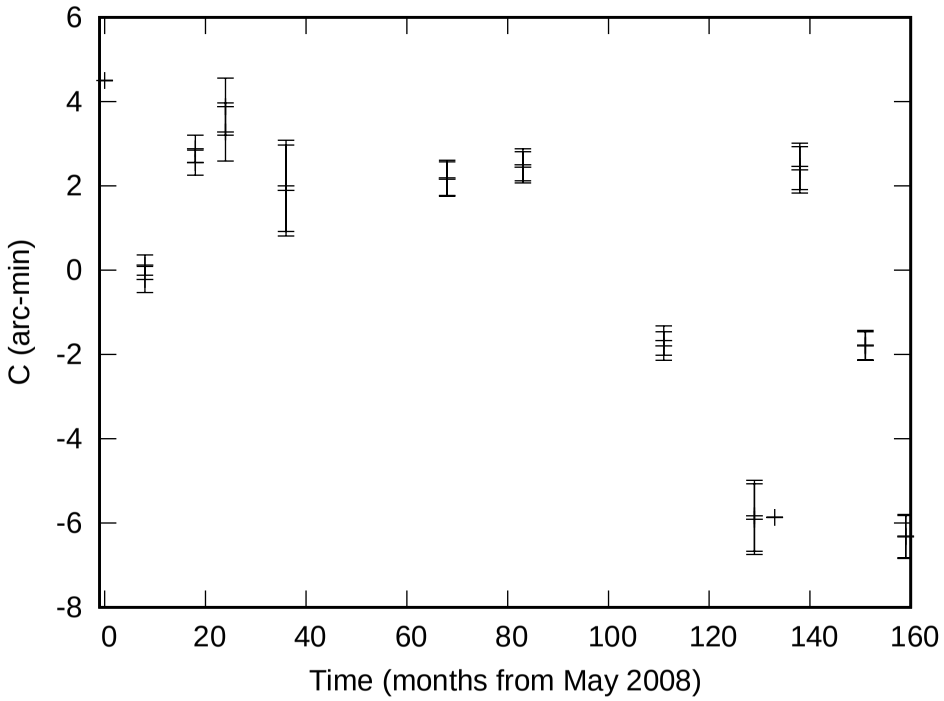

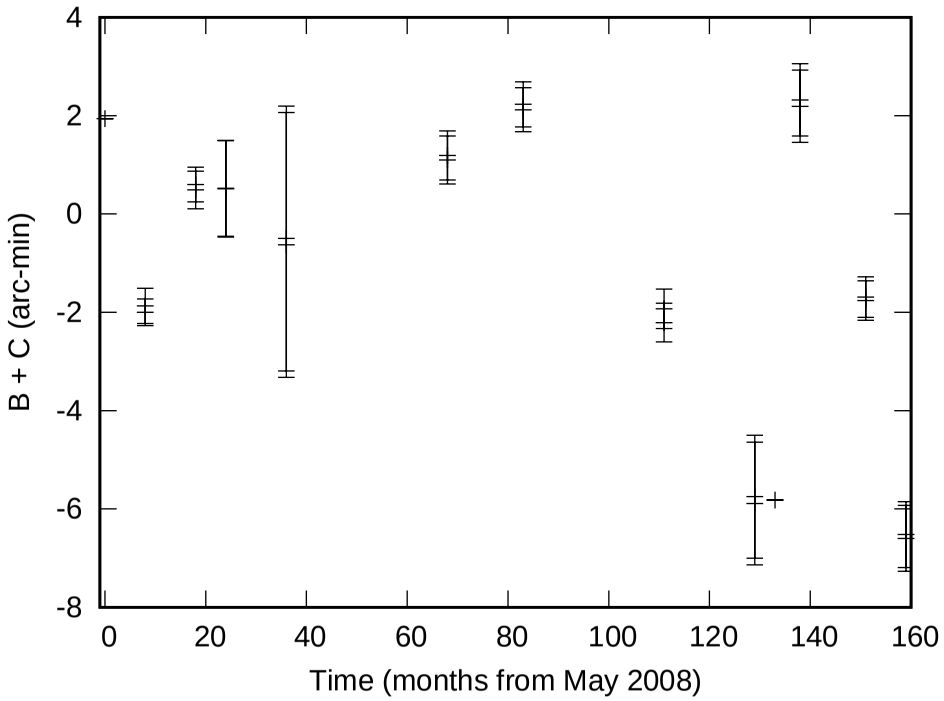

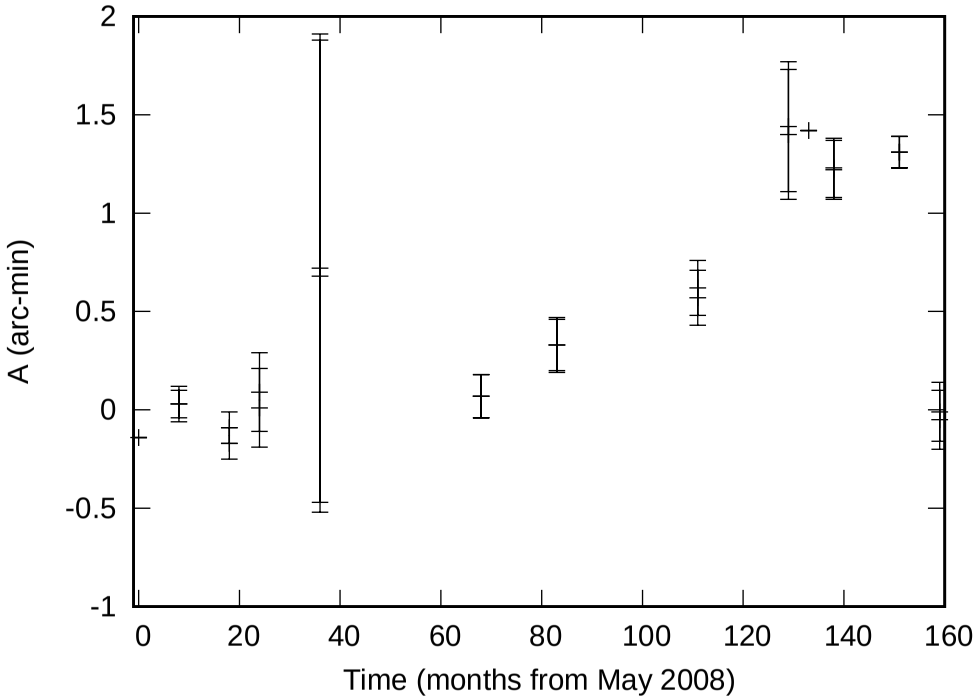

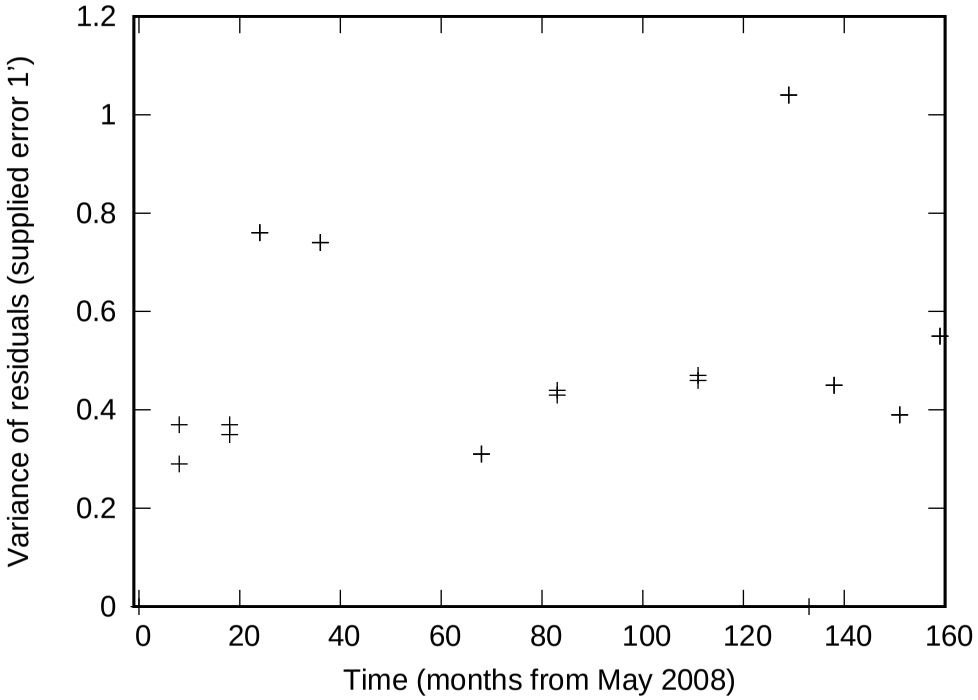

Fig. 1: W03 Azimuth pointing coefficients

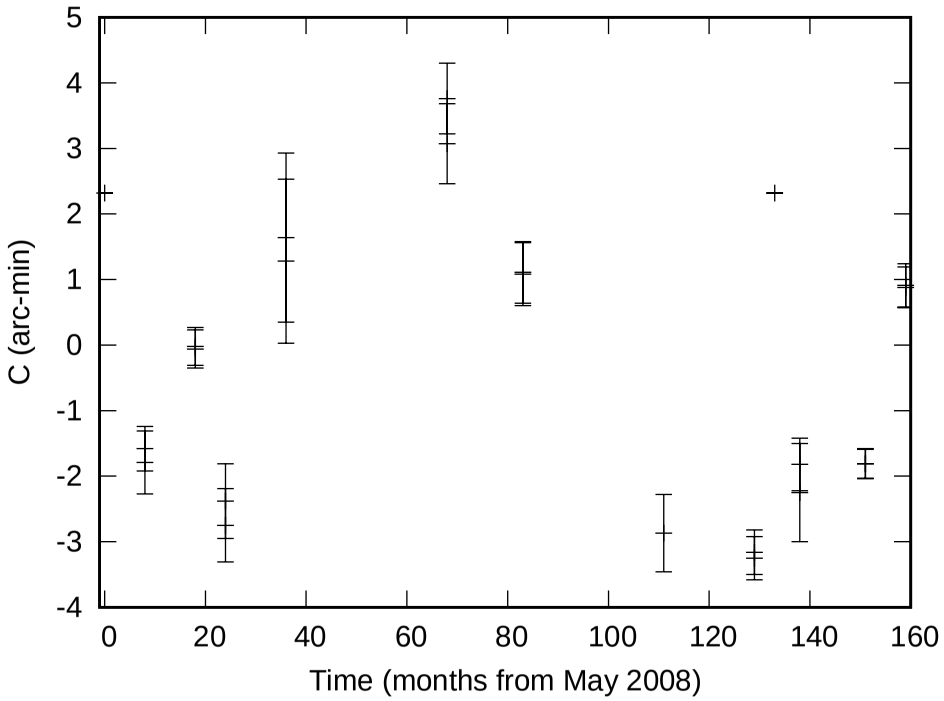

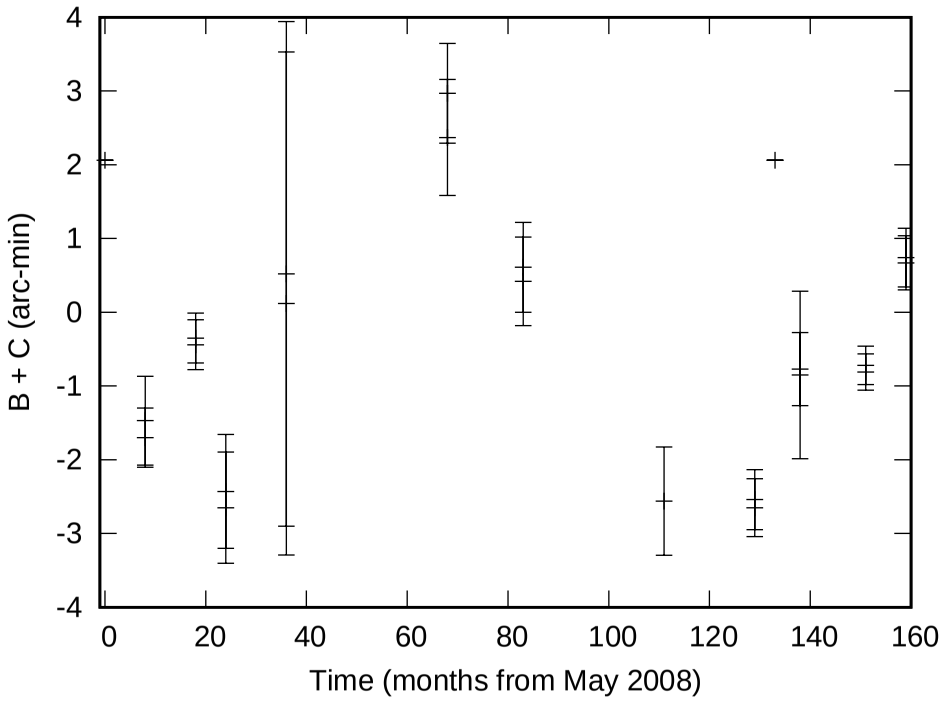

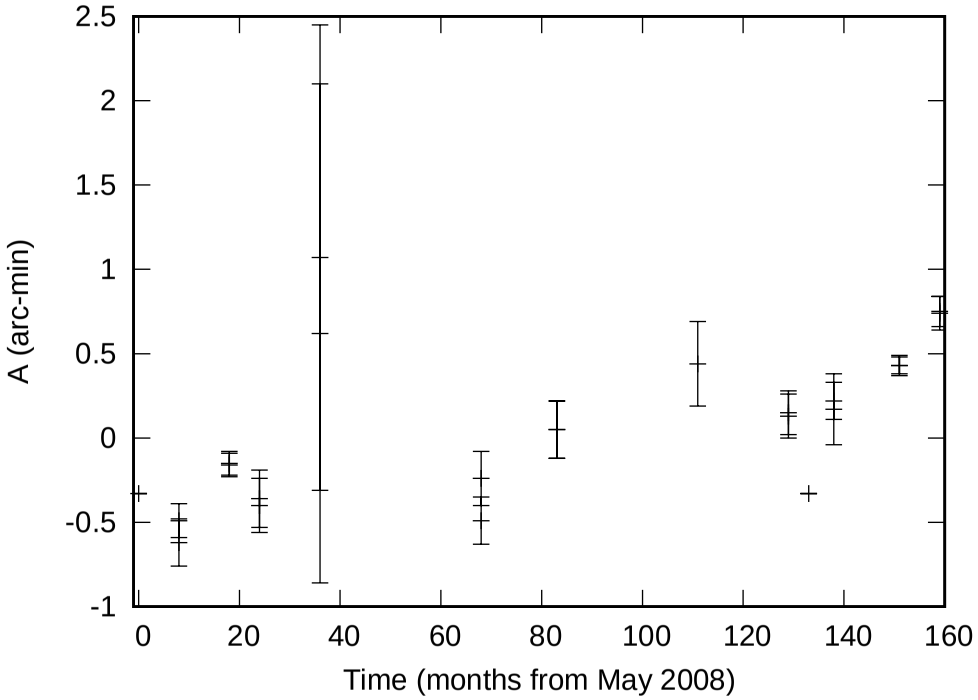

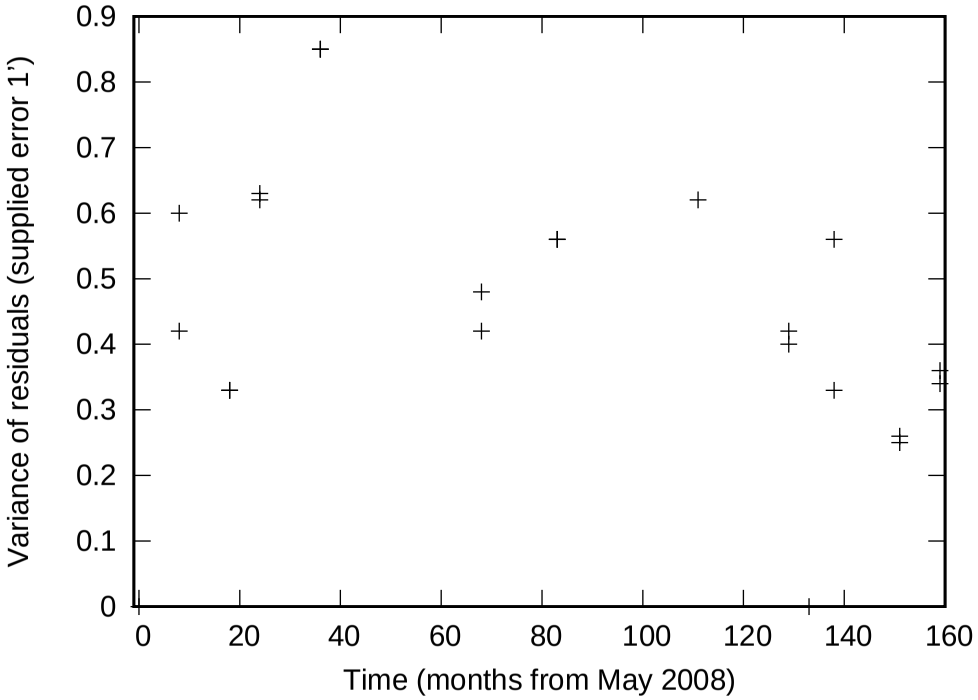

Fig. 1: W04 Azimuth pointing coefficients

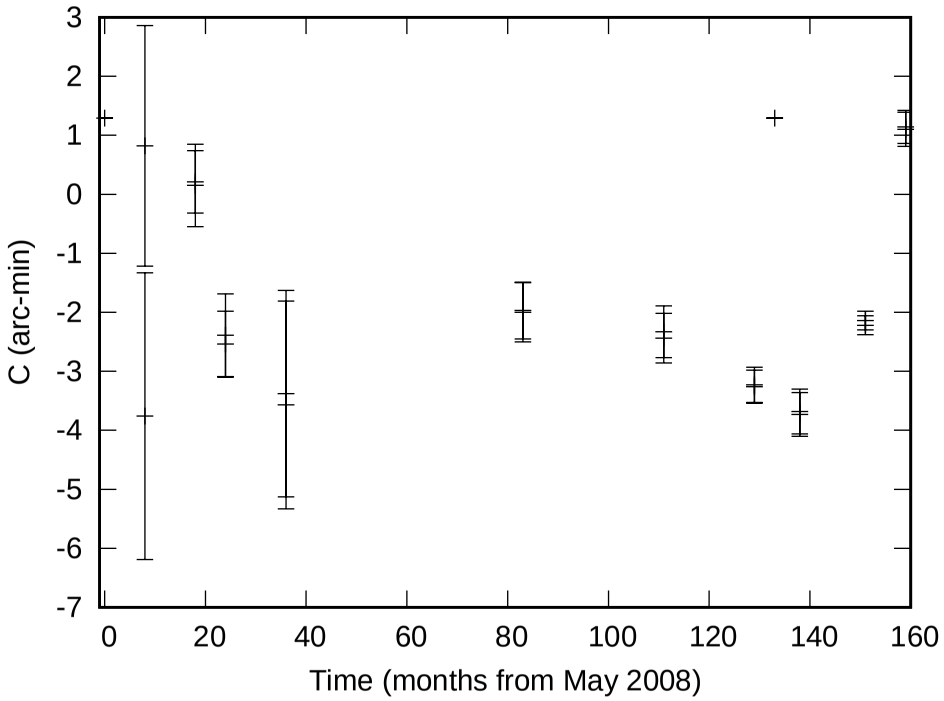

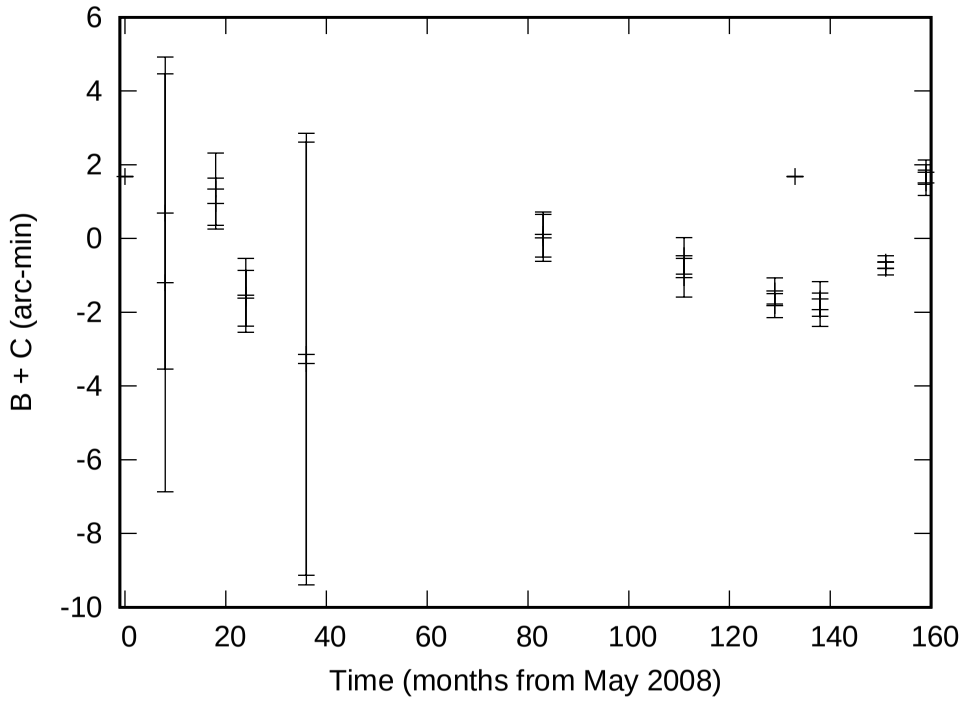

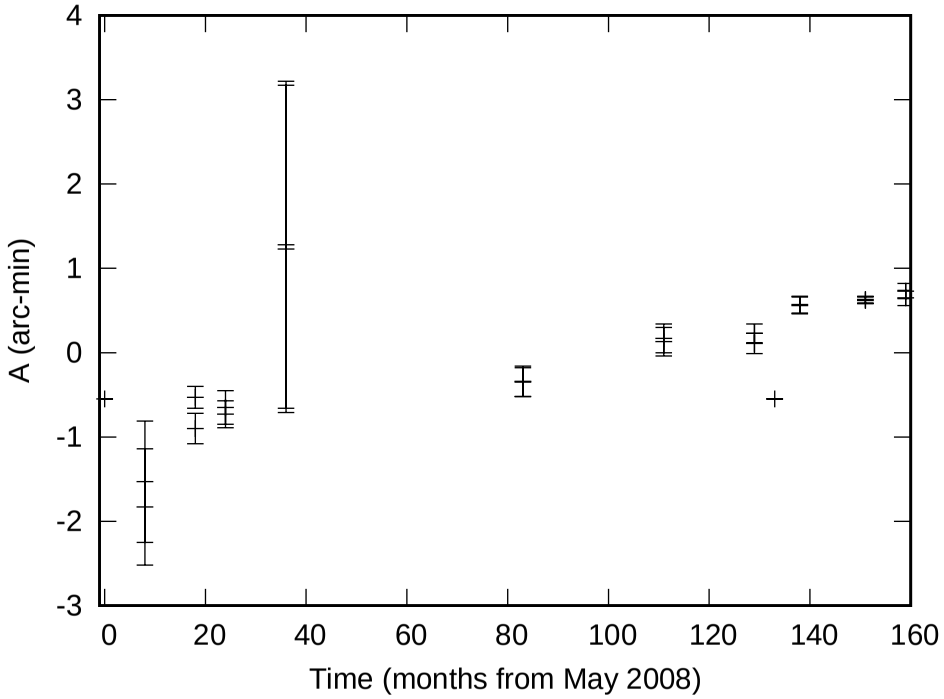

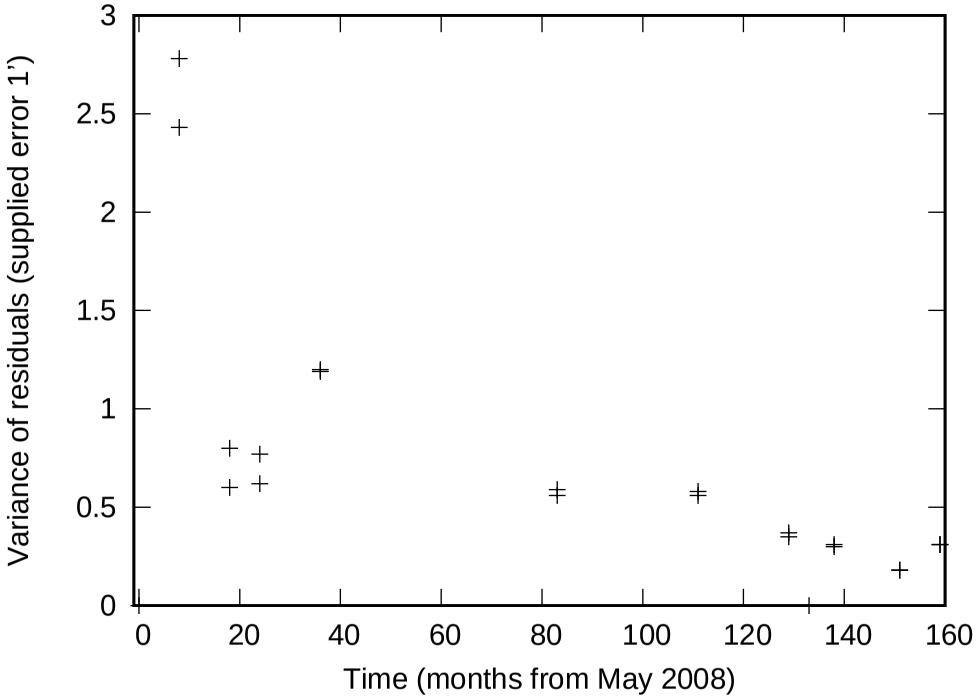

Fig. 1: W05 Azimuth pointing coefficients

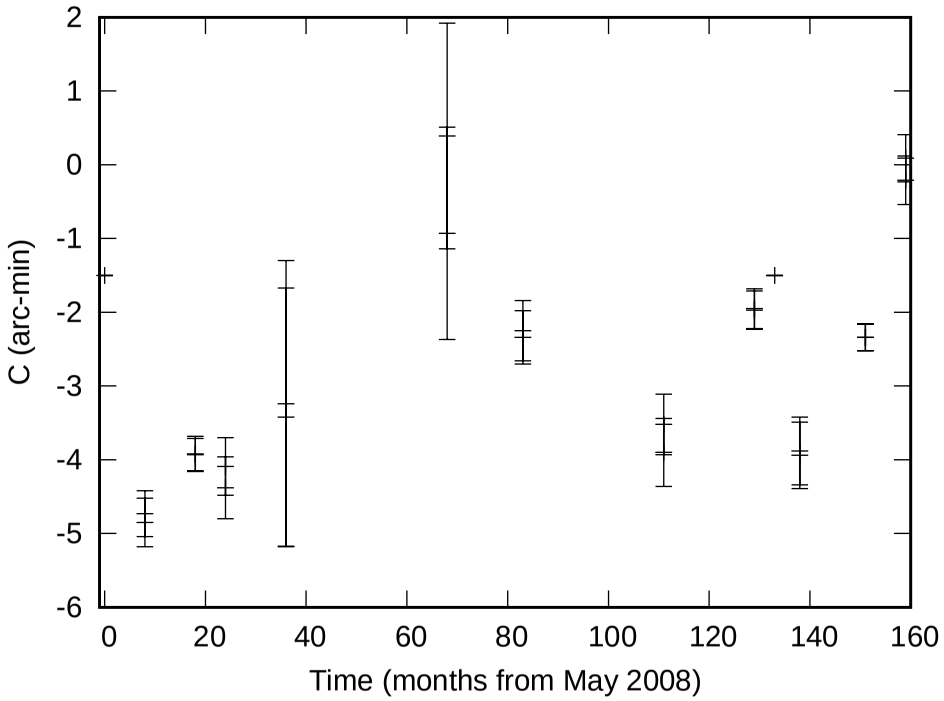

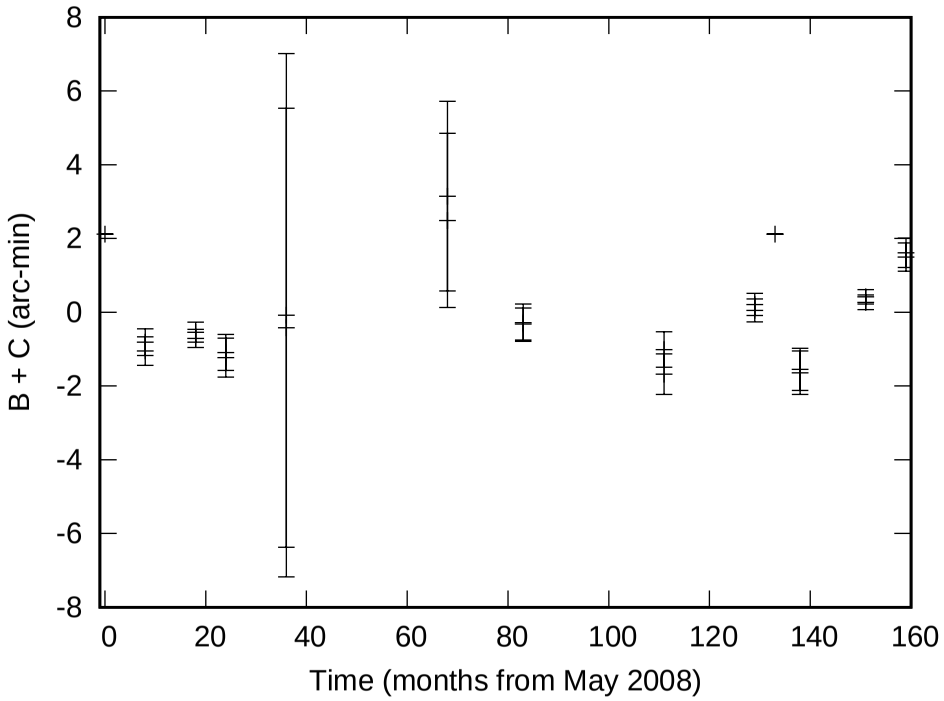

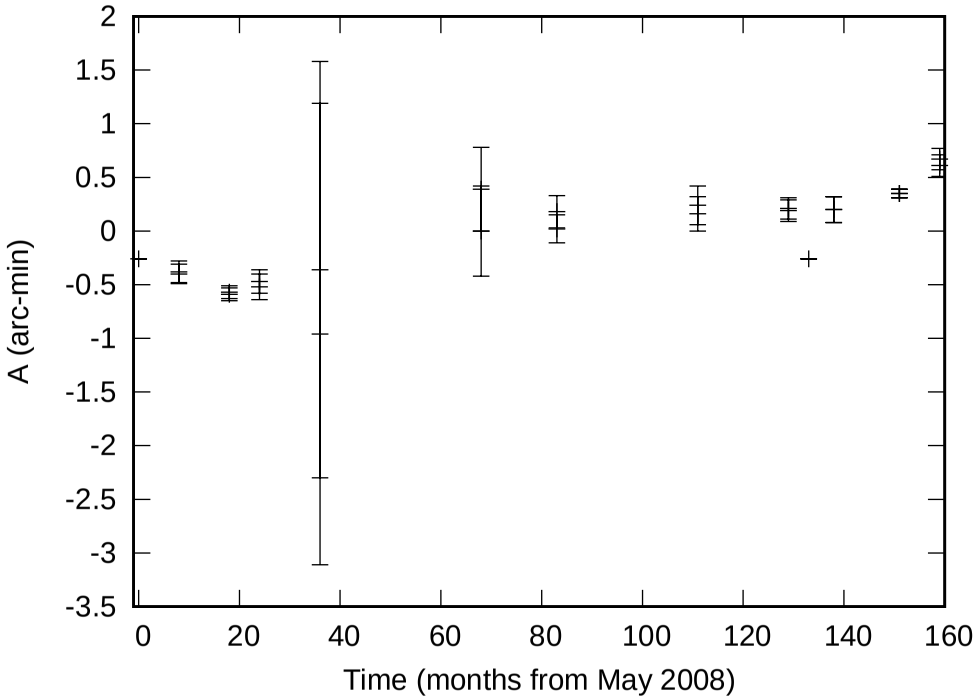

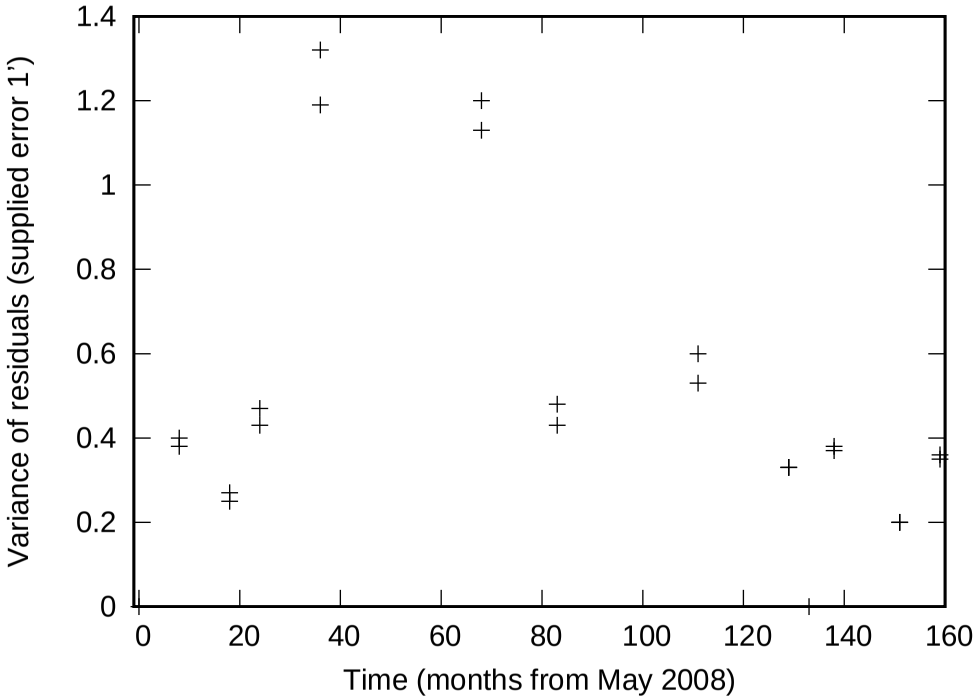

Fig. 1: W06 Azimuth pointing coefficients

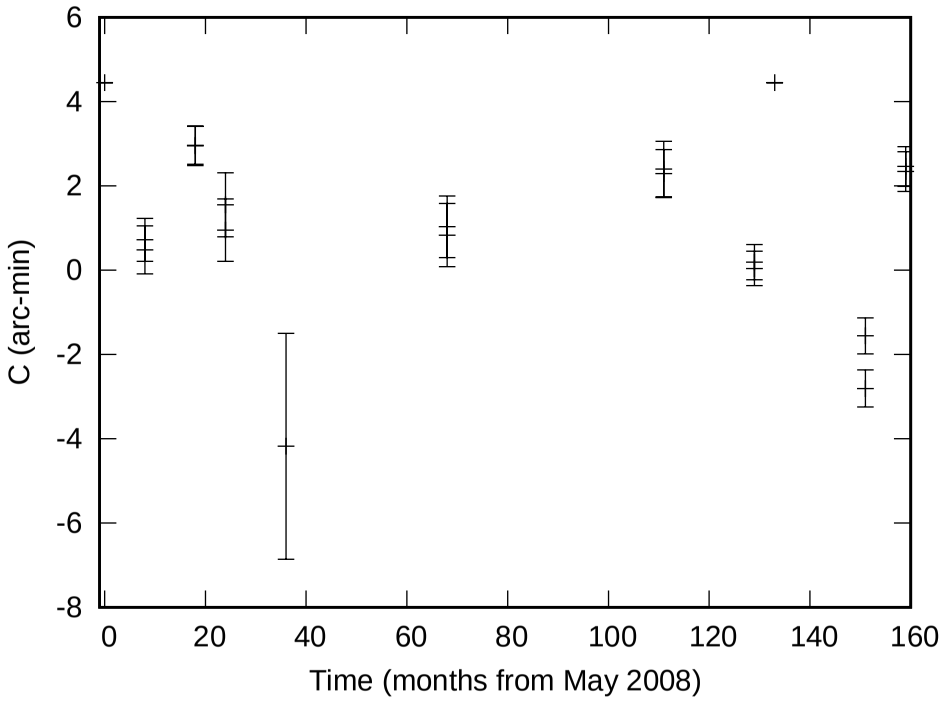

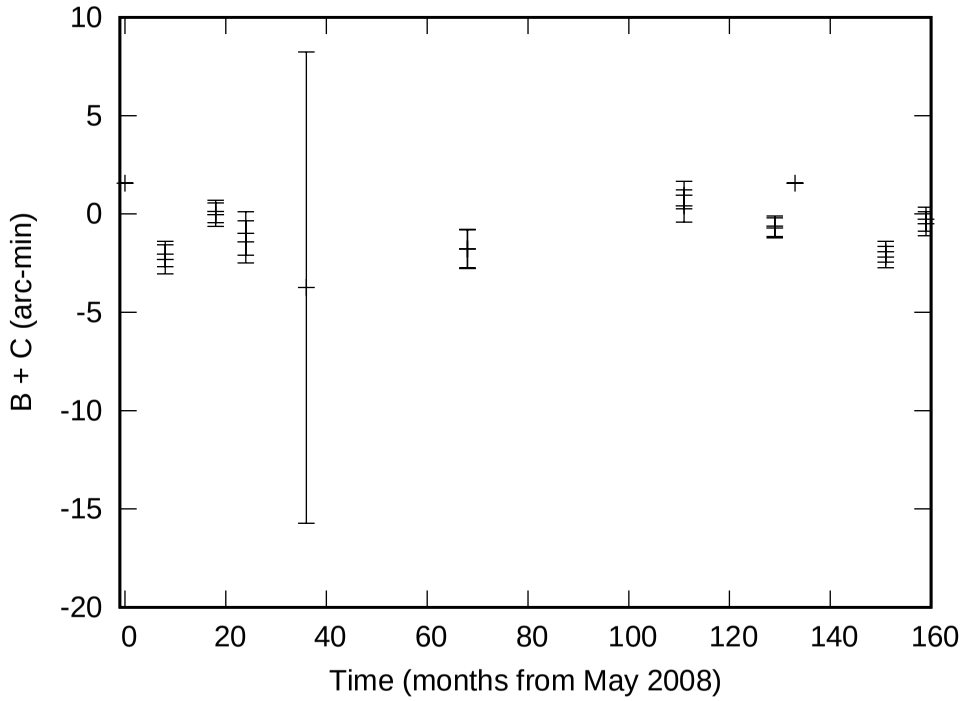

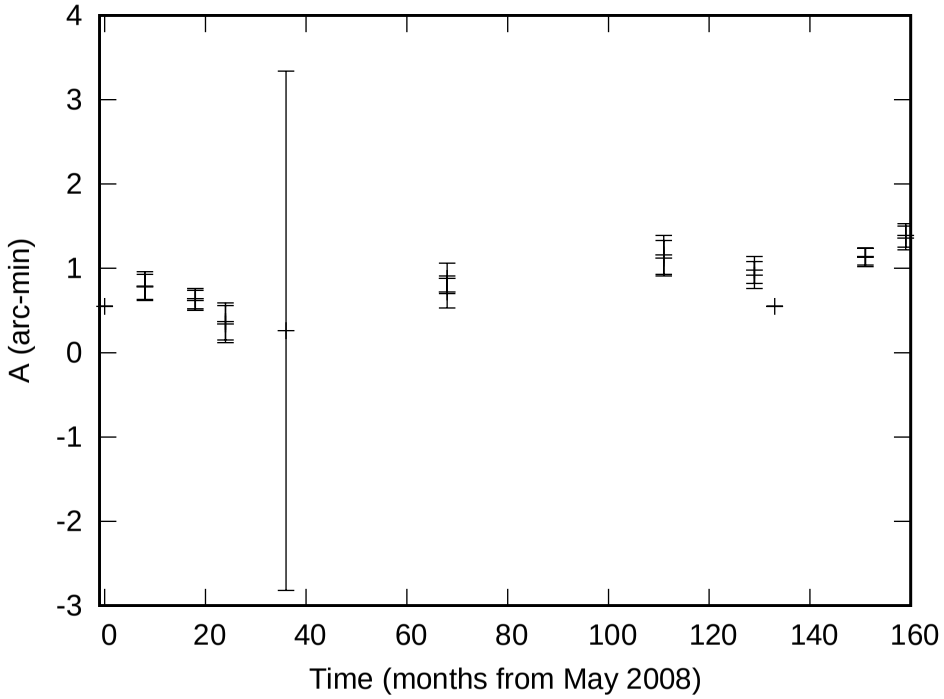

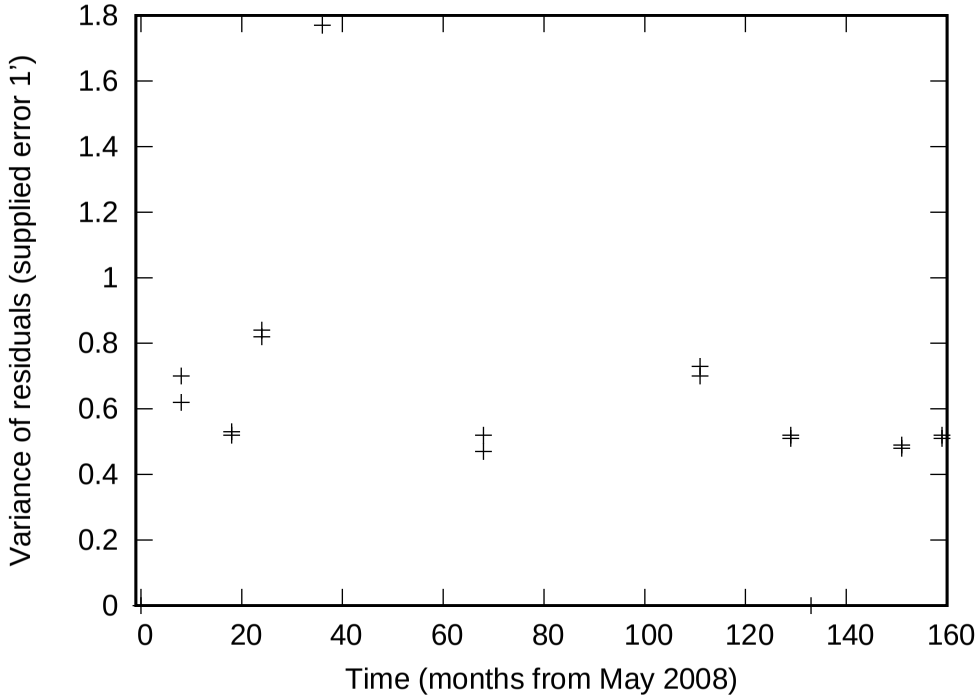

Table -1: Reduced Chi-square of AZ pointing errors
after applying the Jun 19 pointing model

#Antenna-Band-Poln	FIT_STDFIT**2 (AZ)			
#	28Aug17	17Feb19	25Nov19	16Dec20
C00-USB-130	0.13	0.37	0.84	0.91
C00-USB-175	0.12	0.38	0.89	0.90
C01-USB-130	4.54	8.46	3.67	6.05
C01-USB-175	4.45	9.07	3.77	6.18
C02-USB-130	1.39	0.30	2.54	1.72
C02-USB-175	1.02	0.24	2.57	1.72
C03-USB-130	1.24	0.25	0.58	NaN
C03-USB-175	1.35	0.29	0.59	NaN
C04-USB-130	1.99	1.29	NaN	4.28
C04-USB-175	1.85	1.02	NaN	4.28
C05-USB-130	1.00	0.51	0.42	0.75
C05-USB-175	1.22	0.43	0.49	0.77
C06-USB-130	1.66	1.11	1.25	0.33
C06-USB-175	1.77	1.14	1.74	0.30
C08-USB-130	0.16	0.93	0.16	0.30
C08-USB-175	0.19	1.11	0.27	0.28
C09-USB-130	0.51	2.75	0.62	2.46
C09-USB-175	0.48	2.75	0.68	2.45
C10-USB-130	0.39	0.34	0.24	0.97
C10-USB-175	0.39	0.33	0.23	0.94
C11-USB-130	0.91	2.20	0.61	0.39
C11-USB-175	0.85	2.04	0.39	0.40
C12-USB-130	0.41	0.62	0.57	0.42
C12-USB-175	0.43	0.62	0.58	0.45
C13-USB-130	0.15	0.70	0.46	0.96
C13-USB-175	0.14	0.67	0.46	0.95
C14-USB-130	0.25	0.13	0.22	0.23
C14-USB-175	0.25	0.11	0.18	0.23
E02-USB-130	1.13	1.62	0.29	1.00
E02-USB-175	1.08	1.70	0.28	1.01
E03-USB-130	0.37	0.64	0.16	1.41
E03-USB-175	0.36	0.70	0.23	1.40
E04-USB-130	1.29	2.92	1.10	1.20
E04-USB-175	1.32	2.91	1.09	1.17
E05-USB-130	1.04	1.16	0.59	0.36
E05-USB-175	1.05	1.11	0.59	0.38
E06-USB-130	1.10	0.60	0.52	0.95
E06-USB-175	1.38	0.53	0.45	0.92
S01-USB-130	0.34	0.45	0.29	0.21
S01-USB-175	0.31	0.43	0.31	0.23
S02-USB-130	0.83	0.39	0.83	0.67
S02-USB-175	0.81	0.35	0.92	0.69
S03-USB-130	0.47	0.15	0.20	0.51
S03-USB-175	0.52	0.17	0.19	0.52
S04-USB-130	0.76	1.02	0.69	0.84
S04-USB-175	0.79	1.02	0.70	0.84
S06-USB-130	0.99	1.55	1.22	1.47
S06-USB-175	0.54	1.57	1.20	1.45
W01-USB-130	0.42	0.26	0.33	0.15
W01-USB-175	0.38	0.23	0.29	0.14
W02-USB-130	1.19	0.98	2.47	0.73
W02-USB-175	1.14	0.99	2.51	0.74
W03-USB-130	1.71	2.25	1.18	0.96
W03-USB-175	NaN	2.20	0.87	0.96
W04-USB-130	1.07	1.74	1.67	1.21
W04-USB-175	1.04	1.65	1.65	1.22
W05-USB-130	0.50	0.20	0.44	0.28
W05-USB-175	0.67	0.20	0.45	0.28
W06-USB-130	0.77	1.48	NaN	1.65
W06-USB-175	0.80	1.58	NaN	2.24

3.2 Elevation

Measured model parameters as a function time in Months are shown in Fig. 2. Where month no. are measured from May 2008 when the model coefficients were implemented for the first time. The model coefficients for the model of May 2008 are shown by a '+' sign in the plots corresponding to month-0. Also, the existing model coefficients which were last renewed in Jun 2019 are shown by the same symbol for the month 133 in the plots. The value of the angle 'd' as provided by 'gnuplot' often shows $n\pi$ ambiguity. To avoid this issue, we have plotted $\cos(d)$ in Fig. 2. Whenever 'c' was negative, its sign was flipped with a corresponding flipping of sign of $\cos(d)$. As can be seen from Fig. 3, despite fitting Eqn. 2 for each epoch, the reduced χ^2 for E02, E05, E06 were >3 (assuming error in measurements is $1'$) from 2008. E02 errors went down after 2011, while E05 and E06 errors were reduced after 2014. Among the model parameters, 'a' shows sudden change for C06, C09, S04, W01, W02, W03 and W06. Among them, the changes in 'a' are very high for W02 and W06. The parameter 'c' also changed for the antennas C08, C09, S04, S06 and W02. Systematic change is quite common for $\cos(d)$ for several antennas. Sudden change in $\cos(d)$ is noted for W01.

We note that the model values used at GMRT are often quite different than what is determined by independent fitting for all the parameters at each epochs. Therefore, we also checked for the reduced χ^2 of the pointing errors from Aug 2017 after applying the latest pointing model (after May 2008, pointing model was updated for certain antennas in Jul 2017 and then again in Jun 2019), which are shown in Table-2. It shows that for most of the antenna pointing errors have typical reduced $\chi^2 < 1$, though 3 antennas have $\chi^2 > 2$. This indicates the model of Jun 2019 adequately describes the EL pointing errors for almost all the antennas. For S02 and S06 reduced $\chi^2 > 3$. This indicates, EL pointing parameters are not well described by the model for these two antennas. W03 also had moderately high reduced χ^2 ($\sim$2), which needs to be monitored.

Acknowledgements

I thank Nimisha G Kantharia and Vasant Kulkarni for useful discussions. The observations on Jan 26 2014 was done by N. G. Kantharia and the data was shared with me.

References

COESA, US Standard Atmosphere, 1976, NOAA-S/T 76-1562, US Govt. Printing Office, Washington, DC.
Greve, A.; Panis, J.-F. & Thum, C., 1996, A&AS, 115, 379.
Kantharia, N.G; Kulkarni, V. K. & Nityananda, R., 2007, NCRA Technical Report entitled "Towards a pointing Model for GMRT antennas–II".
Roy, S. & Kulkarni, V. K., 2009, NCRA Technical Report entitled "Towards a pointing Model for GMRT antennas–Part III: Model parameters and implementation".

Fig. 2: C00 Elevation pointing coefficients

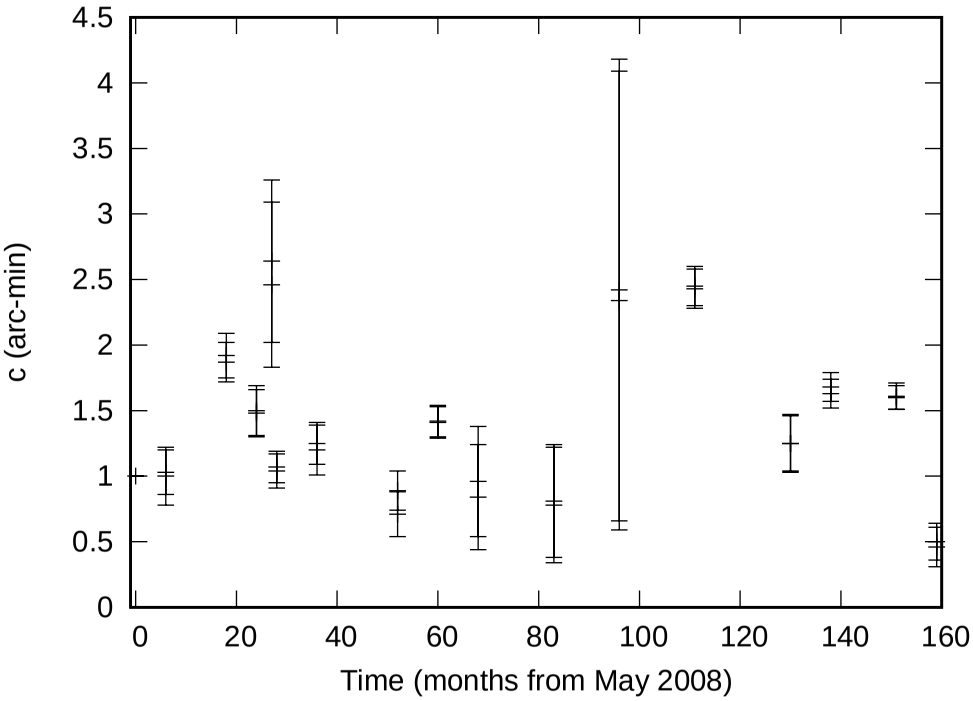

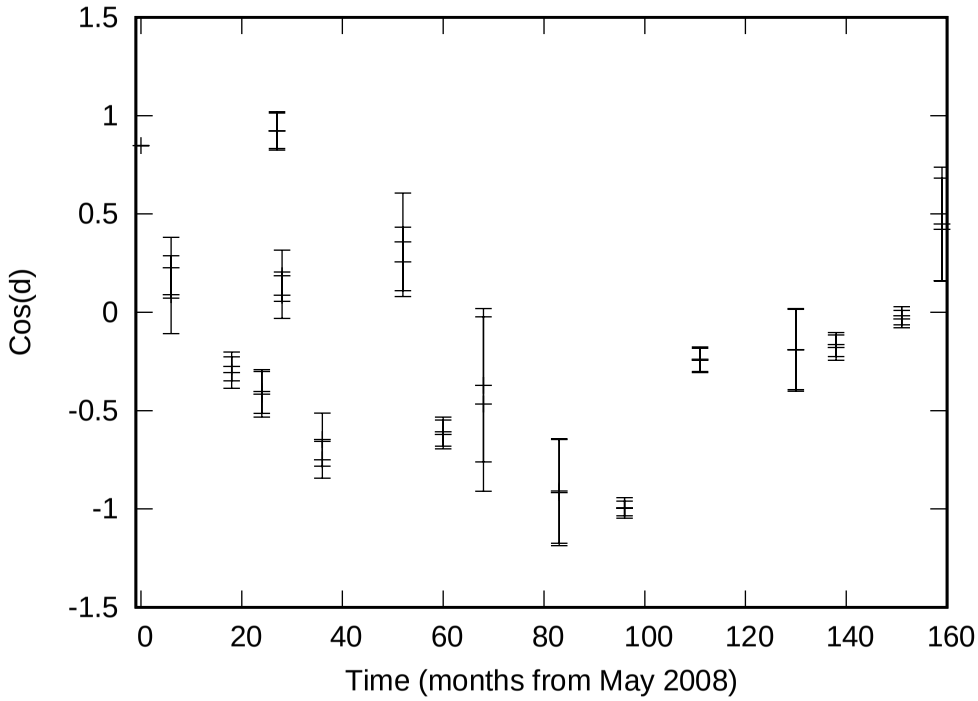

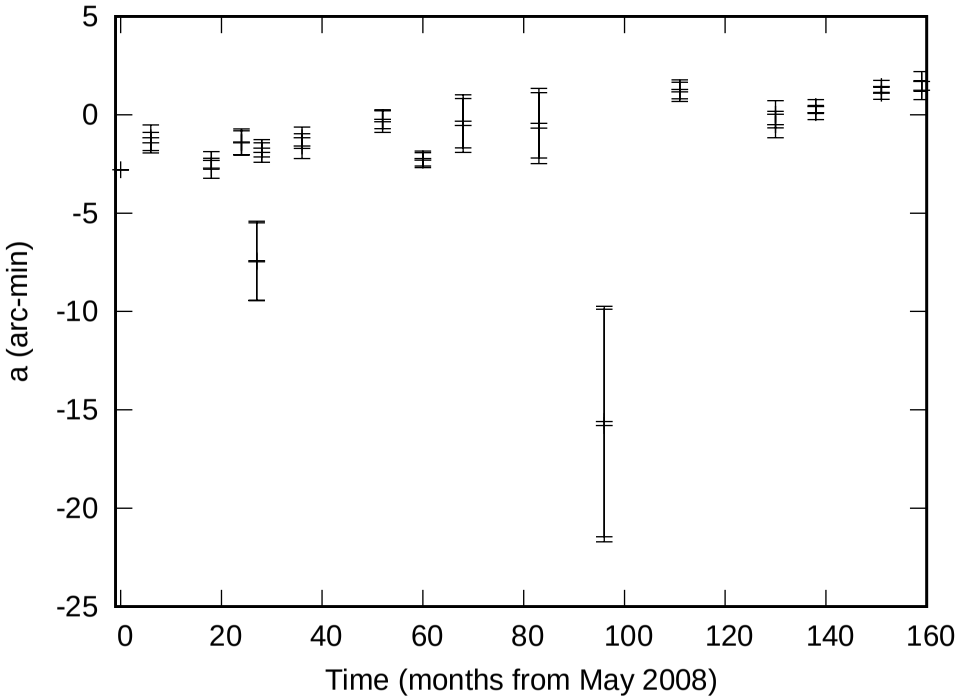

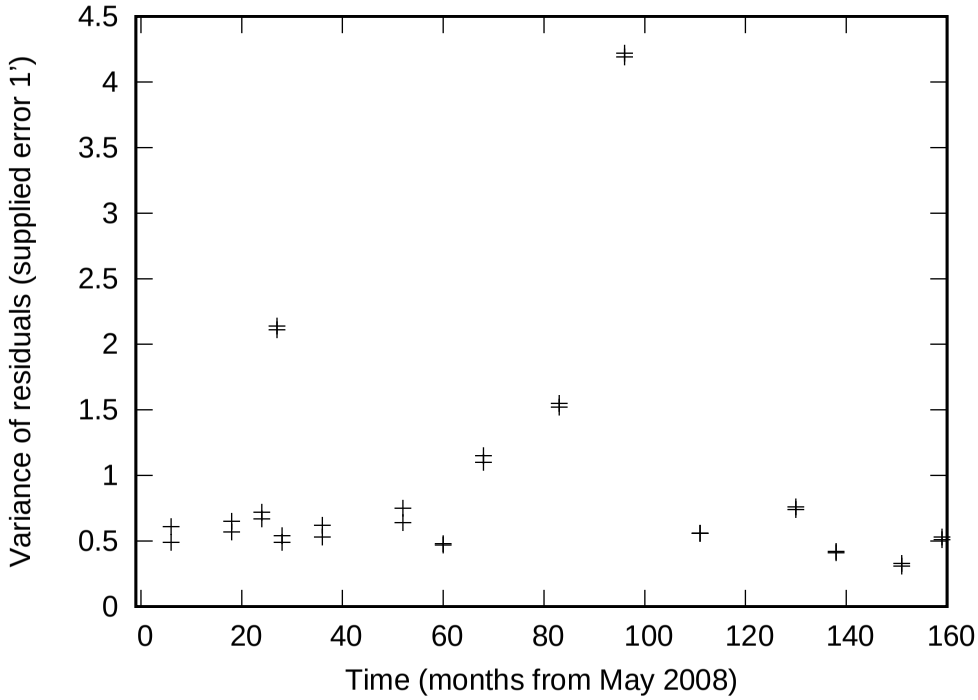

Fig. 2: C01 Elevation pointing coefficients

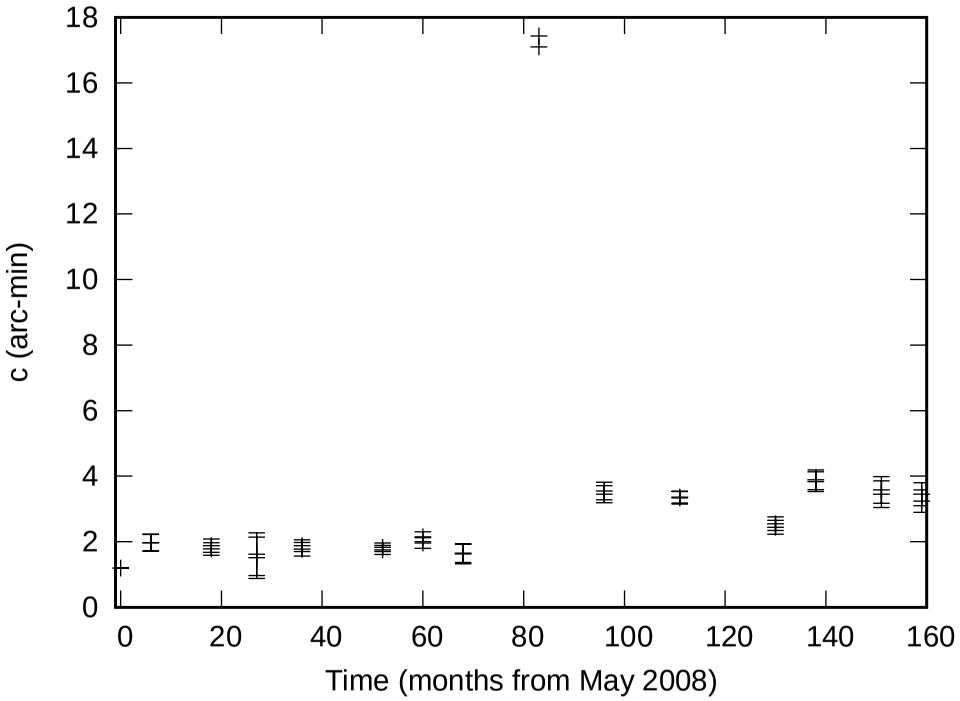

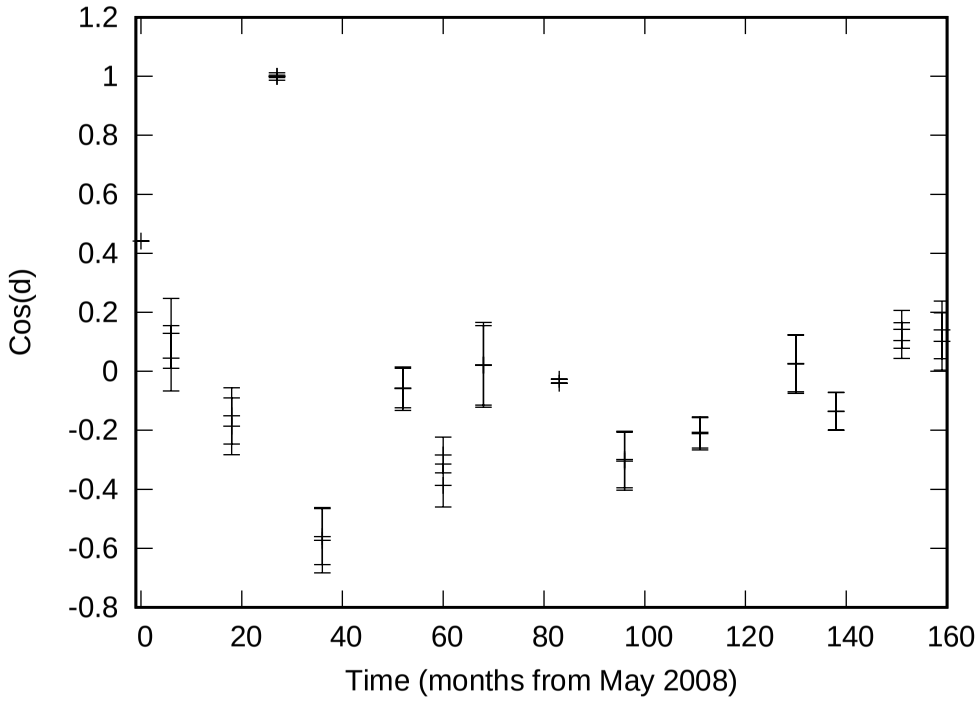

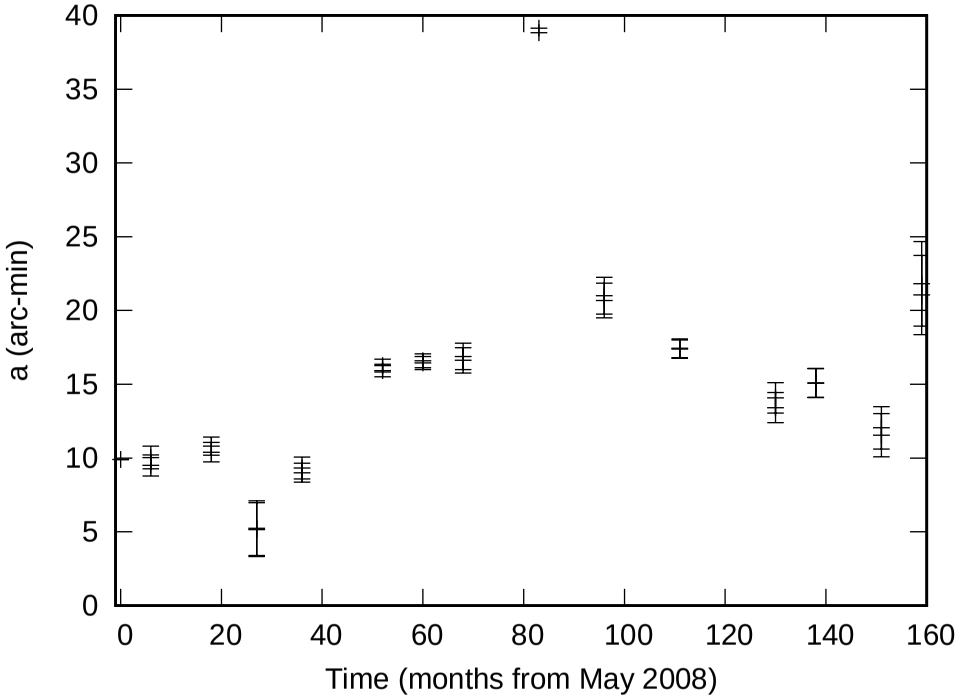

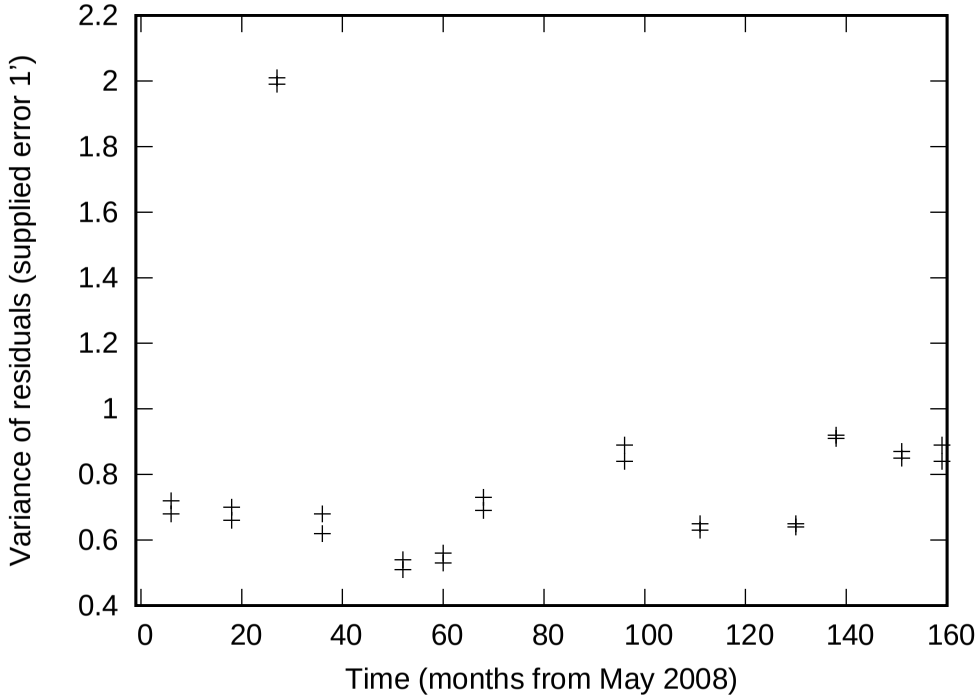

Fig. 2: C02 Elevation pointing coefficients

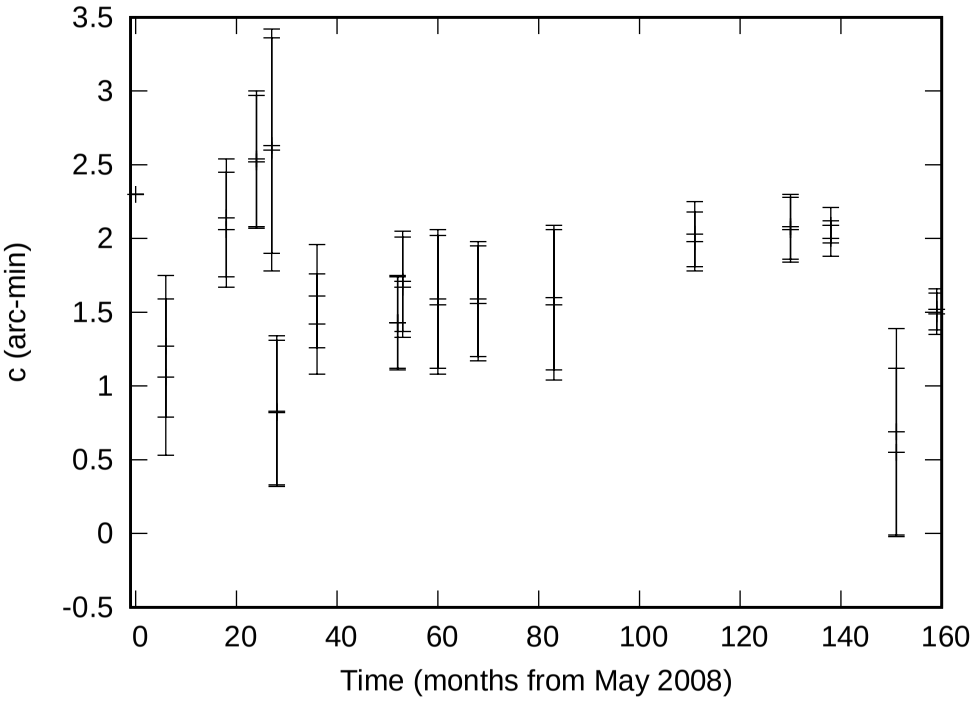

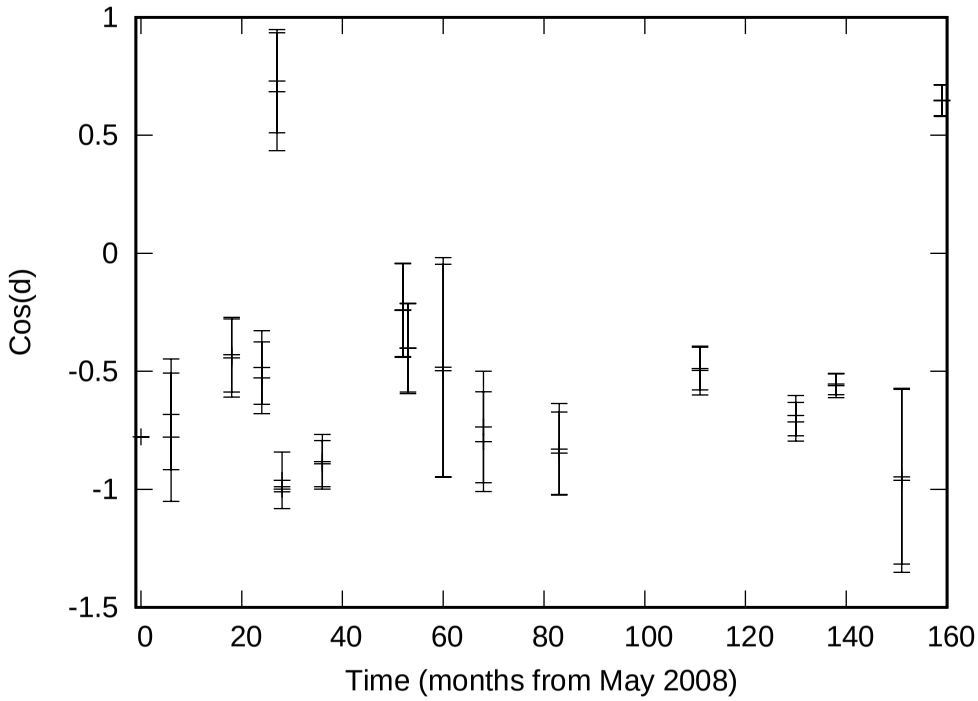

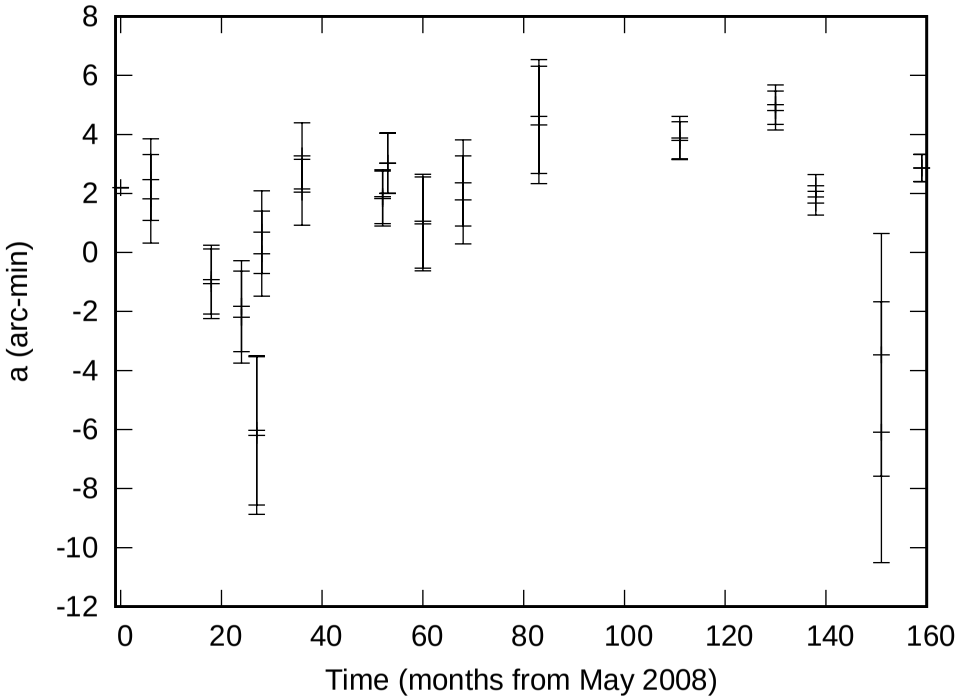

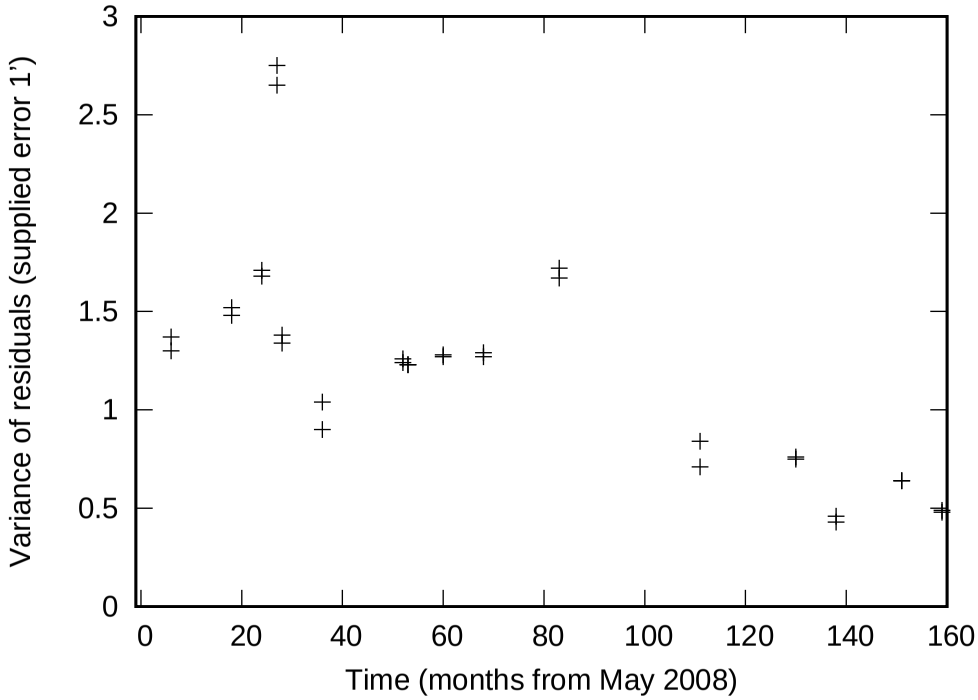

Fig. 2: C03 Elevation pointing coefficients

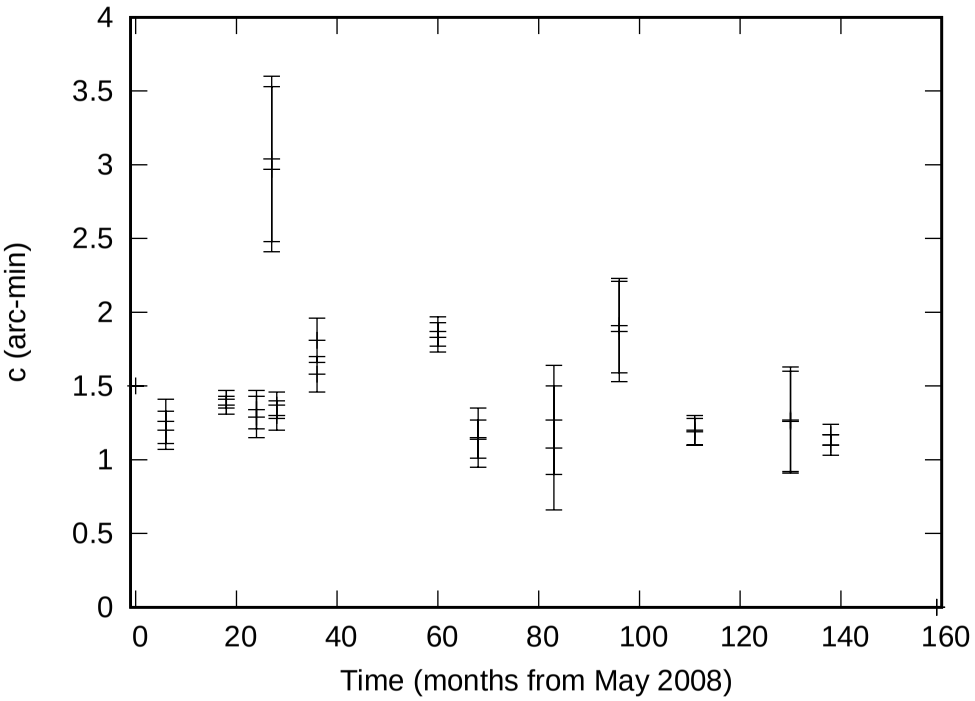

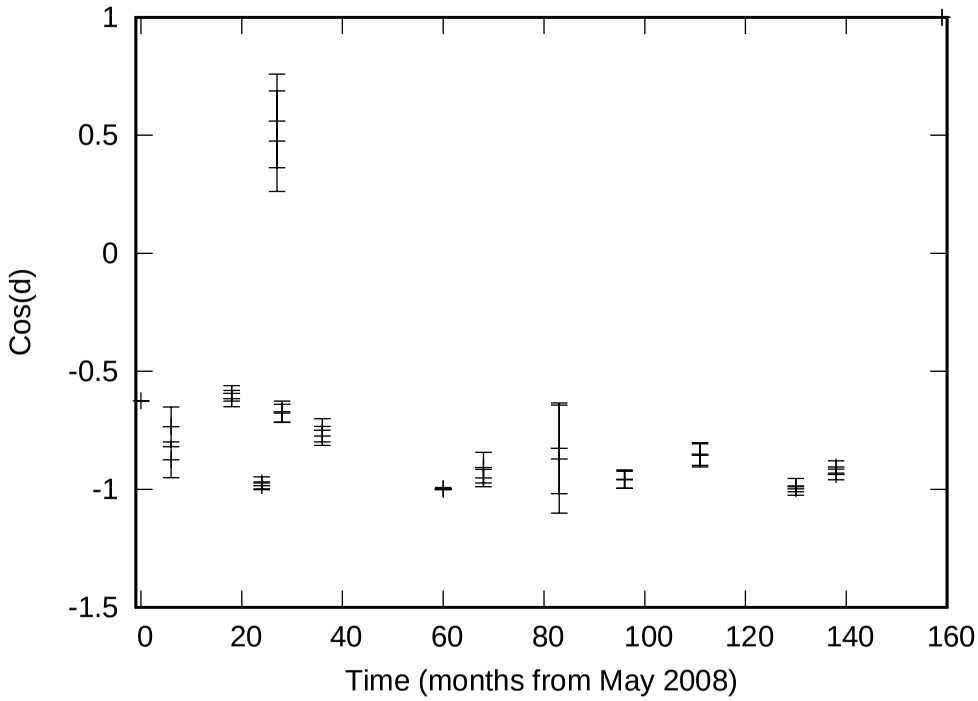

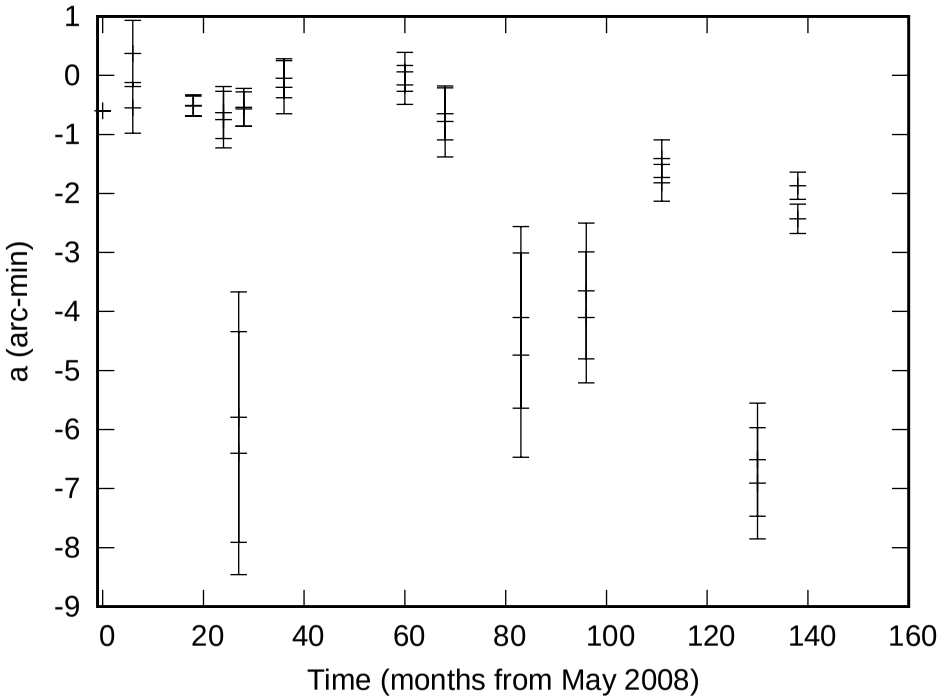

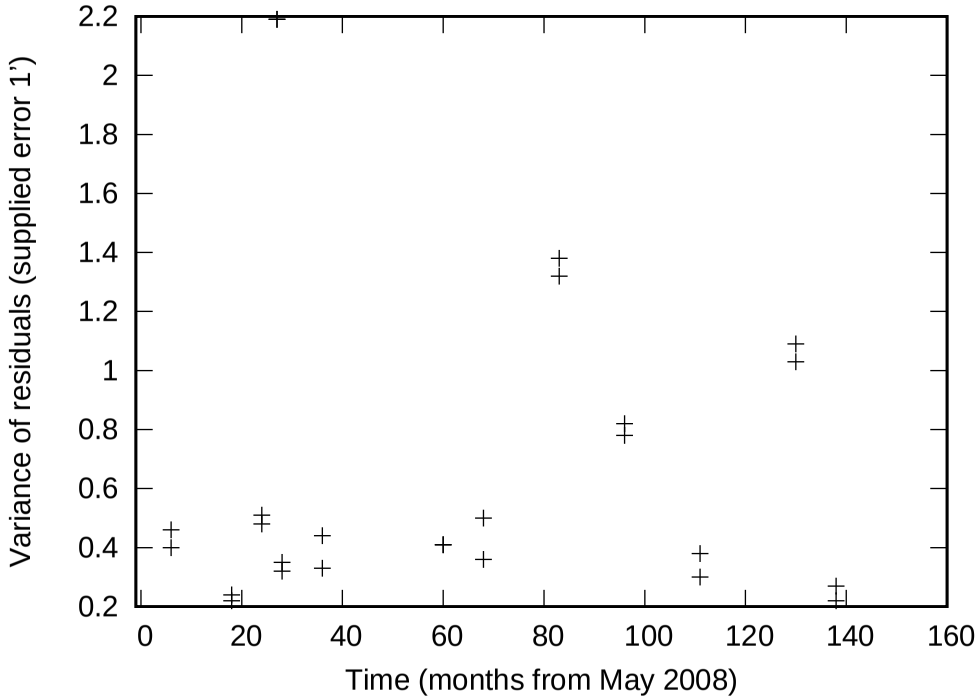

Fig. 2: C04 Elevation pointing coefficients

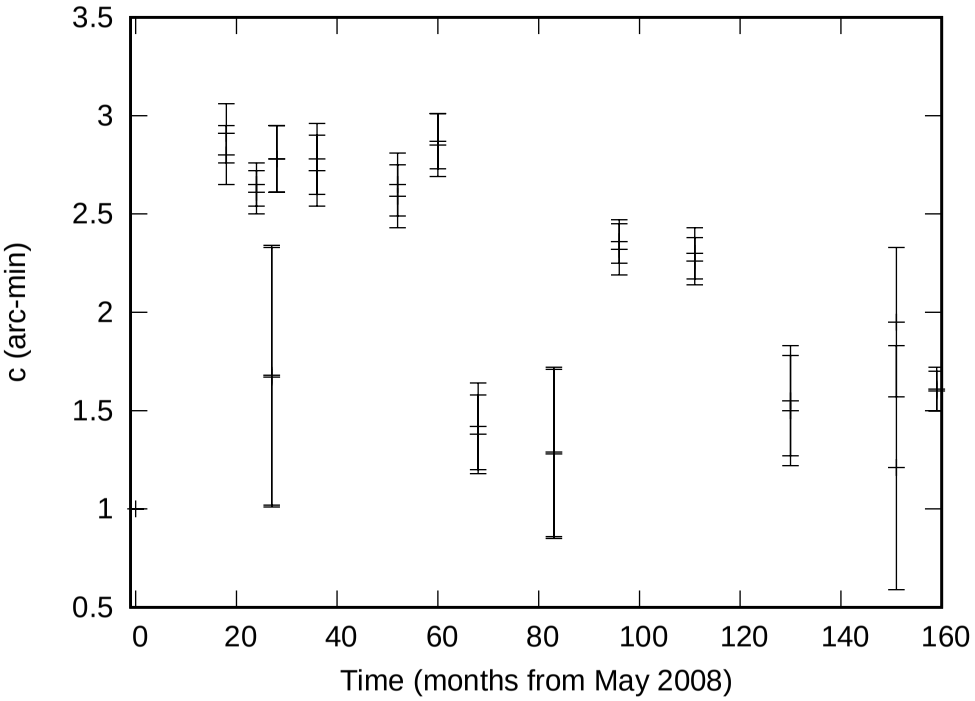

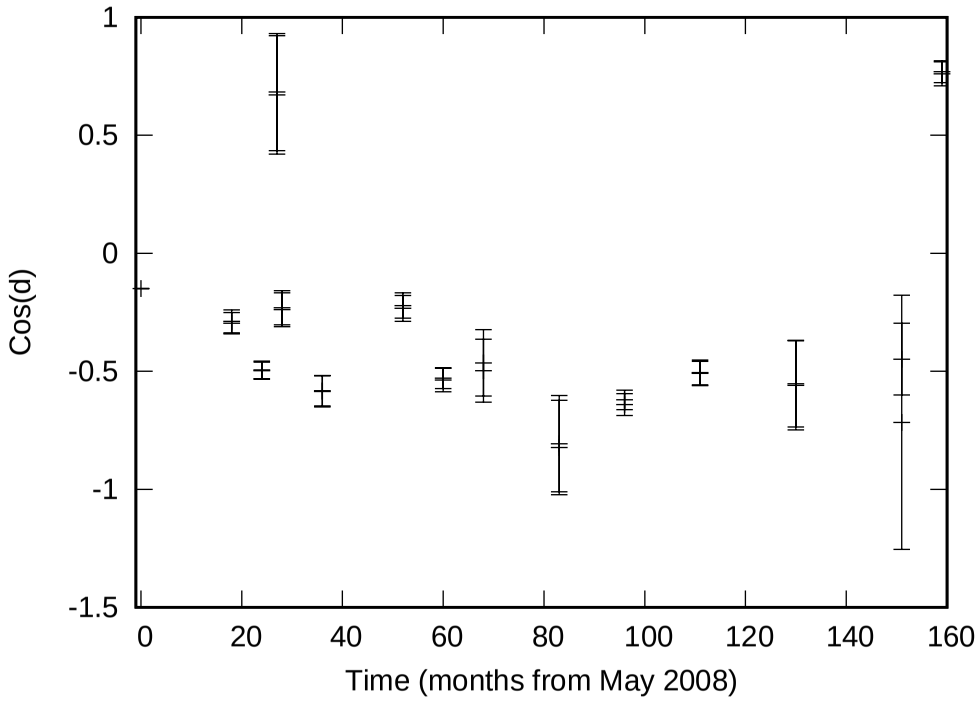

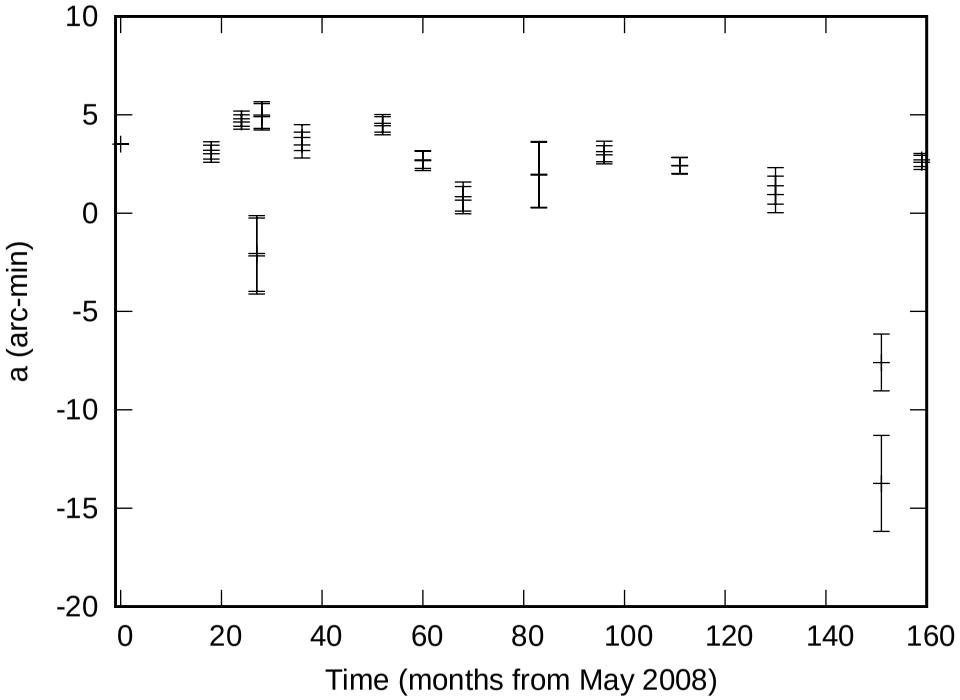

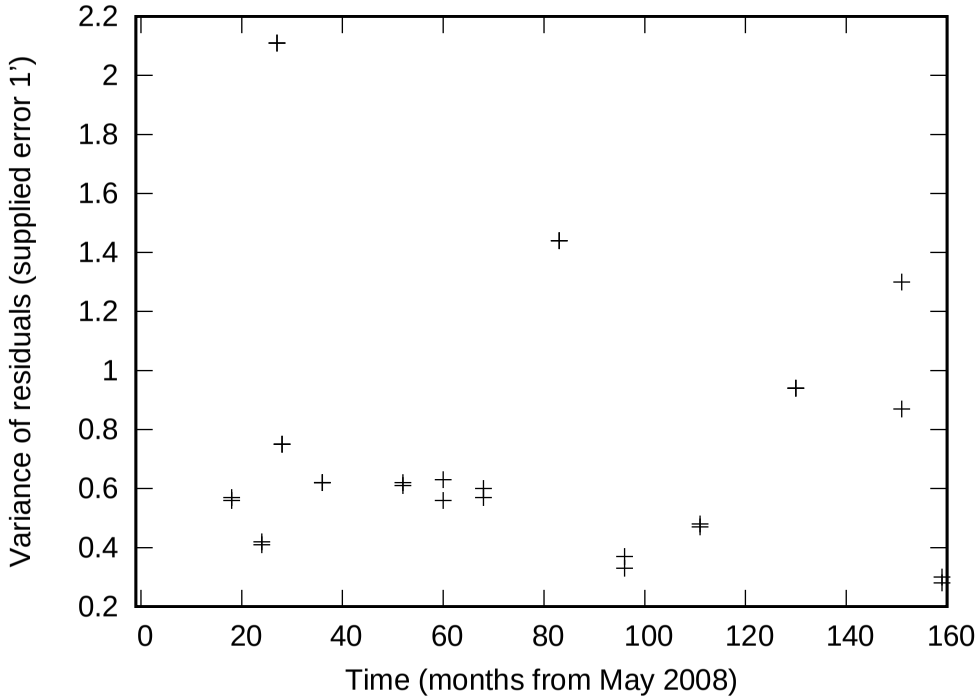

Fig. 2: C05 Elevation pointing coefficients

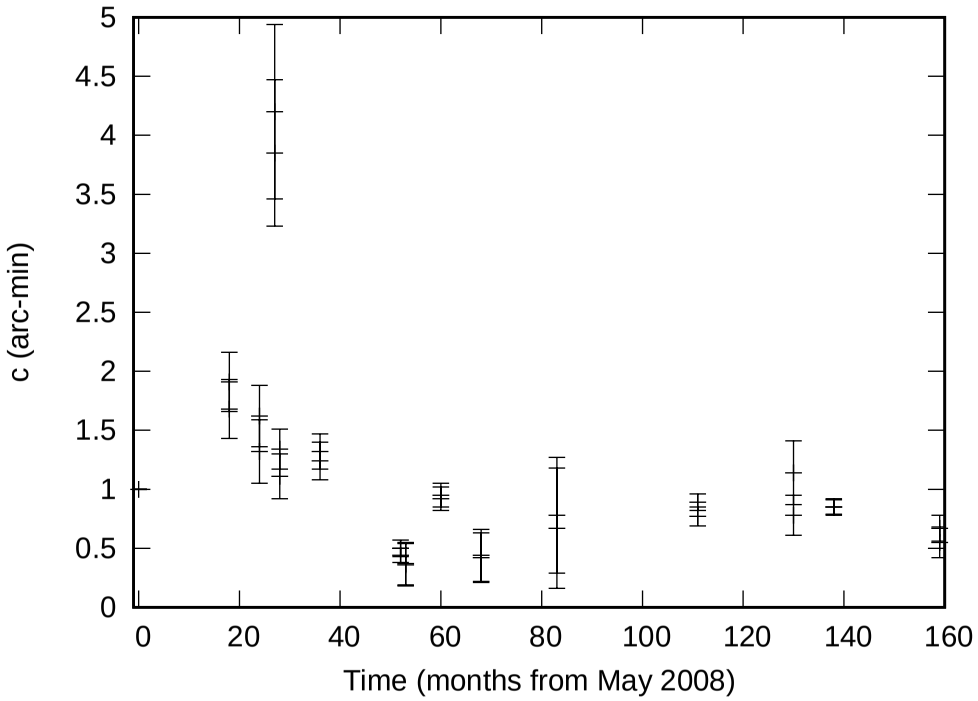

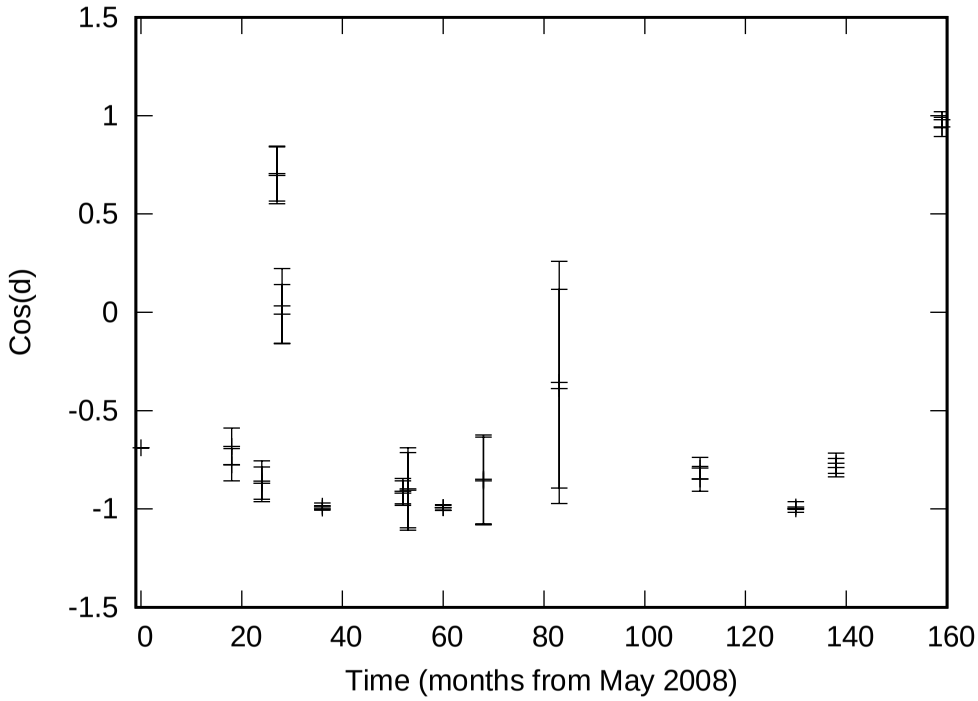

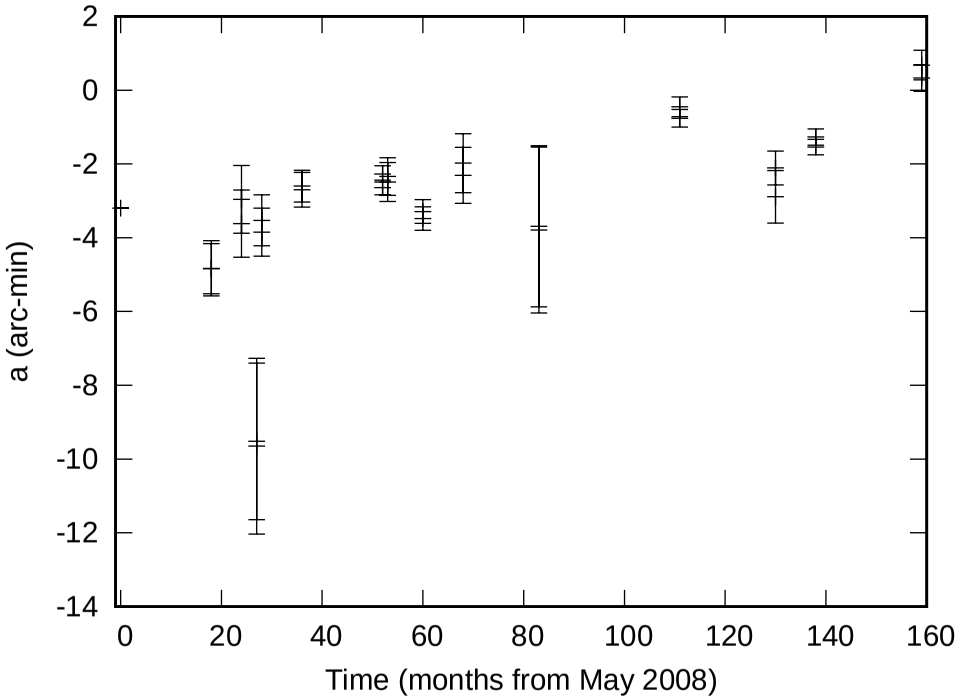

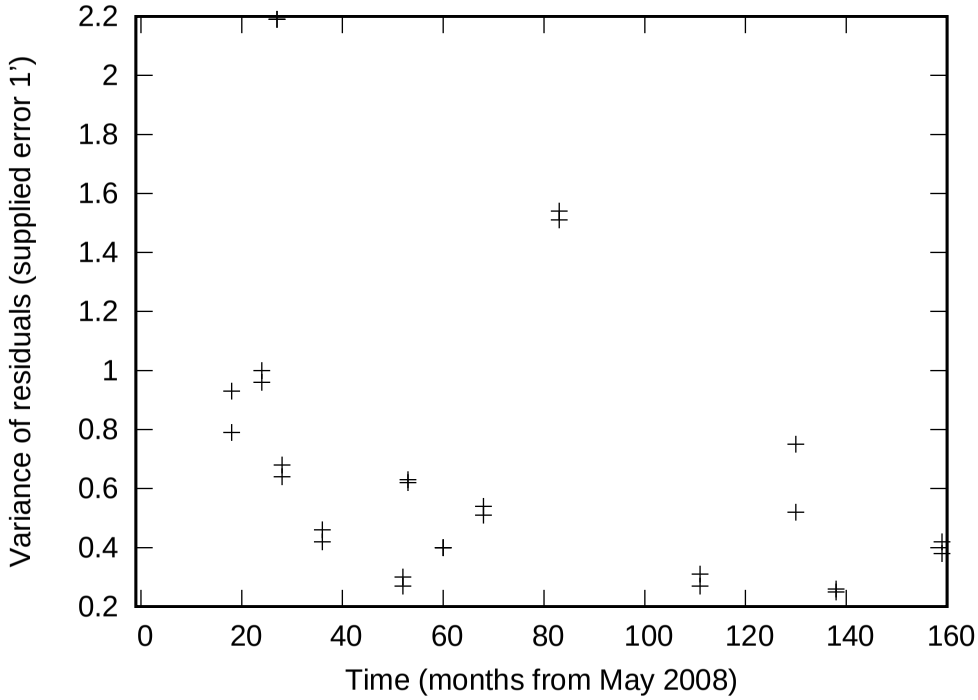

Fig. 2: C06 Elevation pointing coefficients

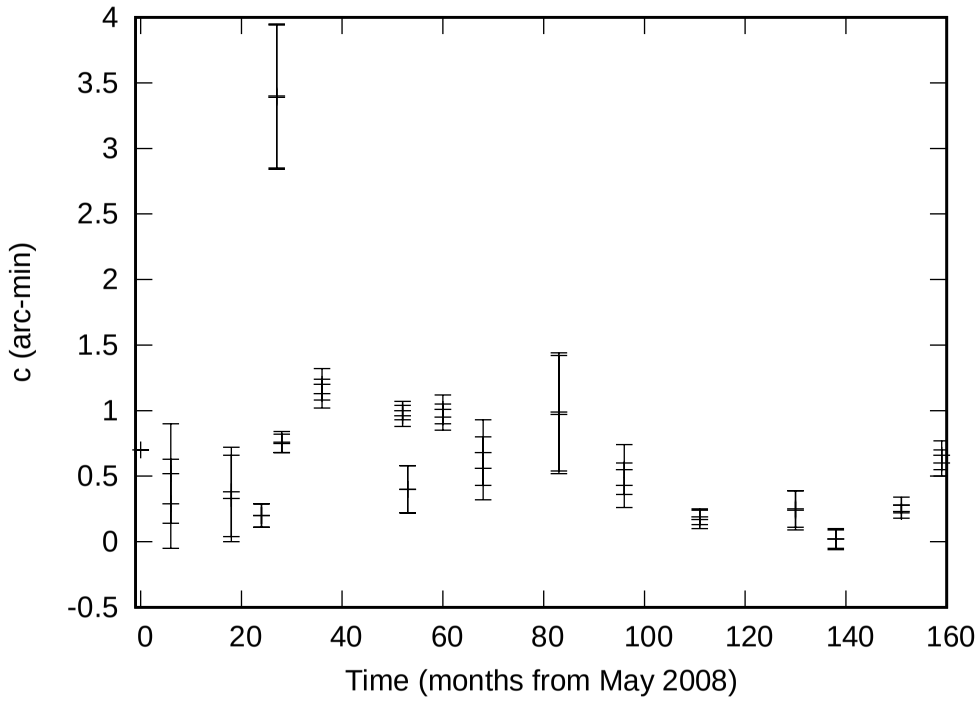

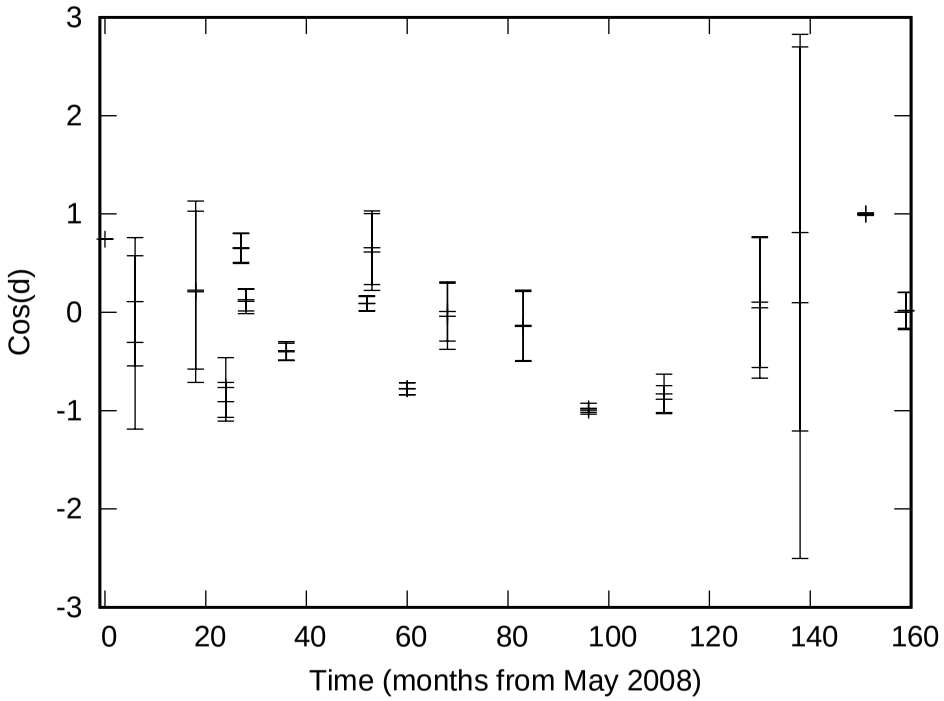

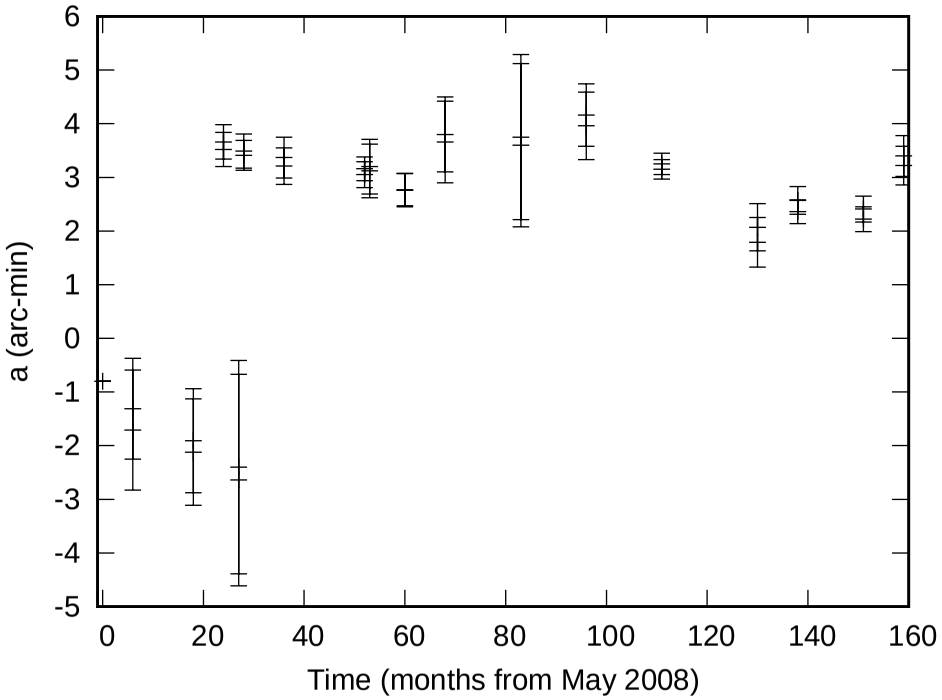

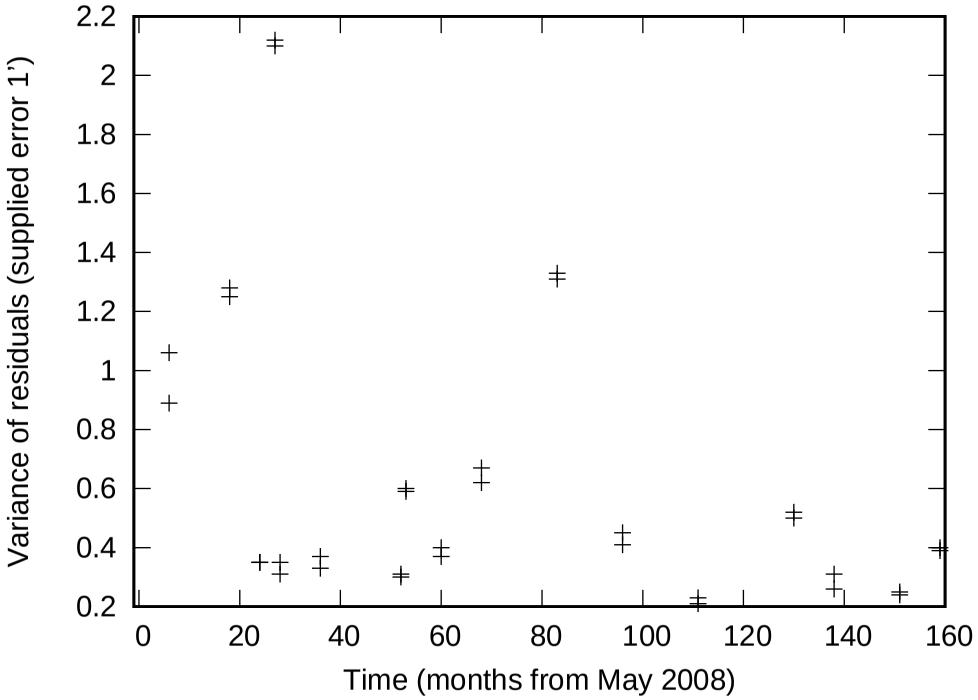

Fig. 2: C08 Elevation pointing coefficients

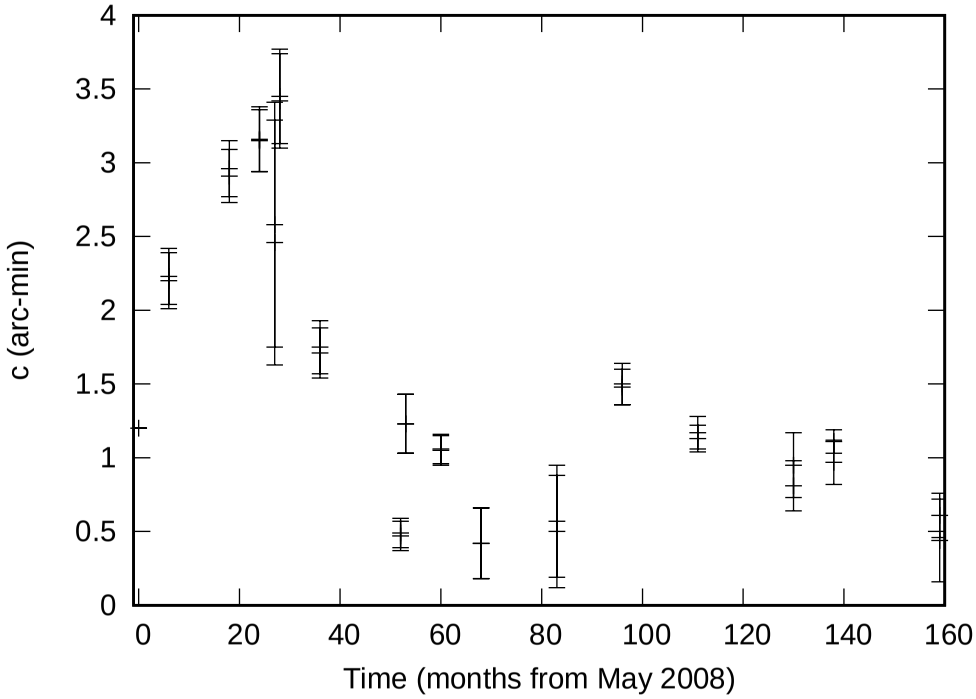

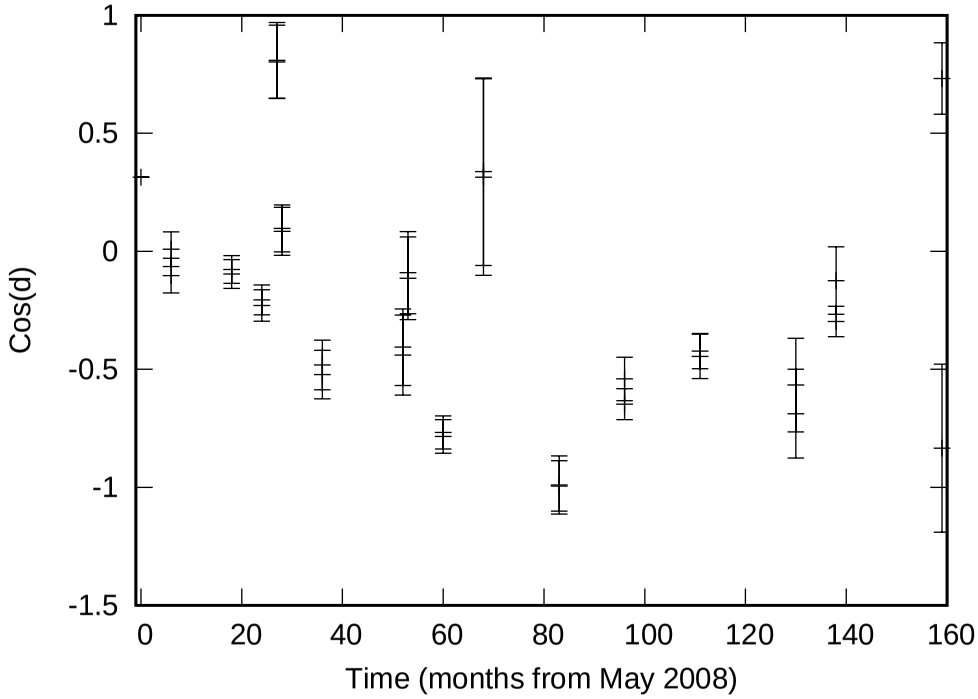

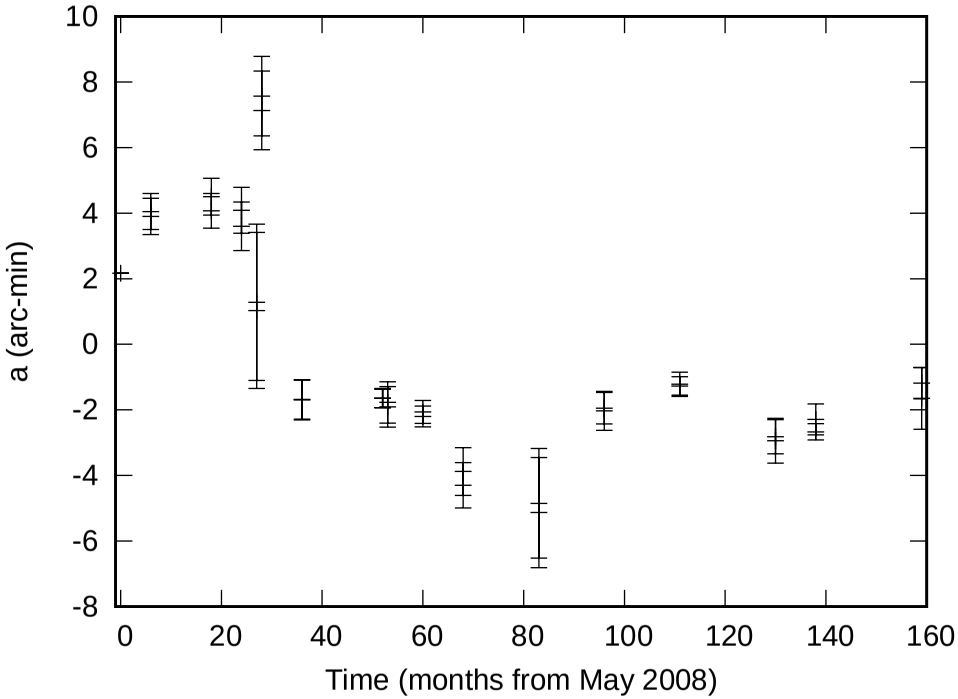

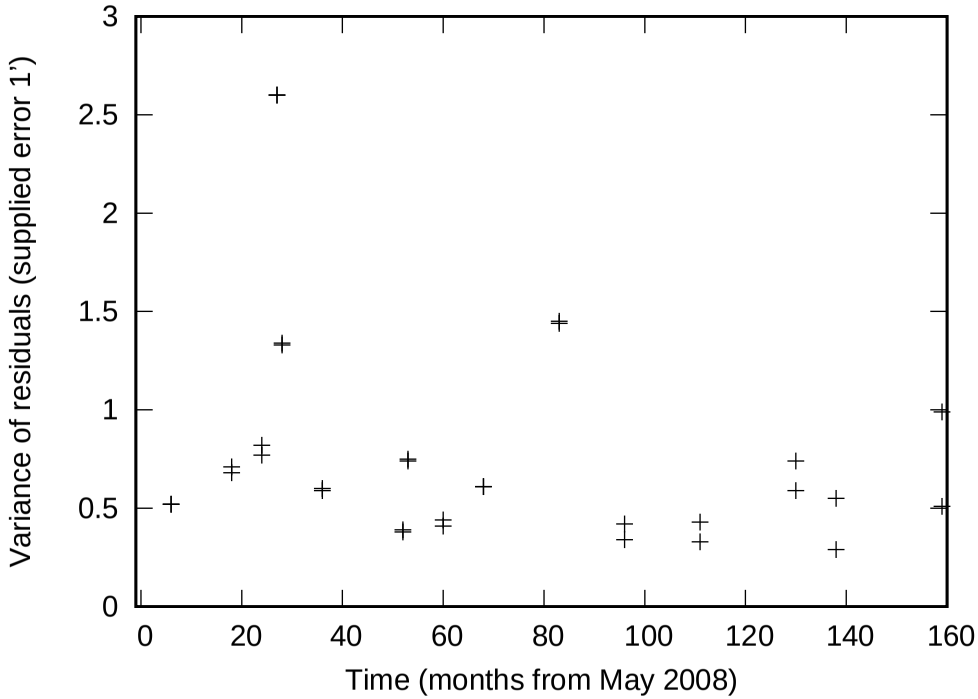

Fig. 2: C09 Elevation pointing coefficients

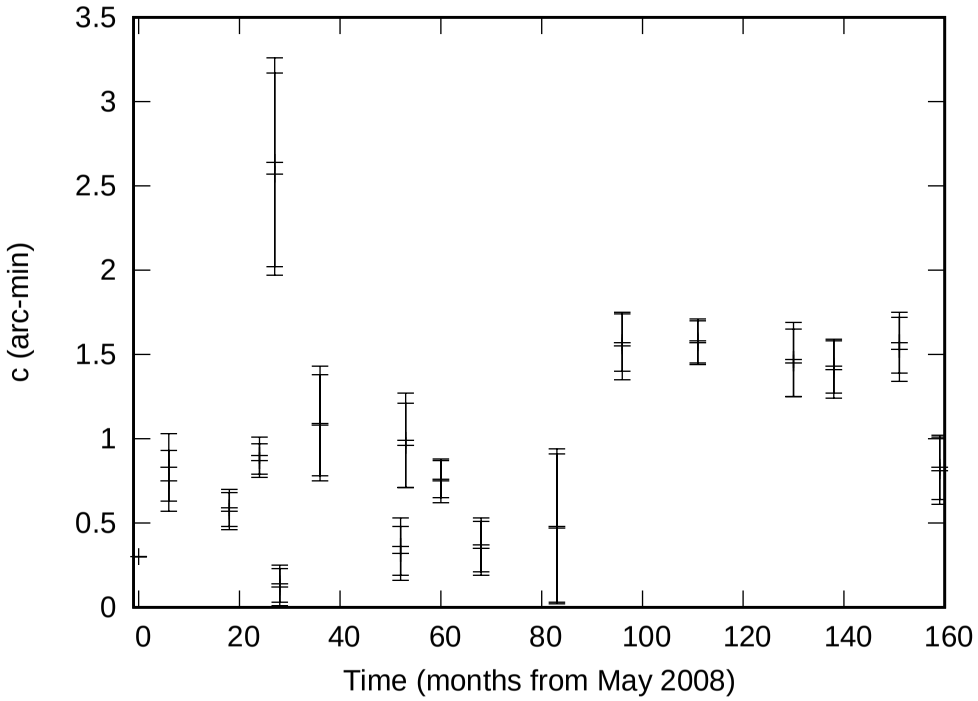

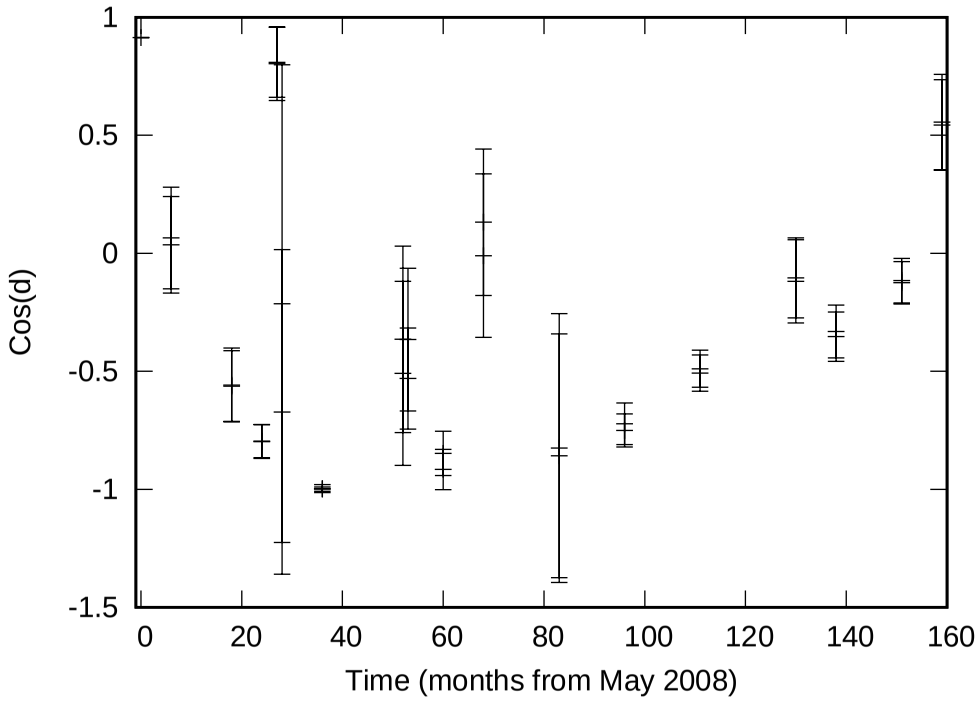

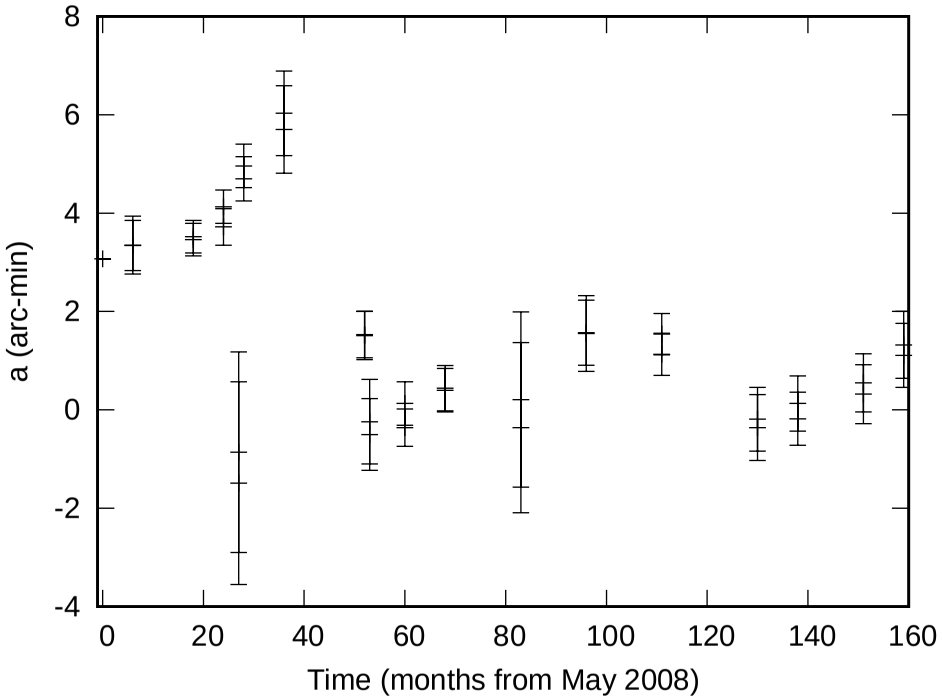

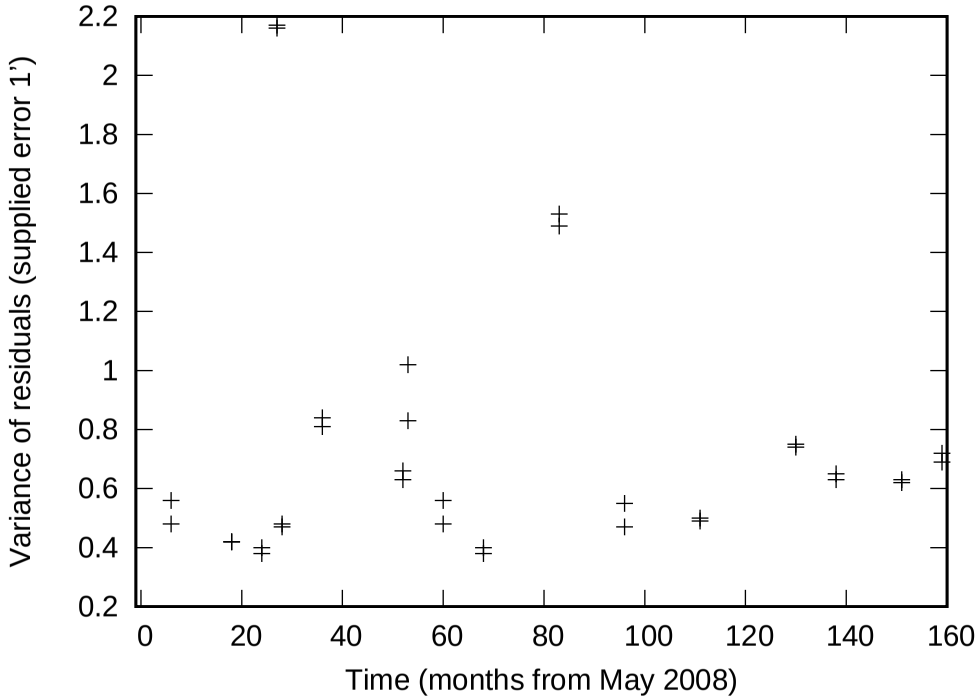

Fig. 2: C10 Elevation pointing coefficients

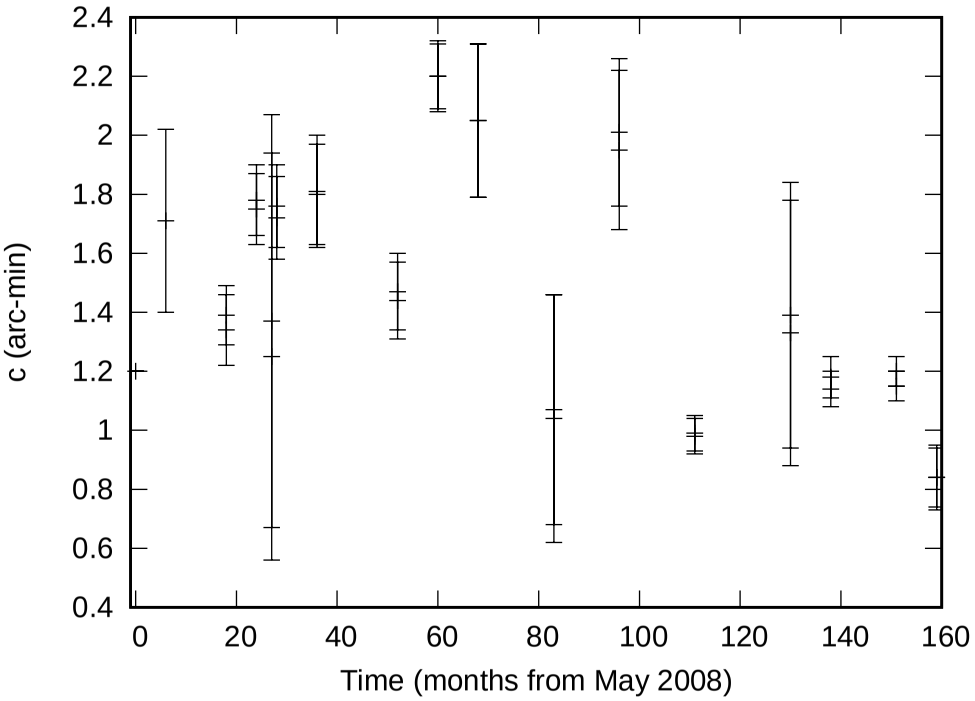

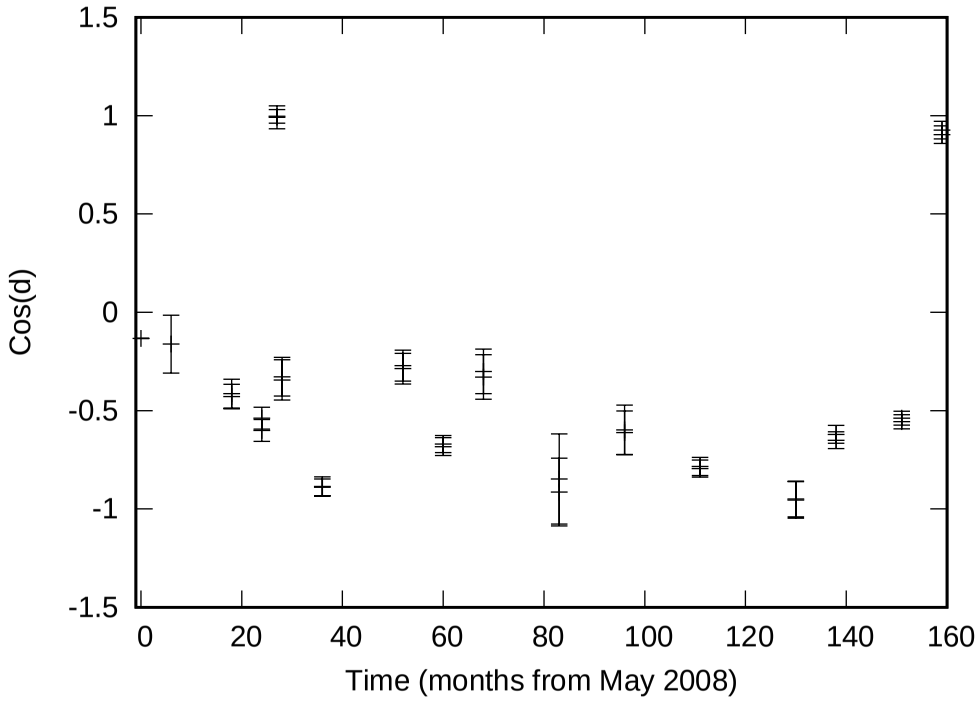

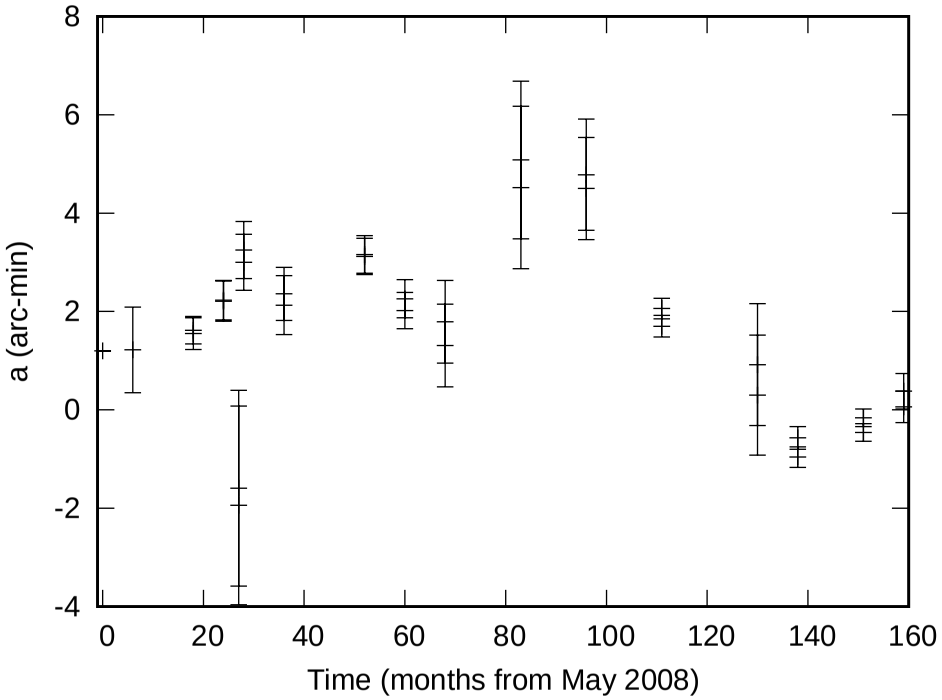

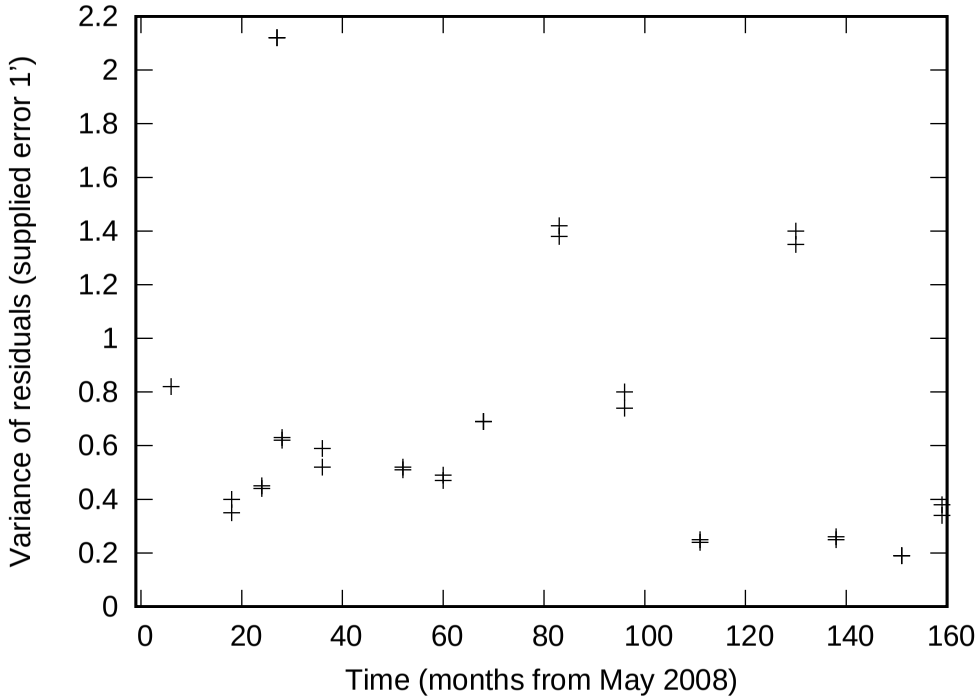

Fig. 2: C11 Elevation pointing coefficients

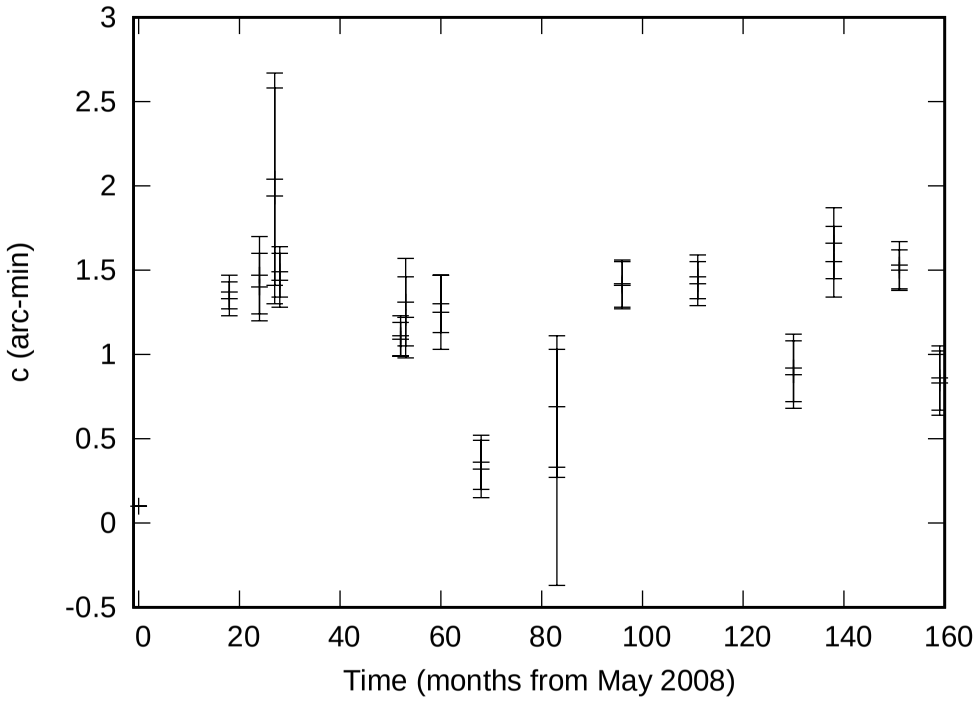

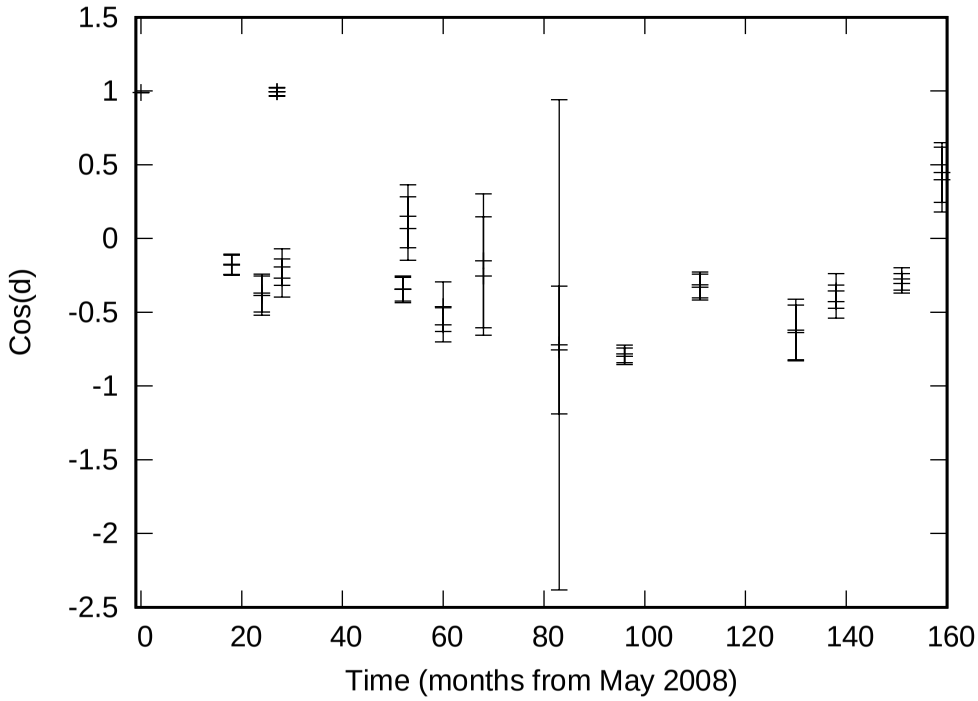

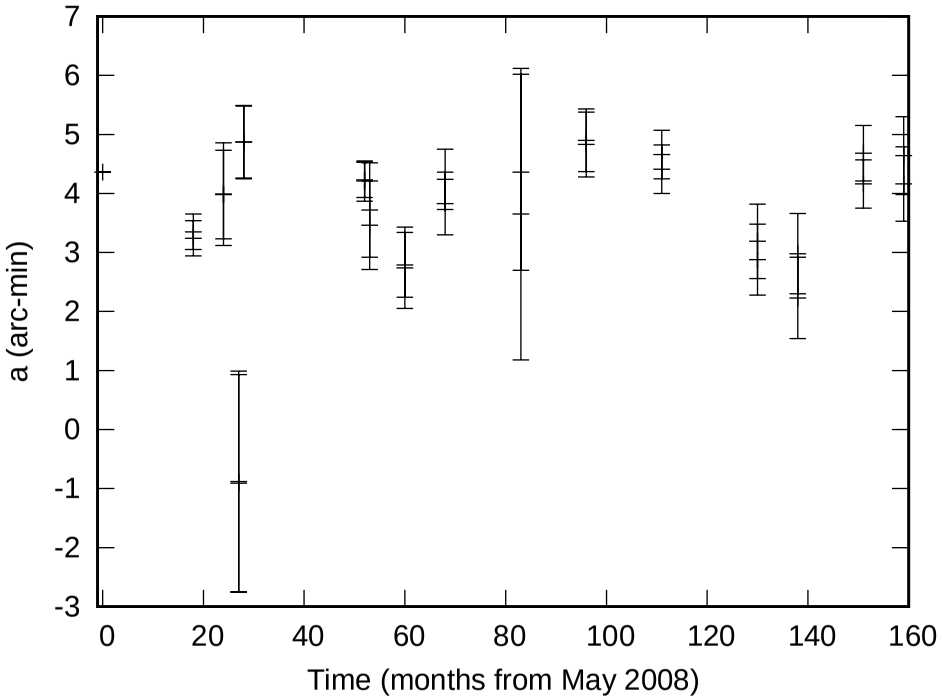

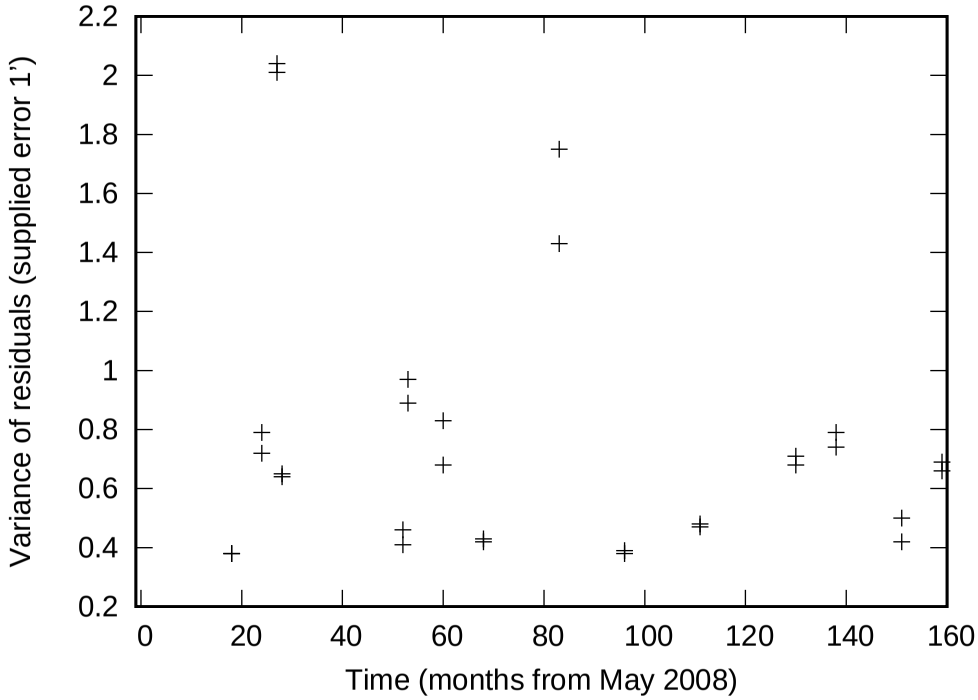

Fig. 2: C12 Elevation pointing coefficients

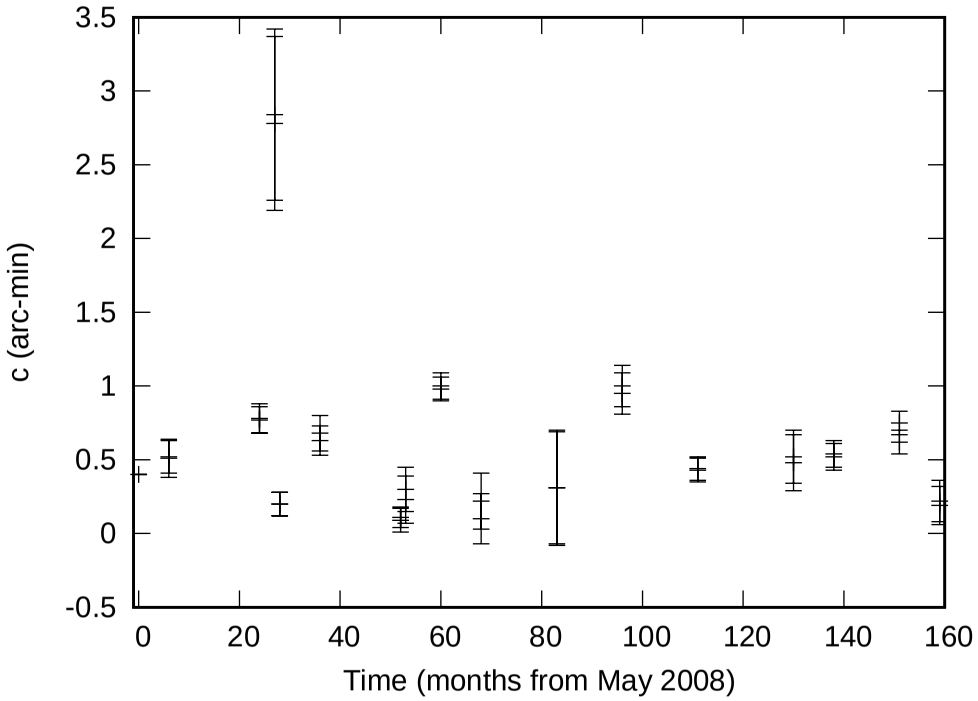

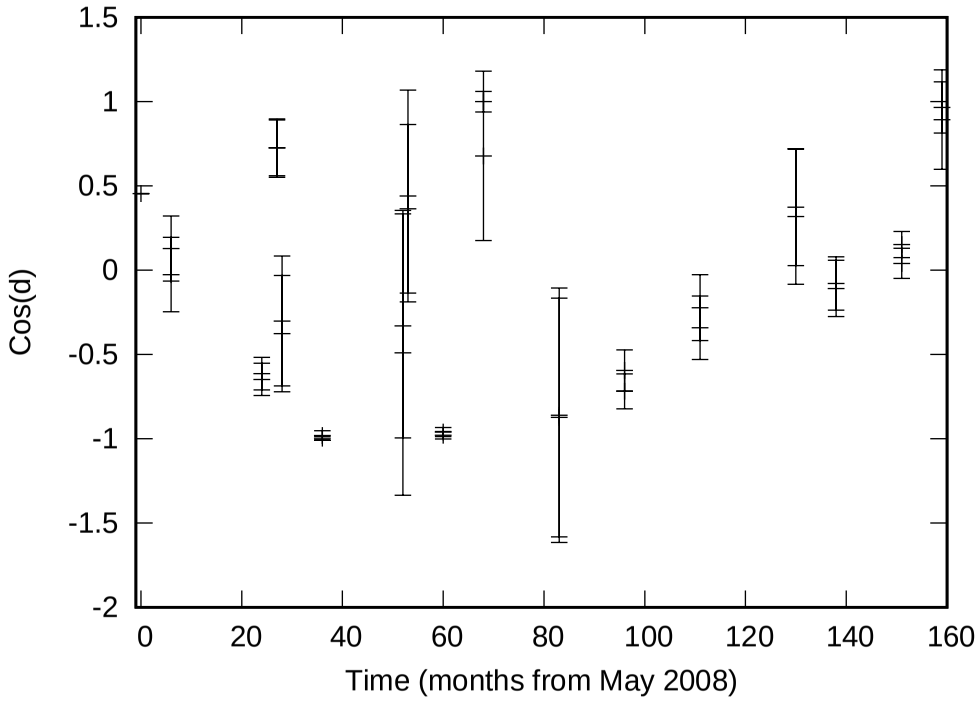

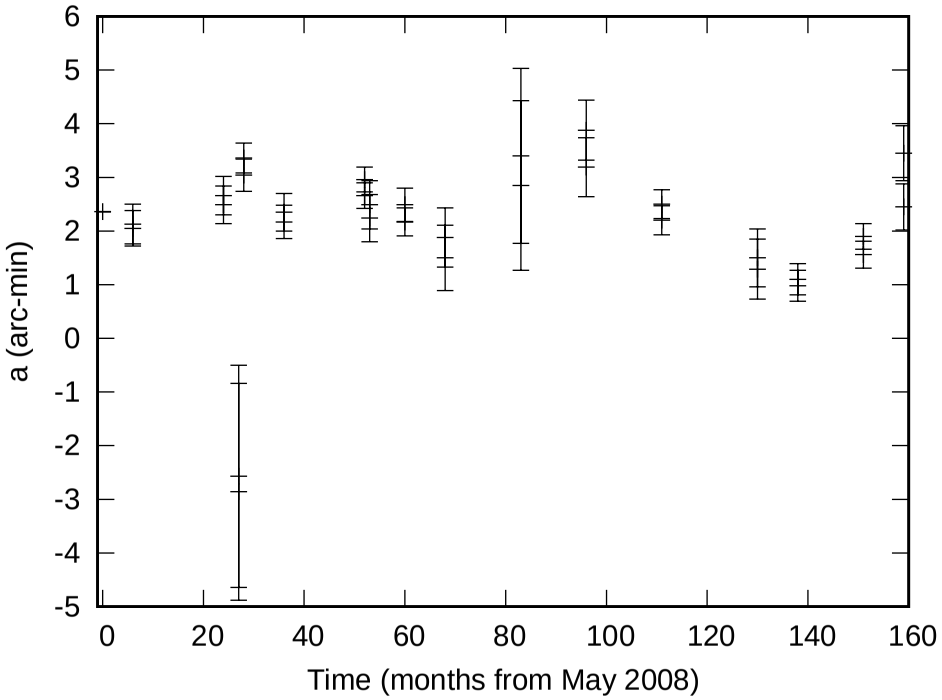

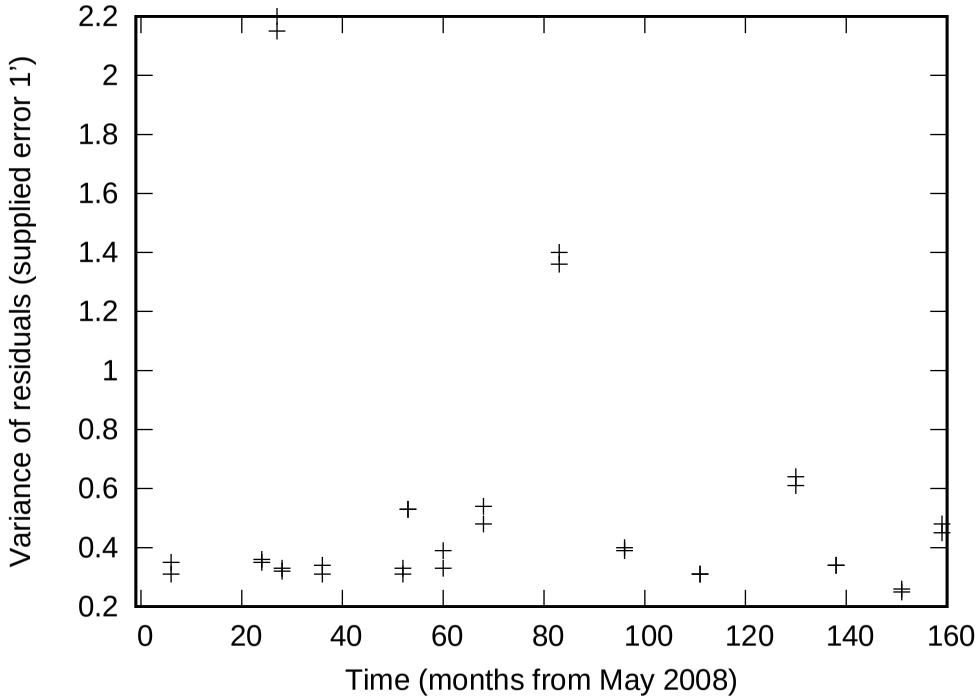

Fig. 2: C13 Elevation pointing coefficients

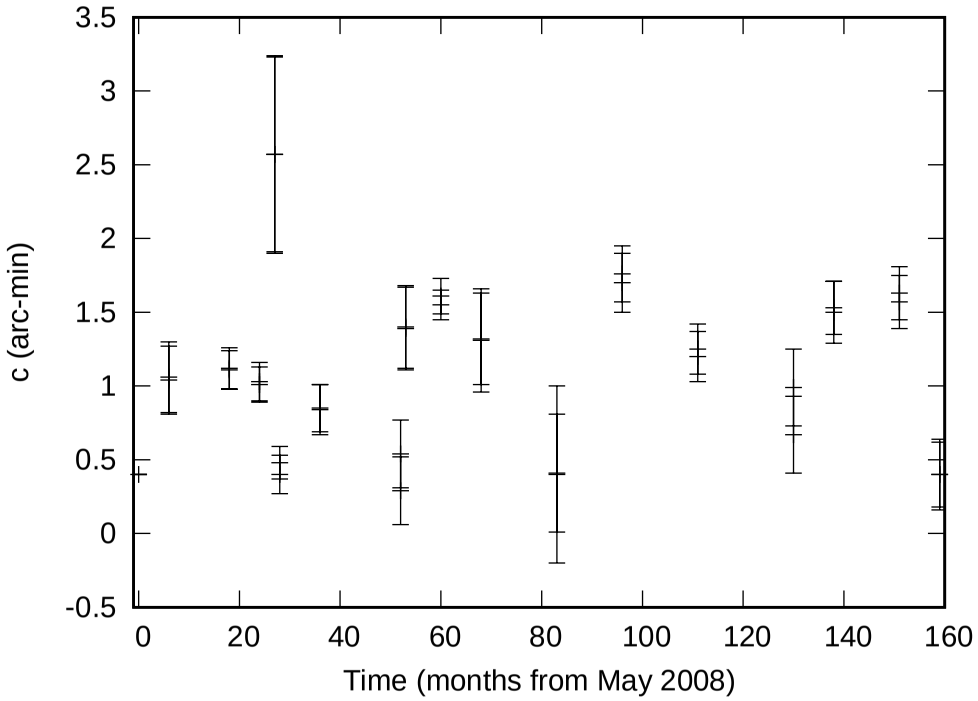

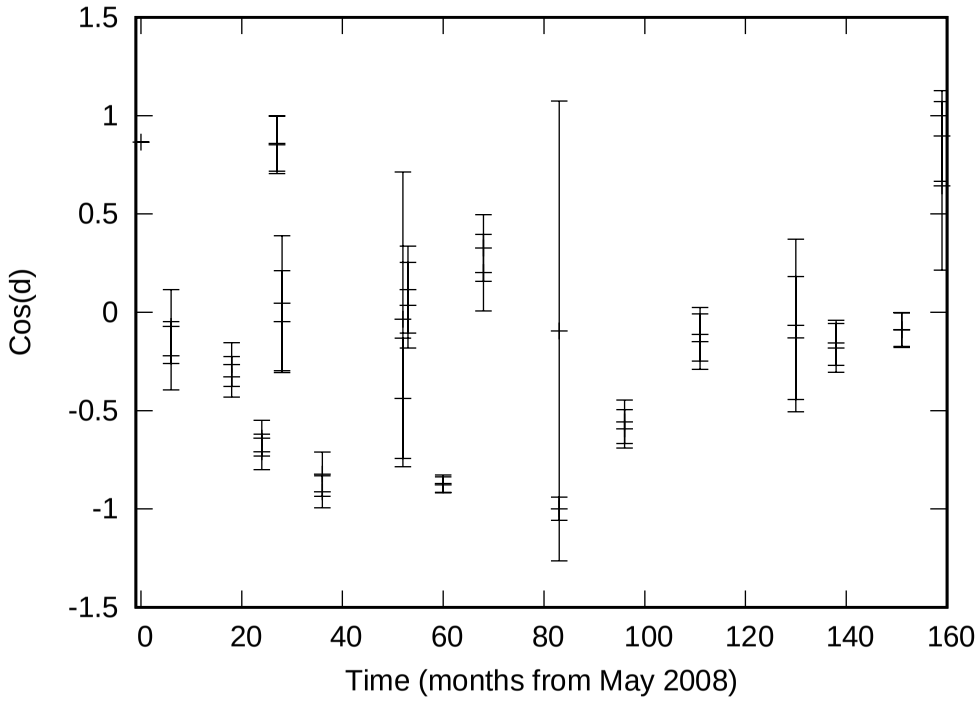

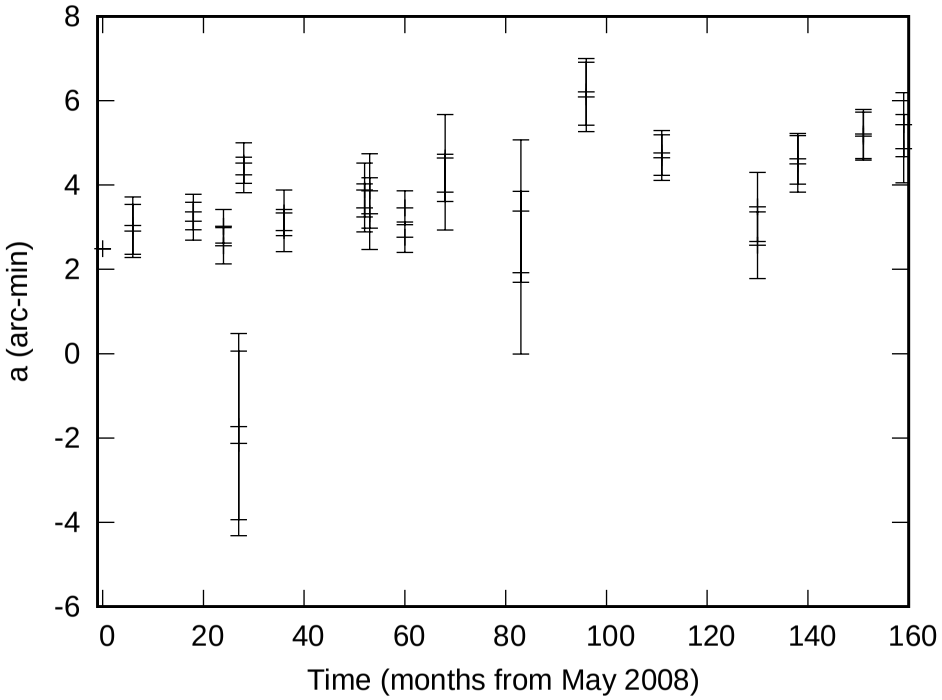

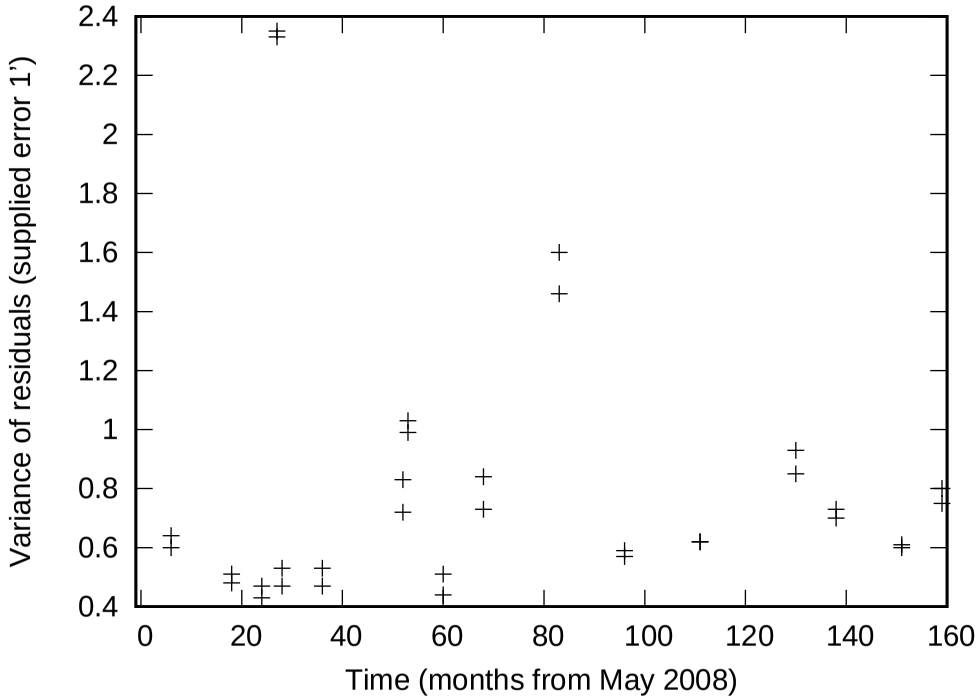

Fig. 2: C14 Elevation pointing coefficients

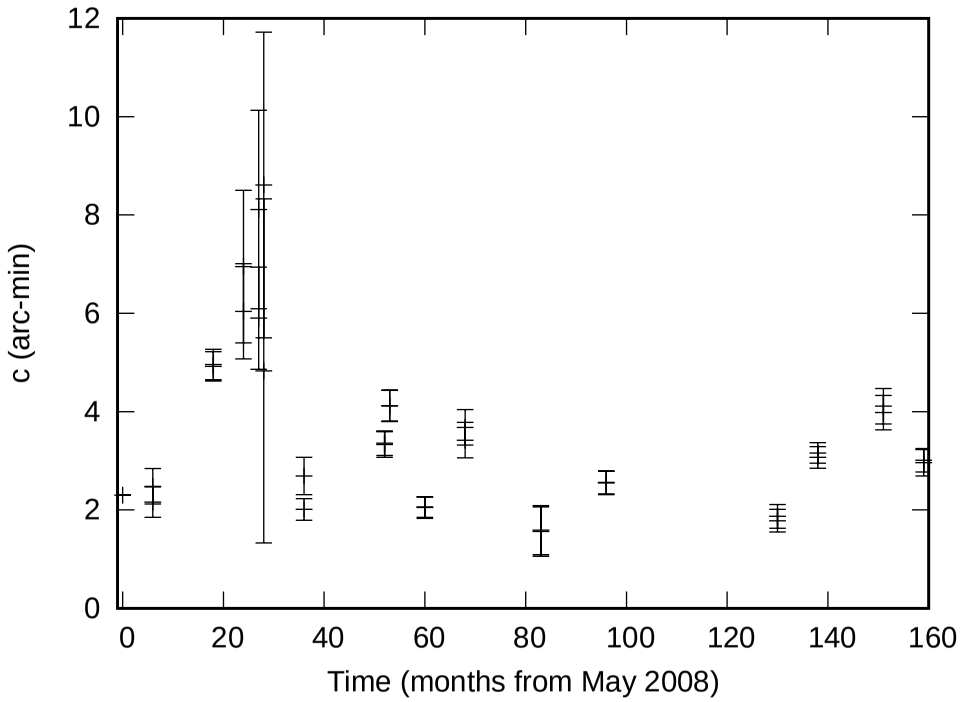

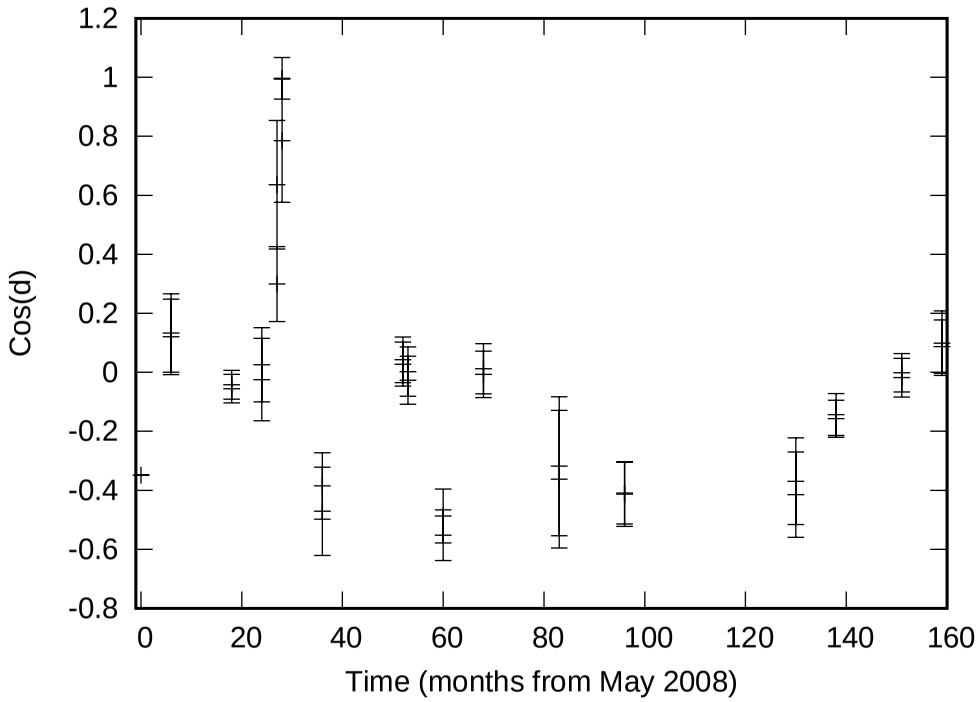

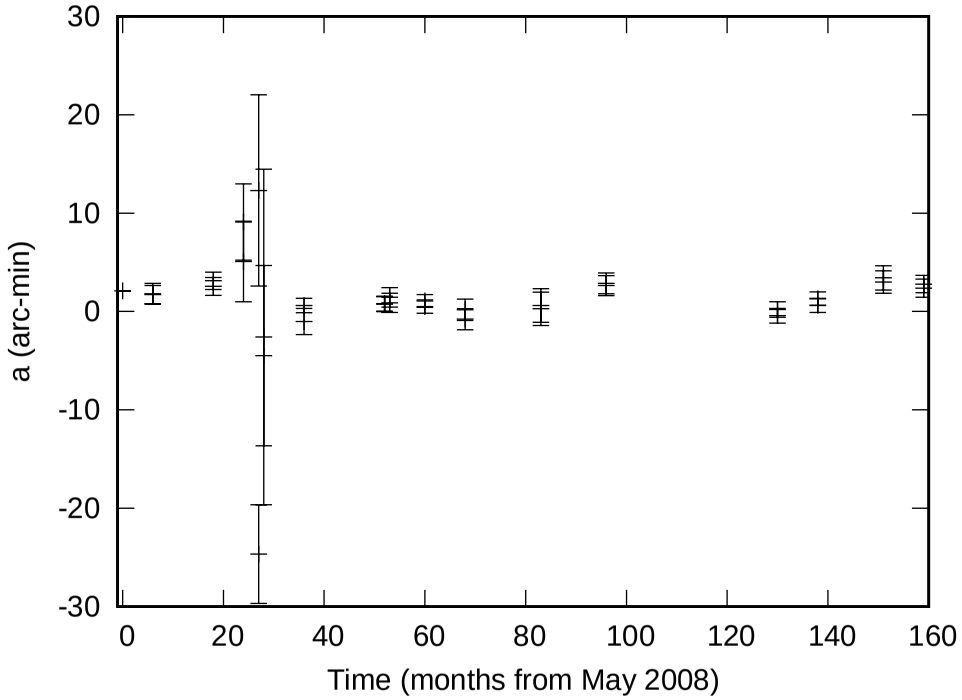

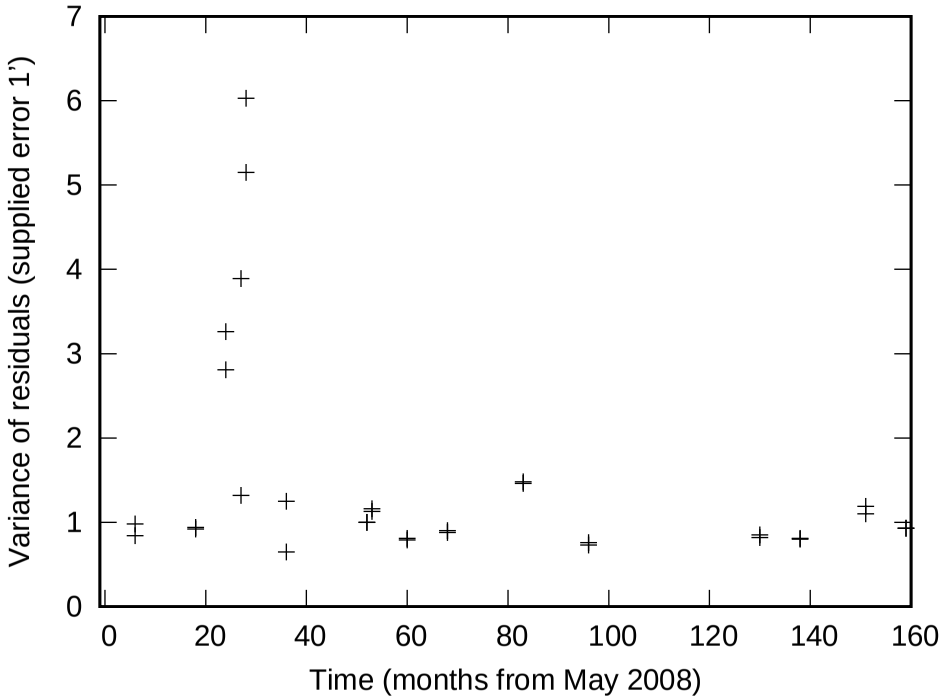

Fig. 2: E02 Elevation pointing coefficients

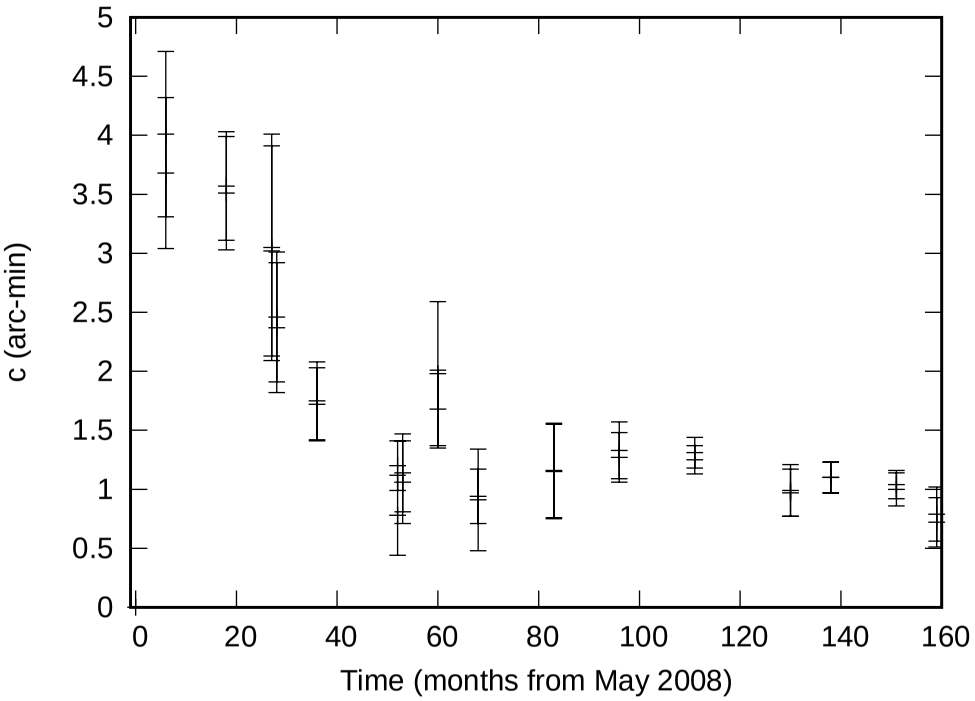

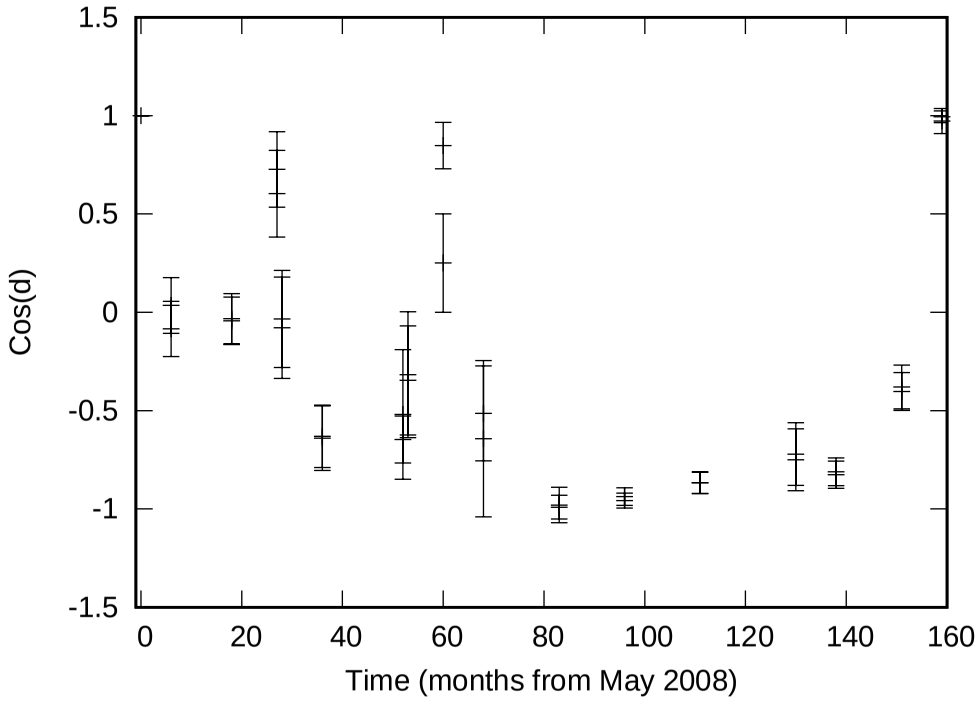

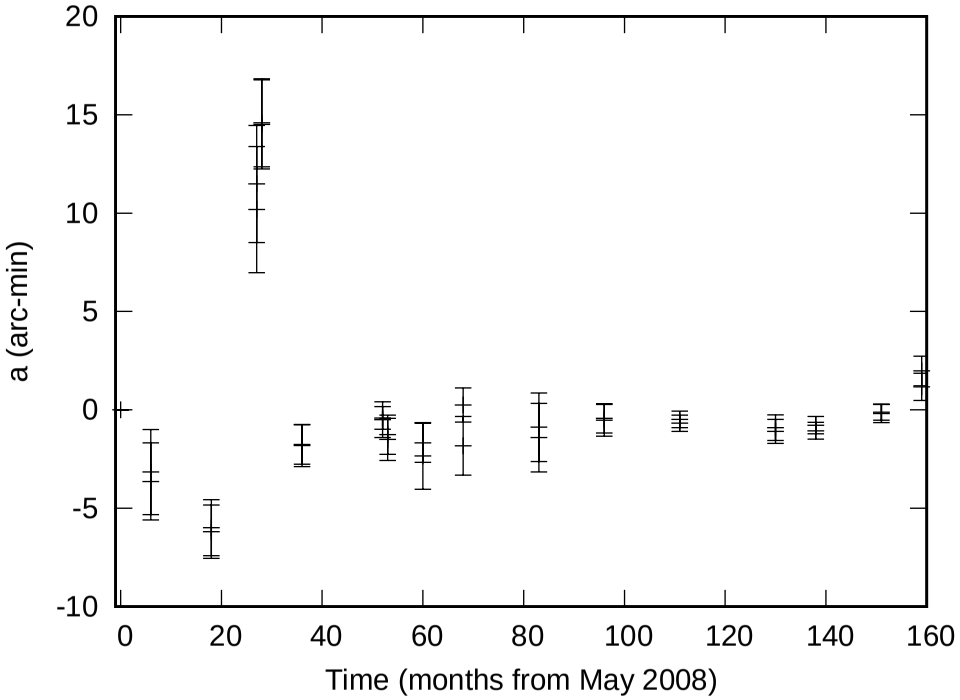

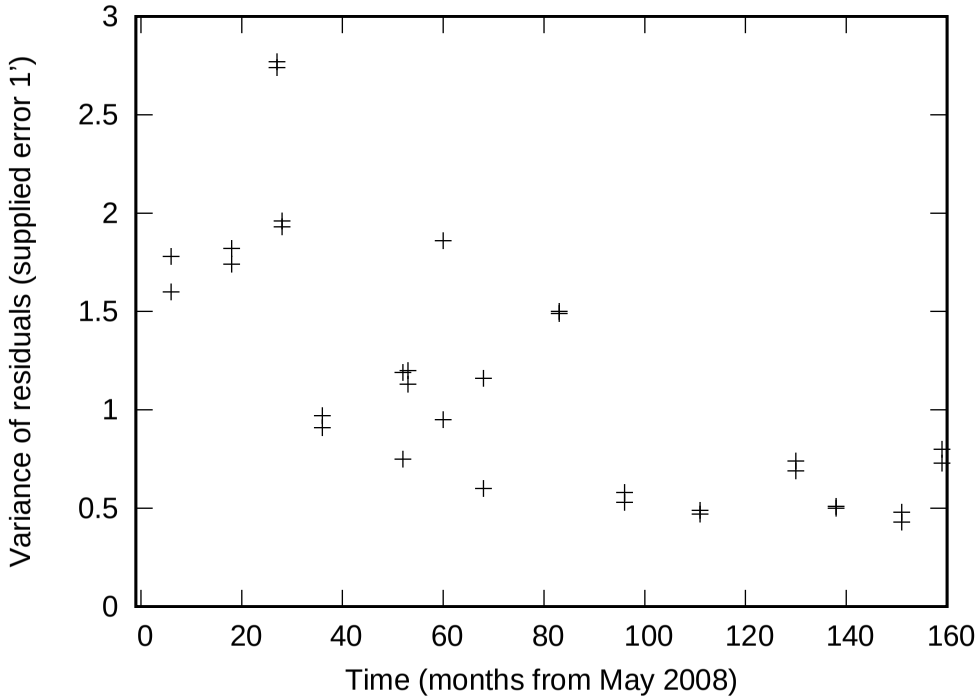

Fig. 2: E03 Elevation pointing coefficients

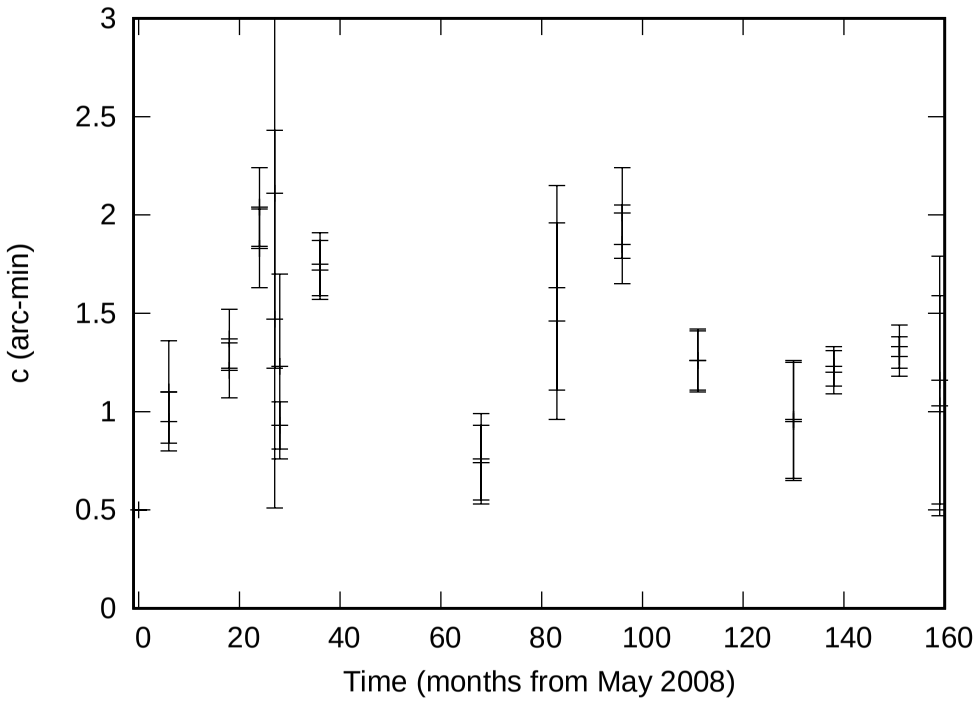

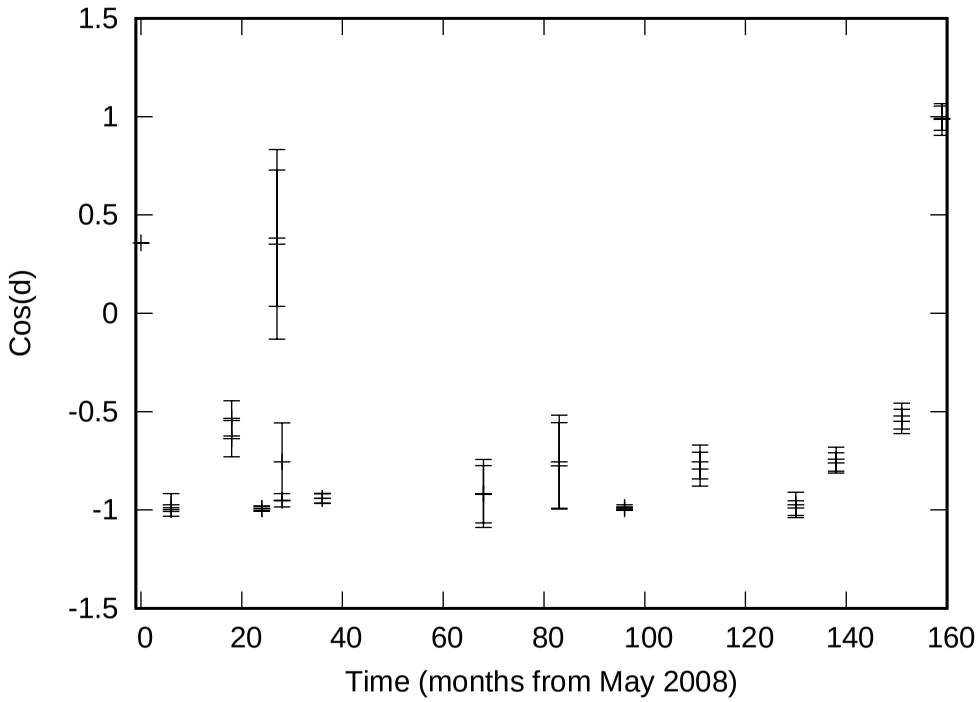

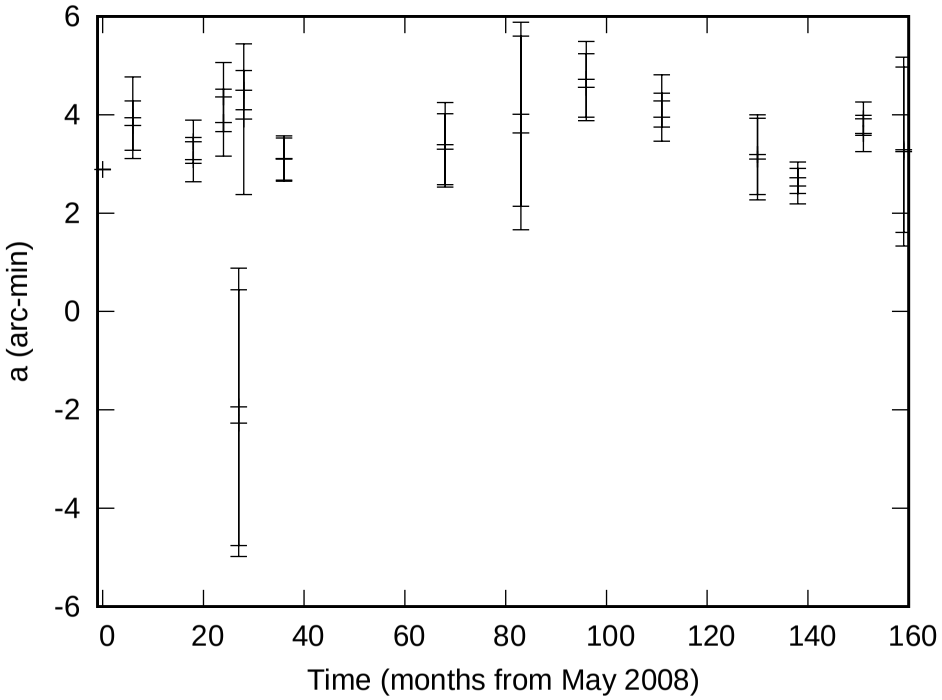

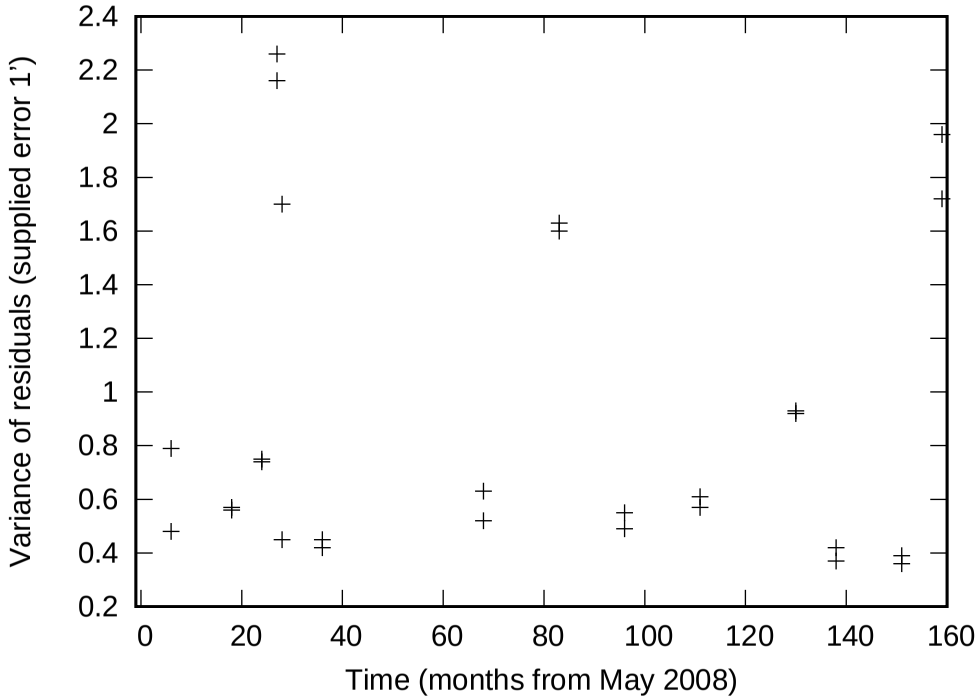

Fig. 2: E04 Elevation pointing coefficients

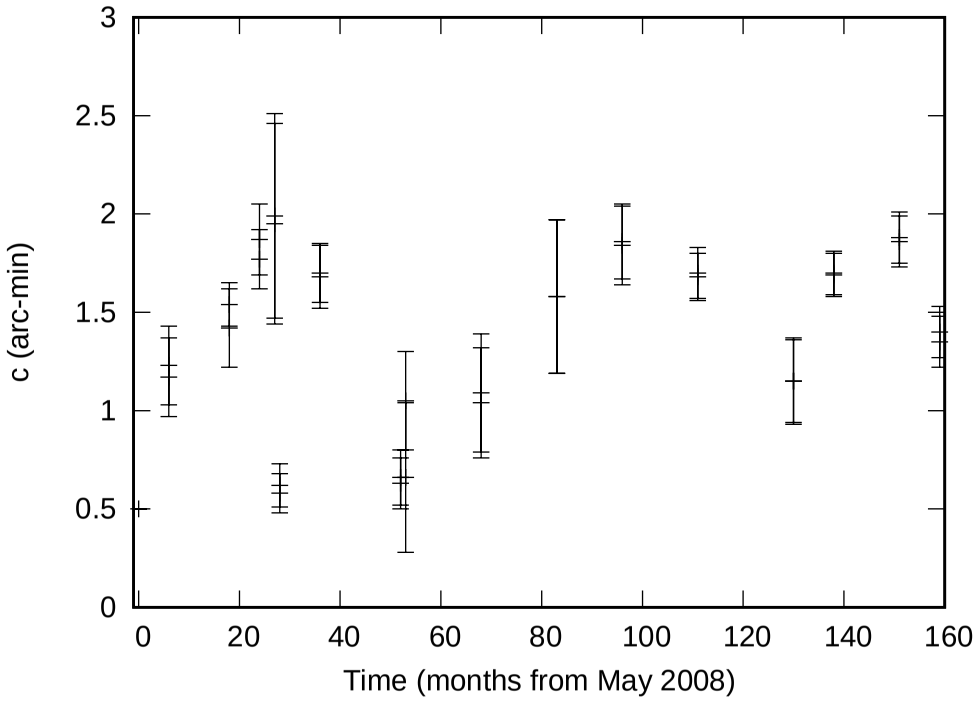

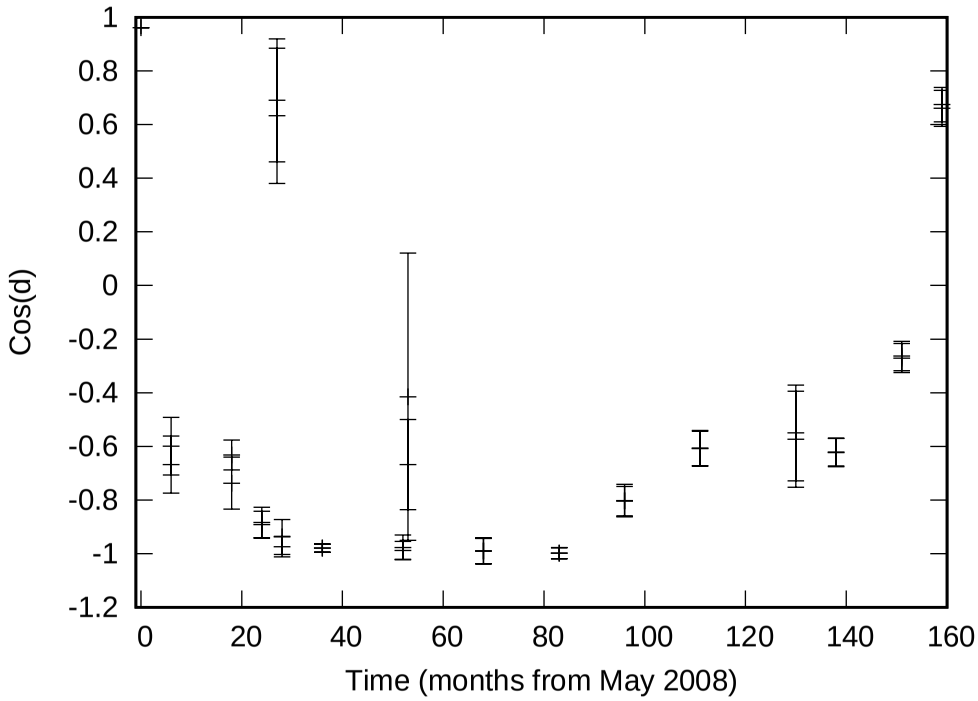

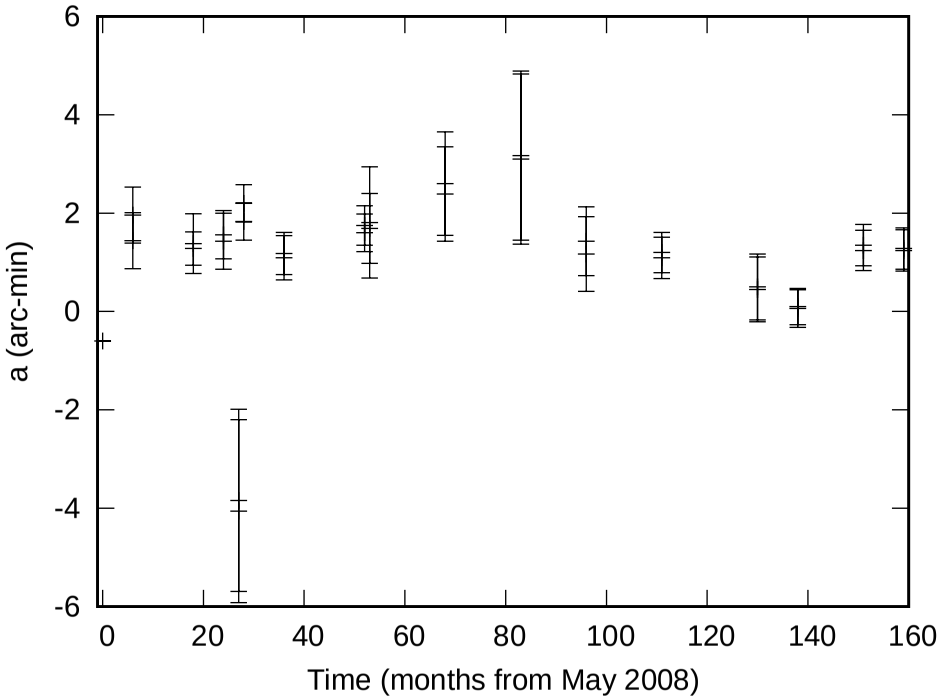

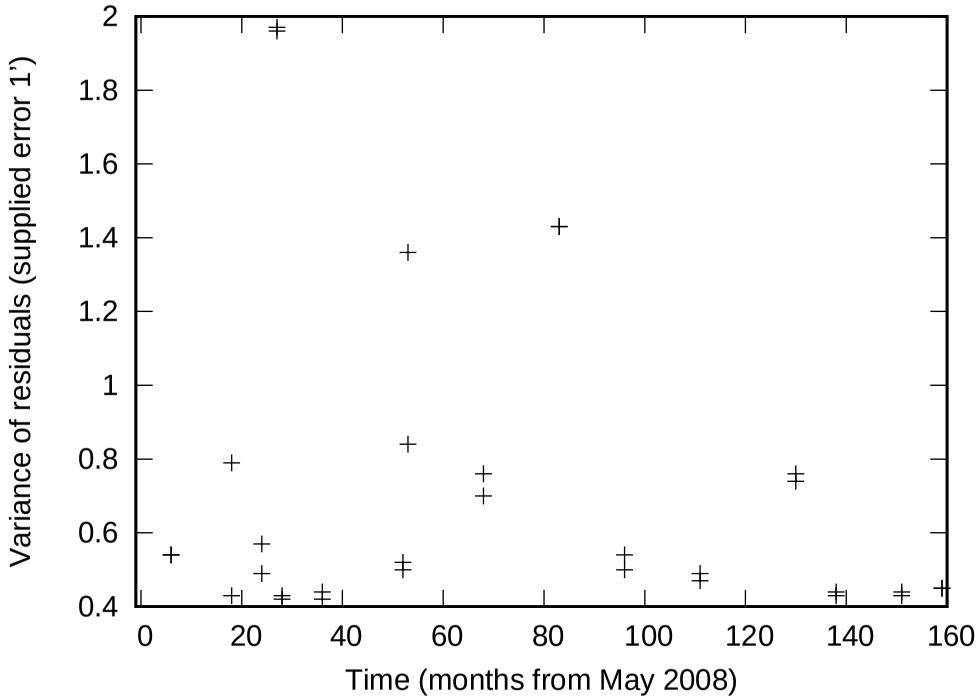

Fig. 2: E05 Elevation pointing coefficients

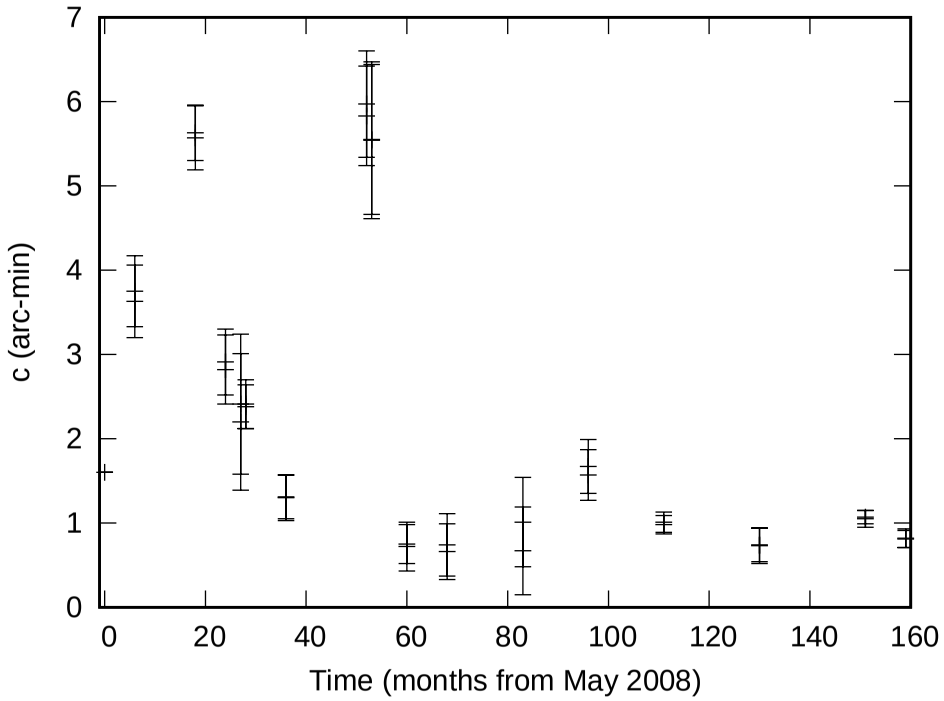

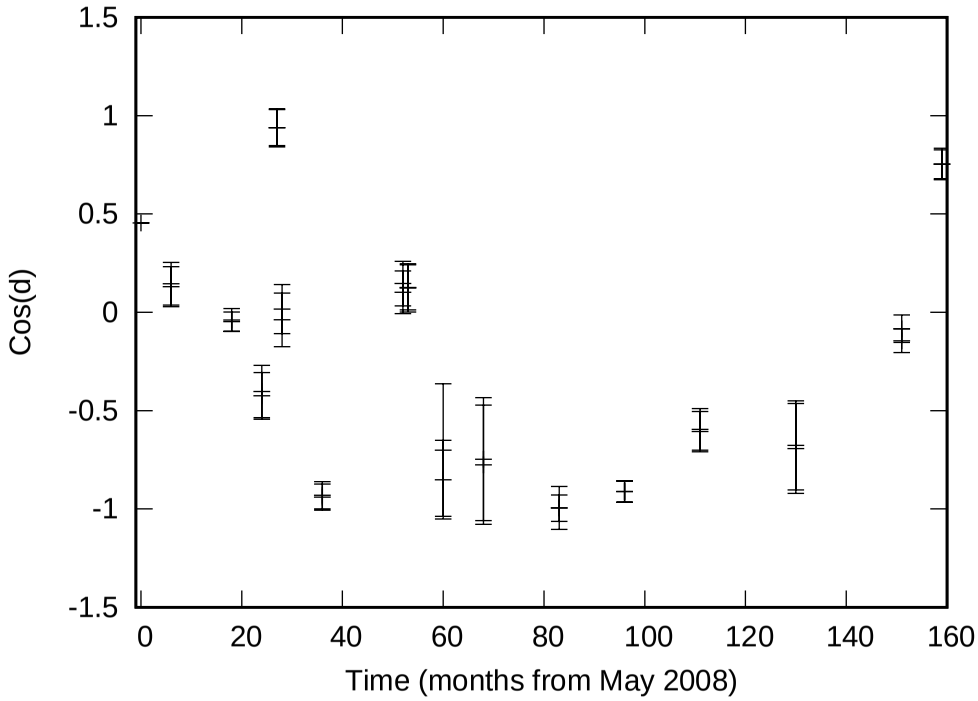

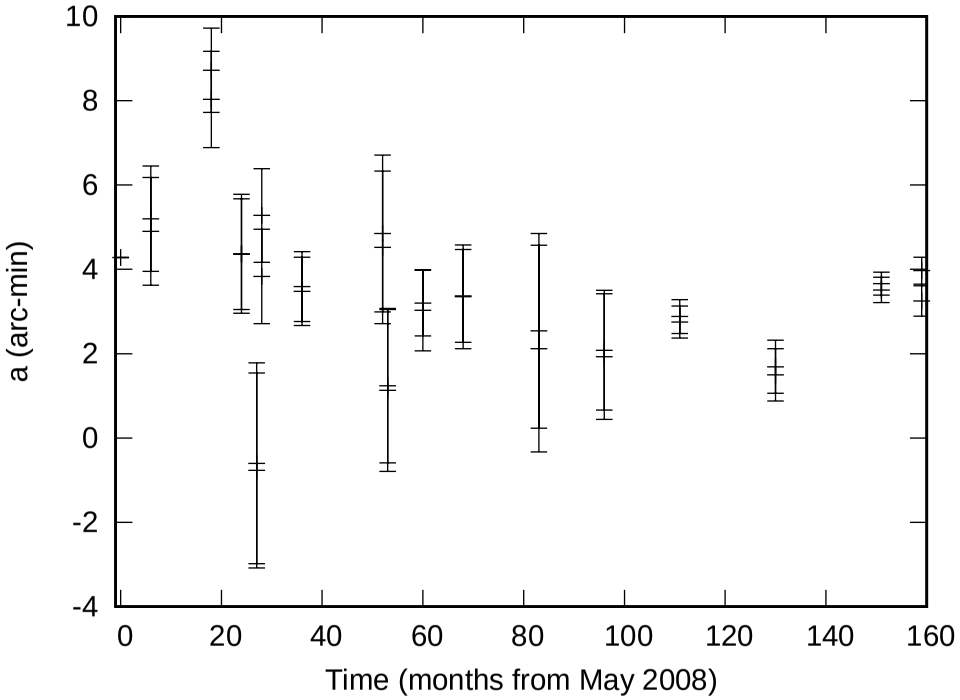

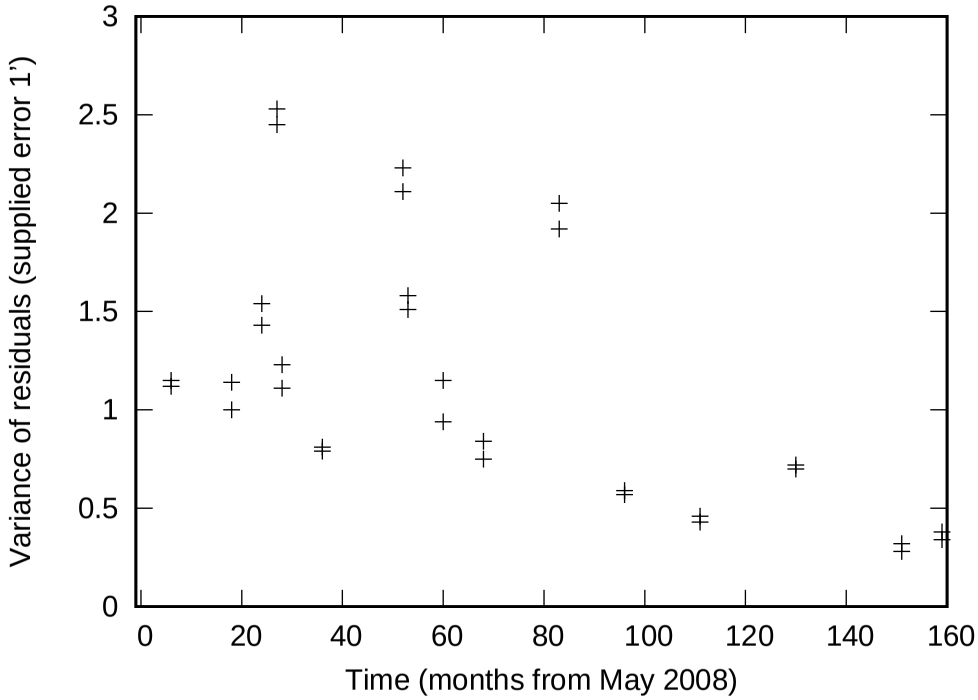

Fig. 2: E06 Elevation pointing coefficients

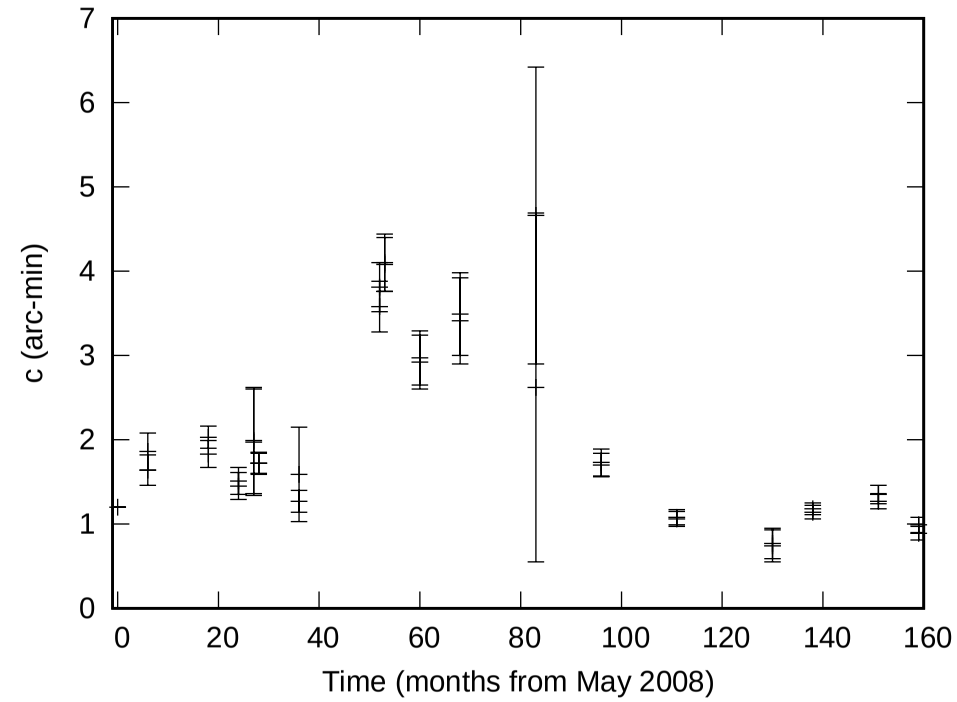

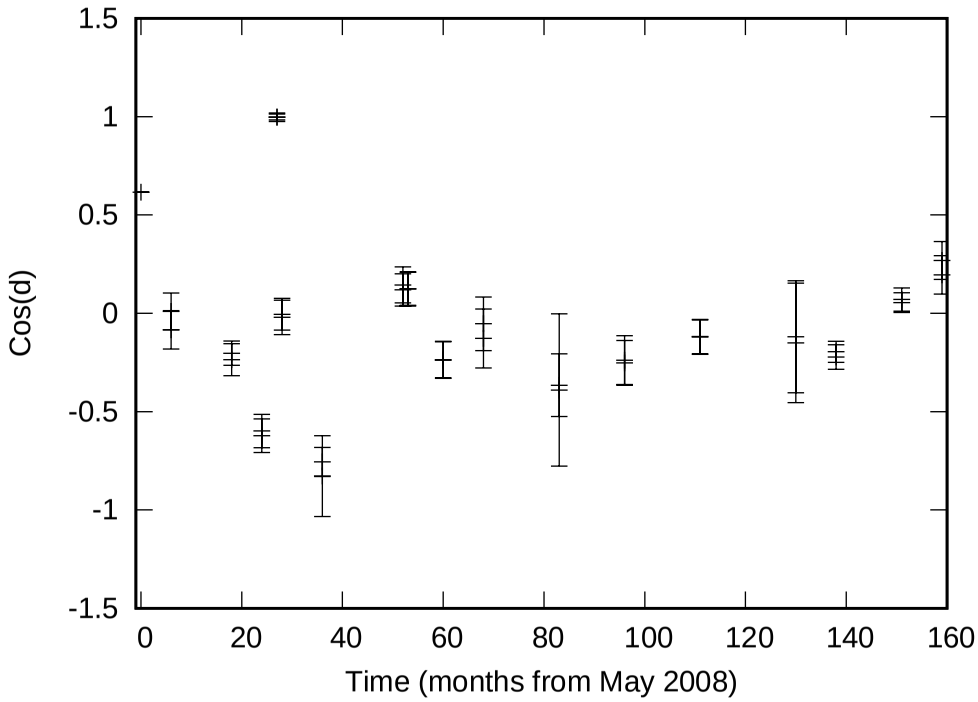

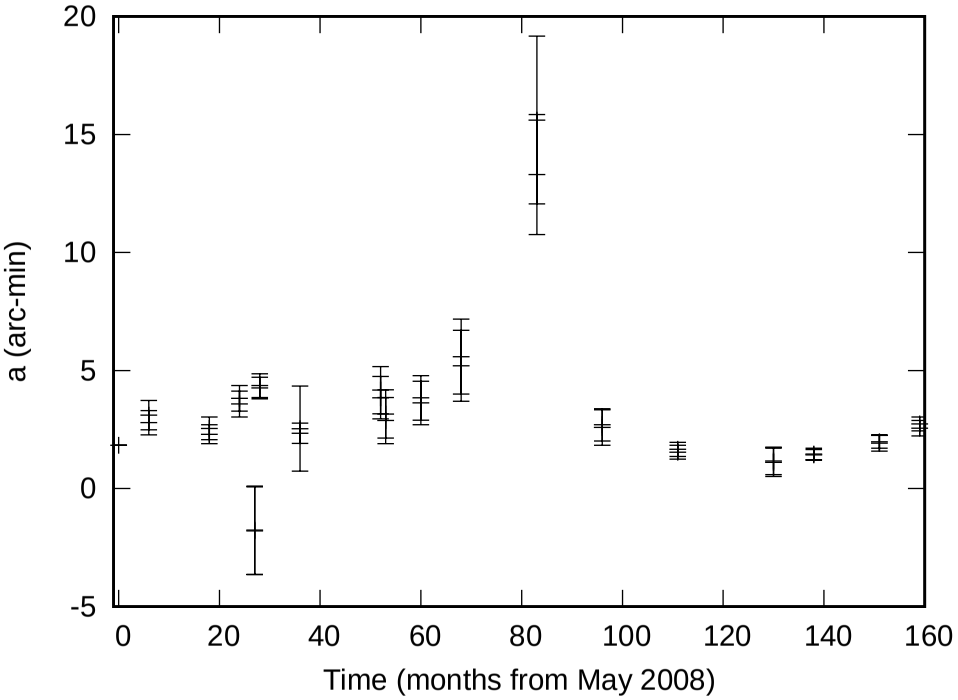

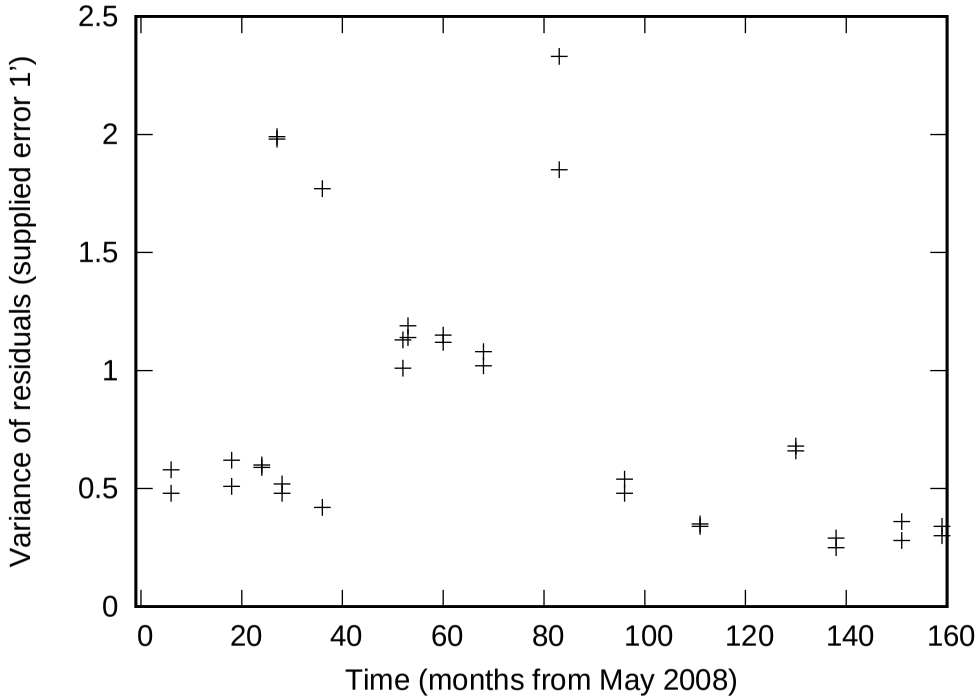

Fig. 2: S01 Elevation pointing coefficients

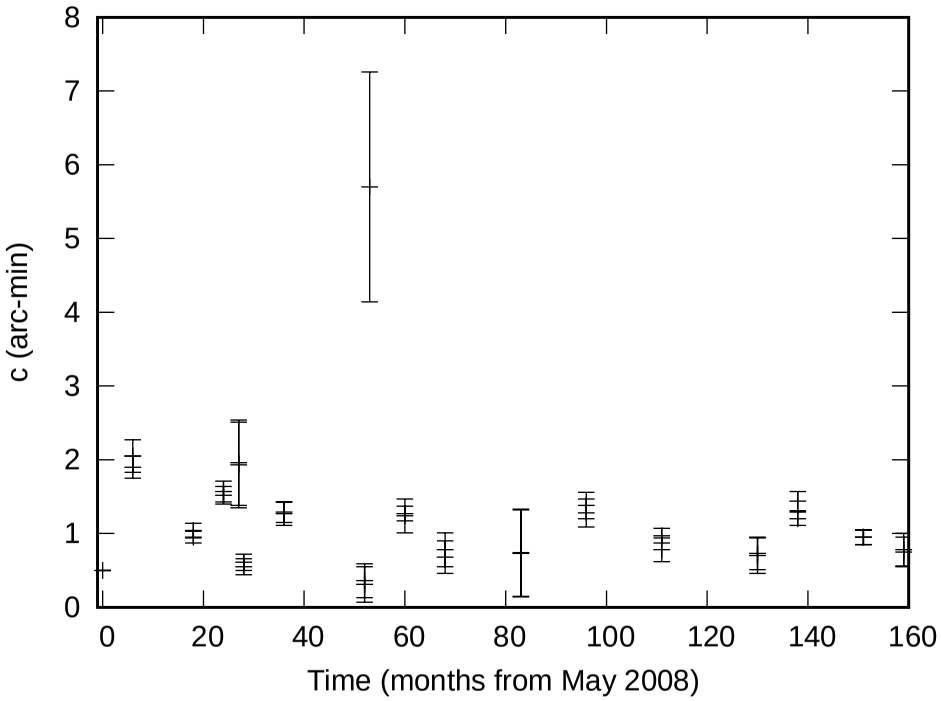

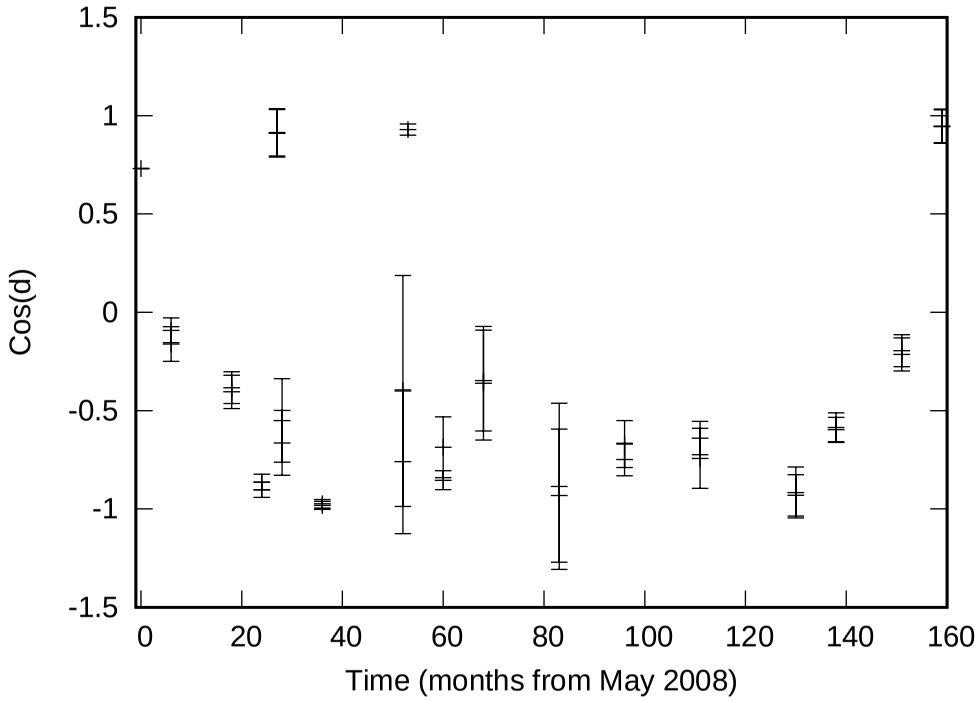

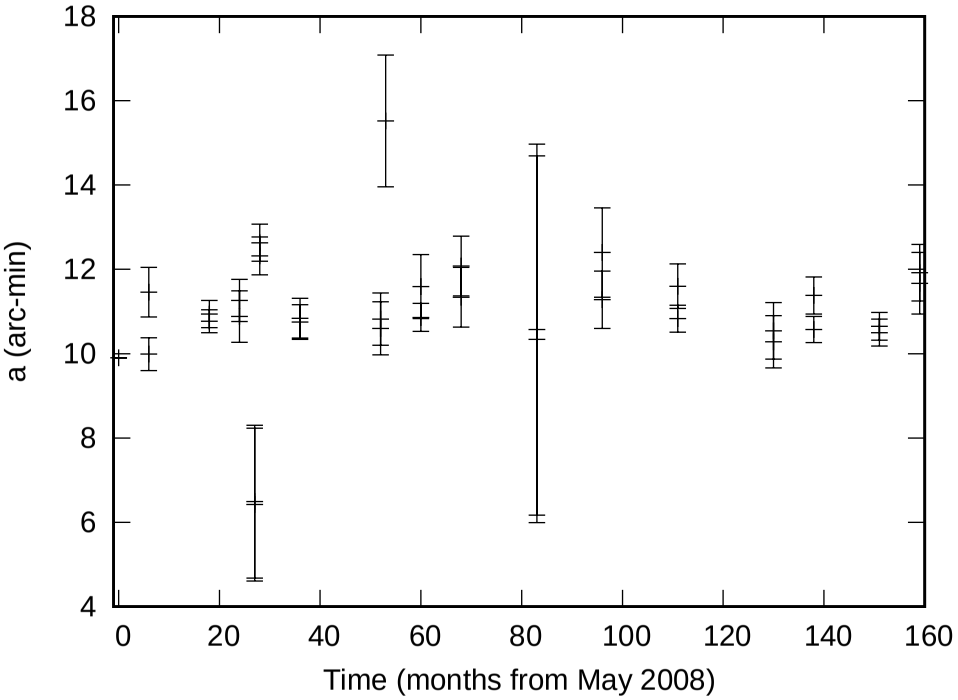

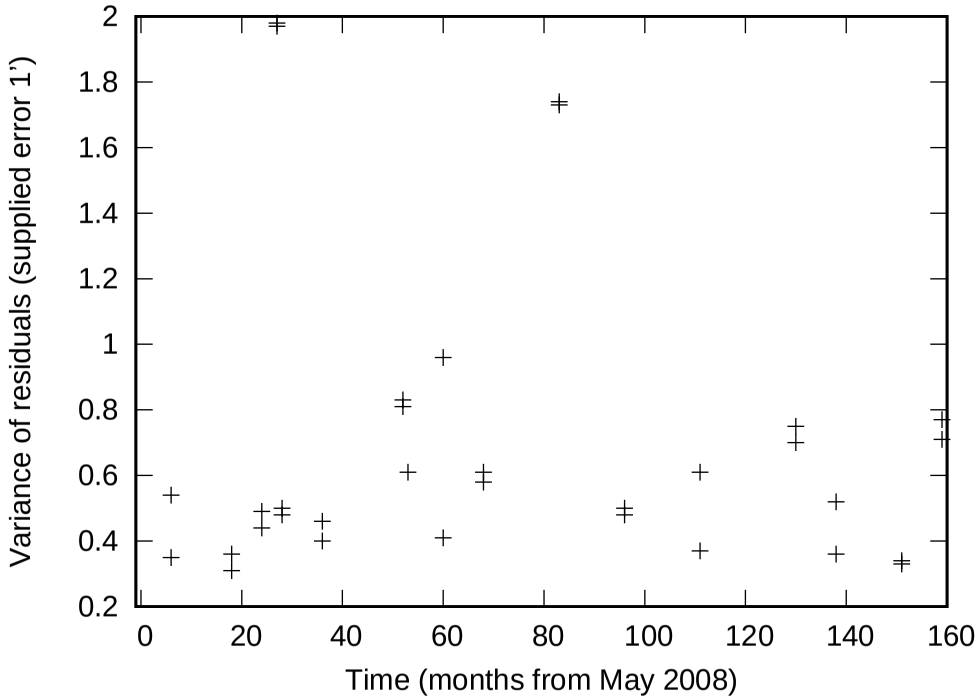

Fig. 2: S02 Elevation pointing coefficients

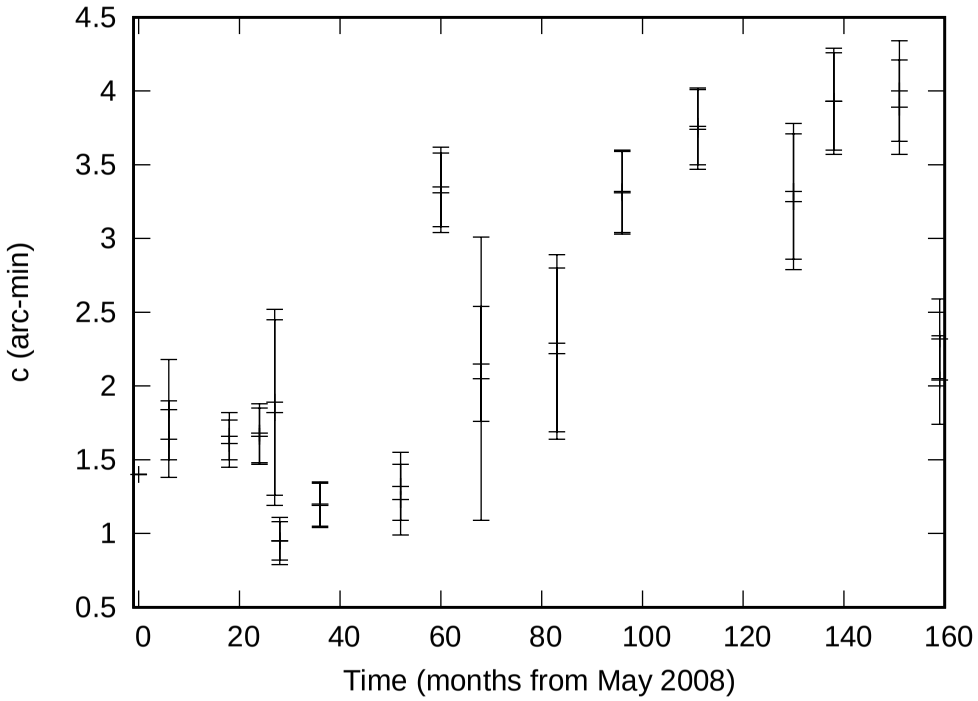

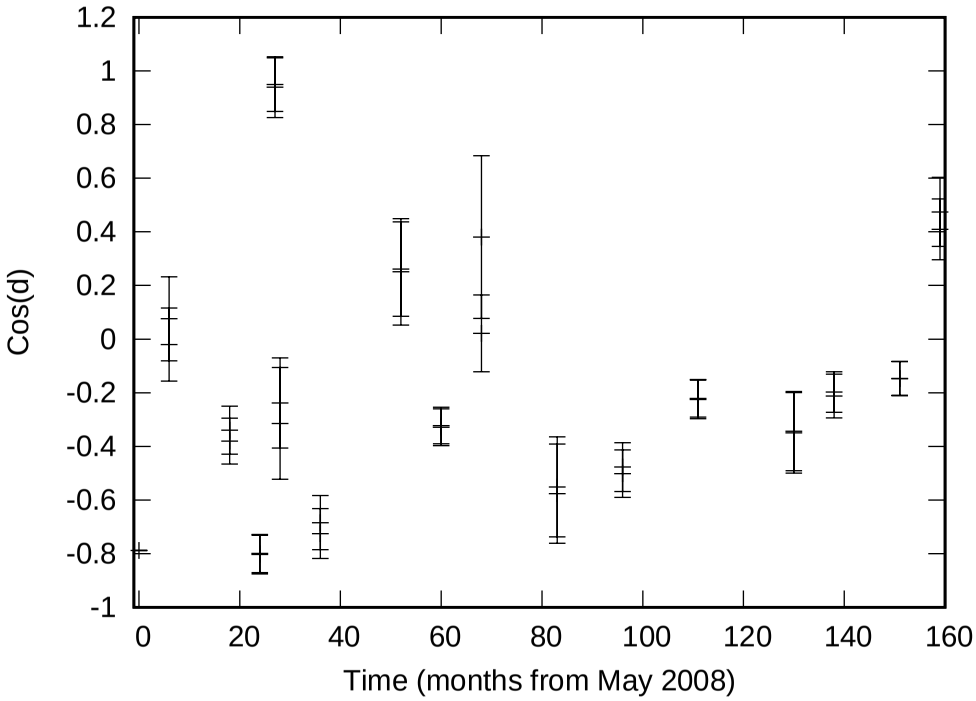

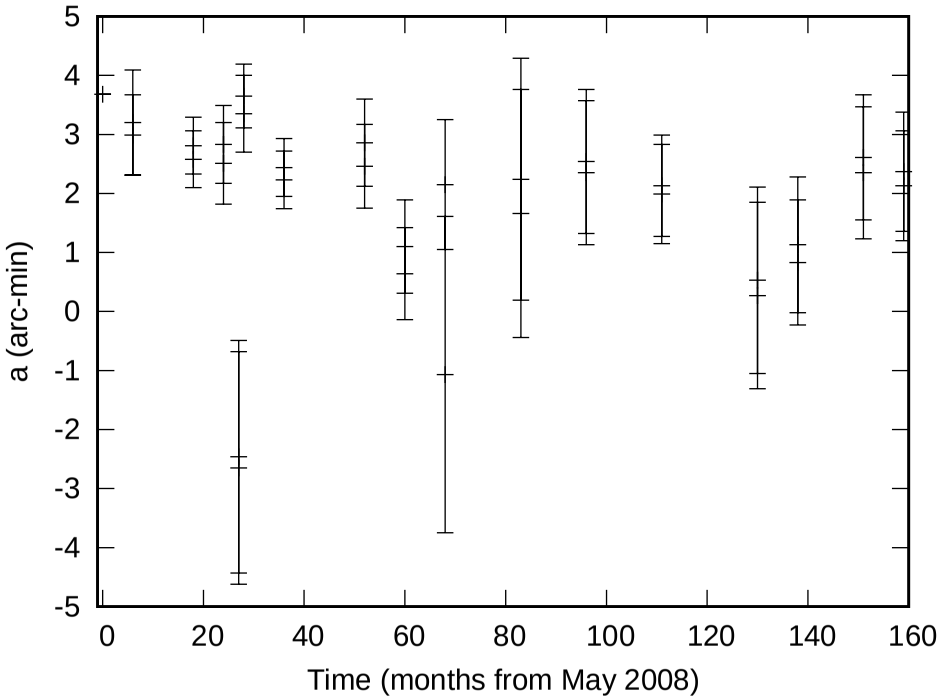

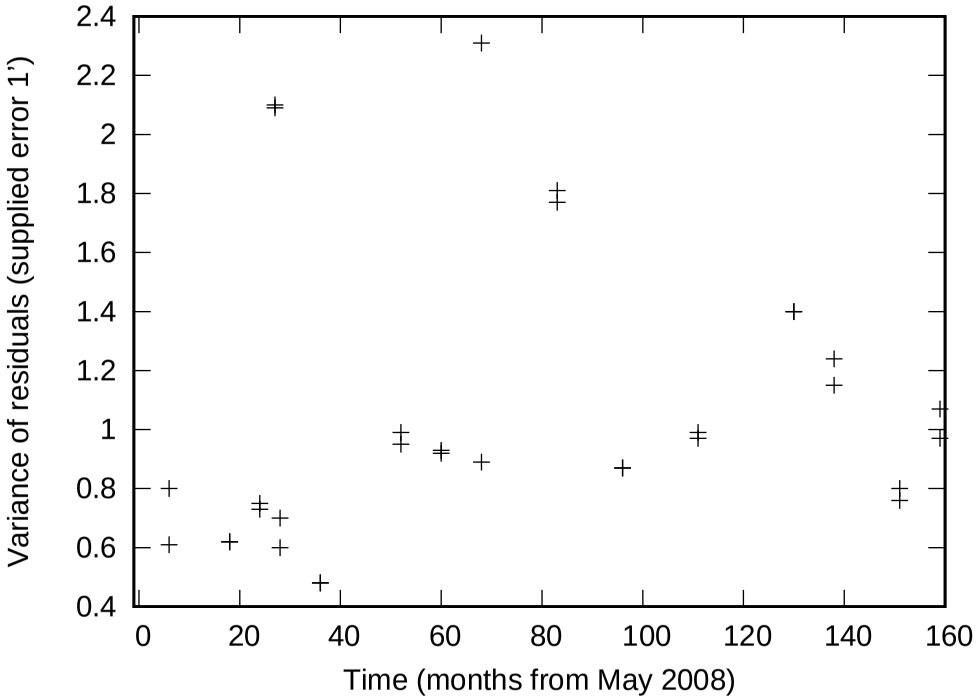

Fig. 2: S03 Elevation pointing coefficients

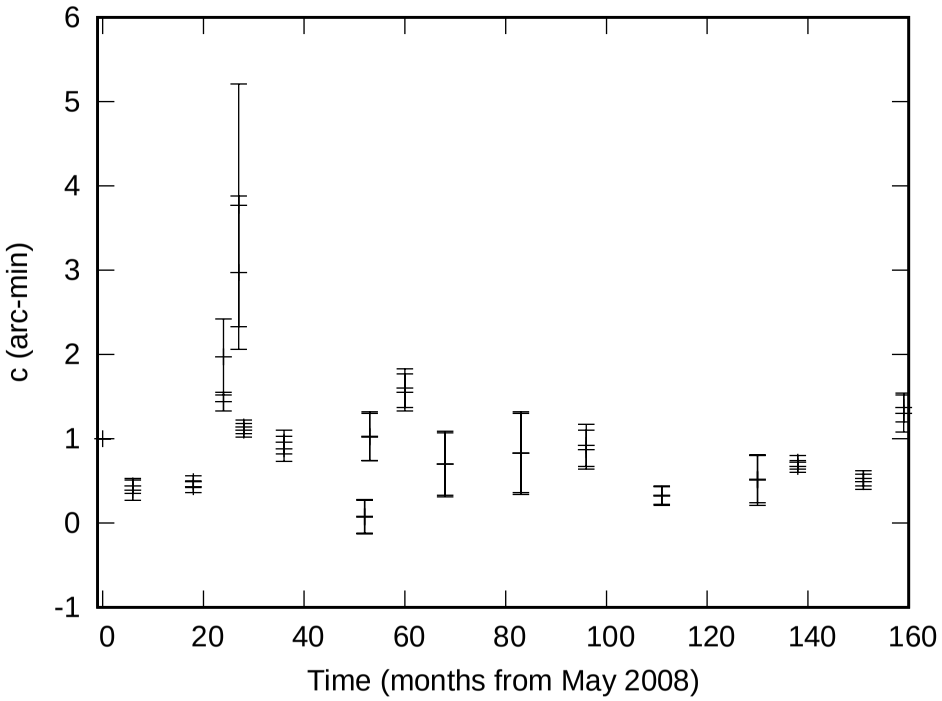

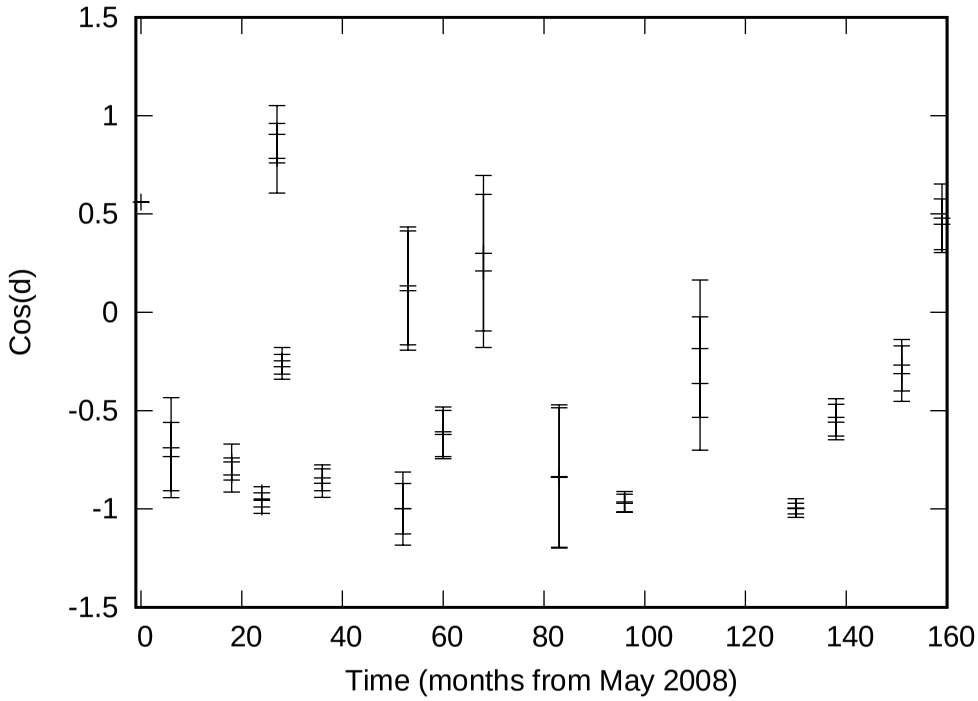

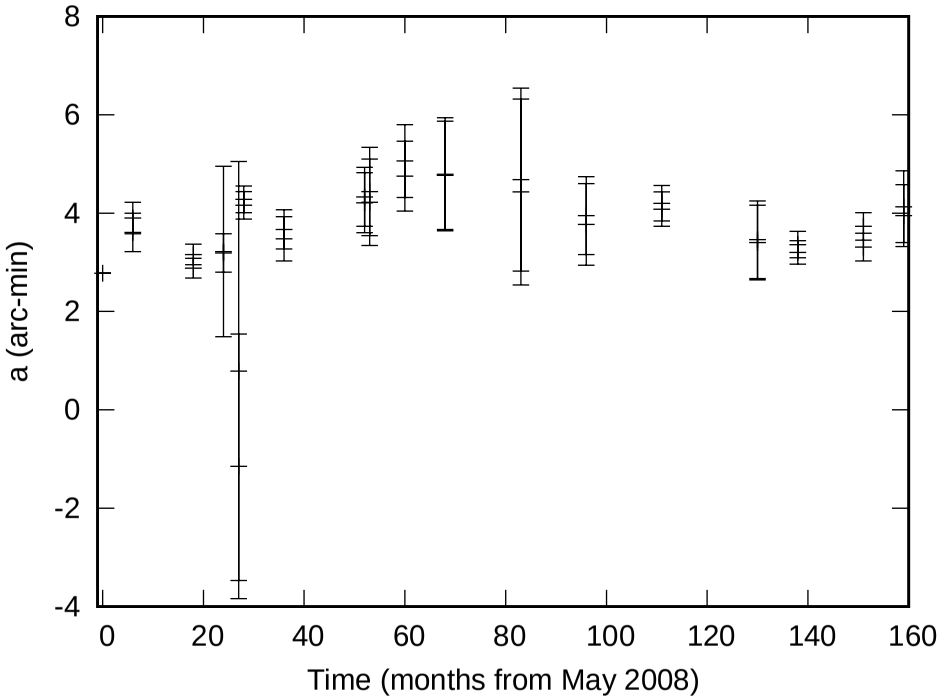

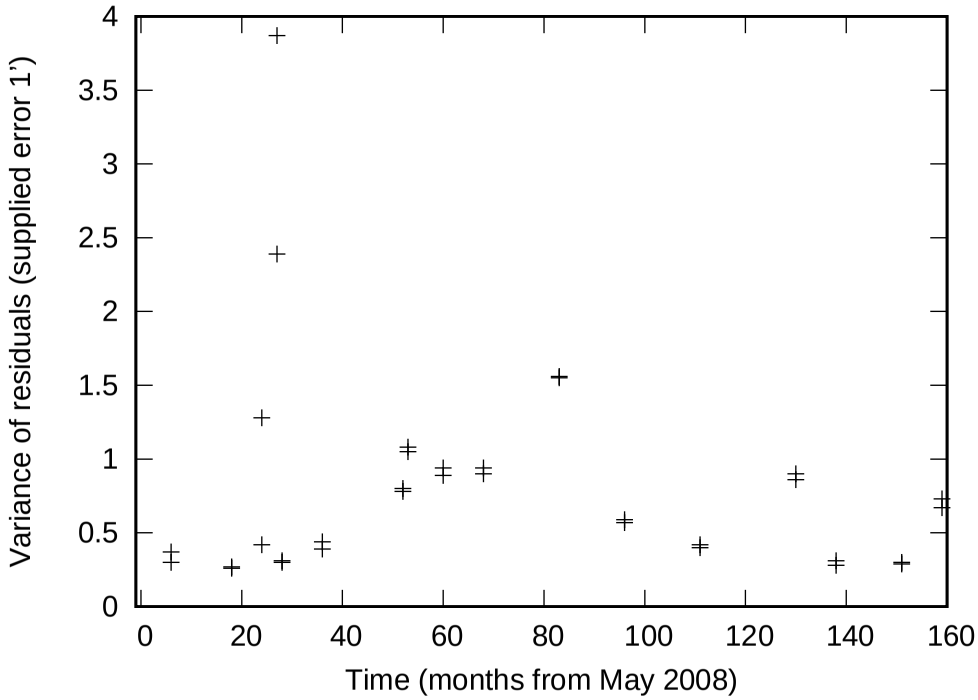

Fig. 2: S04 Elevation pointing coefficients

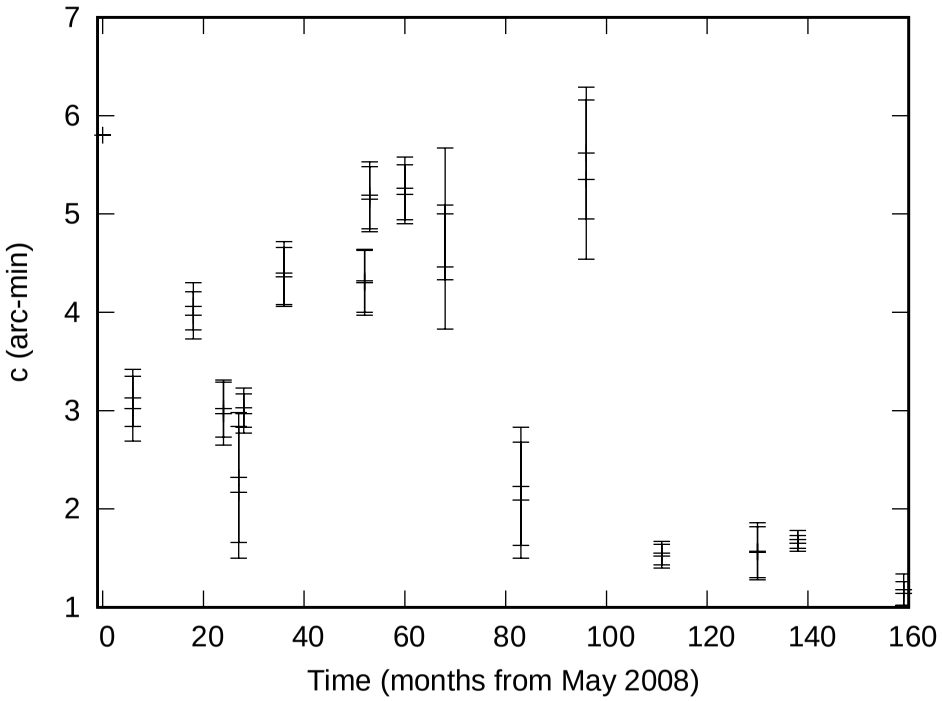

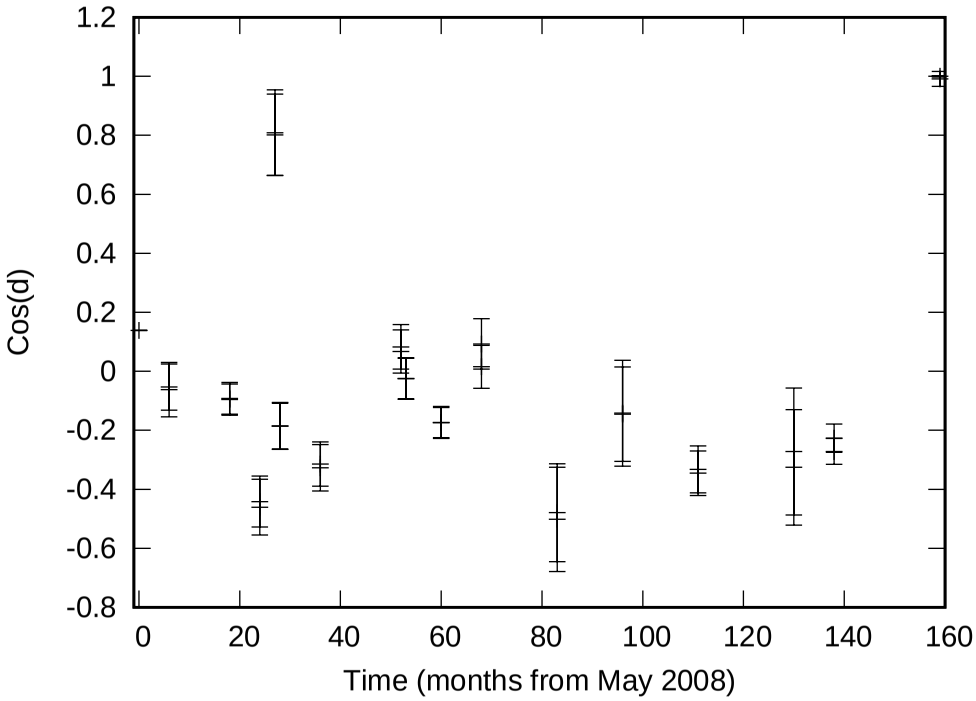

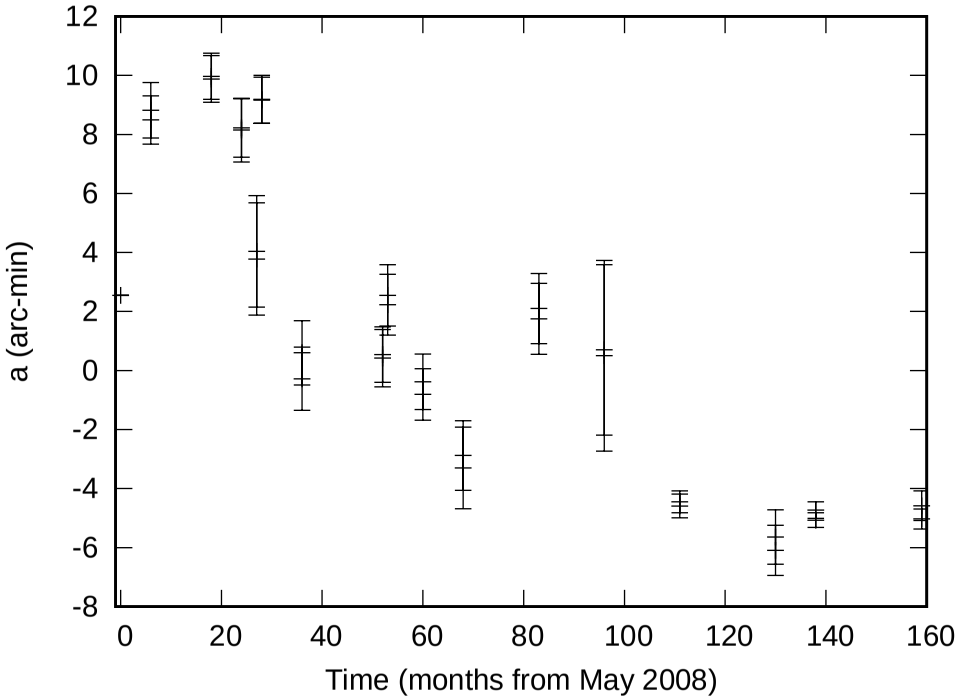

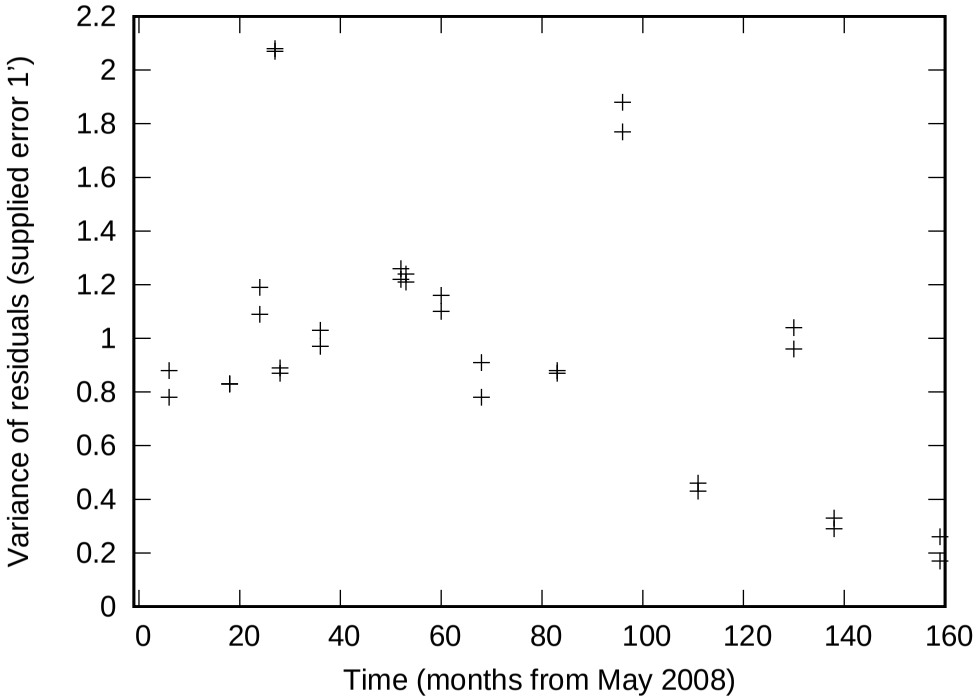

Fig. 2: S06 Elevation pointing coefficients

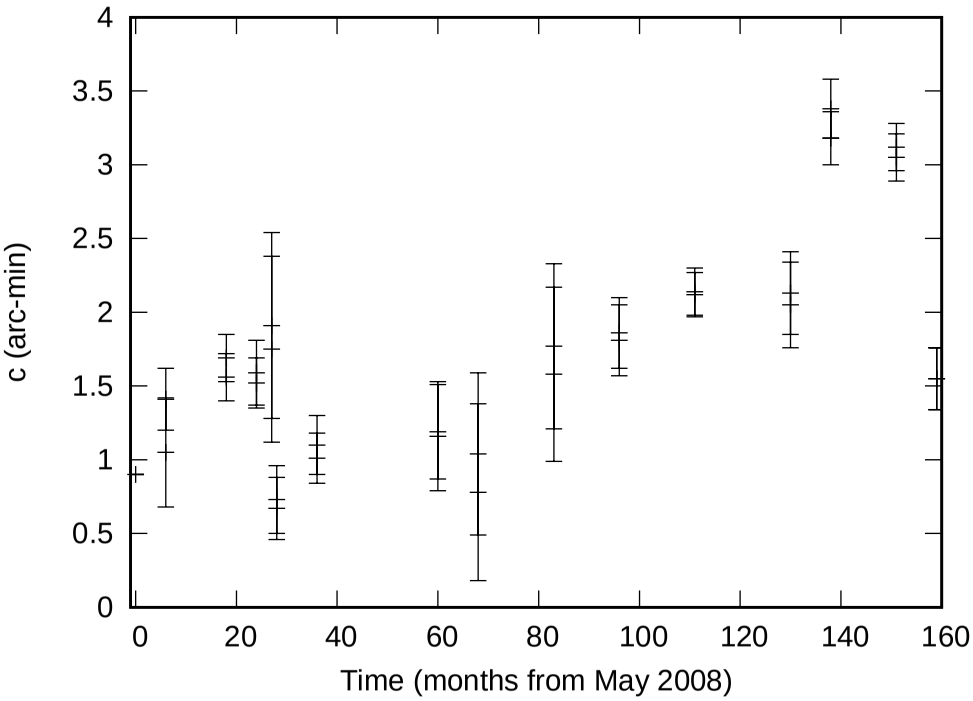

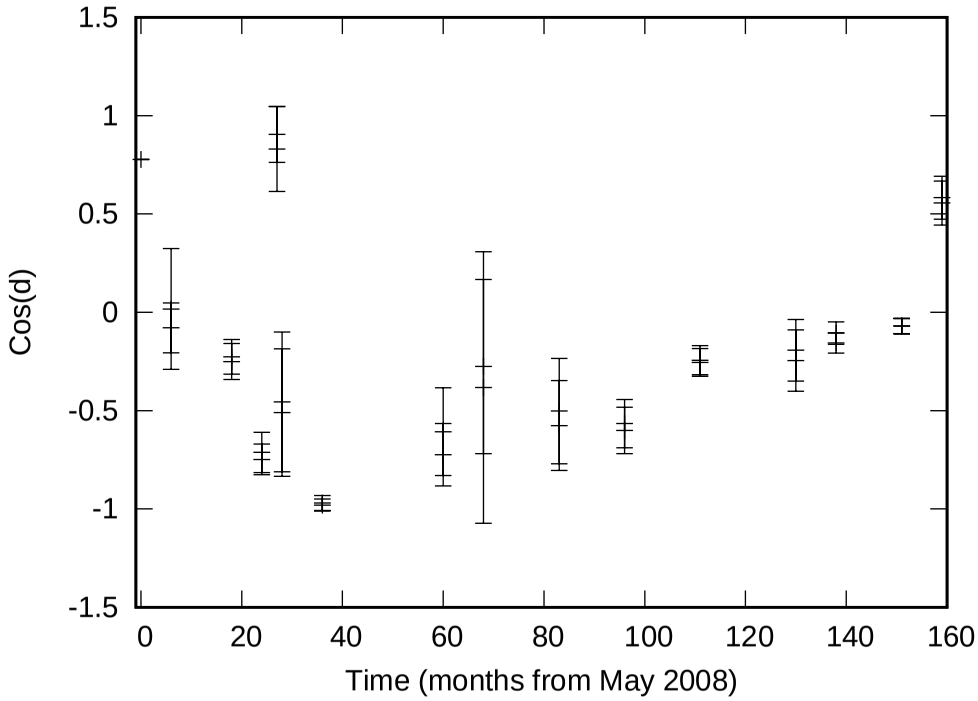

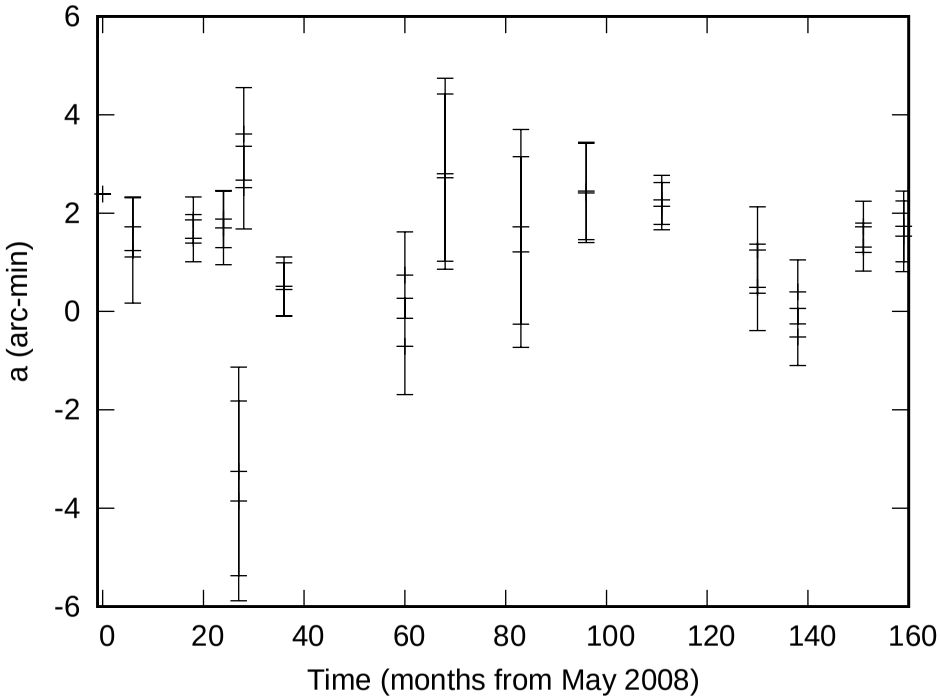

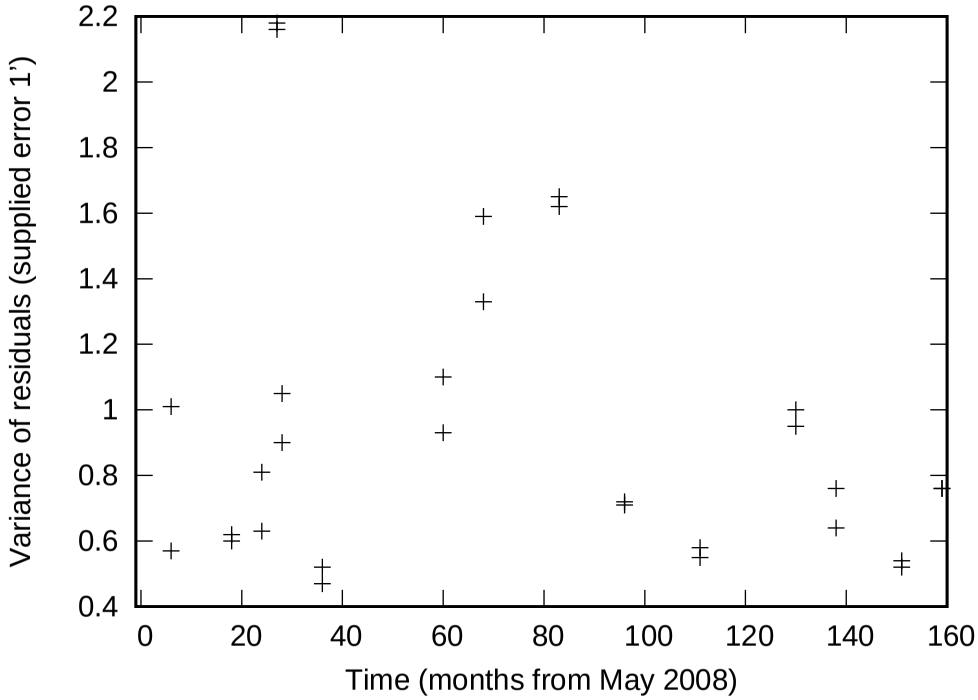

Fig. 2: W01 Elevation pointing coefficients

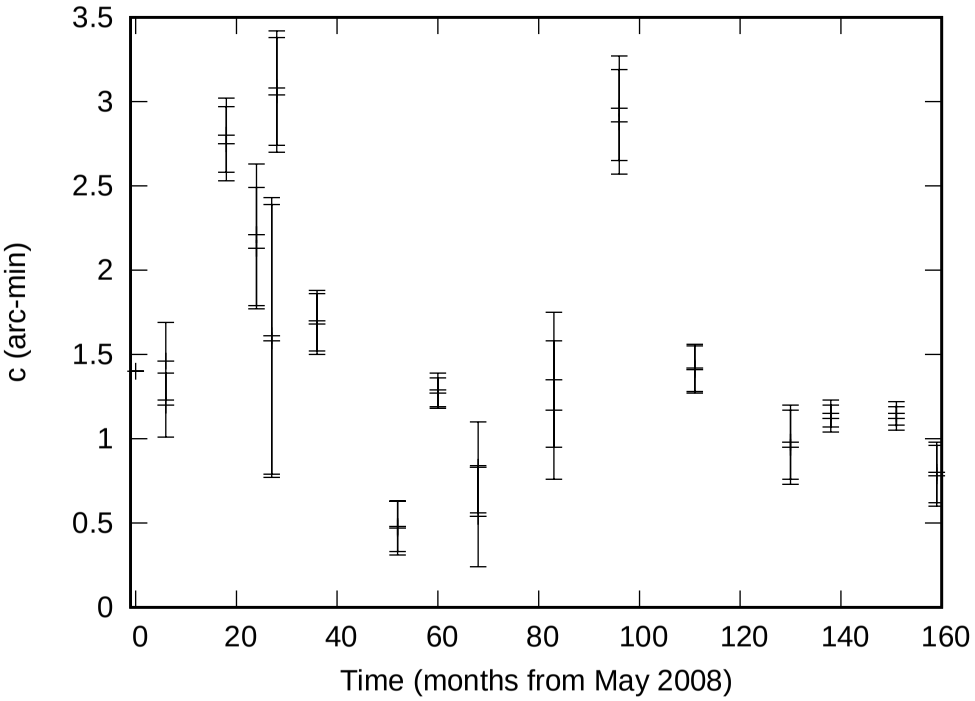

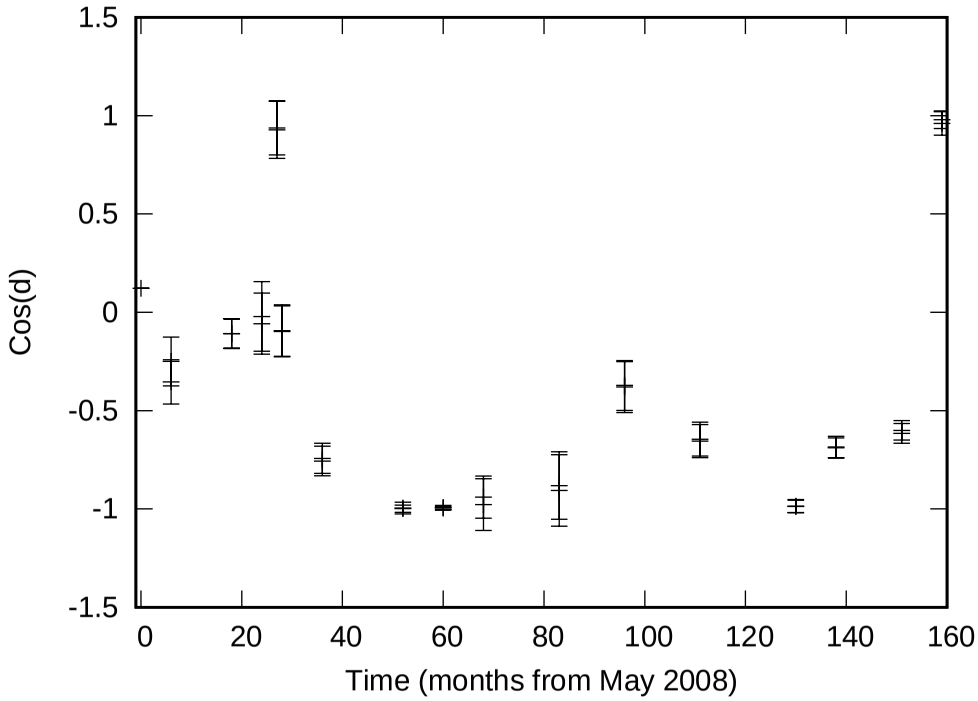

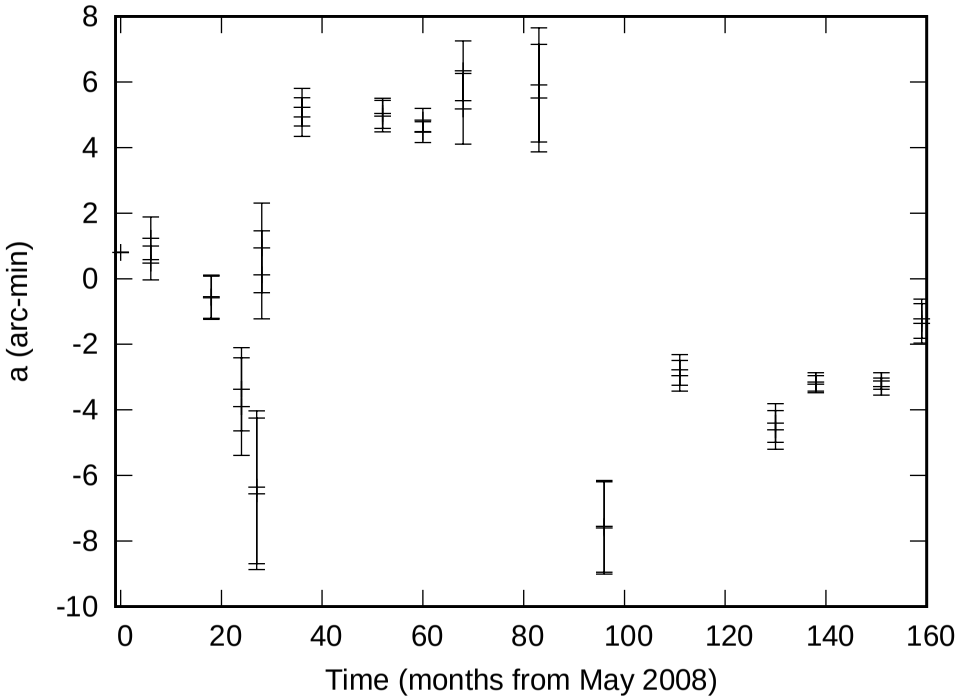

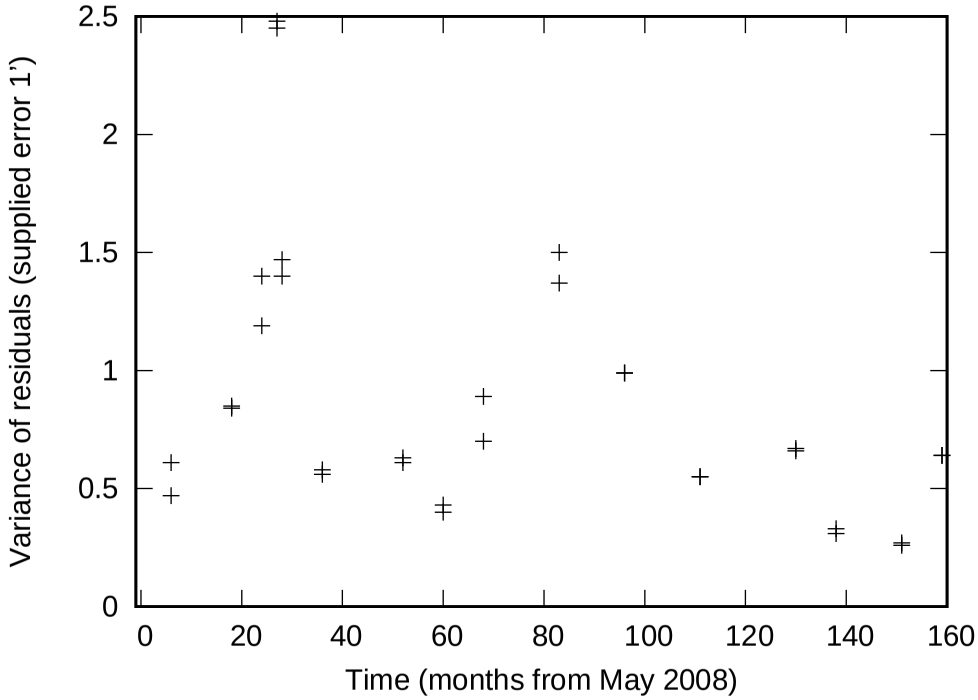

Fig. 2: W02 Elevation pointing coefficients

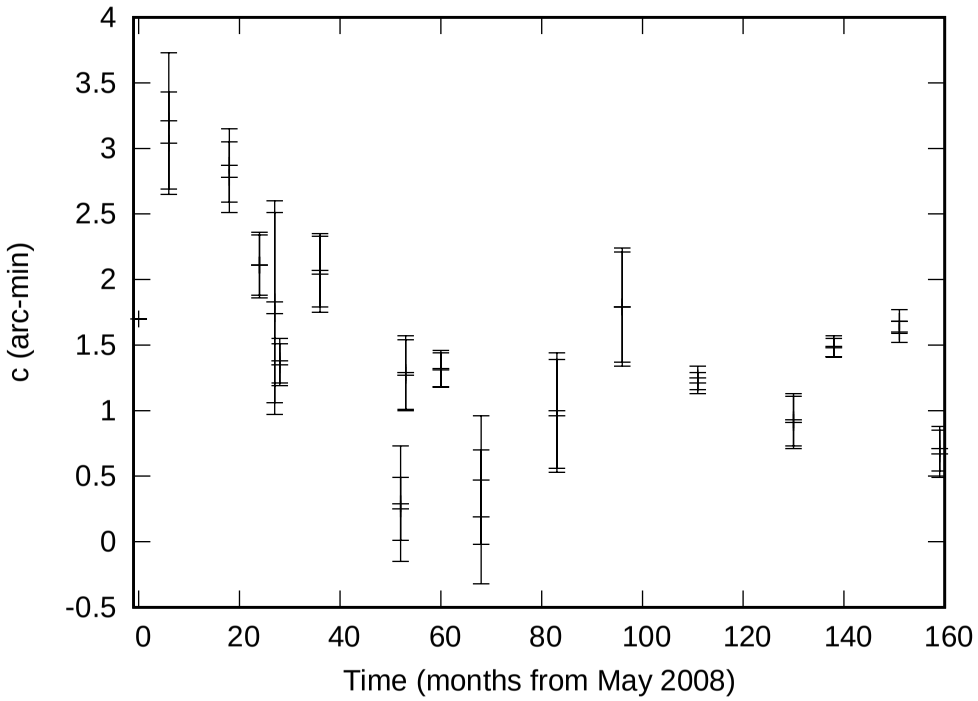

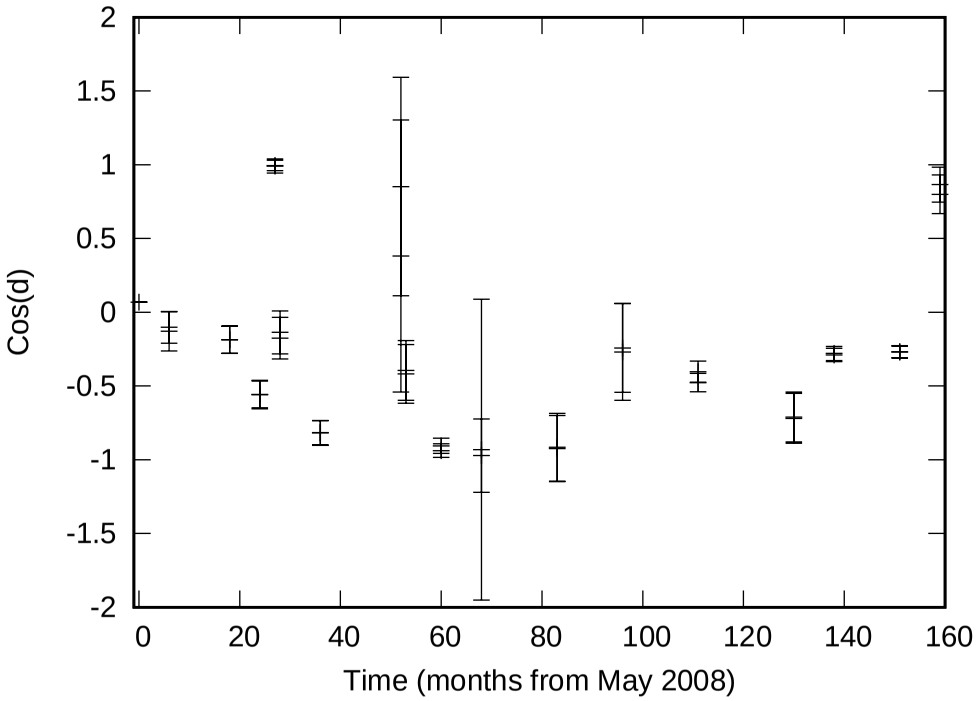

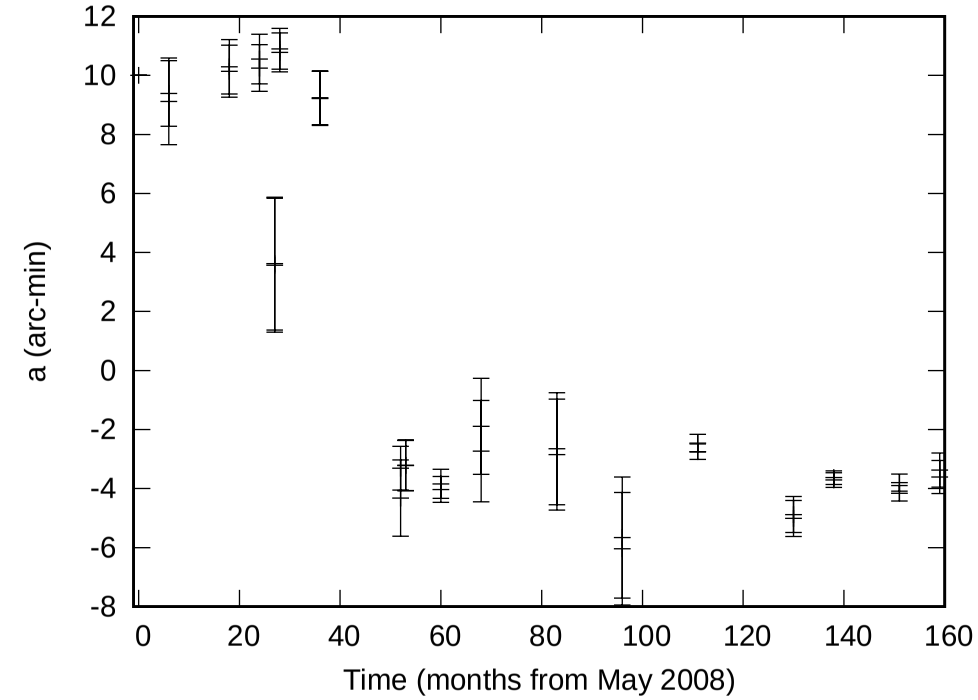

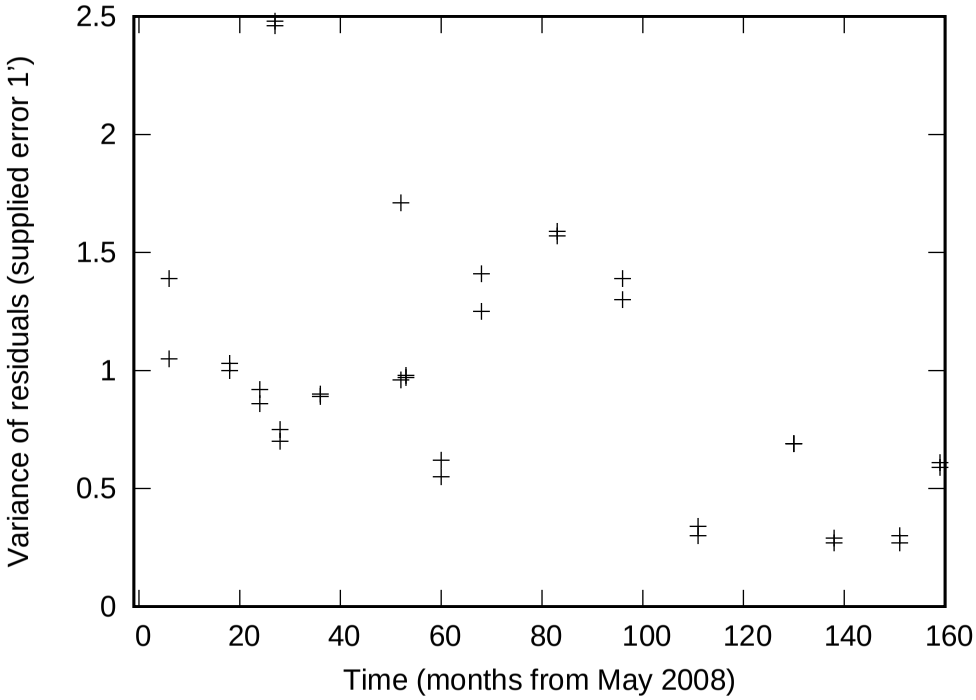

Fig. 2: W03 Elevation pointing coefficients

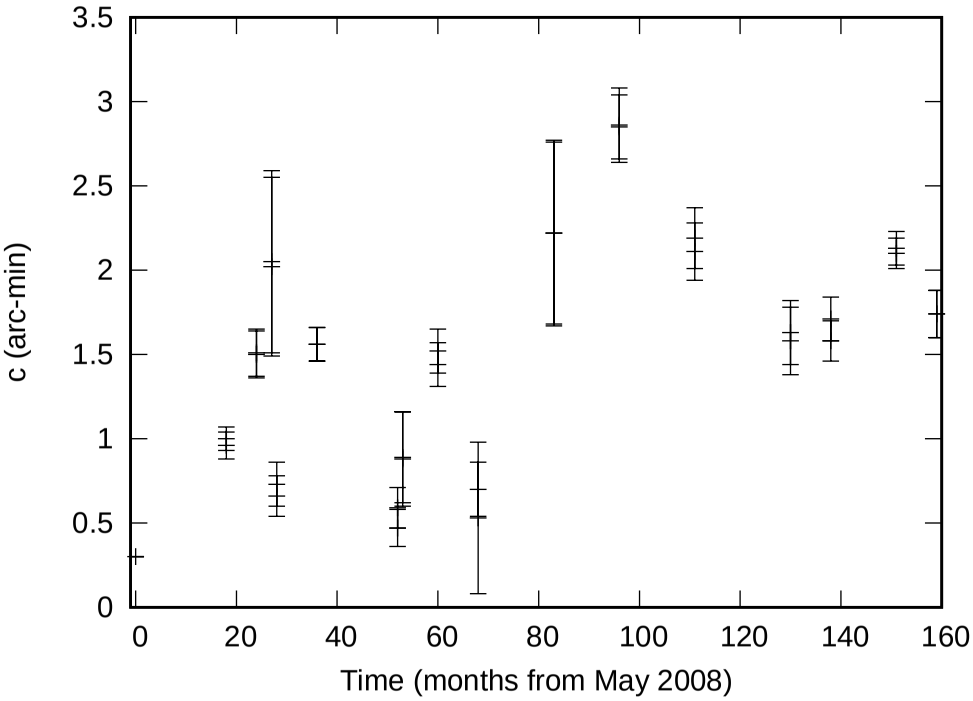

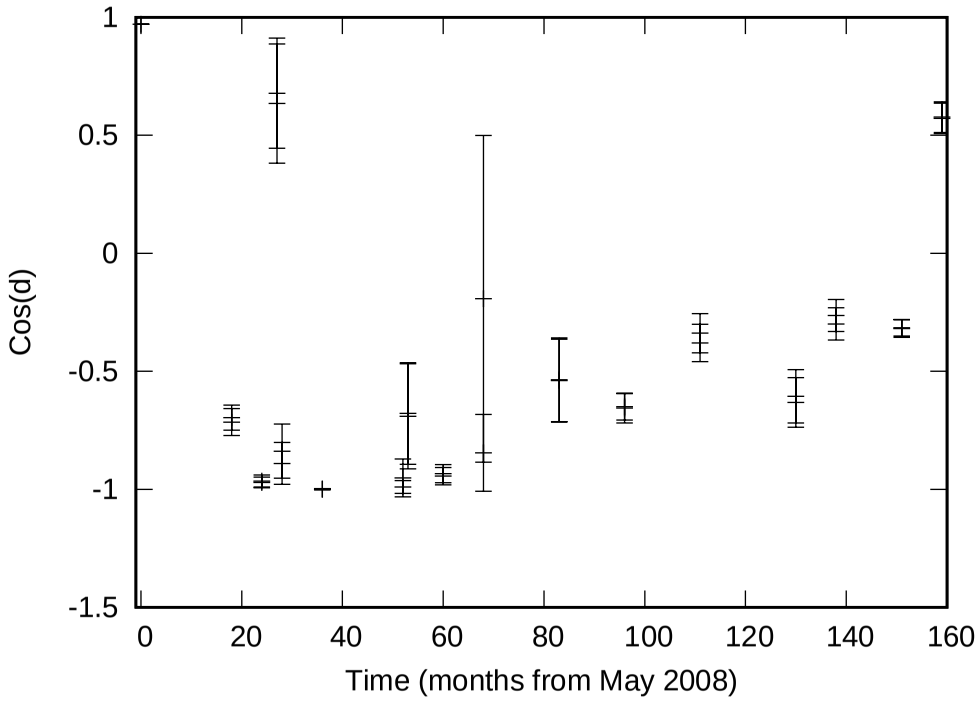

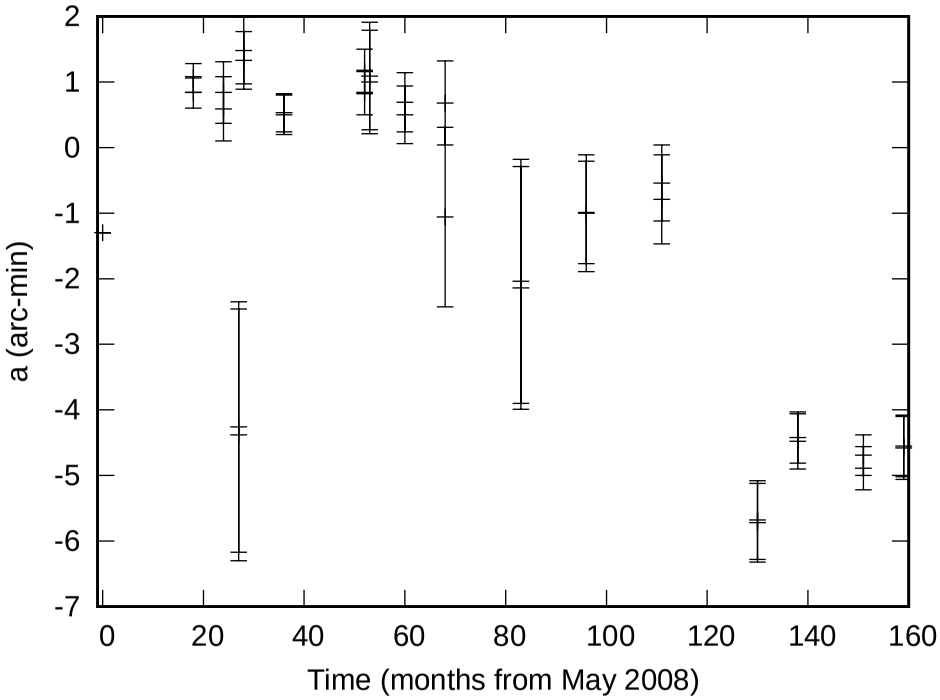

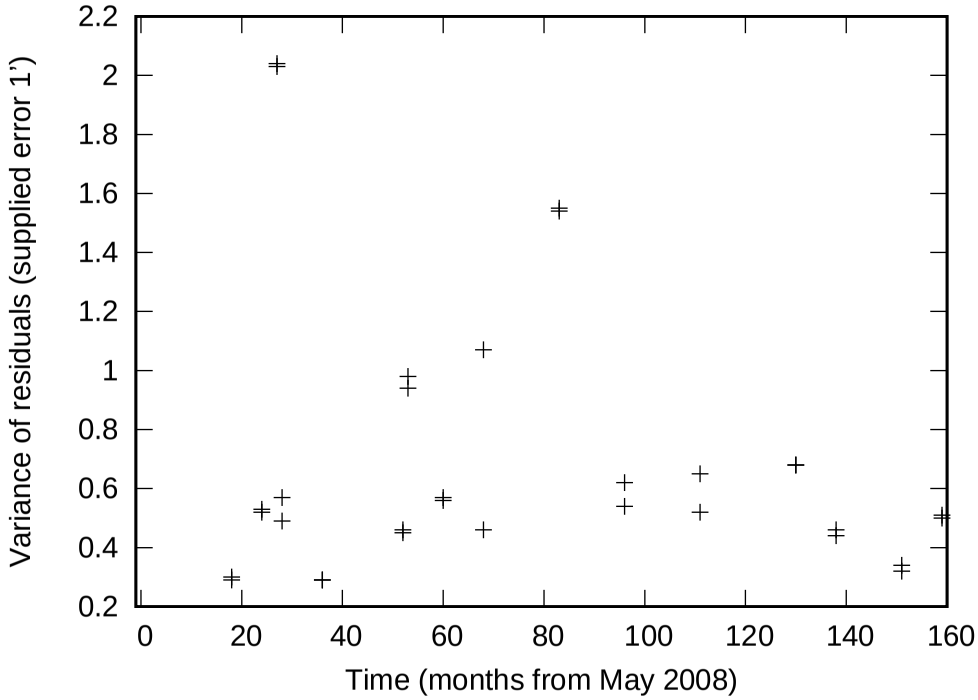

Fig. 2: W04 Elevation pointing coefficients

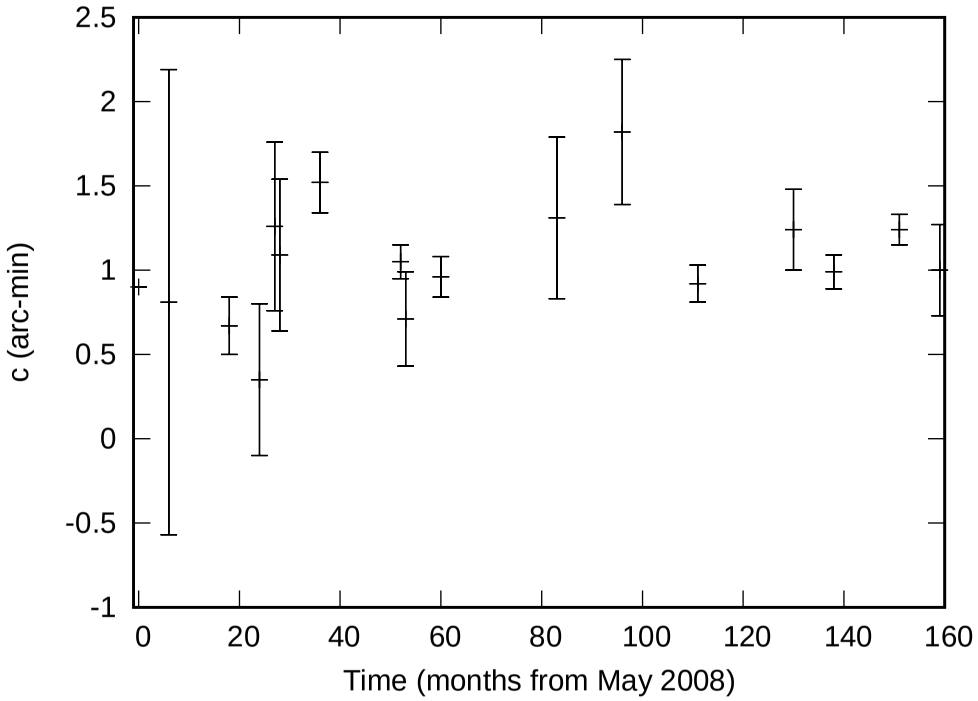

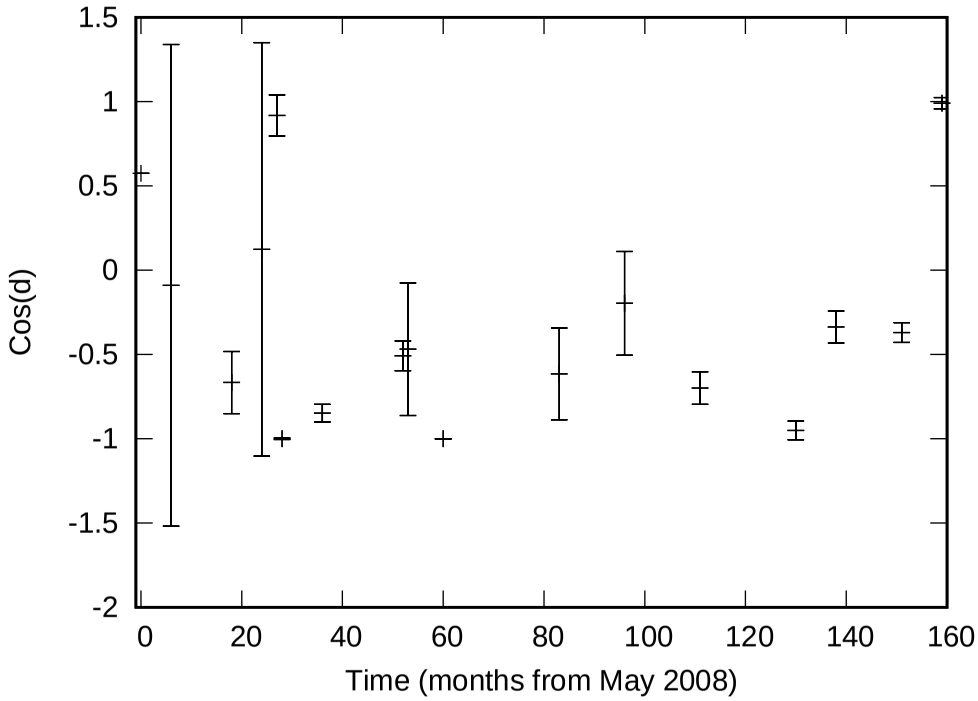

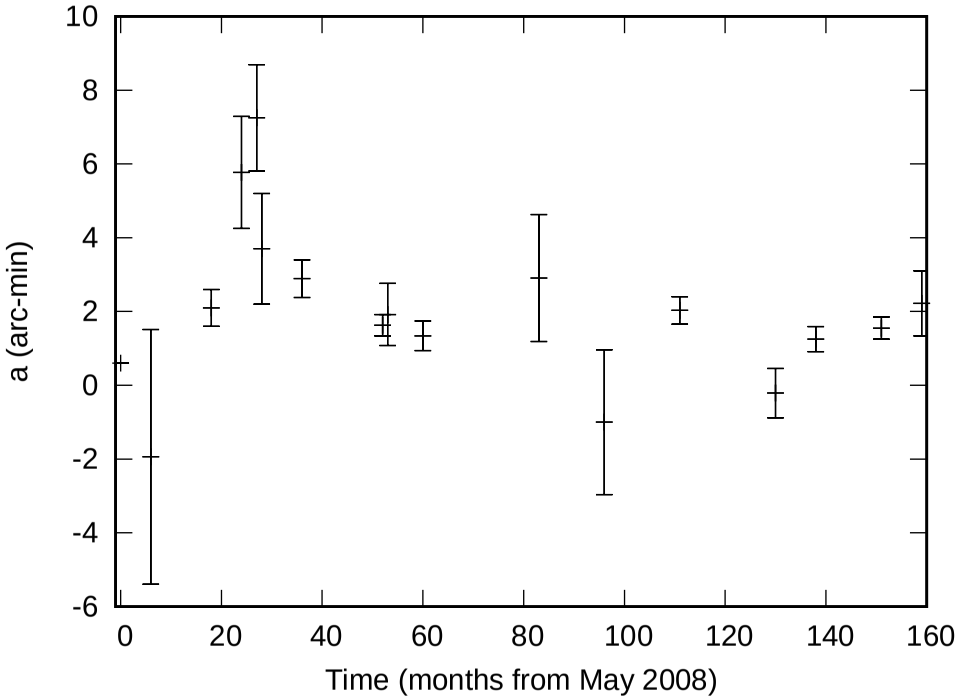

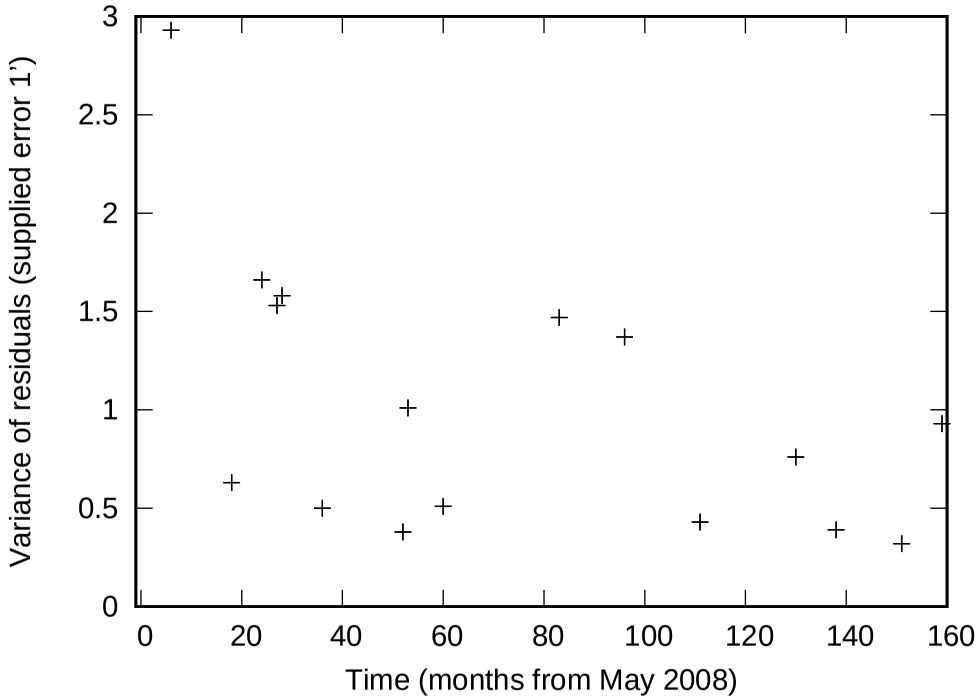

Fig. 2: W05 Elevation pointing coefficients

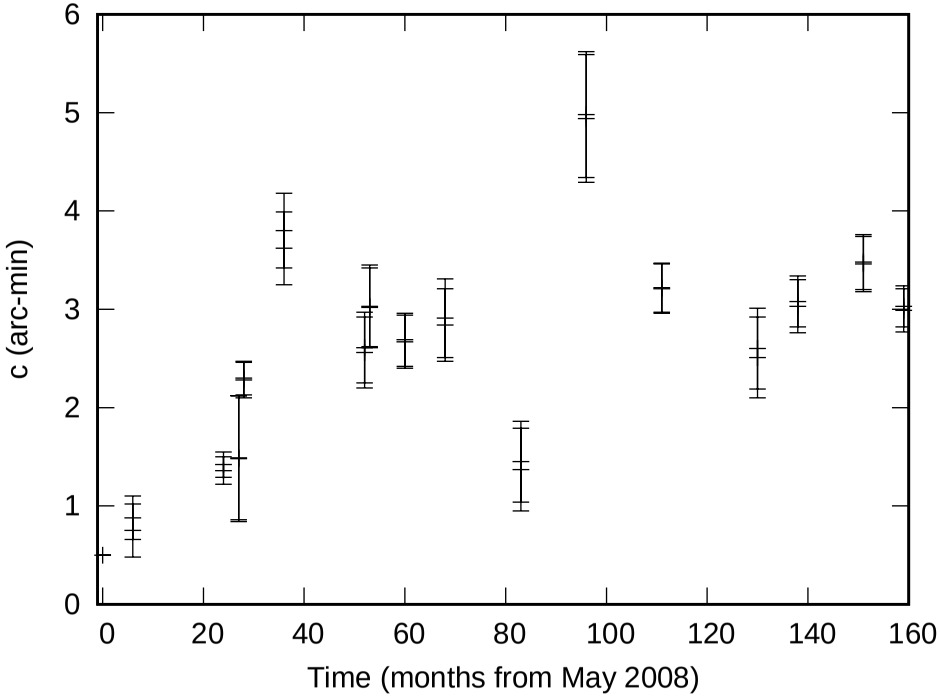

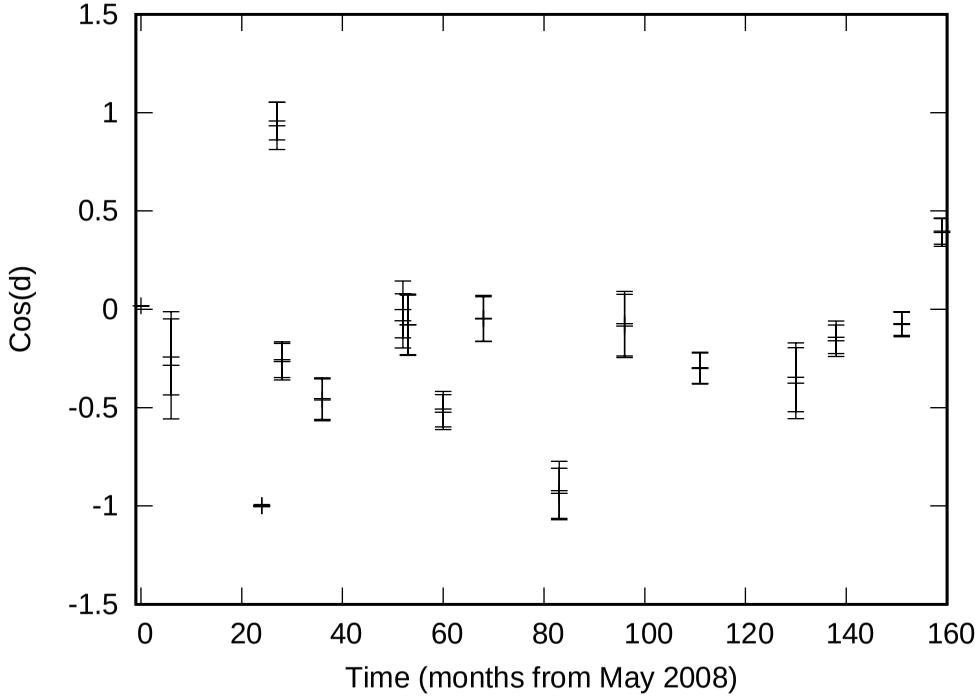

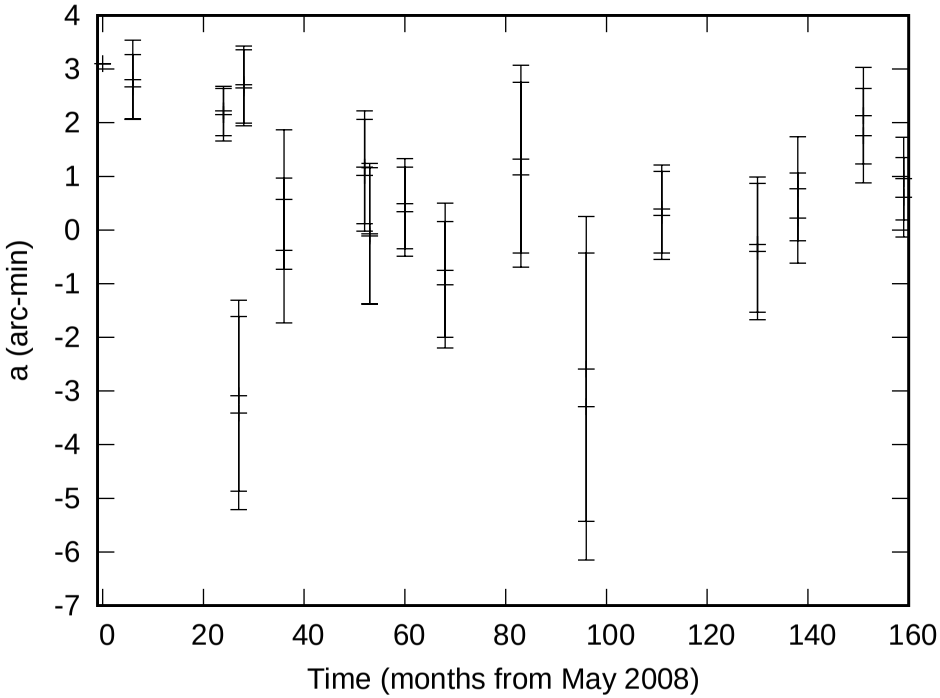

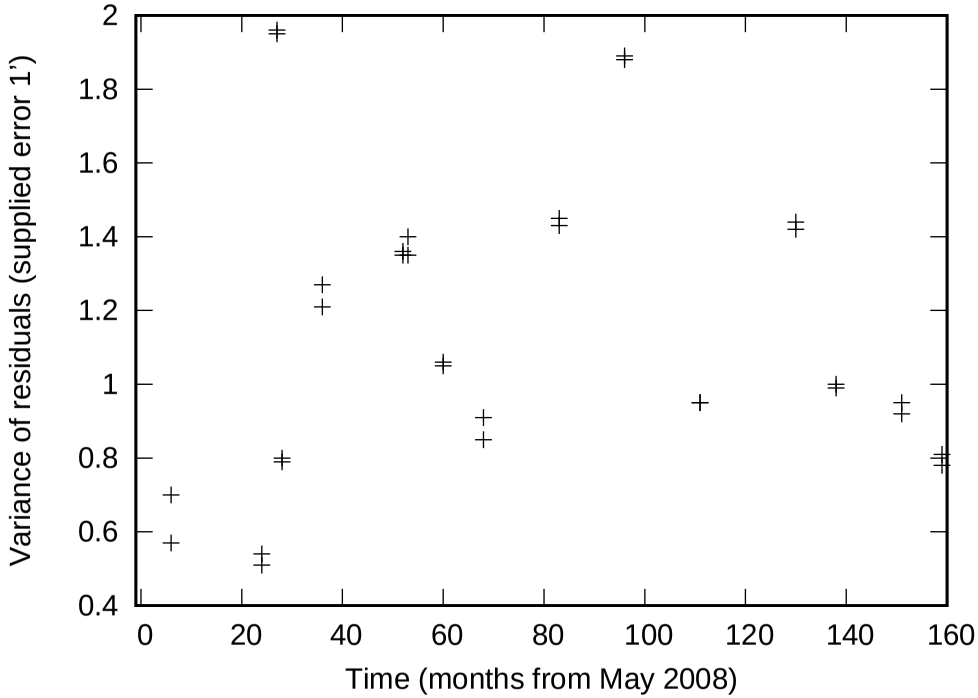

Fig. 2: W06 Elevation pointing coefficients

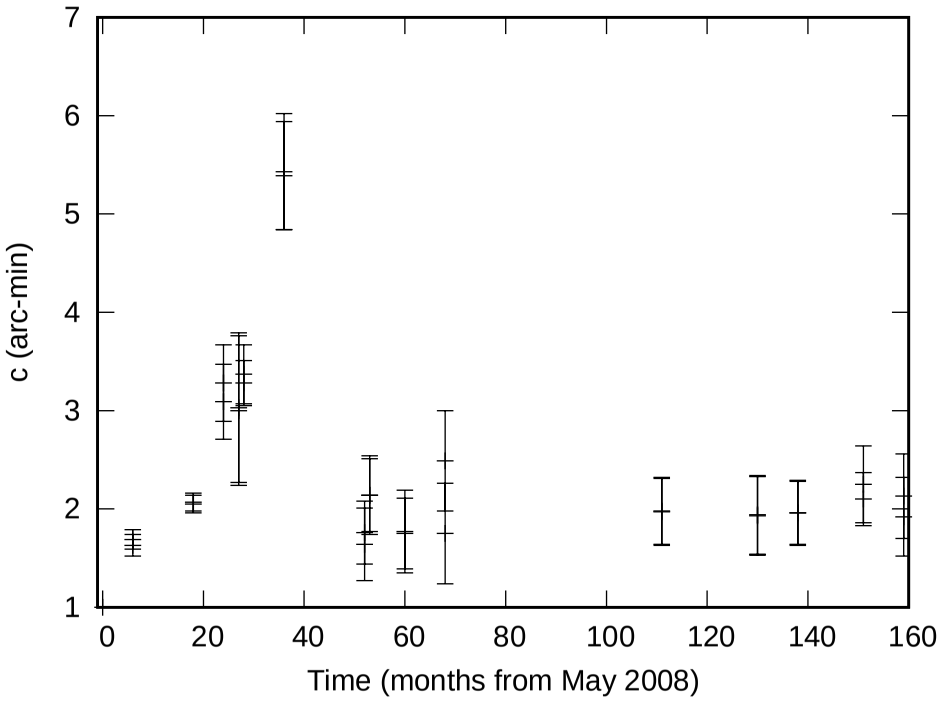

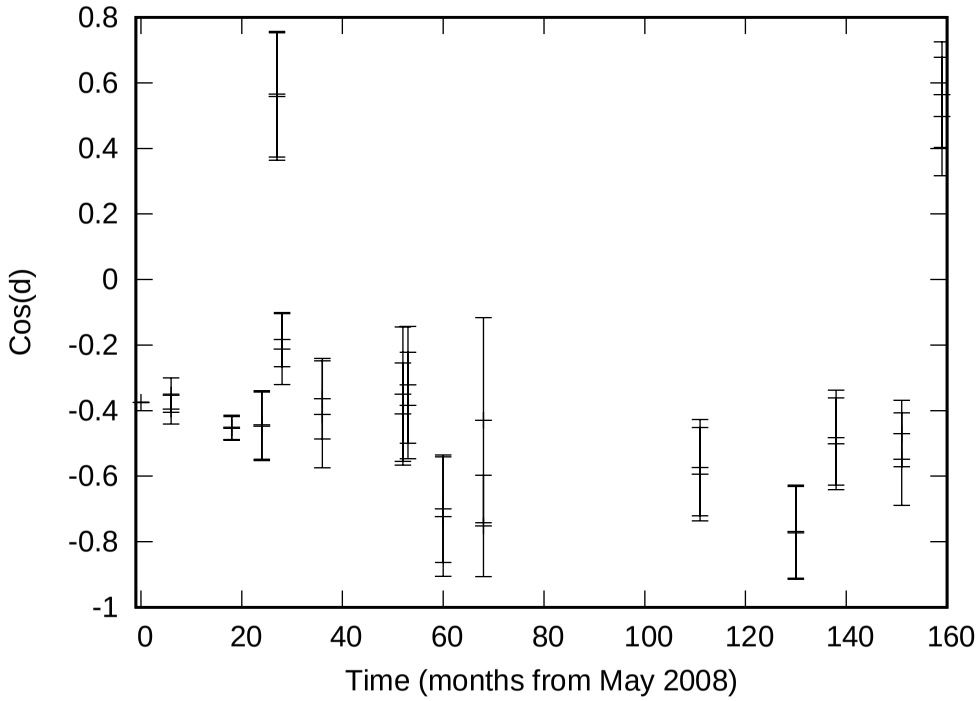

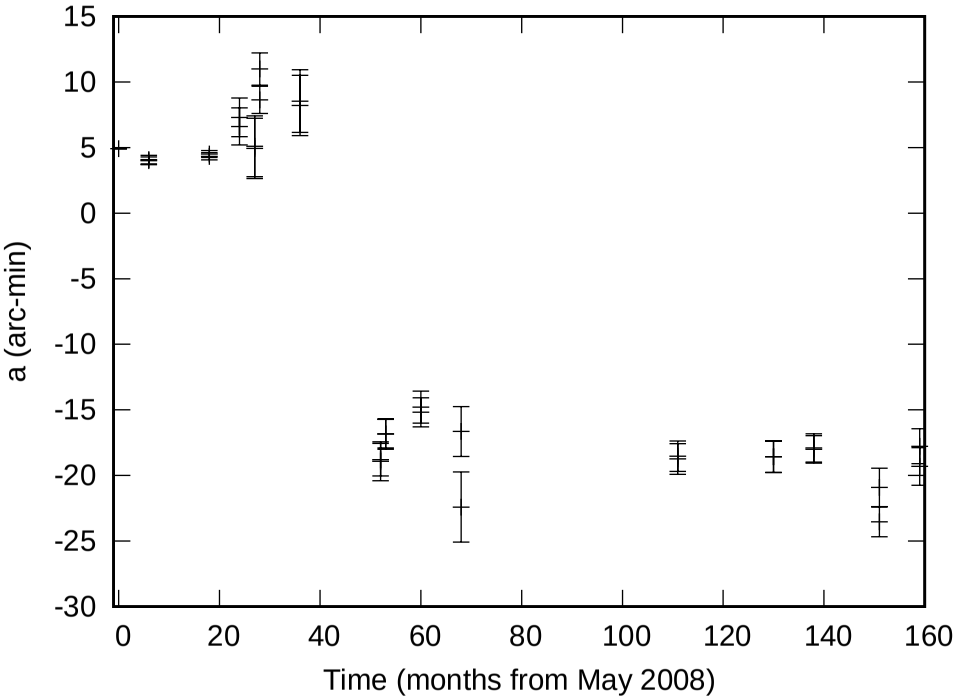

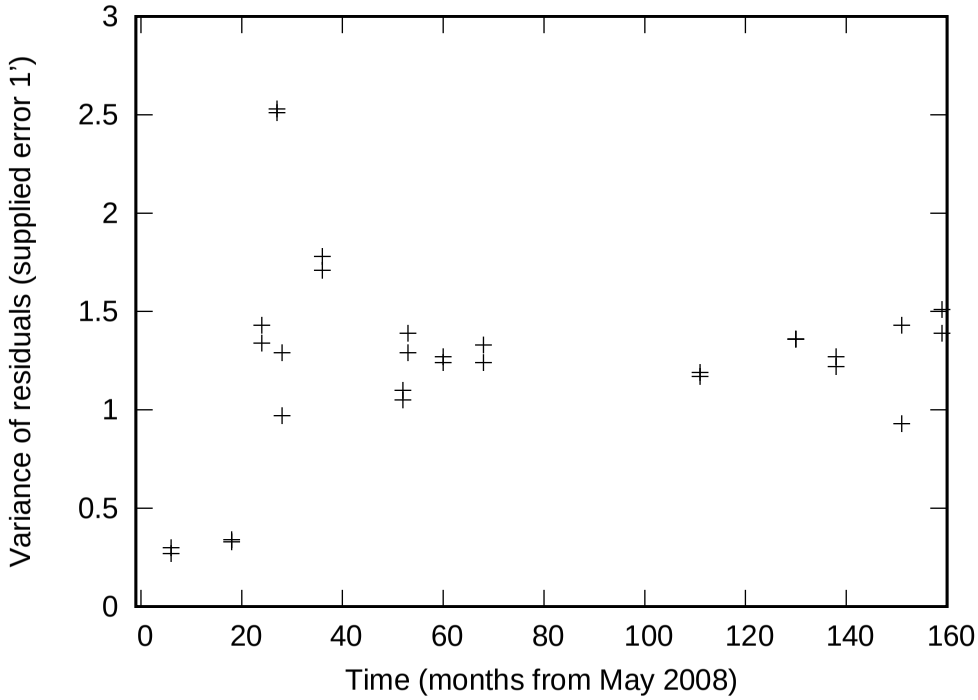

Table -2: Reduced Chi-square of EL pointing errors
after applying the Jun 19 pointing model

#Antenna-Band-Poln	FIT_STDFIT**2 (EL)			
#	23Aug17	03Mar19	14Nov19	02Dec20
C00-USB-130	3.94	1.52	1.77	1.54
C00-USB-175	4.01	1.66	1.91	1.57
C01-USB-130	1.37	0.65	1.60	1.95
C01-USB-175	1.30	0.68	1.67	1.78
C02-USB-130	0.92	1.07	0.46	0.45
C02-USB-175	1.12	1.16	0.46	0.46
C03-USB-130	0.36	3.16	0.46	NaN
C03-USB-175	0.40	3.03	0.38	NaN
C04-USB-130	0.29	1.58	0.46	3.5
C04-USB-175	0.28	1.54	0.38	3.49
C05-USB-130	0.74	0.57	0.49	NaN
C05-USB-175	0.80	0.39	0.55	NaN
C06-USB-130	0.21	0.83	0.41	0.61
C06-USB-175	0.23	0.74	0.42	0.64
C08-USB-130	0.56	0.64	0.35	NaN
C08-USB-175	0.46	0.92	0.41	NaN
C09-USB-130	1.09	1.62	1.38	1.10
C09-USB-175	1.07	1.51	1.31	1.08
C10-USB-130	1.01	3.14	1.30	0.79
C10-USB-175	0.94	3.07	1.13	0.70
C11-USB-130	0.32	0.71	0.88	0.32
C11-USB-175	0.35	0.73	0.76	0.40
C12-USB-130	0.09	0.51	0.24	0.21
C12-USB-175	0.10	0.48	0.23	0.13
C13-USB-130	0.83	1.34	0.85	0.88
C13-USB-175	0.81	1.23	0.85	0.88
C14-USB-130	NaN	1.09	1.22	2.42
C14-USB-175	NaN	0.94	1.14	2.63
E02-USB-130	0.38	0.81	0.56	0.73
E02-USB-175	0.41	0.82	0.51	0.78
E03-USB-130	1.04	1.40	1.31	1.40
E03-USB-175	1.01	1.33	1.19	1.30
E04-USB-130	0.27	0.70	0.27	0.64
E04-USB-175	0.26	0.71	0.28	0.62
E05-USB-130	0.51	0.82	NaN	1.09
E05-USB-175	0.54	0.82	NaN	0.99
E06-USB-130	0.15	0.53	0.08	0.26
E06-USB-175	0.15	0.56	0.09	0.20
S01-USB-130	0.18	0.70	0.25	0.29
S01-USB-175	0.37	0.73	0.37	0.27
S02-USB-130	3.80	3.19	4.56	4.14
S02-USB-175	3.81	3.23	4.62	4.02
S03-USB-130	0.67	0.73	0.41	0.53
S03-USB-175	0.70	0.80	0.45	0.52
S04-USB-130	0.26	0.81	0.10	NaN
S04-USB-175	0.26	0.95	0.15	NaN
S06-USB-130	4.76	5.20	9.66	5.69
S06-USB-175	4.84	5.42	9.69	5.79
W01-USB-130	1.72	2.71	1.44	1.10
W01-USB-175	1.68	2.61	1.41	1.01
W02-USB-130	0.60	1.21	0.36	0.35
W02-USB-175	0.57	1.22	0.36	0.38
W03-USB-130	2.27	2.16	1.91	2.12
W03-USB-175	1.96	2.13	1.61	2.00
W04-USB-130	1.18	1.30	1.39	1.13
W04-USB-175	1.16	1.35	1.36	1.09
W05-USB-130	1.27	2.19	1.00	0.94
W05-USB-175	1.26	2.30	1.01	1.02
W06-USB-130	1.31	1.90	1.45	0.19
W06-USB-175	1.29	1.91	1.35	0.21